Bedforms and sediment transport in the middle Tay Estuary, Scotland: a side-scan sonar investigation

Silke F.K. Wewetzer

This thesis is submitted to the Department of Geology
of the University of St.Andrews
for the Degree of Doctor of Philosophy

March 1997

(i) I, Silke F.K. Wewetzer, hereby certify that this thesis, which is approximately 55,000 words in length, has been written by me, that it is the record of work carried out by me and that it has not been submitted in any previous application for a higher degree.

date 17.3.97 signature of candidate

(ii) I was admitted as a research student in June 1993 and as a candidate for the degree of Ph.D. in June 1993; the higher study for which this is a record was carried out in the University of St. Andrews between 1993 and 1997.

date 17.3.97 signature of candidate

(iii) I hereby certify that the candidate has fulfilled the conditions of the Resolution and Regulations appropriate for the degree of Ph.D. in the University of St. Andrews and that the candidate is qualified to submit this thesis in application for that degree.

date 17.3.97 signature of supervisor

date 17.3.97 signature of supervisor

In submitting this thesis to the University of St. Andrews I understand that I am giving permission for it to be made available for use in accordance with the regulations of the University Library for the time being in force, subject to any copyright vested in the work not being affected thereby. I also understand that the title and abstract will be published, and that a copy of the work may be made and supplied to any bona fide library or research worker.

date 17.3.97 signature of candidate

ABSTRACT

Side-scan sonar techniques have been employed to determine the distribution of various bedforms and their changing asymmetries to tidal currents in the middle reaches of the Tay Estuary on the east coast of Scotland. The field study area is geographically defined by two multi-pier bridges, the Tay Railway Bridge and the Tay Road Bridge, which cross the estuary at Dundee.

This study is an investigation of the bedforms, sediment types and facies variations by means of acoustic remote sensing, coupled with direct sampling of bottom sediments and measurement of current velocities. Full coverage was achieved by systematically surveying the study area by means of side-scan sonar along 42 traverses. The main bedform types recorded in the study area, between autumn 1993 and summer 1995, were dunes. Sonographs were interpreted for dune height, wavelength, length along dune crest, sinuosity, superposition, asymmetry and crest orientation and a statistical analysis was carried out to establish correlations between the various geometrical parameters and water depth and to compare these results with the findings of other researchers. The side-scan sonar surveys were augmented by echo-sounding surveys in parts of the study area where sonographs could not be interpreted in detail. In August 1995, 53 sediment samples were collected to gather ground information to calibrate the sonographs for a more detailed interpretation of sediment types, showing that this part of the estuary is dominated by slightly gravelly sand. The channels are lined with mussels, pebbles and gravel and silty sand and sandy silt accumulates along the shores. Dune asymmetries were indicative of flood dominant current flow and were examined in conjunction with current measurements from eight stations. Bed load transport was estimated from current velocities. Dune morphology, water depth, grain size and current velocity were statistically analysed but no significant relationships could be established.

ACKNOWLEDGEMENTS

A Ph.D. project runs over a few years and many people help in various ways. I wish to thank everyone for their help and support, especially

Rob Duck (Department of Geography, University of Dundee) for being the best supervisor I could have wanted and without whom I would have never come this far

Ian Lorimer of the Tay Estuary Research Centre (TERC) for being a brilliant boatman during fieldwork and for always being around when I needed help of any kind

John McManus for successfully applying for two years of funding and for his comments during the final stage of this thesis

Colin Cameron as well as other members of staff at St. Andrews

Fraser Maxwell for sharing the collection and analysis of the sediment samples

Kath Leys and Sander Onland for spending long days on the Tay with me during current measuring sessions

and my friends and family who kept me going.

This project was funded for two years by the Commission of the European Communities (Human Capital and Mobility Fund) which is gratefully acknowledged.

CONTENTS

Declaration i
Library declaration ii
Abstract iii
Acknowledgements iv
Contents v
Figures viii
Tables xiv
Plates xv

Chapter 1
Introduction 1

Chapter 2
Previous research on the Tay Estuary 4
2.1 Introduction 4
2.2 The setting of the Tay Estuary 4
2.3 Hydrodynamics 9
2.3.1 Fluvial input 10
2.3.2 Marine input 11
2.3.2.1 Tidal progression 11
2.3.2.2 Salinity distribution and variation 13
2.3.3 Mixing of fresh and salt water and the water circulation 14
2.3.4 Other effects 18
2.4 Sediments and sediment transport 19
2.4.1 The reaches of the estuary 23
2.4.1.1 The uppermost, fluviatile sector 23
2.4.1.2 The upper estuary 23
2.4.1.3 The middle estuary 23
2.4.1.4 The lower estuary 26
2.4.2 The channels 26
2.4.3 Sediment sources and transport 29
2.4.3.1 Fluvial input 30
2.4.3.2 Marine input 31
2.4.3.3 Marginal input 31
2.4.3.4 Suspended sediment and turbidity maximum 31
2.4.4 Charting of migratory areas 33

Chapter 3
Surveying equipment 34
3.1 Introduction 34
3.2 Basic principles of acoustic surveying techniques 35
3.2.1 Echo-sounder 41
3.2.1.1 Basic components 42
3.2.1.2 Calibration 45
3.2.1.3 Factors affecting the record 45
3.2.1.4 Applications of echo-sounding 48
3.2.1.5 Lowrance X-16 echo-sounder 48
3.2.2 Side-scan sonar 53
3.2.2.1 Basic principles 53
3.2.2.2 Geometry of a side-scan sonar record 56

3.2.2.3 Design details 59
3.2.2.4 Record interpretation 69
3.2.2.5 Klein Hydroscan Model 401 78
3.2.2.6 Waverley Sonar 3000 79
3.2.3 Position-fixing 80
3.2.3.1 Global Positioning System (GPS) 80
3.2.3.2 Magellan NAV 1000 PLUS GPS receiver 83

Chapter 4
Transverse sedimentary structures in estuaries 87
4.1 Introduction 87
4.2 Classification 87
4.3 Distribution 89
4.4 Size 90
4.5 Shape 93
4.6 Orientation 95
4.7 Superimposed dunes 96
4.8 Migration 97
4.9 Summary 97

Chapter 5
Sedimentary bedforms recorded by side-scan sonar 99
5.1 Introduction 99
5.2 Data collection 99
5.3 Bedform geometries as recorded by side-scan sonar 100
5.3.1 Wavelength 103
5.3.2 Height 114
5.3.3 Length along dune crest 119
5.3.4 Sinuosity 123
5.3.5 Superposition 131
5.3.6 Asymmetry 131
5.3.7 Crest orientation 140
5.3.8 Summary of the interpretation of sonographs 142
5.4 Geometrical parameters of dunes 146
5.5 Conclusions 155

Chapter 6
Sedimentary bedforms recorded by echo-sounding 157
6.1 Introduction 157
6.2 Data collection 157
6.3 Bedform geometry 158
6.3.1 Wavelength 158
6.3.2 Height 163
6.3.3 Superposition 166
6.3.4 Asymmetry 171
6.3.5 Summary of the interpretation of echograms 174
6.4 Comparison of side-scan sonar and echo-sounding survey results 176
6.4.1 Wavelength 176
6.4.2 Height 177
6.4.3 Superposition 179
6.4.4 Asymmetry 180
6.5 Conclusions 181

Chapter 7
Sediment sampling and analysis **183**
7.1 Introduction 183
7.2 Methodology 185
7.2.1 Sediment sampling 185
7.2.2 Preparation of samples for analysis 187
7.2.3 Grain size analysis 187
7.3 Statistical analysis 188
7.4 Results and discussion 189
7.4.1 Description and distribution of sediment types 189
7.4.2 Statistical measures 192

Chapter 8
Current measurements **198**
8.1 Introduction 198
8.2 Equipment and methods 201
8.3 Results 202
8.4 Discussion of the current measurements 226
8.5 Estimation of sediment transport 229

Chapter 9
Key findings, their implications and avenues for future research **237**
9.1 Introduction 237
9.2 Relationships between geometrical parameters of bedforms, sediment size and current velocities 238
9.3 Summary and concluding remarks 245
9.4 Future research suggestions 248

References **253**

Appendix I **266**
Appendix II **268**

FIGURES

Chapter 1

1.1 Location of study area in the Tay Estuary, Scotland. 2

Chapter 2

2.1 Simplified geological map of the Firth of Tay and surrounding districts. 5

2.2 Late-glacial (main Perth) and post-glacial (Flandrian) shorelines and the post-glacial and present-day features of the Tay Estuary and the head of St.Andrews Bay. 8

2.3 Location of sites referred to in the text. 12

2.4 Mid-flood and mid-ebb tidal current patterns in St.Andrews Bay. 15

2.5 Eddy circulation in the Tay Estuary at high water. 17

2.6 Geological cross-section along the line of the Tay Road Bridge compiled from sparker seismic reflection and borehole records. 20

2.7 Migration paths of sediments of marine origin. 21

2.8 The reaches of the Tay Estuary. 22

2.9 Bathymetry of the reach between the Railway and Road Bridges. 24

2.10 Bathymetric cross-sections along the Railway Bridge showing the northerly migration, deepening and final stabilisation of the main channel. 28

Chapter 3

3.1 Typical curves for temperature, salinity, sound velocity and average sound velocity against depth. 36

3.2 A summary of the characteristics of acoustic wave propagation. 39

3.3 Attenuation of seismic waves for an absorption of 0.5dB per wavelength plotted as the effect of absorption on the amplitude of a sound wave reflected at a range of depths 0-1500m. 40

3.4 Tidal levels and datum. 43

3.5 Block diagram showing the main components of an echo-sounder. 44

3.6 Bar check for bottom-mounted transducers. 46

3.7 Echo-sounder depth error resulting from a side echo. 47

3.8 Echo-sounder depth errors resulting from ship motion. 47

3.9 Dry paper trace recorded with the Lowrance X-16. 52

3.10 Artist's impression of a side-scan sonar in operation. 54

3.11 Block diagram showing the main components of a side-scan sonar system. 55

3.12 Side-scan sonar record with corresponding sketch describing the conditions under which the record was made. 58

3.13 Physical extent of acoustic pulse length. 61

3.14 Relationship between range resolution and sonic "footprint". 63

3.15 As viewed from above, the side-scan sonar beam has the highest energy level in a narrow section. This is the main lobe of the sonar pulse that propagates out across the sea bed. 64
3.16 The side-scan sonar beam as viewed from the front or back of the tow fish is very wide. This provides near and far sea floor coverage. 65
3.17 Along-track (transverse) resolution depending on horizontal beam width and range. 67
3.18 Application of time-varying gain (TVG) amplification to a nonconstant signal. 68
3.19 Distortion effects on some common shapes parallel to the line of travel caused by various ship speeds. 71
3.20 Side-scan sonar geometry for horizontal range calculation. 72
3.21 Side-scan sonar geometry for target height calculation based on acoustic shadow. 74
3.22 Side-scan sonar geometry for target depth calculation based on acoustic shadow. 75
3.23 Side-scan sonar geometry showing the impossibility of calculating target depth on the basis of a low tonal colour zone. 76
3.24 Orbital configuration of the 24 GPS satellites consisting of four satellites in each of the six orbital planes. 82
3.25 Satellite coverage available for position fixes. 85
3.26 Low elevation satellite blocked by obstruction. 85

Chapter 4
4.1 Bedform phase diagrams: (a) after Allen (1983); (b) after Leeder (1982) and (c) after Harms *et al.* (1975). 91
4.2 Descriptive terms of plan patterns used for subaqueous bedforms. 94

Chapter 5
5.1 Traverses of the side-scan sonar surveys. 101
5.2 Sonographs of bedforms recorded at the same locality obtained on 03.06.94 and 14.03.95. 102
5.3 Sonographs recorded during flood and slack tidal conditions. 104
5.4 Sonographs recorded during ebb tidal conditions. 105
5.5 Sonograph recorded on Middle Bank where no dunes could be detected in the east-central section. 106
5.6 Good reflections from the steep, lee slopes of small dunes are shown in the lower half of the sonograph. 107
5.7 Dune wavelength during flood and slack tidal conditions as interpreted from side-scan sonographs. 109
5.8 Sonograph recorded in Queen's Road Channel showing dunes interspersed by ribbons of darker tonal intensities characteristic of cohesive silts and fine sands colonised by *Mytilus* beds. 110
5.9 Dune wavelength during ebb tidal conditions as interpreted from side-scan sonographs. 112

5.10	Sonograph showing abrupt changes between areas of flat bed and areas of small dunes.	113
5.11	Dune height during flood and slack tidal conditions as interpreted from side-scan sonographs.	116
5.12	Abrupt changes in dune wavelength and height recorded in Queen's Road Channel showing large dune wavelengths and heights on the left and small dune wavelengths and heights on the right.	117
5.13	Dune height during ebb tidal conditions as interpreted from side-scan sonographs.	118
5.14	Length along dune crest is defined in this thesis as the length of a good reflection from the steep, lee slope of a dune recorded by side-scan sonar.	120
5.15	Length along dune crest during flood and slack tidal conditions as interpreted from side-scan sonographs.	121
5.16	Length along dune crest during ebb tidal conditions as interpreted from side-scan sonographs.	122
5.17	Dune interference pattern recorded on Middle Bank by side-scan sonar.	124
5.18	Patchy, discontinuous signature recorded in the channels by side-scan sonar.	125
5.19	Dune sinuosity during flood and slack tidal conditions as interpreted from side-scan sonographs.	126
5.20	Sonograph showing an area of dunes of generally sinuous in phase shape and a region where no dunes were detected.	127
5.21	Abrupt changes of dune height, wavelength and sinuosity from "patchy, discontinuous" to straight and then to sinuous in phase (from south to north) at the northern edge of the Southern Channel as recorded by side-scan sonar.	129
5.22	Dune sinuosity during ebb tidal conditions as interpreted from side-scan sonographs.	130
5.23	Sonograph showing simple dunes of medium wavelength as defined by Ashley (1990).	132
5.24	Sonograph showing compound dunes: A - platform dune, B - superimposed dune.	133
5.25	Dune superposition during flood and slack tidal conditions as interpreted from side-scan sonographs.	134
5.26	Dune superposition during ebb tidal conditions as interpreted from side-scan sonographs.	135
5.27	Sonograph showing asymmetric dunes.	137
5.28	Dune asymmetry during flood and slack tidal conditions as interpreted from side-scan sonographs.	138
5.29	Dune asymmetry during ebb tidal conditions as interpreted from side-scan sonographs.	139
5.30	Dune crest orientation during flood and slack tidal conditions as interpreted from side-scan sonographs.	141

5.31 Dune crest orientation during ebb tidal conditions as interpreted from side-scan sonographs. 143
5.32 Abrupt change of dune crest orientation recorded in Queen's Road Channel. 144
5.33 Locations of sonographs shown in Chapter 5. 145
5.34 Plot of dune wavelength versus length along dune crest as measured from sonographs (total data set). 149
5.35 Plot of intertidal dune wavelength versus dune height as measured from sonographs recorded during ebb tidal conditions. 149
5.36 Plot of subtidal dune wavelength versus dune height as measured from sonographs. 152
5.37 Plot of intertidal dune wavelength versus dune height as measured from sonographs. 152
5.38 Plot of water depth versus dune height as measured from sonographs (total data set). 154
5.39 Plot of water depth versus dune wavelength as measured from sonographs (total data set). 154

Chapter 6

6.1 Echo-sounding traverses recorded during ebb and flood and slack tidal conditions. 159
6.2 Dune wavelength during flood and slack tidal conditions as determined by echo-sounding. 161
6.3 Dune wavelength during ebb tidal conditions as determined by echo-sounding. 162
6.4 Dune height during flood and slack tidal conditions as determined by echo-sounding. 164
6.5 Dune height during ebb tidal conditions as determined by echo-sounding. 165
6.6 Echogram of simple dunes. 167
6.7 Echogram of compound dunes. 168
6.8 Dune superposition during flood and slack tidal conditions as determined by echo-sounding. 169
6.9 Dune superposition during ebb tidal conditions as determined by echo-sounding. 170
6.10 Echogram of large flood asymmetric dunes. 172
6.11 Dune asymmetry during flood and slack tidal conditions as determined by echo-sounding. 173
6.12 Dune asymmetry during ebb tidal conditions as determined by echo-sounding. 175

Chapter 7

7.1 Positions of collected sediment samples determined by side-scan sonograph interpretation. 184
7.2 Textural classification of sediments after Folk (1974). 190
7.3 Textural classification of sediments after Folk (1974). Distribution is based on sediment samples in correlation with side-scan sonographs. 191
7.4a Distribution of median grain diameter based on sediment sampling in correlation with side-scan sonograph interpretation. 193

7.4b Distribution of median grain diameter after Buller and McManus (1975). 193
7.5a Distribution of sorting characteristics based on sediment sampling in correlation with side-scan sonograph interpretation. 195
7.5b Distribution of sorting characteristics after Buller and McManus (1975). 195
7.6a Distribution of skewness variations based on sediment sampling in correlation with side-scan sonograph interpretation. 196
7.6b Distribution of skewness variations after Buller and McManus (1975). 196

Chapter 8
8.1 Positions of current measuring stations. 199
8.2 Sonograph of the bed at Station A showing ebb dominant dunes recorded during ebb tidal conditions. 204
8.3a Station A: time series plot of surface and bottom current velocities. 206
8.3b Station A: speed and direction of bottom currents. 206
8.4 Sonograph of the bed at Station B showing flood dominant dune asymmetries. 208
8.5a Station B: time series plot of surface and bottom current velocities. 209
8.5b Station B: speed and direction of bottom currents. 209
8.6 Sonograph of the bed at Station C showing flood dominant dune asymmetries. 211
8.7a Station C: time series plot of surface and bottom current velocities. 212
8.7b Station C: speed and direction of bottom currents. 212
8.8 Sonograph of the bed at Station D showing dunes of mixed asymmetries recorded during ebb tidal conditions. 213
8.9a Station D: time series plot of surface and bottom current velocities. 215
8.9b Station D: speed and direction of bottom currents. 215
8.10 Sonograph of the bed at Station E showing flood dominant dune asymmetries. 216
8.11a Station E: time series plot of surface and bottom current velocities. 217
8.11b Station E: speed and direction of bottom currents. 217
8.12 Sonograph of the bed at Station QRC showing flood dominant dune asymmetries. 219
8.13a Station QRC: time series plot of surface and bottom current velocities. 220
8.13b Station QRC: speed and direction of bottom currents. 220
8.14 Sonograph of the bed at Station T2-T showing the "patchy, discontinuous" pattern typical of most channel areas. 221
8.15a Station T2-T: time series plot of surface and bottom current velocities. 223
8.15b Station T2-T: speed and direction of bottom currents. 223

8.16 Sonograph of the bed at Station NOM showing the border between the "patchy, discontinuous" pattern in the northern and central section and "no measurable dunes" in the southern section. 224
8.17a Station NOM: time series plot of surface and bottom current velocities. 225
8.17b Station NOM: speed and direction of bottom currents. 225
8.18 Average and maximum current velocities. 227
8.19 Plot of average current speed (flood and ebb) and corresponding sediment mean grain diameter for all eight stations showing the relationship between grain size, flow velocity and type of sediment movement. 231

Chapter 9
9.1 Plot of mean current speed and mean grain size, as recorded at the current stations, on a bedform phase diagram established by Harms *et al*. (1975). 242
9.2 Sonograph recorded when crossing a convergent front in the Tay Estuary. 251

Appendix II
II.1 Relationship between critical shear stress and mean grain size. 269
II.2 Relationship between the K coefficient in the bed load estimation equation and mean grain size for different values of excess shear stress. 269
II.3 Nomogram for evaluation of bed load transport from measurements of the critical velocity and the coefficient K. 270

TABLES

Chapter 3

3.1 Approximate two-way working ranges of modern active sonar systems. 41

3.2 Pulse width according to lower depth limit. 51

Chapter 4

4.1 Classification of dunes. 88

4.2 Previously used bedform names and their new terminology. 89

Chapter 5

5.1 Correlation coefficients (r_{cc}) computed for linear regression analysis of geometrical parameters of dunes and water depth. 147

5.2 Intertidal bedform size and morphological characteristics. 150

Chapter 8

8.1 Variations of dune parameters (during flood and ebb tidal conditions) and sediment classification at current meter stations. 200

8.2 Comparison between tidal height of side-scan sonar surveys and current measurements. 201

8.3 Average and maximum current speeds and directions. 205

8.4 Results of bed load estimation for one tidal cycle according to the method of Sternberg (1972). 234

Chapter 9

9.1 Mean ebb and flood tidal current speeds, dune dimensions and mean grain sizes at the eight current measuring stations. 241

9.2 Correlation coefficients (r_{cc}) computed between various geometrical parameters of dunes and maximum and average current speeds. 244

PLATES

Chapter 3

3.1 The Lowrance X-16 echo-sounder (192kHz). 49

3.2 R.V. Mya from the Tay Estuary Research Centre (TERC), Newport-on-Tay. 50

3.3 The Waverley Sonar 3000 (side-scan sonar system). 57

3.4 The Magellan NAV 1000 PLUS Global Positioning System (GPS) receiver. 84

Chapter 5

5.1 Photograph of Middle Bank at low water on a spring tide showing the subdivision into three small banks. 111

Chapter 7

7.1 Photograph of van Veen grab modified with the addition of teeth. 186

Chapter 8

8.1 The Braystoke MK 3, 5" Diameter Impeller current meter. 203

Chapter 1

INTRODUCTION

Pritchard (1967) defines an estuary as "a semi-enclosed coastal body of water which has a free connection with the open sea and within which sea water is measurably diluted with fresh water derived from land drainage". Estuaries are characterised by reversing currents, day to day changes in the lunar tidal ranges, tidal modifications by areas of low atmospheric pressure, continuously variable fresh water input from the rivers and are therefore a challenging environment to investigate. Such a complex multivariate environment can only be analysed by a large amount of data collected during a variety of tidal and weather conditions.

The principal aim of this study was to carry out the first systematic side-scan sonar survey of the bed of part of the middle reaches of the Tay Estuary, Scotland (Fig. 1.1), to investigate the bed and establish correlations between the various geometrical parameters of bedforms and water depth. The side-scan sonar survey results were to be augmented by echo-sounding surveys in areas where recorded sonographs could not be fully interpreted. To establish the sediment distribution in the study area direct bottom sampling was to be coupled with the sediment investigation by acoustic remote sensing. A simplified circulation model was to be established by examining dune asymmetries recorded by side-scan sonar in conjunction with current measurements. Bed load transport was estimated from current velocities. The overall aim was to establish correlations between the geometrical parameters of bedforms, grain size of sediments and current velocities.

The study area is geographically constrained by the Tay Railway Bridge and the Tay Road Bridge crossing the estuary to the south of the city of Dundee. Research on bedforms and sediments in both this zone and that of the wider estuary has been undertaken previously, especially by Buller and McManus (1975). Hitherto, however, side-scan sonar has been used only for restricted, small scale surveys within the Tay Estuary but never for a systematic coverage over a relatively large area.

Examination of intertidal bedforms, exposed at low water, limited previous diver observations of subtidal bedforms (Buller and McManus, 1975) and

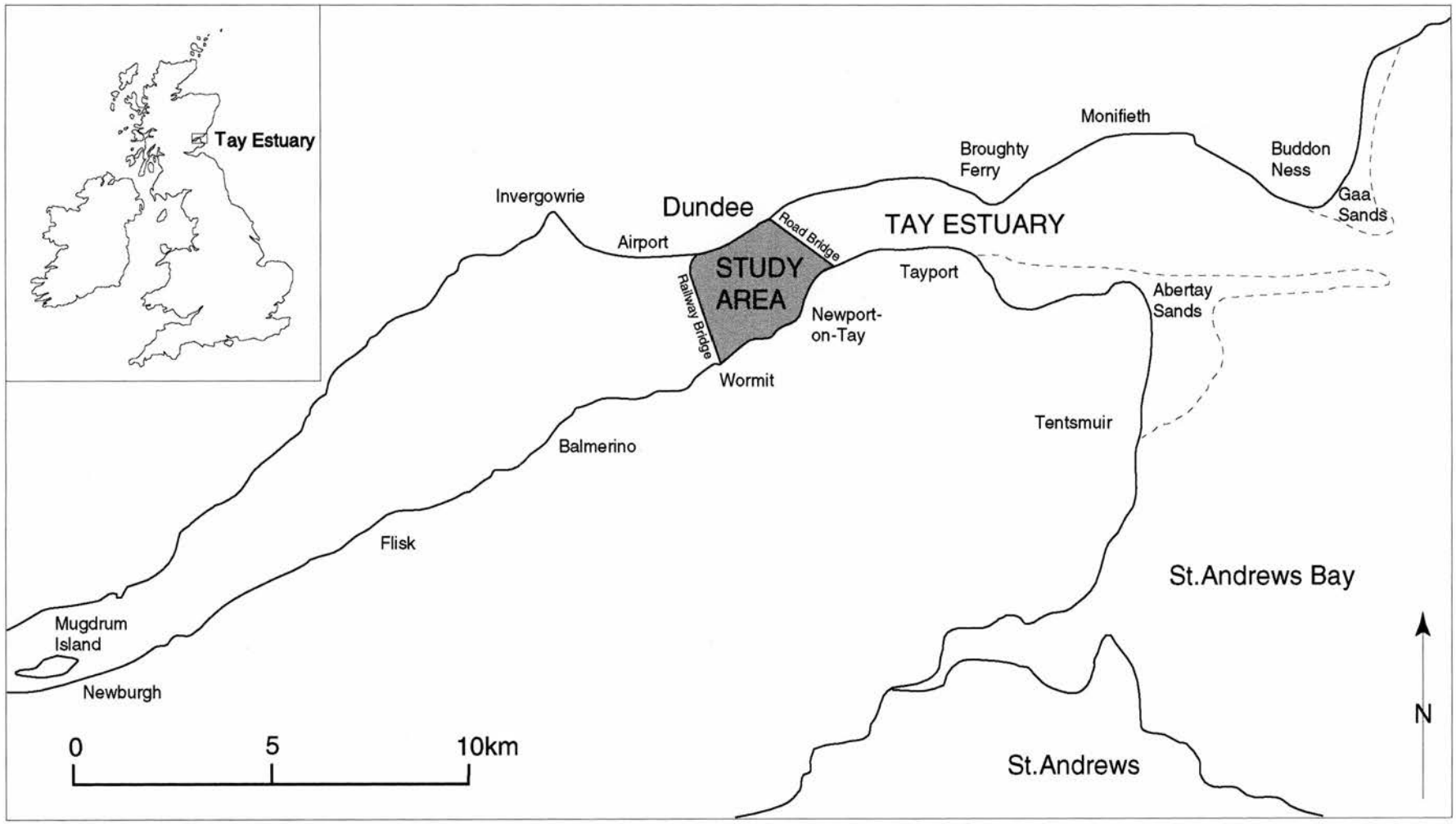

Fig. 1.1: Location of study area in the Tay Estuary, Scotland.

earlier sediment sampling surveys (Buller and McManus, 1975; White, 1992) in the study area have been used to provide additional ground information to support the acoustic remote sensing surveys and the ground information collected in this study. Another reason for choosing this fieldsite was that it is known from previous work (Buller et al., 1971; Buller and McManus, 1971; Buller and McManus, 1975) to be highly dynamic. Earlier work (Buller and McManus, 1975) suggests that much of the sediment in this area is of marine origin and this hypothesis has been tested. It is known that sands cover extensive areas and side-scan sonar was used to look in detail at bedforms and their asymmetry. Every estuary is tidally influenced and one of the aims of this project was to find out which parts of the middle Tay Estuary are dominated by ebb or flood tidal conditions. An attempt is made to establish correlations between bathymetry, bedform geometries, sediment type and tidal water movement. Examination of the types of bedforms, the sources of the sediment and the facies changes should increase our understanding of estuarine dynamics.

The structure of the thesis is as follows: In Chapter 2 an overall review of previous relevant work carried out on the Tay Estuary is given. In Chapter 3 the main equipment such as echo-sounder, side-scan sonar and GPS, used in this study is described. Chapter 4 gives a brief introduction to transverse sedimentary bedforms in estuaries as detected by other researchers and explains the general terminology used in this thesis. Chapters 5 and 6 are the main results chapters of the side-scan sonar and echo-sounding surveys carried out. These results are complemented by the results of a sediment sampling survey and current measurements in Chapters 7 and 8, respectively. The results of the four surveys are discussed in the individual chapters as well as in Chapter 9 which is concluded by a section on suggestions for future research.

Chapter 2

PREVIOUS RESEARCH ON THE TAY ESTUARY

2.1 Introduction

A large number of scientists have carried out research in the Tay Estuary, particularly in the last three decades. The aim of this literature review is to produce a summary of the dynamics and physical processes of sedimentation of the Tay Estuary dealt with by several researchers.

2.2 The setting of the Tay Estuary

The Tay Estuary has been developed along a graben which trends obliquely across the axis of the Sidlaw-Ochil anticline (sometimes referred to simply as the Sidlaw anticline or as the Tay anticline) at the eastern end of the Midland Valley of Scotland (Buller and McManus, 1971; McManus, 1972; Dobereiner and McManus, 1983; Armstrong *et al.*, 1985).

This part of the Midland Valley is principally underlain by rocks of Lower Devonian (Lower Old Red Sandstone) age (Fig. 2.1) which comprise conglomerates, sandstones, siltstones and shales, with contemporaneous lavas of intermediate to basic composition and associated pyroclastic rocks. The Lower Devonian formations were folded during Middle Devonian times by Caledonian orogenic activity. In general the fold axes display the typical Caledonian trend, from north-east to the south-west. Developed beneath Strathmore is a broad syncline, the so-called Strathmore syncline, whilst the adjacent anticline to the south, the Sidlaw-Ochil anticline deforms the lavas and intercalated sedimentary rocks of the Sidlaw and Ochil Hills. After the deposition of Upper Devonian sedimentary rocks in the area, now largely removed by erosion, a period of faulting occurred during which the subsidence of the Tay Graben took place between the near-parallel North Tay and South Tay faults, trending obliquely to the axis of the Sidlaw-Ochil anticline. This permitted the lowering of undeformed Upper Devonian rocks to occupy the central rift beneath the Carse of Gowrie, between the folded Lower Devonian rocks, thus creating the lowlands extending from Bridge of Earn to Dundee.

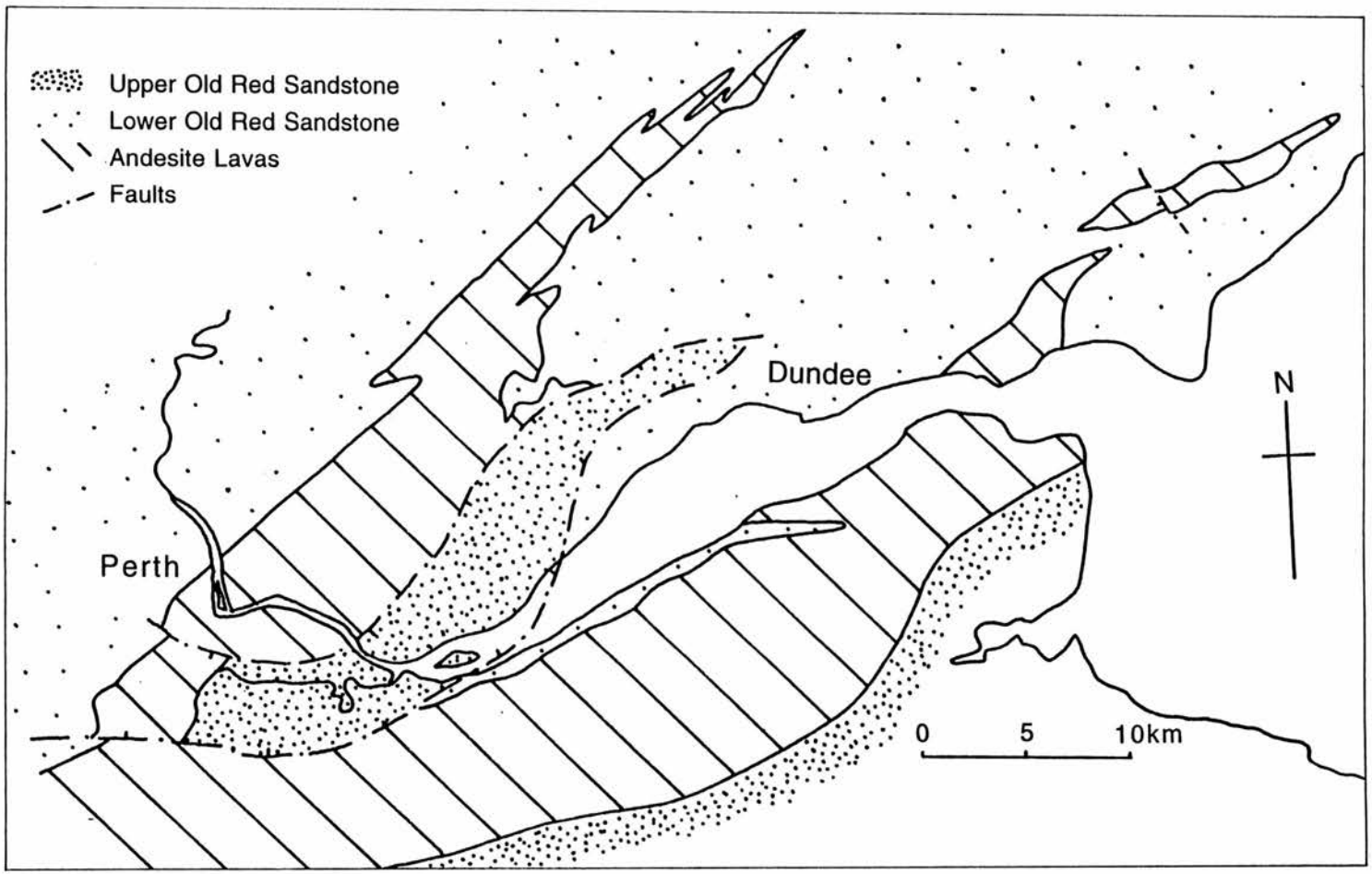

Fig. 2.1: Simplified geological map of the Firth of Tay and surrounding districts (after Buller and McManus, 1971).

The Tay Estuary has been developed along the foot of the Ochil Hills but is separated from the Sidlaw Hills by the lowland Carse of Gowrie. The dip slopes of the Sidlaw Hills rise smoothly from Strathmore, whereas the south-facing, relatively steep, scarp slopes descend to the North Tay fault at the northern edge of the Carse of Gowrie. Similarly, the scarp slopes of the Ochil Hills rise sharply from the South Tay fault and the dip slopes descend away from the Tay towards the south-east (Scarth, 1966).

In detail the relief of this area is determined to a large extent by the various rocks which make up the Lower Devonian formations. Relatively soft sandstones and other sedimentary rocks are intercalated with the volcanic rocks (McManus, 1972). Since the sedimentary rocks are less resistant to erosion than the lavas, they tend to form belts of low ground while the lavas tend to stand out in relief. The lava-dominated hills of the Sidlaws and Ochils form strong positive features and cause a distinct narrowing at the mouth of the estuary between Broughty Ferry and Tayport (Scarth, 1966; McManus, 1972).

It is believed that the current drainage pattern of the Tay was initiated during the Miocene, after the cessation of Tertiary volcanic activity in western Scotland, as a west to east draining system (McManus, 1968; Buller *et al.*, 1971). Hence the river system of the Tay rises in the Grampian Highlands and extends across the Highland Boundary Fault into the northern sector of the Midland Valley (Al-Jabbari *et al.*, 1980) where the waters flow through the Perth Gap into the Tay Estuary (McManus, 1967). The mountainous upper parts of the drainage basin are underlain by mixed assemblages of metamorphic rocks of Precambrian age (Moine and Dalradian Supergroups) (Armstrong *et al.*, 1985; Stephenson and Gould, 1995).

At the onset of the Pleistocene glaciation the principal drainage is believed to have flowed seawards through the Perth Gap, i.e. through the resistant volcanic rocks of the Sidlaw Hills (Buller *et al.*, 1971). This has been postulated by means of the analysis of the stratigraphy of the deposits in large numbers of boreholes, drilled in the Perth area, which indicate the existence of a buried channel of such dimensions that it could have resulted only from the erosive action of a major stream (McManus, 1967).

During the Pleistocene the whole area was covered by ice and repeated advances and retreats in the region modified all valleys and most watersheds (McManus, 1968; Buller *et al.*, 1972; Al-Jabbari *et al.*, 1980). Due to the development of large ice sheets, world-wide sea level dropped by some 80-100m. During each ice-retreat the lower valleys were inundated by the sea so that estuarine conditions were far more extensive than today (McManus, 1966). The principal ice flow entered the Tay Estuary by way of Strathearn (McManus, 1972). Each successive ice advance removed the soft drift deposits laid down during the previous retreat (McManus, 1966) and deposited a new mantle of till during its subsequent retreat (Buller *et al.*, 1971). Four synglacial lowerings of sea level enabled the Tay to cut deeply below the present sediment-covered floor. The resultant buried channel is, according to borehole analyses, asymmetrical in cross-section and in the Dundee area extends to approximately 72m below O.D. (McManus, 1966 and 1968).

The early stages of ice retreat from the Tay Estuary were contemporaneous with depressed land levels so, although the ice thickness was probably over 100m, it was partly buoyed up by sea water at the seaward extremity (McManus, 1972). The glacial till is mantled by a widespread deposit of laminated silty clays with thin sand layers incorporating occasional boulders and pebbles (McManus, 1966 and 1972). Simpson (1933) indicated that, during the deposition of this so called Arctic Clay, ice was in close proximity to the head of the estuary. Consequently, fine rock-flour material was released into the estuarine waters throughout the year and substantial quantities settled out (McManus, 1966). According to McManus (1972) the early phases of this sedimentation took place in deep water where no tidal currents would have disturbed the bottom. The water was probably strongly stratified, a thick layer of saline marine water beneath a thin layer of freshwater, providing an ideal environment for the flocculation and subsequent settling of clays. As the waters became shallower due to siltation, less fine material was retained and progressively coarser sediments were deposited.

Following the final retreat of ice from the area, rapid isostatic uplift of the crust took place. This resulted in a general fall of relative sea level and left behind a distinctive suite of raised beaches (Armstrong *et al.*, 1985) (Fig. 2.2), best developed in the weaker sandstones (Scarth, 1966) and which

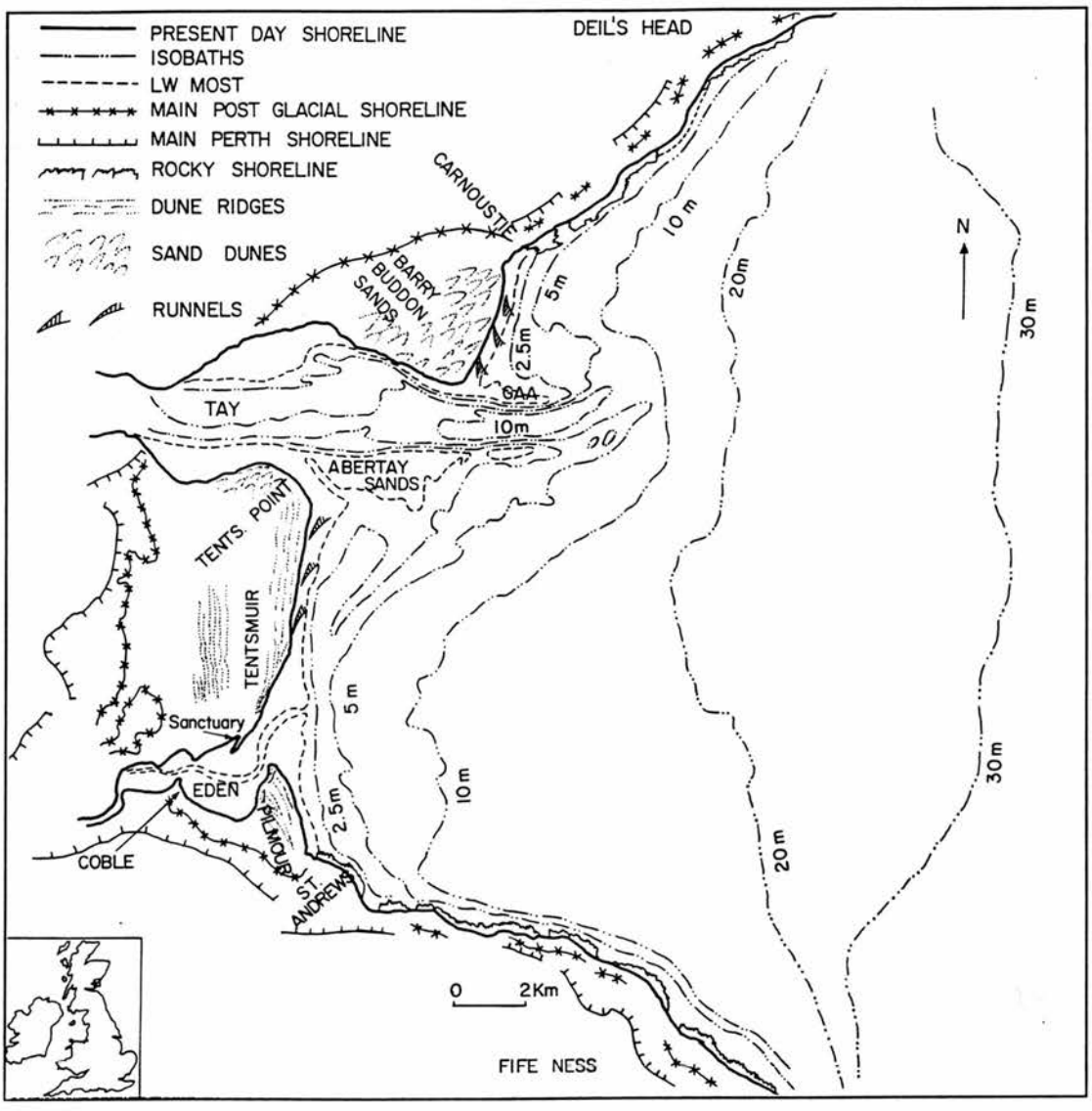

Fig. 2.2: Late-glacial (main Perth) and post-glacial (Flandrian) shorelines and the post-glacial and present-day features of the Tay Estuary and the head of St.Andrews Bay (after Ferentinos and McManus, 1981).

have been extensively investigated by Sissons *et al.* (1965). At this time climatic amelioration was swift and runoff streams developed extensively, cutting into bedrock and the early unconsolidated sediments towards a base level around 39m below O.D. (McManus, 1972). This is known from evidence of boreholes and geophysical surveys (McGuinness *et al.*, 1962) which have also revealed that the fill of this early valley is capped by a gravel deposit which occupies a relatively shallow position beneath the modern surface. Along the line of the Tay Railway Bridge it is identified at 15m below O.D. while at the Road Bridge the gravel descends from 8m below O.D. to 27m below O.D. towards the centre of the present estuary (Mc Manus, 1972).

McManus (1972) explains the origin of the gravel bed as follows: Wave activity extensively eroded marginal materials in the lower parts of the catchment area as the Rivers Tay and Earn re-established their courses across unconsolidated glacial debris. As the sea level rose the next time, the Tay Estuary silted up with coarse sands and fine gravels in the channels, medium and fine sands on the sand banks and very fine, partly laminated silts on the marginal mudflats. In the meantime the sea level fell and rose again. During the next fall a thin layer of peat was deposited on the exposed tidal flats which were covered with intertidal silts during the following sea level rise (Armstrong *et al.*, 1985). Again the sea level fell and this time a thicker layer of peat was deposited. This was followed by a relative rise of sea level which was again associated with the deposition of an inter-tidal silty clay formation, the so-called Carse Clay (Armstrong *et al.*, 1985; Buller *et al.*, 1975). The final fall to the present sea level was associated with erosion as well as accumulation of the modern estuarial deposits, especially in the middle reaches of the estuary (McManus, 1972).

2.3 Hydrodynamics

Pritchard's (1967) definition of an estuary being "a semi-enclosed coastal body of water which has a free connection with the open sea and within which sea water is measurably diluted with fresh water derived from land drainage" is used here. Water movements in estuaries are of complex nature. They are primarily governed by tidal and freshwater inputs, the resultant flow being modified by bed and channel configurations, salinity and silt load variations (Buller *et al.*, 1971; Charlton *et al.*, 1975). The tidal

range varies mainly with the lunar cycle but can also be modified by local and regional weather patterns. The input of freshwater depends mostly on the season and the rainfall. Salinity variations are the result of these two varying controls (Charlton *et al.*, 1975; Williams and West, 1975).

2.3.1 Fluvial input

The quantity of fresh water entering an estuary depends on climate, physiography, geology and vegetation cover of the hinterland. Strong relief causes orographic rainfall. Physical characteristics of rocks affect the quantity and freedom of flow (infiltration) while the density of vegetation cover determines the rate of run-off (Buller *et al.*, 1975).

The Tay Estuary receives most of its freshwater from a 6,500km^2 catchment area (Buller *et al.*, 1975; Dobereiner and McManus, 1983). The major draining systems are the Rivers Tay and Earn which contribute the greatest volume of freshwater of any river basin in the UK (McManus, 1968; Pontin and Reid, 1975). Most of the catchment area is situated in highland terrain on metamorphic rock (Dobereiner and McManus, 1983). Rainfall varies greatly from 760mm annually in the lower and drier south-eastern part of the basin to 3,200mm annually in the Highlands (Al-Jabbari *et al.*, 1980). In the higher regions much of the precipitation falls as snow and may be retained for lengthy periods before being released between February and April due to a rise in air temperature (Al-Jabbari *et al.*, 1980; Dobereiner and McManus, 1983). The river discharge is therefore greatest between February and April and then decreases to a minimum in summer (McManus, 1968 and 1986b; Pontin and Reid, 1975).

According to McManus (1986a) and Charlton *et al.* (1975) long term gauging has revealed that the mean daily flow for the Tay-Earn system is 198m^3/s and can increase to a maximum of 1,465m^3/s or decrease to a minimum of 35m^3/s. Daily average flow figures also indicate that the River Earn contributes approximately 16% (31m^3/s) and the River Tay approximately 84% (167m^3/s) of the total inflow with the catchment ratios being 15% and 85% respectively (Pontin and Reid, 1975; McManus, 1984). During extreme floods, the maximum surface water velocity approaches 4m/s on the River Tay and 3m/s on the River Earn. Since about 1950 peak flow in the winter is partially reduced by storage in

Hydro-Electric reservoirs, conversely summer flow is enhanced by release of this stored water (McManus, 1986b).

2.3.2 Marine input

Unlike the variable fluvial input into the estuary, the marine input is quite regular depending mainly on the tidal cycle and can be occasionally modified by storms and sustained variations in barometric pressure. The major components of marine input are tidal progression and salinity variations. Buller *et al.* (1972) give an estimate of 127×10^9l of saline water passing into the estuary during a neap tide.

2.3.2.1 Tidal progression

Tidal motion in the North Sea has been described by Proudman and Doodson (1924) as three Kelvin waves of which the most northerly has its amphidromic centre about 60km off the south-western coast of Norway. This Kelvin wave generates a tidal wave travelling in a southerly direction across the mouth of the Tay Estuary (Charlton *et al.*, 1975) leading to a tidal range of 4.0-6.0m (Buller *et al.*, 1975) or, as mentioned by McManus (1986b), of 3.5-5.0m from neap to spring conditions. The tidal reach is approximately 50km long with its landward limit 3km north of Perth (Buller *et al.*, 1975; McManus, 1986b) (Fig. 2.3).

At the seaward end of the estuary the tidal wave is symmetric but it becomes progressively distorted landward from Flisk (Fig. 2.3) (McManus, 1986b). The motion and distortion of the tidal wave depend upon the buffering effects of freshwater discharge, the morphology of the bed over which it passes, the roughness characteristics of the sedimentary deposits (Buller *et al.*, 1975) and especially on the variations in cross-section (Charlton *et al.*, 1975). Charlton *et al.* (1975) also note that the Road Bridge is an obstruction for the tidal wave unlike the Railway Bridge which is built perpendicular to the tidal flow. It may, however, cause small changes even though a delay of the tidal wave should be detectable. Since every tide is slightly different in character only a statistical analysis of data for conditions before and after the construction of the bridge would show this. No such data exist.

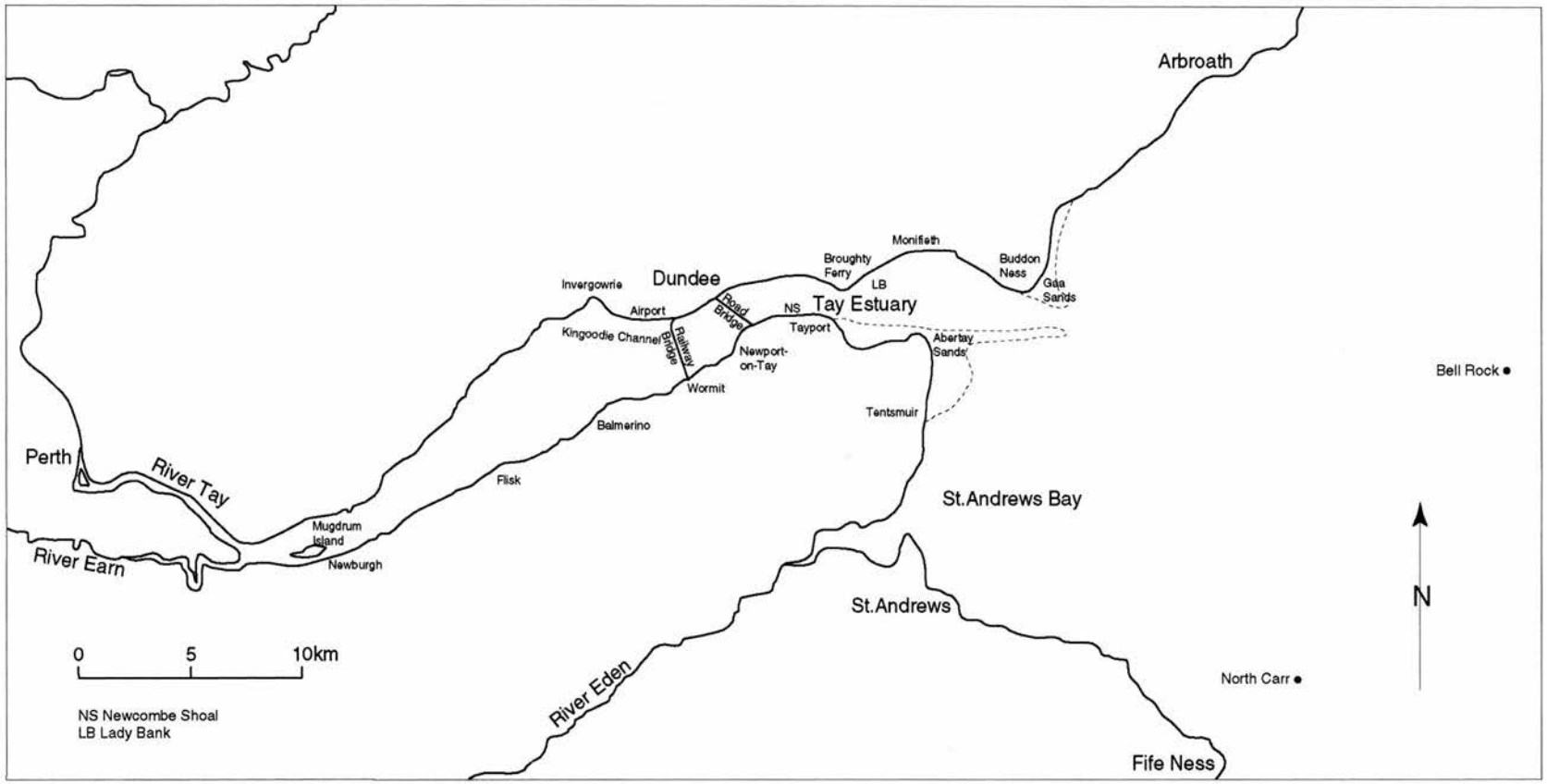

Fig. 2.3: Location of sites referred to in the text.

Duck and Dow (1994) used side-scan sonar and echo-sounding to survey along the Railway Bridge. The sonographs revealed the presence of columnar structures which are interpreted as the fallen piers of part of the first Tay Railway Bridge. These piers lie approximately north-south across the estuary and effectively present a virtually continuous barrier to bottom water currents over a distance of ca. 470m off the southern shore.

In general the tidal delay, the time between high water at the mouth of the estuary and its landward limit near Perth, is about two hours (Buller *et al.*, 1975) but other figures have also been given; for example 50 minutes between Dundee and Perth (Dobereiner, 1982).

2.3.2.2 Salinity distribution and variation

The Tay is generally a partially mixed estuary in which the salinity values as well as the limit of salt penetration up the estuary are determined by freshwater discharge and tidal range (Williams and West, 1975; Dobereiner and McManus, 1983; McManus, 1984). During low river flow the salinity intrusion extends to the Newburgh region (Williams and West, 1975; McManus, 1984) although Mill recorded in 1885 that some fishermen say that salt can be tasted at Perth during very dry summer weather and at high spring tides. Under most conditions the limit of salt penetration both at high and low water lies west of the Railway Bridge (McManus, 1984).

McManus and Wakefield (1982) have measured water salinity variations through complete tidal cycles at several locations in the Tay Estuary. This has revealed an increase of salinity to a peak value up to two hours after high water, following an initial post-high water sag. Repeated measurements taken at three sites across the Dundee-Newport-on-Tay reach have given different salinity values. The northern waters are more saline on the flood tide than on the ebb, and the southern fresher on the flood than on the ebb. This gives an indication, in connection with float tracking experiments, of the estuarine circulation, which is examined in Section 2.3.3.

McManus (1982) plotted the variation of salinity against current speed to obtain a visual representation of the behaviour of water. He found that the range of salinities in the headwaters is smaller than in the middle estuary

and that the range decreases seawards although it has a higher average value. The comparison of these plots showed that the ranges of variation of both salinity and current speed are greater on spring than on neap tides.

Williams and West (1975) state that the salinity variation at Newport-on-Tay (Fig. 2.3) shows a greater difference between surface and bottom values at high water than at other times in the tidal cycle; about 20g/kg near the channel bed and about 19g/kg near the surface. They also found evidence in their measurements at Broughty Ferry, Newport-on-Tay and Balmerino for a net upstream movement of water near the bottom and a net seaward movement of water in the upper layers during the flood tide. The explanation for this phenomenon can be found in the different density values for salt and freshwater. Relatively dense sea water enters the estuary along the bed whilst less dense out-flowing river water moves seawards near the surface hence producing a form of density stratification (McManus, 1984).

2.3.3 Mixing of fresh and salt water and the water circulation

An essential feature of a study of circulation in an estuary is an understanding of the interaction between fresh river water moving seaward and denser saline sea water flowing landward. The mixing of the tidal and fluvial components produce density gradients which result in a characteristic non-tidal circulation in estuaries (Williams and West, 1973 and 1975).

The tidal volume entering the Tay varies from $130 \times 10^6 m^3$ on extreme neap tides to $623 \times 10^6 m^3$ on extreme spring tides, giving a ratio of 1 to 5 (Charlton *et al.*, 1975). A freshwater spate coincident with neap tides produces a fresh to salt water ratio of 1:2, whereas on spring tides this ratio is 1:10 (Buller *et al.*, 1975). In the summer, when freshwater flows are low, the ratio can increase to 1 to 50, and exceptionally to 1 to 200 (Cunningham, 1896).

The coastal segment of the floodstream runs south-south-west past Arbroath and divides into two streams (Fig. 2.4): one turns west to enter the Tay Estuary while the other continues south-south-west before forming a clockwise eddy between St.Andrews Bay and the Abertay Sands. It

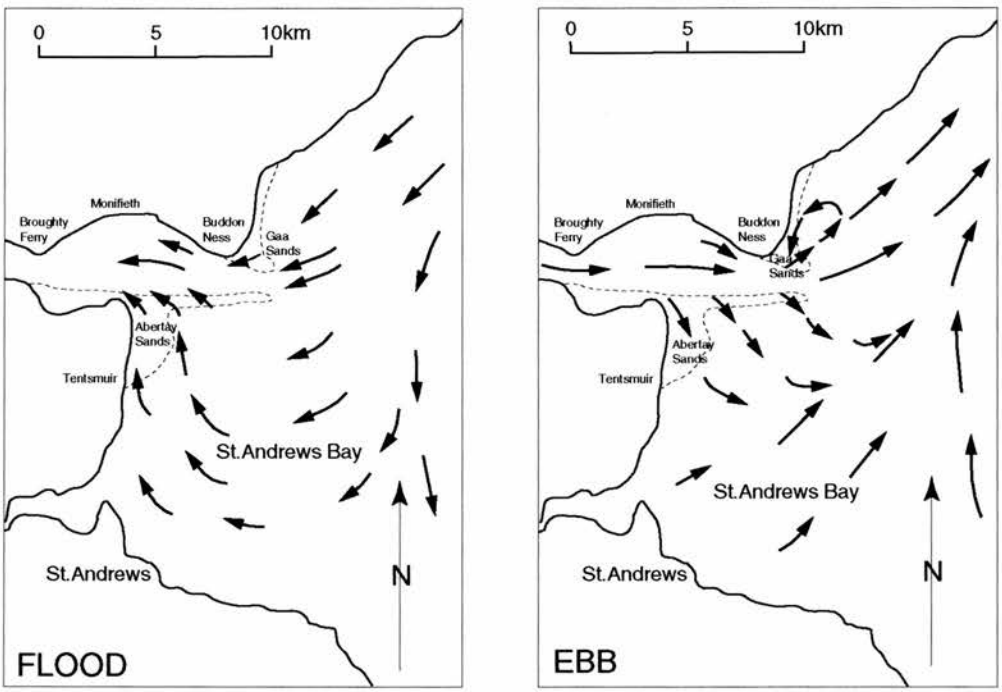

Fig. 2.4: Mid-flood and mid-ebb tidal current patterns in St.Andrews Bay (after Ferentinos and McManus, 1981).

sweeps along the Tentsmuir shoreline and then spills over the Abertay Sands finally entering the estuary (Ferentinos and McManus, 1981). These tidal currents generally flow with a maximum velocity of 1m/s (Green, 1975a). During the ebb tide the water flows eastwards out of the Tay Estuary entrance and then continues in a north-easterly direction (Fig. 2.4). Its momentum leads to the formation of an ebb jet to the north of the estuary mouth where it establishes an anticlockwise eddy (Ferentinos and McManus, 1981).

Charlton *et al.* (1975) have investigated the tidal and freshwater induced circulation in the Tay Estuary and found the following: the flood tide tends to enter the estuary over the full width of the mouth with a moderately dominant current in the main Navigation Channel. Once the flood tide overflows the drying banks within the estuary, it tends to follow fairly wide paths largely governed by the geometry of the estuary and its bedforms. The flood flow over the Abertay and Gaa Sands joins the main channel which widens out into the Monifieth Bay area before being constricted by the narrows between Tayport and Broughty Ferry where the flood flow tends to concentrate on the south side. Since this is the deepest part of the estuary, no major increase in stream velocity has been recorded. Between the road and the Railway Bridge the flow is fairly uniformly distributed between the channels although the main Navigation Channel is on the south side. West of the Railway Bridge the main flow keeps to the Southern Channel but an appreciable flow spreads over the mud and sand flats on the north side. As the tide turns at high and low water, complex imbalances appear to build up between residual dynamic energy in the main channels and opposing surface gradients resulting from movement of the tidal waves. This induces a series of rotational eddy lenses (Fig. 2.5), forming before the full opposing tidal current becomes dominant. They can last for up to 30-45 minutes. The ebb flow drains off the flats and tends to concentrate in the main channels. West of the Railway Bridge it flows strongly in the main southerly channel. Between the bridges it swings towards the south bank at Newport-on-Tay, then heads through the Road Bridge in a more northerly direction towards Dundee and Broughty Ferry where it tends to the north side. It remains in the main Navigation Channel in the Monifieth Bay area and most of water flows out of the estuary in a north-easterly direction.

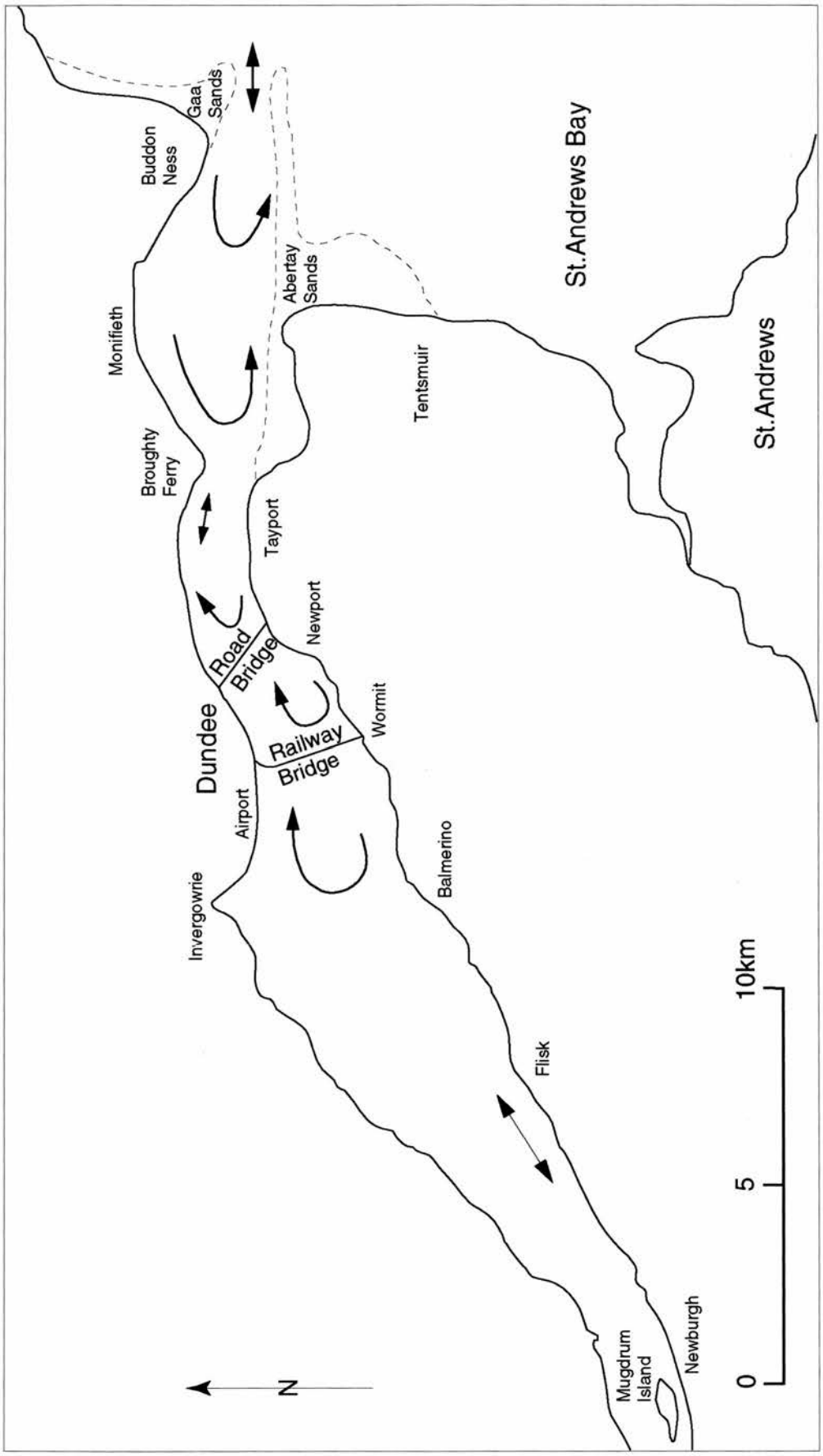

Fig. 2.5: Eddy circulation in the Tay Estuary at high water (after Charlton *et al.*, 1975).

McManus and Wakefield (1982) support these results with their investigations of salinity variation and float tracking between the two bridges but show anticlockwise rotation at high water and not clockwise as Charlton *et al.* (1975) claimed. As mentioned earlier, higher salinity values have been measured on the flood tide in the Queen's Road Channel. At the beginning of the ebb tide the more saline waters flow from the Queen's Road Channel southward into the main Navigation Channel and then move towards the southern shore. There they mix with the less saline waters. This results in a circulation pattern in which waters containing more salt flow seawards past points on the southern side of the channel than have been carried past these points on rising tide. Therefore the salinity detected at a point off the southern shore usually rises after high tide to reach its peak value as much as two hours after high water.

2.3.4 Other effects

Wind records from Bell Rock (Fig. 2.3) lighthouse 35km off the coast (lat 56°26'04"N, long 2°22'30"W) show that the most prevailing and dominant winds in St.Andrews Bay are from the south-west and west, but also not uncommon and as strong are winds from the north-east and south-east (Ferentinos and McManus, 1981; McManus, 1986b). A steady wind on an extensive area of shallow water such as an estuary can significantly modify water levels or gradients. Charlton *et al.* (1975) quote an estimate that a rise of water level of 1.9m between Buddon Ness and Newburgh can be generated by a wind of 25m/s (approximately 10-11 on the Beaufort scale) along the estuary.

North-easterly and south-easterly winds are known to have produced waves with significant heights of up to 5m in St.Andrews Bay (McManus, 1986b) but these directions follow in turn the most frequent waves from the south-west, recorded on North Carr (Fig. 2.3) light vessel 2km off Fife Ness (Ferentinos and McManus, 1981). In general, waves as well as wave-induced currents are the most important mechanisms causing shoreline changes; their major contribution being the transport of sediment along the coastline (Sarrikostis and McManus, 1987).

Another effect which can alter the mean sea level temporarily (Charlton *et al.*, 1975) is a persistent high or low of atmospheric pressure. In the estuary this is felt as a general lowering or raising of tidal levels which may

amount to 20-30cm. A moving frontal system which produces a rapidly changing pressure can also change the time of travel of the tidal wave within the estuary.

2.4 Sediments and sediment transport

The present day estuarine deposits mantle a complex sedimentary fill (Fig. 2.6). Present day channels cut deeply into this fill, exposing peats and partially consolidated clays and silts on the channel floor where gravels are normally the only stable deposits. In addition to these sediments are those entering the estuary. Sands are mainly provided by the sea. They migrate into the upper estuary along channels and sand banks (Fig. 2.7) becoming lifted into the water column during peak tidal flow (McManus, 1986b). Fine sediments are derived from the river catchment and well over 90% of the solids are transported in suspension. Silt and clay sized particles become entrapped in the gravitational circulation system and may therefore spend many tides migrating up and down the estuary (McManus, 1986b; McManus and Alizai, 1987).

Models rarely take into account the differing behaviour of sands and fine suspensions as they travel through the constantly changing estuarine system. Instead they are based on steady-state experiments and hence not suitable for the discussion and interpretation of the natural situation (Green, 1975b).

For most sedimentological purposes the Tay Estuary may be divided into distinct sectors (Fig. 2.8):

a) the uppermost, fluviatile sector
b) the upper estuary and
c) the middle estuary divided into upper and lower reaches
d) the lower estuary

(McManus, 1968 and 1972).

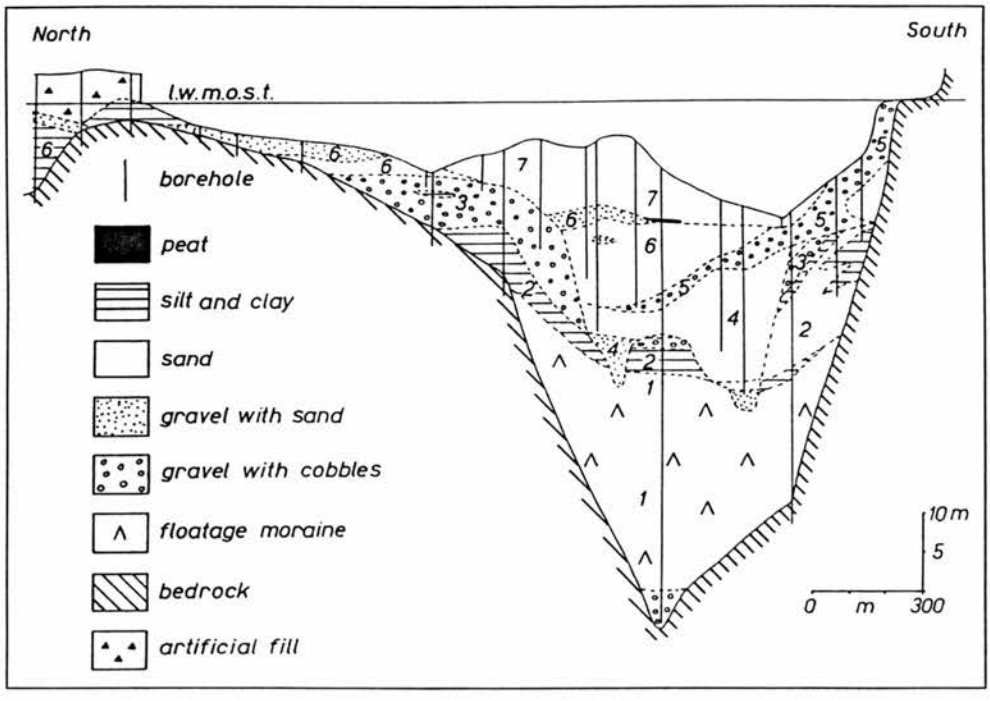

Fig. 2.6: Geological cross-section along the line of the Tay Road Bridge compiled from sparker seismic reflection and borehole records. Note the asymmetry of the buried channel.
l.w.m.o.s.t.=low water mark of spring tides
1: ablation tills (boulder clays) associated with retreating ice; 2, 3: mainly sands and gravels associated with ice readvance (approximately 10,500 years b.p.); 4: pre-Flandrian fill of the first post-glacial estuary (8,500 years b.p.); 5: gravels of Flandrian transgression (6,000 years b.p.); 6: fill of the second estuary culminating with peat (approximately 5,500 years b.p.); 7: modern estuarine sands of the eastern end of Middle Bank (after Duck and McManus, 1989).

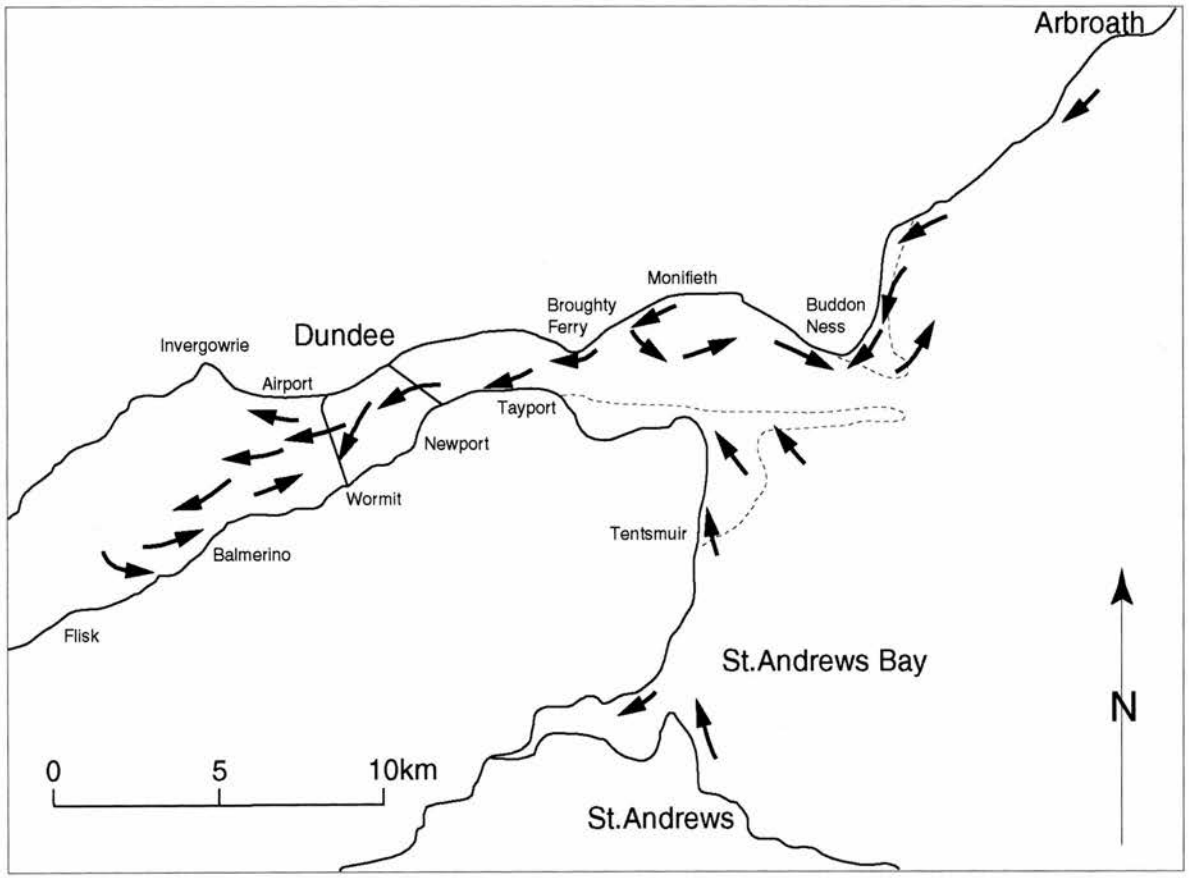

Fig. 2.7: Migration paths of sediment of marine origin (after McManus, 1986b).

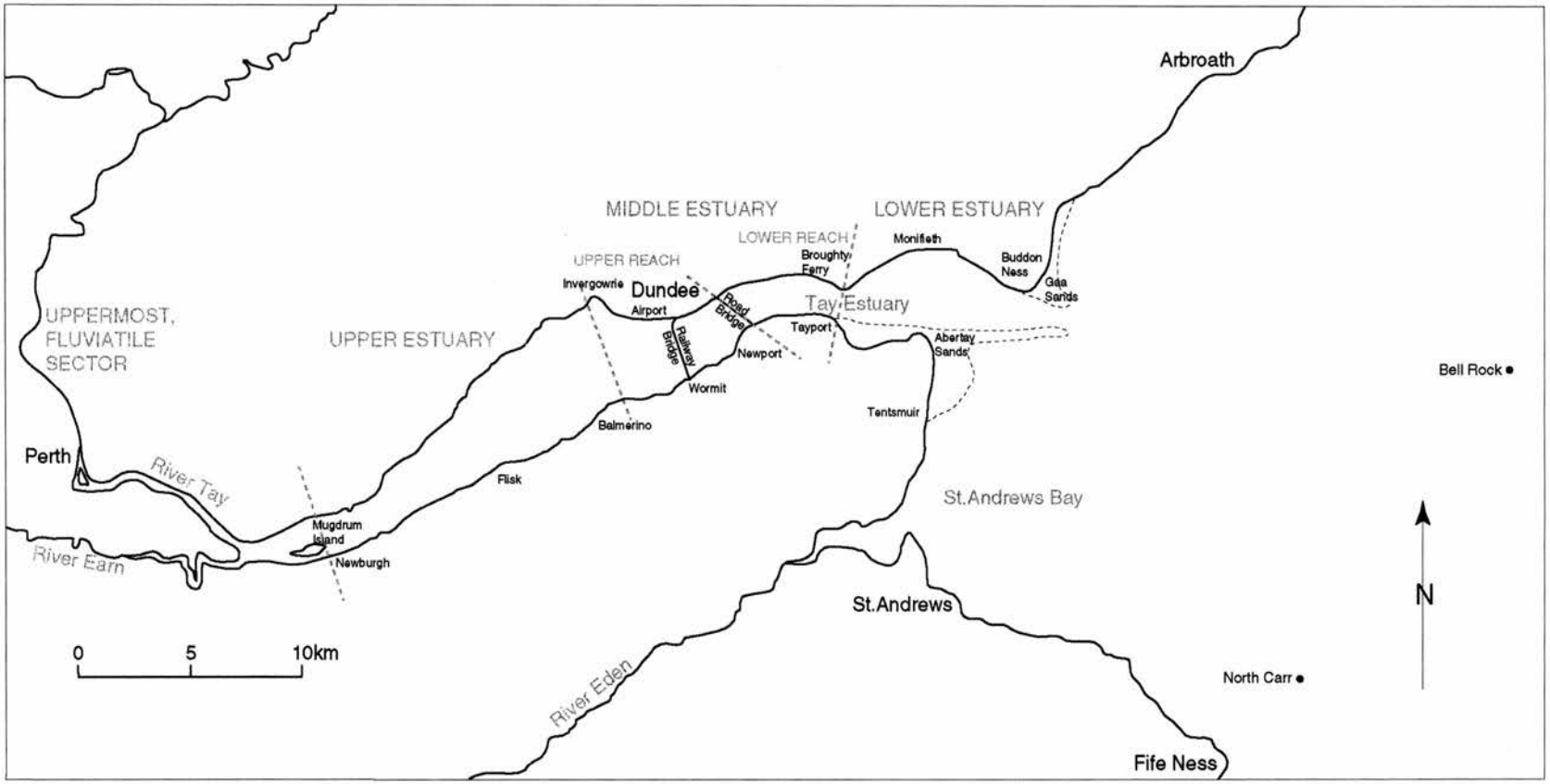

Fig. 2.8: The reaches of the Tay Estuary (after Buller *et al.*, 1971).

2.4.1 The reaches of the Tay Estuary

2.4.1.1 The uppermost, fluviatile sector

Here the Tay is generally an eroding river (McManus, 1966) (Fig. 2.8). The stream bed cuts into silty clays with the aid of pebbles and sand passing seaward. These coarse materials decrease in size downstream (McManus, 1968). Just below Perth the coarse sand and fine gravels form point bars. In the channel and on the banks between Perth and Newburgh solid rocks can be found exclusively on the southern side (McManus, 1966).

2.4.1.2 The upper estuary

The upper estuary extends from Newburgh to Balmerino-Invergowrie (Fig. 2.8). Its northern side is characterised by a classic estuarine succession of marshes at or above high water in front of which are mottled fine silty sands (McManus, 1968 and 1972). The outer margin of the tidal flats rises sharply from the channel, the latter being floored with gravels as well as coarse and medium sands typically showing lower flow regime structures such as dunes and ripples (McManus, 1979 and 1984). The tidal flat surface has a very subdued relief broken by a drainage network of which some channels may retain more than 1m of water at low tide (McManus, 1984).

2.4.1.3 The middle estuary

The upper middle estuary extends from Balmerino-Invergowrie to the Road Bridge (Fig. 2.8). This unstable area is dominated by sand, migrating sand banks, migrating channels and large as well as small-scale ripples. The sands become coarser towards the east with the channel sands being slightly coarser than the sand bank sediments (Buller *et al.*, 1971).

In the reach between the Railway and Road Bridges Middle Bank (Fig. 2.9) embodies the textural, morphological, structural and hydrodynamic features which are typical of all middle estuarine sand banks (Buller *et al.*, 1971). This mobile complex acts as a natural divide between the Queen's Road Channel to the north and the main Navigation Channel to the south (Buller *et al.*, 1971; Williams and West, 1973; Buller and McManus, 1975).

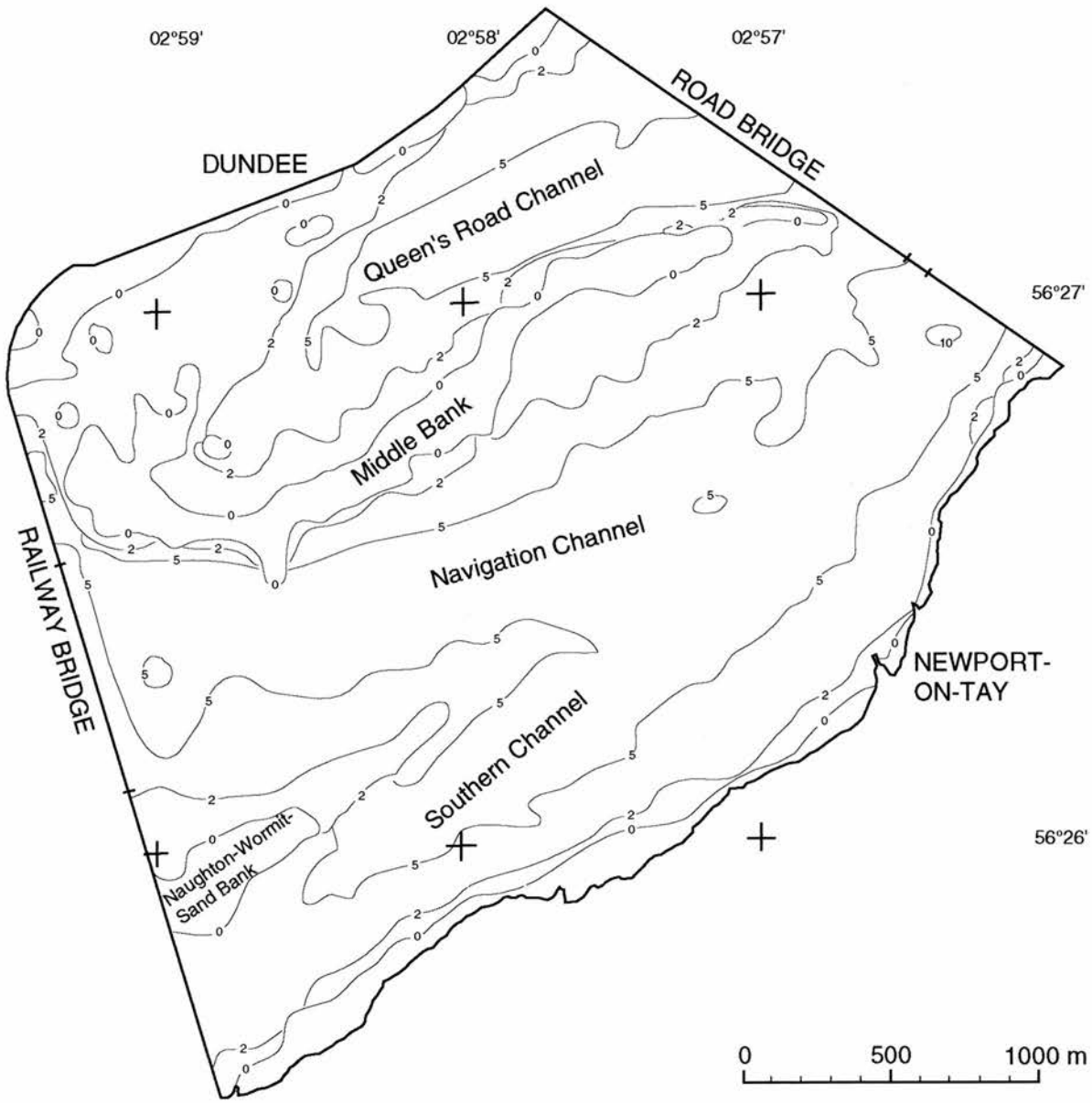

Fig. 2.9: Bathymetry of the reach between the Railway and Road Bridges (after Admiralty, 1994).

Middle Bank is the largest positive feature in this sector being over 1km long and up to 200m wide (Buller *et al.*, 1971). It formerly described a 25-26 year cycle of motion but appears to have stabilised in position since the building of the Road Bridge. Earlier the main bank had been divided into two smaller banks; the western section migrating towards the Railway Bridge where it sub-divided into an irregular group of small banks and shoals while the eastern bank remained static or migrated only slightly towards the Road Bridge. When this dissemination was complete, migration reversed until the main bank was reformed (Buller and McManus, 1971; Buller *et al.*, 1971). Only east-west movements have been recorded in this area, never south-north movements (Buller and McManus, 1971).

Buller *et al.* (1971) give a detailed description of Middle Bank to which the following refers. At highest spring tides the bank is covered by 3m of water. When the bank is fully exposed it consists of four large to very large dunes separated by shallow depressions. The westernmost dune is 50m long, its eastern neighbour 250m, the third dune 250m and the easternmost dune 500m. On and around each of these large to very large dunes are large and small-scale ripples of various geometries, ripple fans, spurs and other sedimentary structures. The seaward flowing ebb currents move parallel to the long axis of the bank. During the first few hours of ebb flow the water surface over the bank is flat or only ruffled by wind-induced waves. Standing waves are formed especially along the northern and eastern margins of the bank by water passing obliquely over the bank into deeper water. As the water shallows and the current speeds increase, the more subtle topographic features of the submerged bank are reflected by surface boils and standing waves. Two alternating large to very large dunes emerge first, one of which is the most westerly described above. Between them the water flows from the south-west to the north-east causing some modification to the large-scale ripples emerging on the lower large to very large dunes. When all four large to very large dunes have surfaced, the shallow depressions in between serve as overspill channels for water on the southern side to move northwards and enter the Queen's Road Channel. The final drainage of the bank is mainly radial although small-scale ripples form perpendicular to large-scale ripple troughs. Buller *et al.* (1971) end their detailed description with an important observation stating that rough weather creates sufficient wave activity to completely plane off all surface features.

White (1992) has carried out detailed work on the morphology of Middle Bank. She generally concludes that the bank is of a longitudinal form within the estuary with dunes, current ripples and catenaries having formed transverse to the flow while bars, runnels and any lineations are parallel. The bank emerges by up to 2m at low spring tides, run-off flow being mostly perpendicular. No exposed areas of Middle Bank are entirely dune free.

The lower middle estuary extends from the Road Bridge to Broughty Ferry-Tayport. In this sector stable large to very large dunes form the Newcombe Shoal situated south of an area showing systematic zonation of sediment away from the channel towards each bank (Buller *et al.*, 1971; McManus, 1972). This channel is dominated by coarse sands which decrease in grain size towards the banks in the south and north. The fastest currents and therefore the coarsest sands occur in the main Navigation Channel. During both ebb and flood flow the Newcombe Shoal is outlined by undulant or hydraulic jump standing waves. Turbulence around this margin is intense and current speeds attained over this feature are comparable with those in the channel (Buller *et al.*, 1971).

2.4.1.4 The lower estuary

The seaward or lower sector of the Tay Estuary (Fig. 2.8) is characterised by marine conditions. Laterally sands mark the northerly Lady Bank off Monifieth from where beaches and backing dunes extend to Buddon Ness (McManus, 1972). Beyond Buddon Ness the entrance channel to the Tay is bordered by the Gaa Sands to the north and by the Abertay Sands to the south (McManus, 1984). The two bar complexes act as a partial barrier protecting the seaward end of the estuary from the severest wave activity of the North Sea (McManus, 1972).

2.4.2 The channels

The channels of the River Tay have cut their beds into relict pebbles, boulders and stiff clays which provide an almost immovable lining (Buller, 1975). The uppermost reaches of the estuary from Perth to Newburgh occupy fluvial channels with limited areas of marsh on either side. This part was artificially deepened in the 19th century and cuts into partially consolidated Late Glacial laminated silts. The channel continues along the

southern shore past Newburgh while a largely natural and partly silted channel curves around the northern side of Mugdrum Island. As far as Balmerino the main Navigation Channel is close to the southern shoreline, then swings northwards and broadens as it approaches the Railway Bridge (McManus, 1984). Beneath the Railway Bridge the subordinate Kingoodie Channel which drains the northern tidal flats flows into the main Navigation Channel. The dunes in the Kingoodie Channel are flood oriented and therefore indicate derivation of sediment from the sea (Buller and McManus, 1975). In the middle reaches the single channel is replaced by three separate channels - Queen' s Road, main Navigation Channel and Southern Channel - with intervening sand banks, the largest being Middle Bank (Dobereiner and McManus, 1983). In this sector the estuary is constricted by the outcrop of lava on the southern shore and the largely artificial waterfront of Dundee. The latter includes the reclaimed land on which the Riverside Airport, playing fields, the landfall of the Railway Bridge and a series of docks and industrial sites are built (McManus, 1984). East of the Road Bridge a single channel exists.

Channel bottom sediment types vary considerably. In the uppermost fluviatile sector the bed is lined mainly with boulders and pebbles (McManus, 1972) which decrease in size downstream (McManus, 1968). In the upper estuary the main Navigation Channel is floored with coarser sands which migrate seawards along the channel bed. The middle estuary is characterised by unstable bedforms (McManus, 1972). Here the channel sediments are again contrasted by the balance between erosion and deposition. The general pattern of these sediments is controlled by the distribution of current speeds. Hence the faster flowing channel waters deposit only coarse sand which is superseded northwards and southwards by decreasing particle sizes as the water shallows and current speeds lessen (Buller, 1975). The main Navigation Channel at the Railway Bridge is migratory (Fig. 2.10). Since the construction of the bridge the water depth has steadily increased. In the central area, beneath the navigation spans, the bed is cut into thick silty sands which are particularly susceptible to erosion and transport, the result being no restriction upon bed movement. During the construction of the Railway Bridge, the main Navigation Channel passed beneath the bridge's central high girders. In subsequent years the channel migrated to the south, then recovered to its central position and continued to move north of the navigation spans. In the late 1950s and early 1960s the channel stabilised itself and lowered

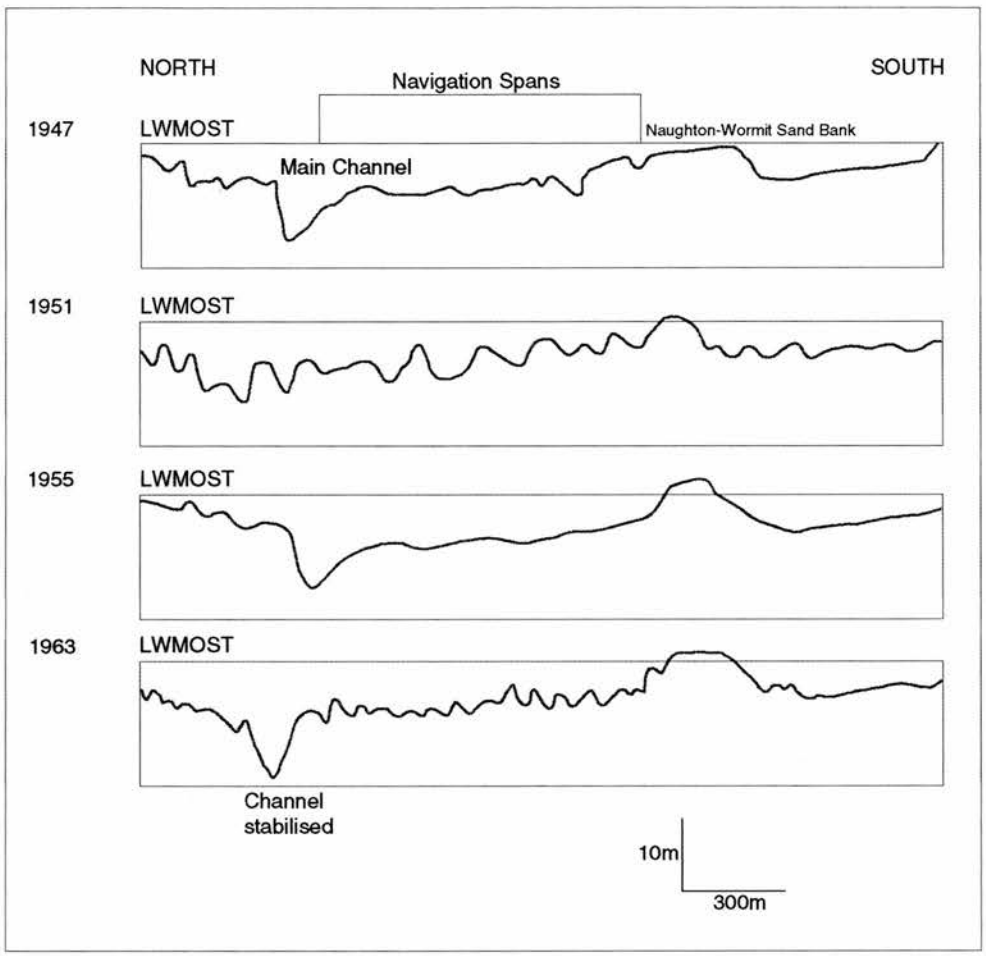

Fig. 2.10: Bathymetric cross-sections along the Railway Bridge showing the northerly migration, deepening and final stabilisation of the Main Channel (after Buller and McManus, 1971).

the bed from previous mean depths between 9.0-10.5m to over 15.0m below watermark of spring tides. By 1971 this deeply eroded cut had been partly filled by present-day mobile very fine sands (Buller and McManus, 1971). At the Railway Bridge the waters in the main Navigation Channel were, in 1983, only 8m deep at low water while in the lower estuary between Broughty Ferry and Tayport they were still over 25m deep (Dobereiner and McManus, 1983).

Mussel beds as indicators of an obvious marine influence can be found as far west as the Queen's Road Channel as well as in the main Navigation Channel towards the Road Bridge (Buller *et al.*, 1971). Further east the lower estuary is fully characterised by marine conditions including beaches along the shoreline (McManus, 1968) and a relatively stable channel (McManus, 1972).

The dunes and ripples in the channels of the Tay Estuary show asymmetrical crestal orientations. This is linked to the flow patterns associated with individual flood and ebb dominant channels and sections of single channels (Buller *et al.*, 1975). The dunes lining the channels can move up to 0.3m/hr. Some reverse migration direction with tidal phase but those dunes which are 3m or higher retain their dominant ebb or flood orientation (McManus, 1986b).

2.4.3 Sediment sources and transport

The establishment of a detailed sediment budget for the Tay Estuary must address river, marine and marginal inputs (McManus, 1986b). Materials entering the estuary are transported by moving waters as bed load, in suspension or in solution (Al-Jabbari *et al.*, 1980). Bed load grains are transported close to the bed by rolling or saltation. The suspended load grains are transported by the flow and the forces of turbulence in random paths within the main body of flow (Buller *et al.*, 1975). An important statement is made by McManus (1986b) in saying that the water circulation patterns and the sedimentation processes make it difficult for sediment to escape seawards. Therefore research ongoing around 1986 concentrated on the internal circulation of the estuary.

2.4.3.1 Fluvial input

The sediment load carried downstream depends upon the river discharge which varies considerably from year to year and from season to season (McManus, 1986a). During floods, coarse material is transported while during calmer conditions only finer particles are mobile, buoyed up by local turbulent eddies in the water column (Al-Jabbari *et al.*, 1980). The main tributaries of the Tay Estuary are the Rivers Tay and Earn. The River Tay flows through many lochs of its drainage basin and it is believed that this largely removes the coarse fraction of the original fluvial load (Al-Dabbas and McManus, 1987).

Quantities of river derived sediments have been estimated by direct and indirect methods. Direct methods included the use of VUV traps to estimate bed loads. They have a 70% trap efficiency but are, according to Al-Jabbari *et al.* (1980), unreliable in the Tay due to the irregular gravelly and boulder strewn beds. Estimation of solute concentration was undertaken by means of a conductivity bridge and suspension concentrations using a siltmeter. The indirect methods estimate sediment discharge through rating and flow duration curves. McManus (1986b) gives estimates for the total solids load in an average year using the above mentioned instruments: 1,056,000t of which 30,000-50,000t is sand and pebbles transported as bed load, suspension load comprises between 25-40% of organic matter (around 250,000t) like solid organic debris, soils, peats, plants or living organisms. In dry years the total solids load can decrease to 600,000t of which 18,000t is carried as bed load.

Buller *et al.* (1975) discuss the fluvial sediment input and state that the River Tay supplies most of the suspended load into the estuary while the River Earn supplies most of the bed load material. Al-Ansari and McManus (1979) investigated the sediment discharge from the River Earn. Their direct determination showed that in an average year 180,000t of solids enter the estuary of which less than 3% travels as bed load and nearly 80% is moved during the four winter months. They concluded that no indirect method of load estimation yield result came close to those obtained by direct measurement.

2.4.3.2 Marine input

The only study of marine sediment input is that of Al-Dabbas and McManus (1987). They state that the rate of lateral growth of sand dominant deposits indicated by charting is greater than the supply of fluvially derived sand. Since there is almost no fresh sediment input derived from erosion of estuarine cliffs and also only limited redistribution of earlier bed sediments, a marine source of sand must be involved. Al-Dabbas and McManus (1987) used shell fragments as indicators of bed sediment transport into the Tay Estuary. Their results point to a migration of sediment into the estuary from the sea with transport on to the tidal flats of the upper estuary prior to deposition. This is a pattern observed by many researchers worldwide (Meade, 1969).

2.4.3.3 Marginal input

Marginal input does not play a major part in the Tay because the amount of material eroded from shorelines is small. Broad tidal flats along the northern coast signify that accretion dominates and elsewhere cliffs, mainly composed of andesitic lavas, as well as the artificial waterfront of Dundee are not susceptible to erosion (Al-Jabbari *et al.*, 1980).

2.4.3.4 Suspended sediment and turbidity maximum

As mentioned earlier, material entering the estuary is transported by moving waters as bed load, in suspension or in solution (Al-Jabbari *et al.*, 1980). Estuaries contain higher suspended sediment concentrations than river and sea waters (Dobereiner and McManus, 1983). The suspended sediment load refers to the product of suspended sediment concentration and current speed, defining suspended sediment as the dry weight to volume concentration of suspended particles with individual diameters greater than 0.45μm (Buller, 1975). The zone containing enhanced levels of suspension concentration is often termed the "turbidity maximum" (Dobereiner and McManus, 1983) although Buller (1975) prefers the term "zones of high suspended sediment concentration". Waters of increased turbidity occur in the reaches where fresh and salt waters meet, where the salinity gradients are greatest. This zone varies in position not only with neap or spring tidal cycles but also in response to river runoff, nevertheless the turbidity maximum zone remains within the estuary under

all conditions. At low tide during high river flows (370m³/s on an average 5.0m spring tide) the concentration peak is situated between the bridges but moves landward as the river discharge decreases (Dobereiner and McManus, 1983).

Suspended sediments are carried during floods as well as during low discharge conditions with varying concentrations depending on freshwater discharge (Al-Jabbari *et al.*, 1980). Dobereiner and McManus (1983) measured maximum suspension concentrations on the ebb phases of neap tides and on spring flood tides. Buller (1975) states that the volume of water and its areal coverage on high spring tides ensures that, during ebb flow, water is charged with high concentrations of suspended sediment and directed from the tidal flats into the surface and mid-depth waters of the main Navigation Channel. While the upper estuarine waters are still ebbing, the tide already floods from the sea acting as an effective barrier for further seaward motion hence resulting in the cumulative formation of a zone of high suspended sediment concentration. As the flood tide becomes fully established the zone is diluted and dispersed. According to Buller (1975) the highest series of concentrations, and the appearance of a major zone of high suspended sediment concentrations, occurs throughout the entire estuary at about three hours before low water. During neap tides a smaller area is covered at high water, uncovered at low water and the current speeds are much lower so that the quantities of transported suspended sediment are also lower. The suspended sediment laden waters draining from the eastern catchment of Invergowrie Bay flow through Kingoodie Channel and do not join the main Navigation Channel until they reach the area between the bridges. However, Weir and McManus (1987) have found that the zones of high suspended sediment concentrations vary in position and intensity and established a systematic correlation with wind speed and direction. Generally these authors found turbidity maxima west of the Tay Railway Bridge.

As freshwater enters brackish estuarial reaches some of the soluble matter becomes precipitated and some of the material, principally clay minerals, flocculates resulting in deposition (Al-Jabbari *et al.*, 1980). It is believed that, as the salt content of the water rises, the increased electrolyte concentrations enhance interparticulate attractions which promotes flocculation (McManus, 1979; Dobereiner and McManus, 1983).

Where suspension concentrations are increased, the high numbers of particles present cause an increased probability of interparticle collisions which results in the growth of aggregates (Dobereiner and McManus, 1983). The greatest aggregate diameters measured by Dobereiner and McManus (1983) have been found towards the seaward end of the turbid waters. They suggest that the growth of aggregate size is linked with salinity and pH since all three increase in concentration or value in the same area. This hypothesis has not yet been confirmed within the Tay Estuary but conforms to patterns observed in other estuaries (Dyer, 1986).

2.4.4 Charting of migratory areas

Historically, migratory areas can be determined from pre-existing bathymetric charts (Buller and McManus, 1971) while nowadays this is often monitored by means of remote sensing. Cracknell *et al.* (1982) and McMillan (1983) studied the sand bank and sediment dynamics in the Tay Estuary using Landsat Multispectral Scanner data (MSS). The images had to be processed to achieve comparability with scenes of different times/dates as well as with the Ordnance Survey maps and Admiralty Charts. The main problem encountered for mapping sand banks was the need for low tide imagery which fortunately was available. After suitable processing the Landsat data produced sand bank maps which compared favourably with the Ordnance Survey maps and Admiralty Charts. The method therefore provides a quick method of updating maps. Anderson (1989) applied different remotely sensed data. He used the Daedalus Airborne Thematic Mapper (AADS) 1268 which gives a higher resolution, is therefore more accurate, and could be used for updating maps.

Chapter 3

SURVEYING EQUIPMENT

3.1 Introduction

The problems of locating objects underwater have intrigued and challenged investigators for generations (Yules and Edgerton, 1964). Since light and radar waves are too easily attenuated within the water column, sound is the only useful medium in the sea for obtaining information over distances or rather depths (Stride, 1961). This acoustic equipment is called sonar which stands for SOund Navigation And Ranging. Further details at close range can then be obtained by divers, a television device or camera or by sediment sampling (Chesterman *et al.*, 1958; Williams, 1982). Several methods for surveying a relatively large area of the sea floor in a short time are available and the selection of a particular technique mainly depends on the type of survey. Parameters like water depth, manoeuverability of the vessel and type of submarine terrain have to be taken into account. Even relatively simple sonar systems can yield a tremendous amount of information on the sea bed if systematically employed or as part of a succession of techniques. Acoustic remote sensing of the sea floor includes bathymetric surveying (echo-sounding), which provides quantitative information of the water depth and usually forms a basis for other kinds of marine survey; acoustic imaging (side-scan sonar) is most often used in a qualitative sense to determine the geomorphology of the bed and to detect obstacles; and sub-bottom profiling which is related to the physical properties of the substrate and involves the detection of sub-surface reflectors (Moustier and Matsumoto, 1993). All three geophysical survey techniques provide a rapid means for assessing the major geological and sedimentological characteristics of an area (Sly, 1981). Since the latter is not relevant to this project it will not be discussed further.

Even though there have been continuous improvements in acoustic equipment and techniques since their introduction during World War I, most of the basic principles have remained the same. The main emphasis is still on accurate position fixing and calibration of the seismic record from known ground information. Major advances have been in the increased sophistication of the surveying equipment, with improved

resolution and reliability, and the associated signal processing and recording facilities. The survey results are still subject to the same constraints imposed by water depth, sea state and the weather as well as the human operator (Dobinson and McCann, 1990). In the near-shore environment the major difficulty is the shallow water depth since it limits the size of the survey vessel. The sea state and the weather are of great importance in any marine survey since they can prevent the successful operation of geophysical equipment being towed behind the survey vessel as well as increasing the ambient, background seismic noise levels.

3.2 Basic principles of acoustic surveying techniques

All seismic reflection systems function in a similar way. They consist of three basic components:

1) an energy source or transducer that emits acoustic pulses at specific power and frequency levels
2) one or more receivers that pick up the transmitted acoustical "echoes" after they are reflected back from the seabed
3) a recording instrument that converts the reflected acoustical signals to electrical signals which, in turn, are converted into a more permanent record (Williams, 1982).

These geophysical remote sensing techniques do not provide a direct measurement of distance but measure the two-way travel time of a pulse of acoustic energy from a vessel to the sea bed and back, and convert this to water depth (Hooper, 1979). This two-way travel time (t) is related to the depth (d) by the equation:

$$d = \frac{1}{2}vt \qquad (1)$$

after McQuillin and Ardus (1977)

where v is the velocity of sound in the transmitting medium. The velocity is dependent on the temperature, salinity and pressure of the medium (Fig. 3.1). In sea water the velocity increases approximately 4.5m/s per 1°C increase in temperature, 1.3m/s per 1‰ increase in salinity and 1.7m/s per 100m increase in depth. The velocity is usually between 1470 and 1540m/s and for approximate calculations the value of 1500m/s is accepted (Ingham, 1975). Empirical formulae have been developed for the calculation of the velocity of sound in water but it should be

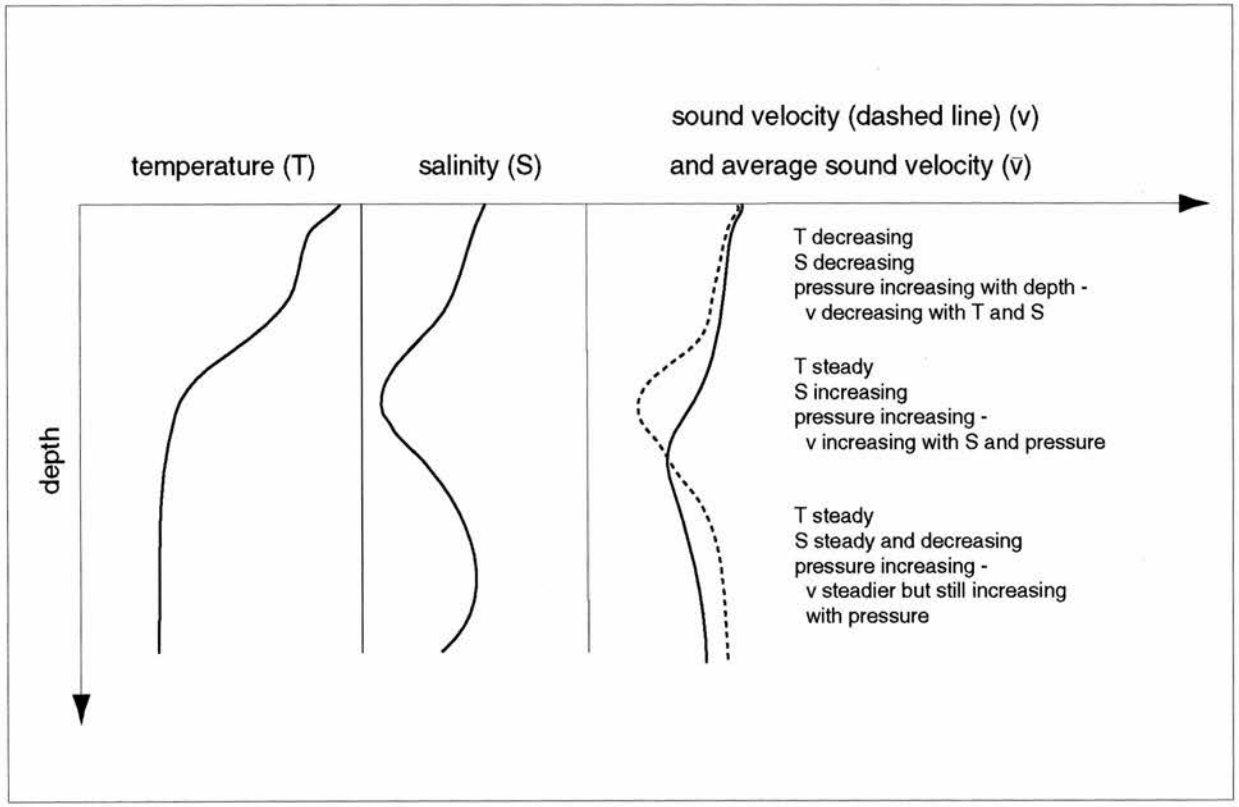

Fig. 3.1: Typical curves for temperature, salinity, sound velocity and average sound velocity against depth (after Ingham, 1975).

remembered that the value required for the calibration of sonar instruments is the average velocity between source and target.

A transducer generates acoustic energy which is propagated through the water. With increasing distance from the source more energy will be attenuated. When the acoustic wave reaches a target, parts of the wave will be reflected and others refracted. Some of the reflected wave will, after further attenuation, reach the receiver as an "echo". The strength of this echo depends on the power of the original transmission as well as its propagation through the medium and its reflection from the target. Most pulses of acoustic energy are generated electrically and have a similar frequency and wave form to the electrical pulse. On the way to a reflector, such as the sea bed, the acoustic energy may be partially reflected at a boundary between layers of contrasting acoustic impedance (Z) where

$$Z = \rho \cdot v \qquad (2)$$

after Beer (1983)

the product of water density (ρ) and seismic velocity (v). Both ρ and v depend on temperature and salinity. In a partially mixed estuary the upper, freshwater layer would have a higher acoustic impedance than the lower layer of salt water (see Example 3.1). If the impedance contrast between two layers is high, a high proportion of the transmitted energy will be reflected which results in a strong return signal shown in dark tones on the sonograph.

Example 3.1:

density of upper layer:	1.01 x 10^3kg/m^3
density of lower layer:	1.02 x 10^3kg/m^3
speed of sound in upper layer:	1495m/s
speed of sound in lower layer:	1525m/s
acoustic impedance in upper layer:	1.510 x 10^6kg/m^{2}s
acoustic impedance in lower layer:	1.555 x 10^6kg/m^{2}s

The direct incidence reflection at a boundary between layers of contrasting Z is expressed in terms of the reflection coefficient (C_r):

$$C_r = \textit{pressure reflected/pressure incident} \qquad (3)$$

or, in the case of the example of the partially mixed estuary,

$$C_r = \frac{Z_{salt} - Z_{fresh}}{Z_{salt} + Z_{fresh}}$$

after Beer (1983).

In the example this would lead to a reflection coefficient of 0.015 which can also be related to the effective target strength (*TS*) expressed as:

$$TS = 20 log_{10} C_r \qquad (4)$$

after Beer (1983)

and is used as another term to quantify the level of reflection. Although acoustic pulses are less easily attenuated in water than light or radar waves, the viscosity of water still has a frictional effect on sound waves. Their energy is dissipated by the viscosity and converted into heat. The lost energy of an acoustic pulse is expressed as the absorption coefficient (α) which is quoted in decibels (dB) per wavelength (λ):

$$\alpha = \frac{27.3}{E_t / E_d} \qquad (5)$$

after McQuillin and Ardus (1977)

where E_t is the transmitted energy and E_d the dissipated energy. The viscous effects are greater at higher frequencies resulting in higher attenuation but decrease as the temperature rises. A summary of the characteristics of acoustic wave propagation is shown in Figure 3.2.

The wavelength (λ) is the length of a cycle expressed in distance units and is related to the frequency (f) which is the number of cycles repeated during one second of time, measured in Hz, as follows:

$$v = f\lambda \qquad (6)$$

after Hobbs *et al.* (1981).

Thus, according to equations (5) and (6), if one wave of low frequency and one of high frequency were to be transmitted through the same medium at the same speed and the same absorption (α), the higher frequency wave would be more easily attenuated than the lower over the same distance (see Example 3.2, Table 3.1 and Figure 3.3).

Example 3.2:

if v=1500m/s and α=0.5dB/λ

then

a frequency of 10Hz would have a wavelength of λ=150m

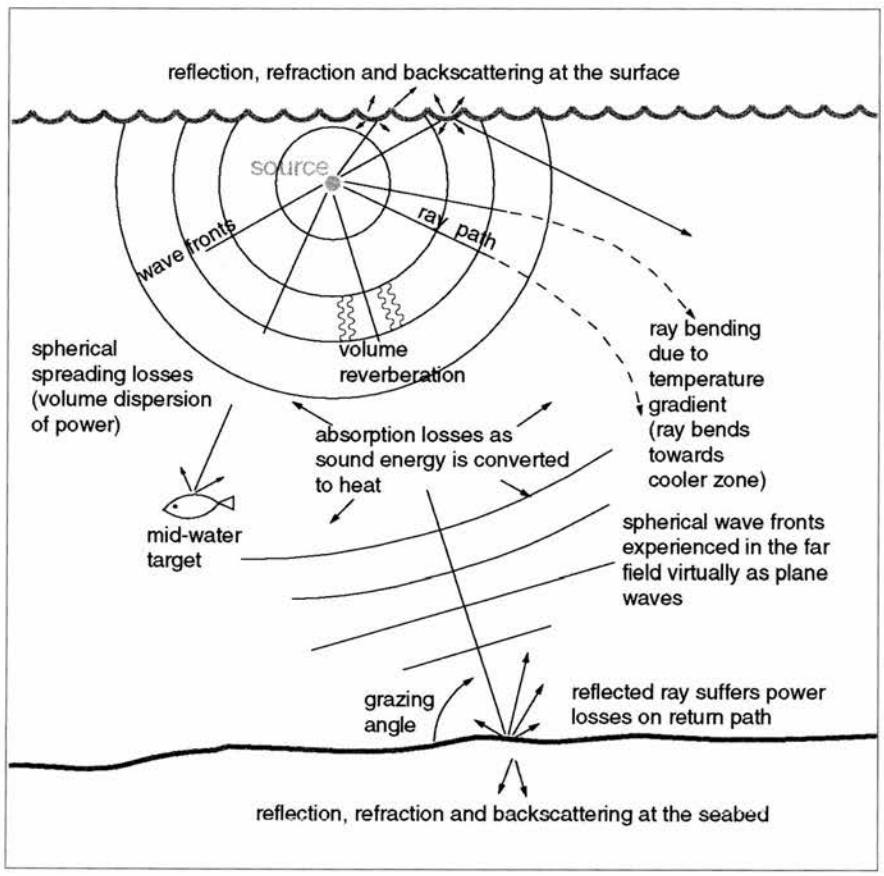

Fig. 3.2: A summary of the characteristics of acoustic wave propagation (after Ingham, 1975).

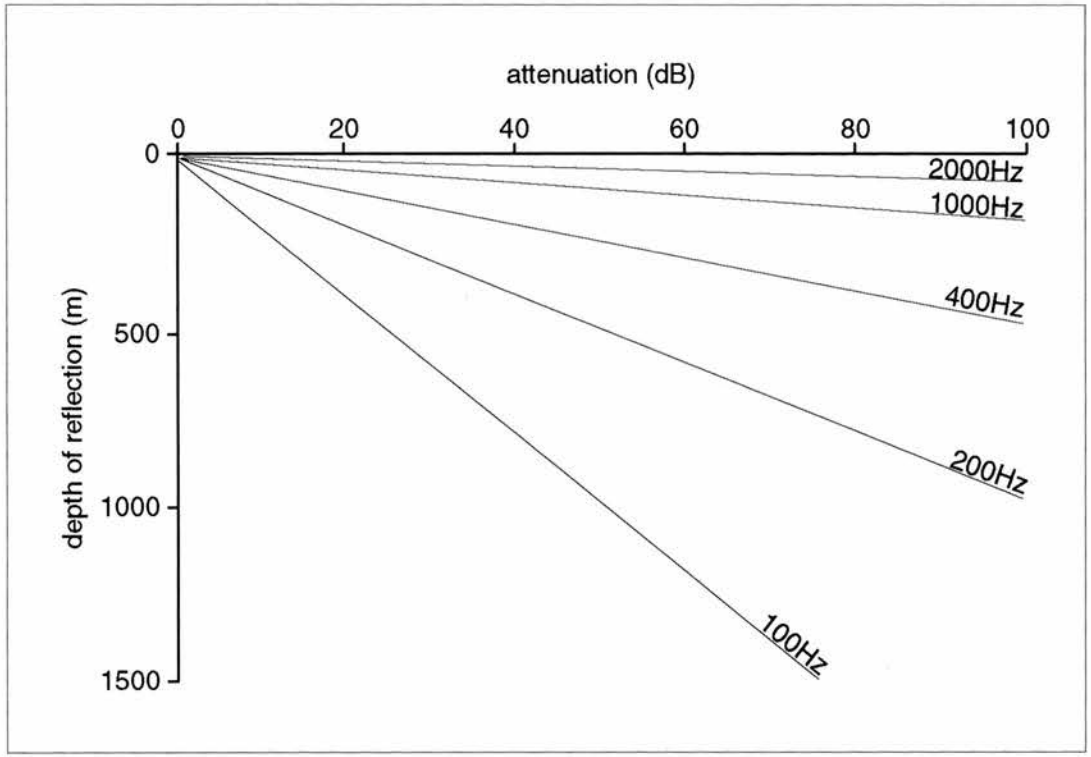

Fig. 3.3: Attenuation of seismic waves for an absorption of 0.5dB per wavelength plotted as the effect of absorption on the amplitude of a sound wave reflected at a range of depths 0-1500m (after McQuillin and Ardus, 1977).

and

a frequency of 100Hz would have a wavelength of λ=15m

therefore

the 10Hz wave would be attenuated due to absorption by 0.5dB over 150m

while

the 100Hz wave would be attenuated by 5dB over the same distance

Table 3.1: Approximate two-way working ranges of modern active sonar systems (Fish and Carr, 1990).

Frequency	Wavelength	Distance
100 Hz	15 m	1000 km or more
1 kHz	1.5 m	100 km or more
10 kHz	15 cm	10 km
25 kHz	6 cm	3 km
50 kHz	3 cm	1 km
100 kHz	1.5 cm	600 m
500 kHz	3 mm	150 m
1 MHz	1.5 mm	50 m

This relationship between frequency and attenuation has important implications since the decibel scale is a logarithmic scale such that an attenuation of

$$1\text{dB} = 20\log_{10}\frac{A_a}{A_o} \qquad (7)$$

after McQuillin and Ardus (1977)

where A_a is the attenuated amplitude and A_o is the original amplitude. Thus an attenuation of 20dB is equivalent to a reduction in amplitude of a seismic wave to one tenth of its original value, a 40dB attenuation is a reduction to one hundredth and a 60dB attenuation to one thousandth.

3.2.1 Echo-sounder

The most elementary and most widely used sonar search technique is the vertical beam sonar (Yules and Edgerton, 1964) usually called the echo-sounder. It measures the time interval between transmission of an

outgoing pulse and detection of the reflected sea bed return, which is converted into water depth, and gives a display of the sea bed profile. Depth measurements have to be corrected for tidal effects as well as adjusted to a datum reference such as O.D. (Newlyn) (Dobinson and McCann, 1990) (Fig. 3.4). Because the vertical beam configuration yields information only about that area of the bottom directly beneath the vessel this technique has restricted applications. The depth accuracy depends mainly on the sea state but is usually better than 0.1m.

3.2.1.1 Basic components

All echo-sounders consist of the following basic components (Fig. 3.5):

a) pulse generator - to provide electrical power
b) switching unit - to pass this power to the transducer
c) transmitting transducer - to convert the electrical power to acoustical power and project the acoustical power into the sea water medium
d) receiving transducer - to receive reflected sound power and convert it into electrical signals
e) receiving amplifier - to step up the amplitude of very weak echoes to enable them to activate the recording system
f) recorder - which usually controls the emission of electrical energy to the transducers, times the interval between transmission and reception of the acoustic pulse, converts the time interval to range and presents the resulting data

(Ingham, 1975).

The "picture" seen on an echo-sounder record is built up by a series of sweeps of a stylus across recording (electro-sensitive) paper. The recorder motor drives the stylus belt and the paper drive rollers, thereby providing the two axes of depth and ship travel for the sea bed profile. The forward movement is represented by the movement of the paper trace. The stylus moves from top to bottom with each outgoing acoustic pulse and represents the depth measurement by marking the trace at the instant of transmission and at the receipt of the returned echo. The speed of the stylus movement has to be synchronised with the vessel's speed and calibrated for the approximate velocity of sound in water (see Section 3.2). Many modern forms of echo-sounders use video displays which have the disadvantage of not giving a permanent record unless

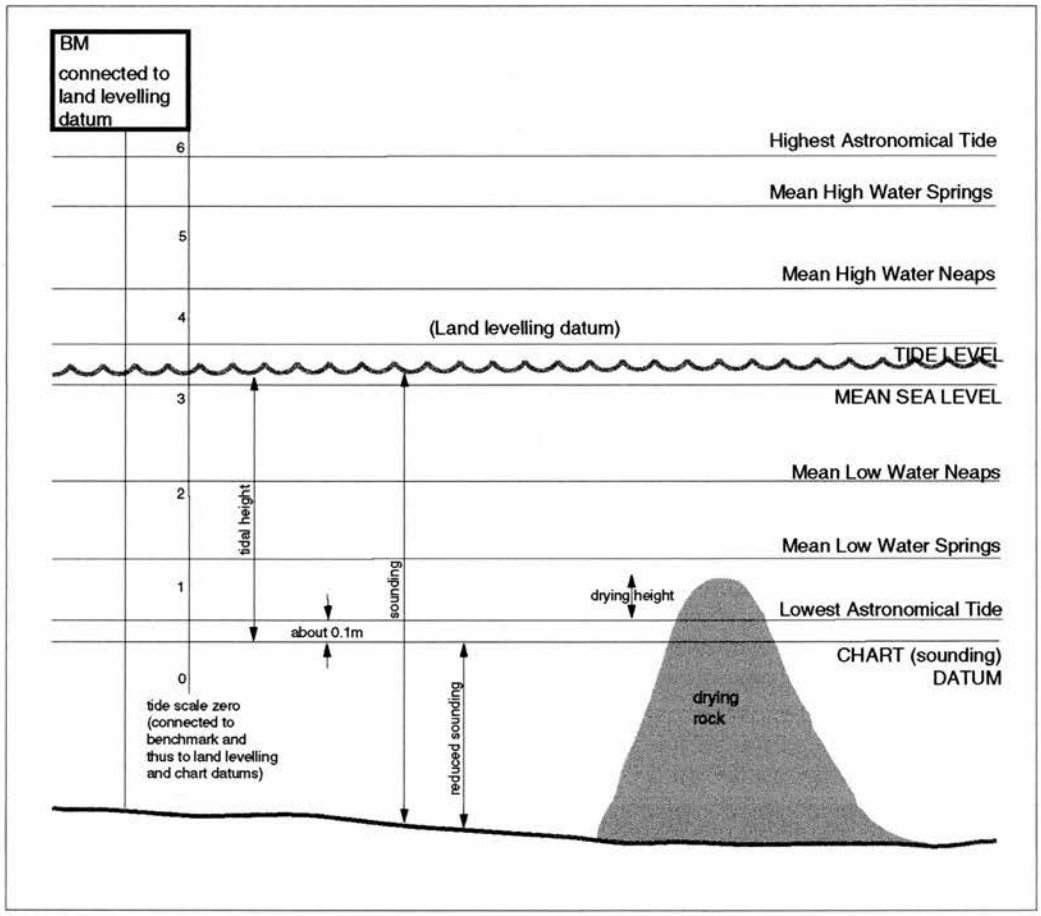

Fig. 3.4: Tidal levels and datum (after Ingham, 1975).

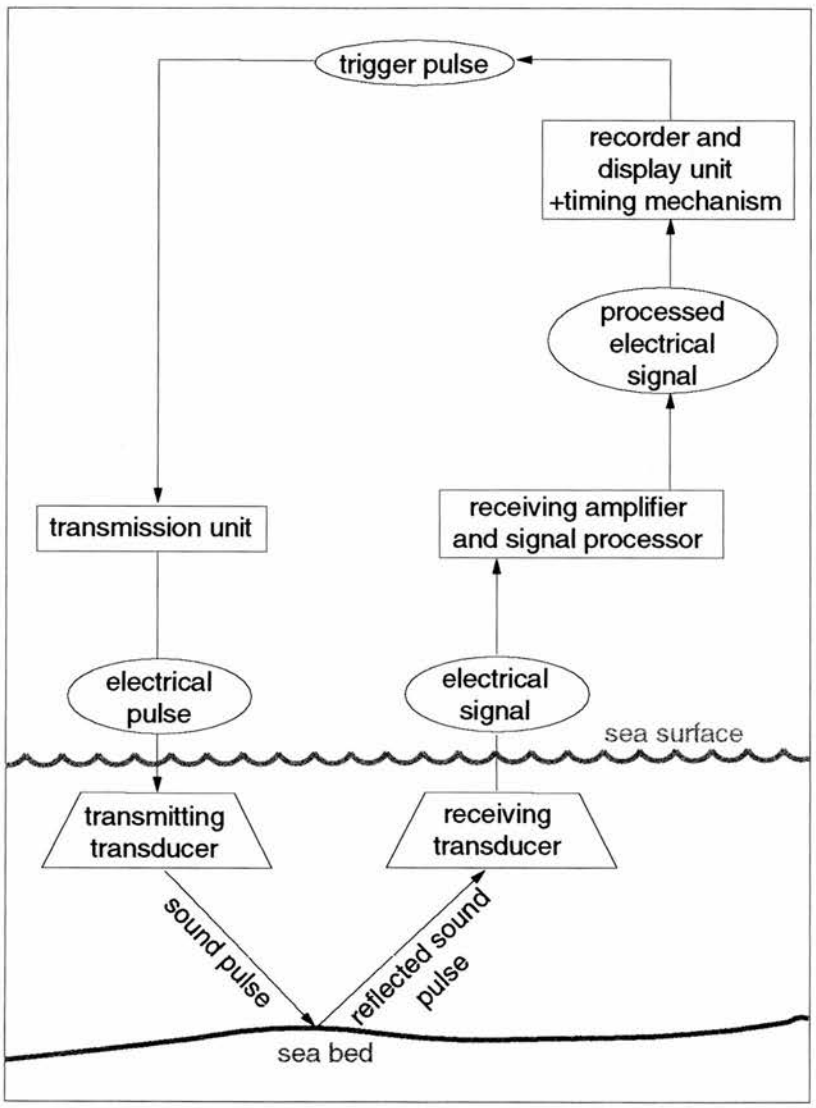

Fig. 3.5: Block diagram showing the main components of an echo-sounder (after McQuillin and Ardus, 1977).

they record the data digitally and offer a play-back facility. The record on dry paper is produced by burning away the surface of the paper to expose black graphite beneath as the stylus current passes through the paper. The width of a paper record is naturally limited and the range of scales offered are confined within these dimensions so that the paper width might represent a depth range from 10m to 1000m (Ingham, 1975). The continuous paper record is periodically marked with lines relating to the ship's position fixes, recorded simultaneously in order to determine the relationship between the ship's position and the echo-sounding record (McQuillin and Ardus, 1977).

3.2.1.2 Calibration

A survey echo-sounder should be calibrated at least at the beginning and/or end of survey operations. This is usually done by employing the "bar check". An iron bar is lowered successively in steps of 1m beneath the transducer suspended from two lines (Fig. 3.6). The corresponding depths are recorded and read off from the paper record. If any errors occur, the stylus speed and the zero settings can be adjusted to eliminate them. This should also include the velocity settings depending on the survey environment since the speed of sound varies in salt and freshwater. In a tidal environment the recorded depth will vary according to the height of the tide at the time. Therefore, all depths must be reduced to a constant datum level which involves the recording of tidal level readings throughout the survey and adding or subtracting the adjustments as appropriate before plotting the measured depths (Hooper, 1979).

3.2.1.3 Factors affecting the record

There are some factors which should be considered when interpreting echo-sounder records. Most of these are associated with fake echoes. Because the beam of the echo-sounder spreads out as a cone, the most direct sound path to the bed may not be vertically under the transducer. This may cause errors when looking specifically at the roughness or slope of the bed although it will result in the recording of the minimum depth (Fig. 3.7). In rough weather conditions ship motion due to the wind and waves also cause errors in depth recordings (Fig. 3.8). Air bubbles in the water, fish with gas-filled swim bladders and seaweed with gas-filled

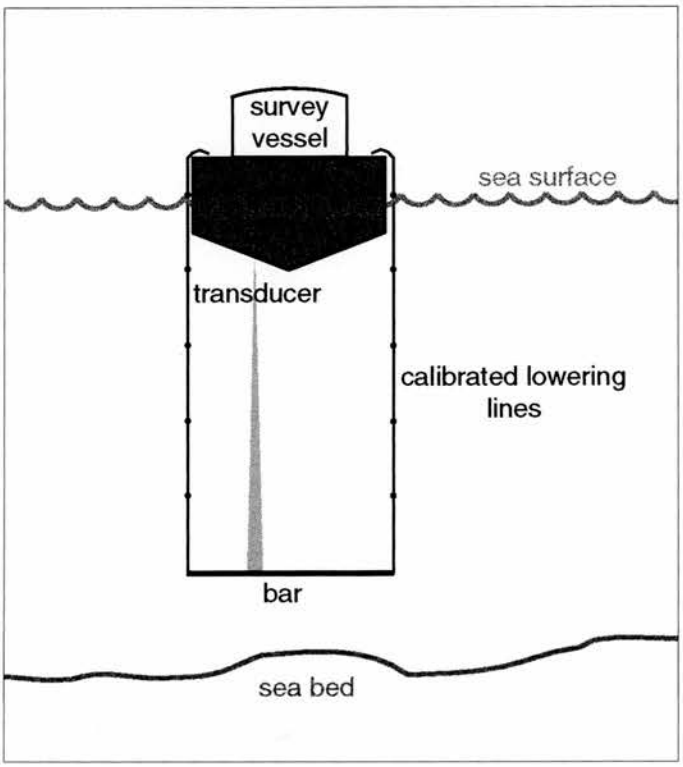

Fig. 3.6: Bar check for bottom-mounted transducers (after Hooper, 1979).

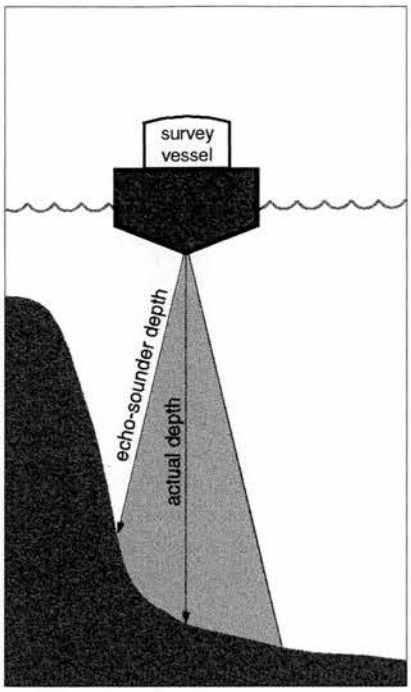

Fig. 3.7: Echo-sounder depth error resulting from a side echo (after Hobbs, 1981).

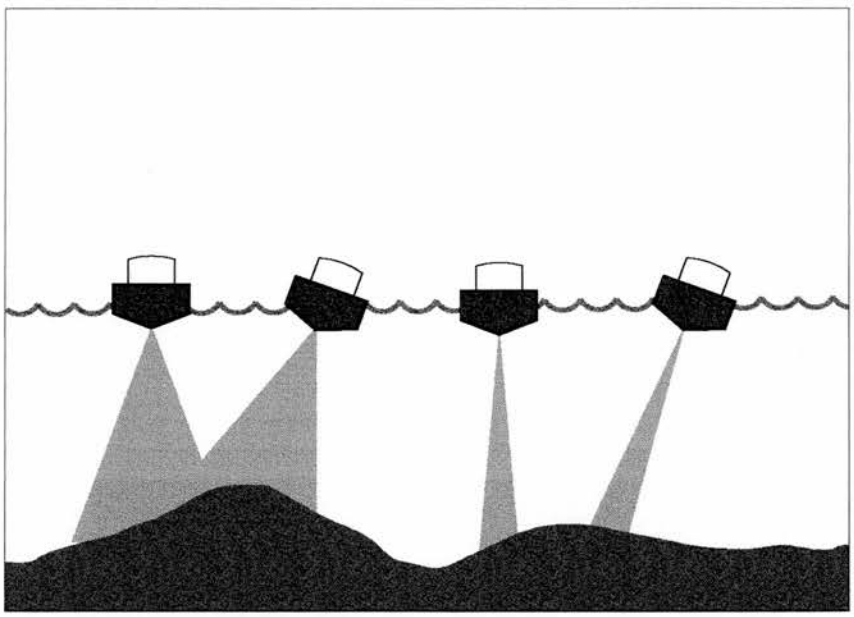

Fig. 3.8: Echo-sounder depth errors resulting from ship motion (after Hobbs, 1981).

bladders cause the reflection of the acoustic pulse and the seabed return is lost. Sometimes "ghost echoes" above the seabed can be observed. These are usually produced by layers of fluid mud or other high concentrations of suspended sediment (Hooper, 1979), but can only be detected when high frequency transducers are used since low frequencies penetrate through these layers and are only reflected by higher density substrates.

3.2.1.4 Applications of echo-sounding

Vertical beam sonar is most useful for simple bathymetric surveys as well as in some special applications when the position of an object of interest has been located by another technique, like side-scan sonar, and the elevation of the object above the bottom as well as the size has to be determined (Yules and Edgerton, 1964). This can include measurements of sand waves, dunes and ripples where best results are achieved by running transverse to the crestal orientations. Sand waves produced in predominant tidal flows have crests which extend across the direction of flow so that transverse sounding lines might easily miss the deepest or shallowest parts of the bedforms and the characteristic wave-shape might escape identification from the contoured soundings (Ingham, 1975). These restricted limitations of the echo-sounder are overcome by the side-scan sonar technique which can cover a large area in a short time.

3.2.1.5 Lowrance X-16 echo-sounder

The vertical beam sonar employed in this study was the Lowrance X-16 echo-sounder (Plate 3.1). It operates at a frequency of 192kHz (192,000 cycles per second) and its depth accuracy is within 0.6%. Like most echo-sounders, this instrument transmits and receives acoustic pulses from a single transducer - the LHT-108A which was mounted in the hull of the R.V.Mya (Plate 3.2) based at the Tay Estuary Research Centre (TERC) at Newport-on-Tay. The transducer emits an acoustic pulse vertically downwards with an 8° cone angle. The size of the insonified circular area of the sea bed depends on the water depth and increases accordingly. The circular area of reflection is called the Fresnel zone (ω) and depends on the frequency (f) of the source pulse (described in

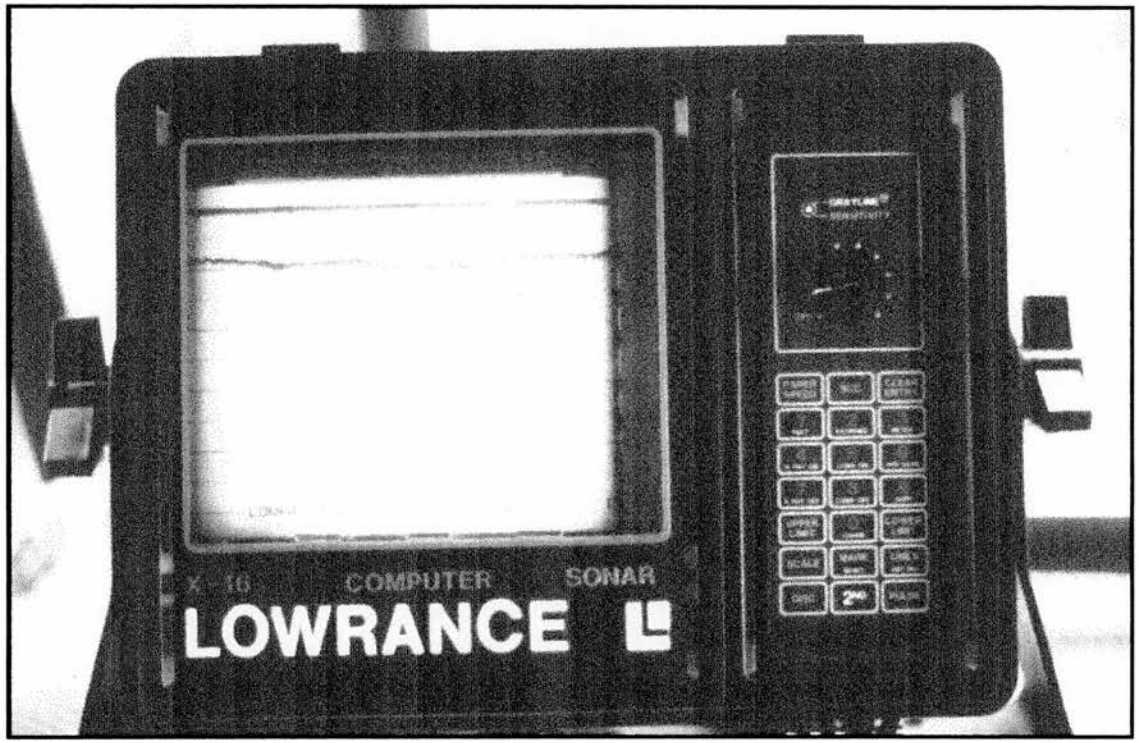

Plate 3.1: The Lowrance X-16 echo-sounder (192kHz).

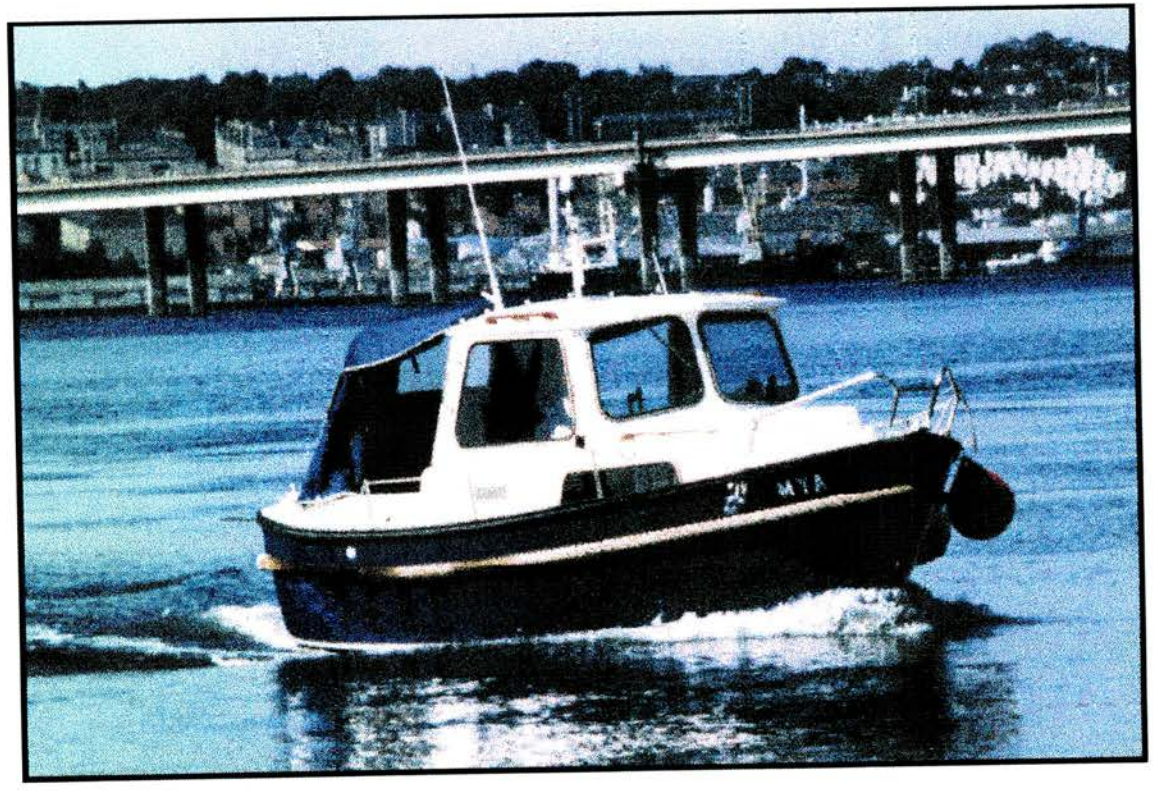

Plate 3.2: R.V. Mya from the Tay Estuary Research Center (TERC), Newport-on-Tay.

terms of wavelength assuming either a constant or average velocity value) and the depth (d) of the reflecting object and is expressed as:

$$\omega = (2d\lambda) \quad (8)$$

after Keary and Brooks (1991).

The system automatically controls the pulse width and varies it according to the lower depth limit as shown in Table 3.2.

Table 3.2: Pulse width according to lower depth limit (Lowrance, 1985).

lower limit (in m)	initial transmit pulse width (in µs)
10	110
20	130
30	160
40-200	200

Since the resolution or the ability to separate targets is diminished when the pulse width is increased, it is important to use the minimum lower depth limit and therefore a longer pulse width. For example: A 200µs transmitted pulse width will allow the unit to display two targets which are only 15cm apart but if the pulse width is increased to 400µs those two targets will merge.

The Lowrance X-16 is a truline recorder giving a permanent depth profile on a dry paper trace (Fig. 3.9). Like other acoustic devices it does not measure depth directly but the two-way travel time of a sound pulse which is converted into depth. Therefore, the trace of an echo-sounder shows the profile of depth changes along a traverse of a survey vessel. The marking stylus is attached to a belt located at the right edge of the recording paper. The top of the paper is marked with the so called zero mark and represents the surface of the water. The bottom line shows the chosen lower depth limit and can be read in feet, fathoms or metres (in this study metres were chosen). To receive a continuous record the paper speed should be adjusted according to the depth range. For detailed sonographs the paper speed should be set to maximum but this may lead to gaps in the record in deeper water. Since the maximum

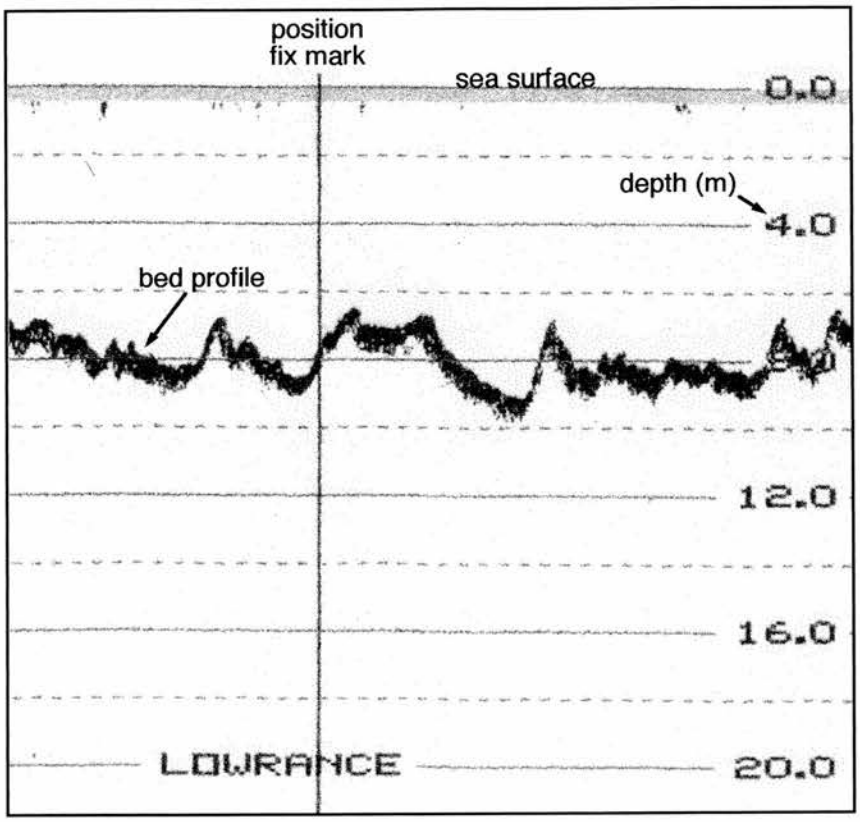

Fig. 3.9: Dry paper trace recorded with the Lowrance X-16.

depth in the fieldwork area does not exceed 30m, the control was set to the fastest paper speed throughout the surveys.

3.2.2 Side-scan sonar

In 1929 sound was first used to examine the sea bed when Wood, Smith and McGeachy developed the prototype echo-sounder (Flemming, 1976). It was soon found out that this method could be used to detect underwater objects by turning the transducer into the inclined or even horizontal mode (Fig. 3.10). To maximise the coverage obtainable per traverse, dual channel systems were developed scanning to both the port and starboard side of a vessel simultaneously, hence doubling the effective coverage and reducing the operating time to survey an area. This equipment was then effectively evolved during the Second World War to detect submarines (D'Olier, 1979) but the first operable sideways-looking sonar was not built until 1961 at the National Institute of Oceanography in England by Tucker and Stubbs (Flemming, 1976). Although it was primarily developed to detect man-made objects (i.e. submarines), its ability to locate features with positive and negative relief such as rock outcrop, sand waves, channels, wrecks and to distinguish between major sediment types has made it an important underwater remote sensing technique (Duck and McManus, 1985).

3.2.2.1 Basic principles

Like the echo-sounder the side-scan sonar is an active sonar system which transmits sound and records the returning echo. At the heart of the system is the transducer which converts the oscillating electric field produced by the transmitter into a mechanical vibration which is then transferred into the water as the sound pulse (Fig. 3.11). The sound travels away from the transducer through the water until it strikes the sea bottom or an object. Only a fraction of the outgoing sound will be scattered back to the receiving transducer (Yules and Edgerton, 1964; Johnson and Helferty, 1990). The detected energy is amplified and presented on some kind of display, i.e. a paper recorder or video and is called sonograph.

The main features which distinguish side-scan sonar from most other forms of sonar are: sideways look, dual channel, towed body and narrow

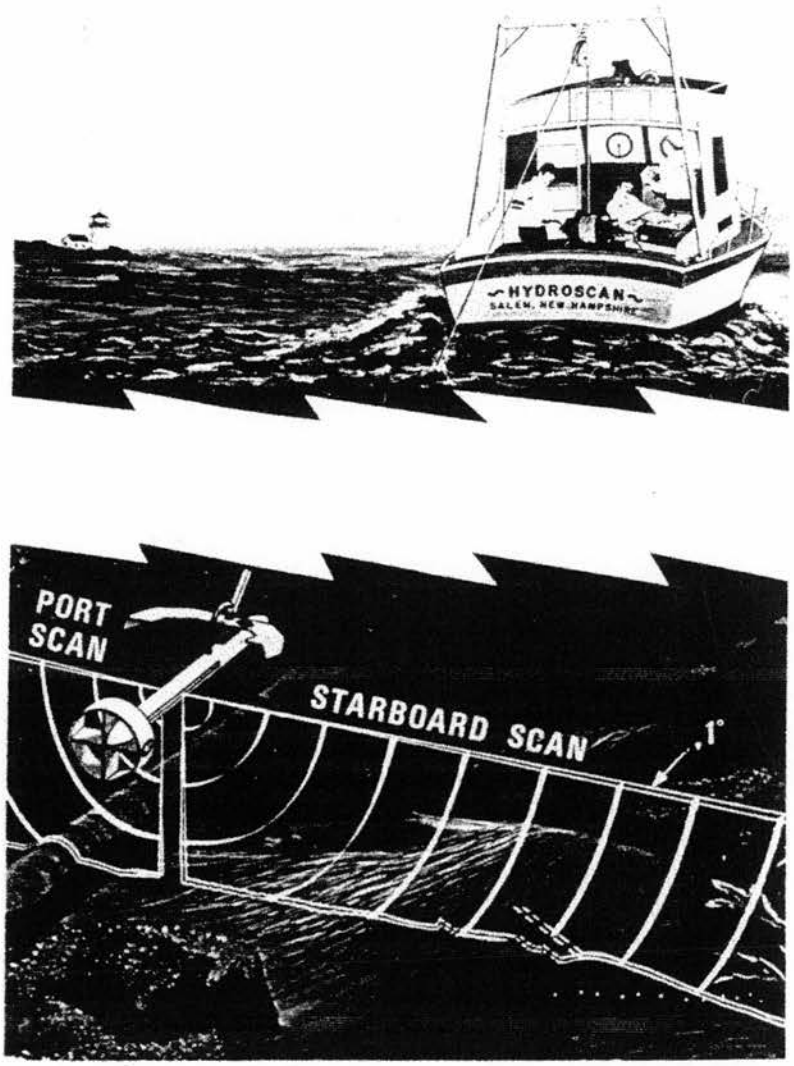

Fig 3.10: Artist's impression of a side-scan sonar in operation (after McQuillin and Ardus, 1977).

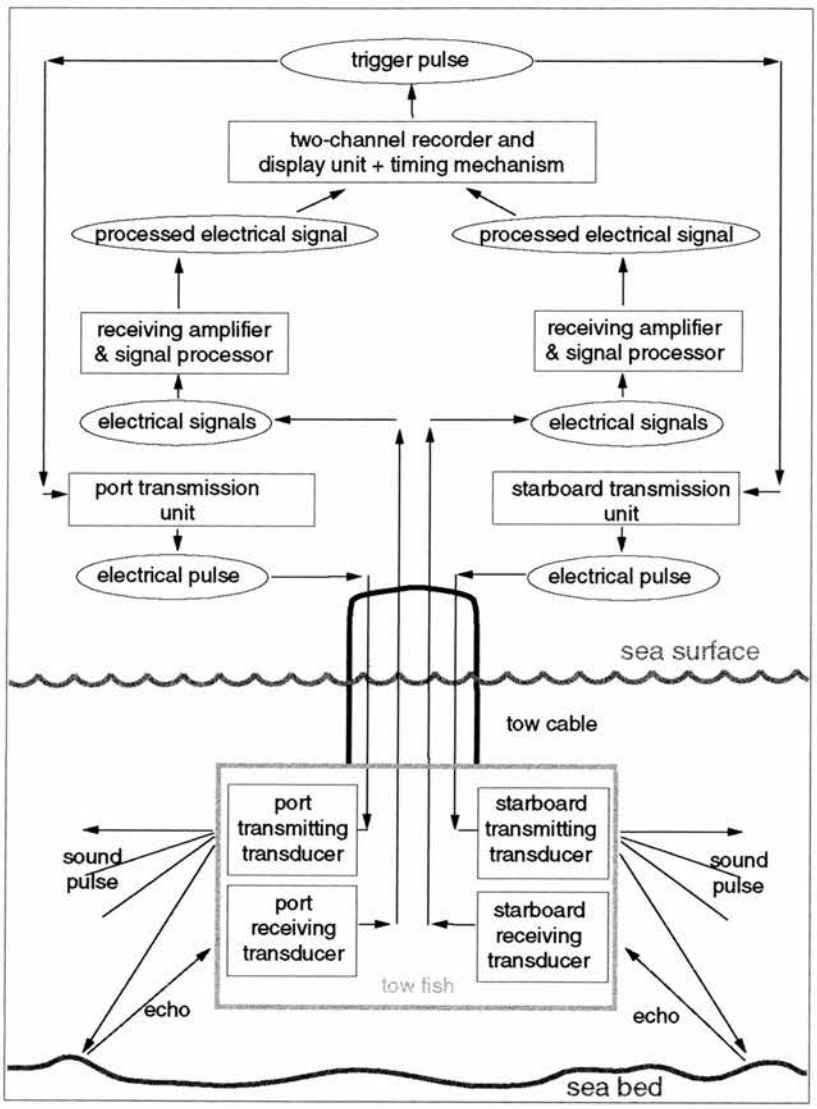

Fig. 3.11: Block diagram showing the main components of a side-scan sonar system (after McQuillin and Ardus, 1977).

horizontal but wide vertical beam angle. As mentioned above sonars were originally used only to measure water depth directly beneath a ship or to locate large objects in the water or resting on the bottom. In order to decouple the sonar from the ship's motion the transducers are mounted in a streamlined, hydrodynamically balanced body called tow fish. If this tow fish is hauled on the end of a long cable relatively close to the bed in order to provide detailed information, there is a chance that it may get damaged or even lost through collision with the sea floor (Belderson *et al.*, 1972).

The system recorder processes the echo of the transmitted acoustic signal. The stronger the echo, the darker the mark on the paper. The sonograph is built up by a succession of scan lines giving a continuous record (Tucker, 1966). In a dual-channel system both channels are printed onto the same roll of recording paper showing the survey line in the middle and printing the echoes of the port and starboard transducers to the left and right. The paper advance is related to the forward motion of the fish while the range is shown across the width of the paper (Bryant, 1975). Since the recording process is instantaneous, the opportunity is given to take a position fix as soon as the contact appears (Yules and Edgerton, 1964) bearing in mind that the vessel's position is not the position of the tow fish.

A basic system consists of a graphics recorder, an electromechanical tow cable and a tow fish containing the acoustic transducers (Plate 3.3).

3.2.2.2 Geometry of a side-scan sonar record

The geometry of side-scan sonar is the key to understanding and interpreting sonographs. Since the sonar measures and displays the ranges of reflectors from the transducers housed in the tow body at some depth below the water surface everything must be referred to this position (Klein, 1985). It is important to remember that the technology is based upon the elapsed time between the outgoing pulse and the returned reflection from a target in the environment (Fish and Carr, 1990).

Since the same transducer emits and receives the pulse, the first transmitted pulse will be a strong signal and therefore produce a dark mark on the record of the port and starboard channels (Fig. 3.12). This

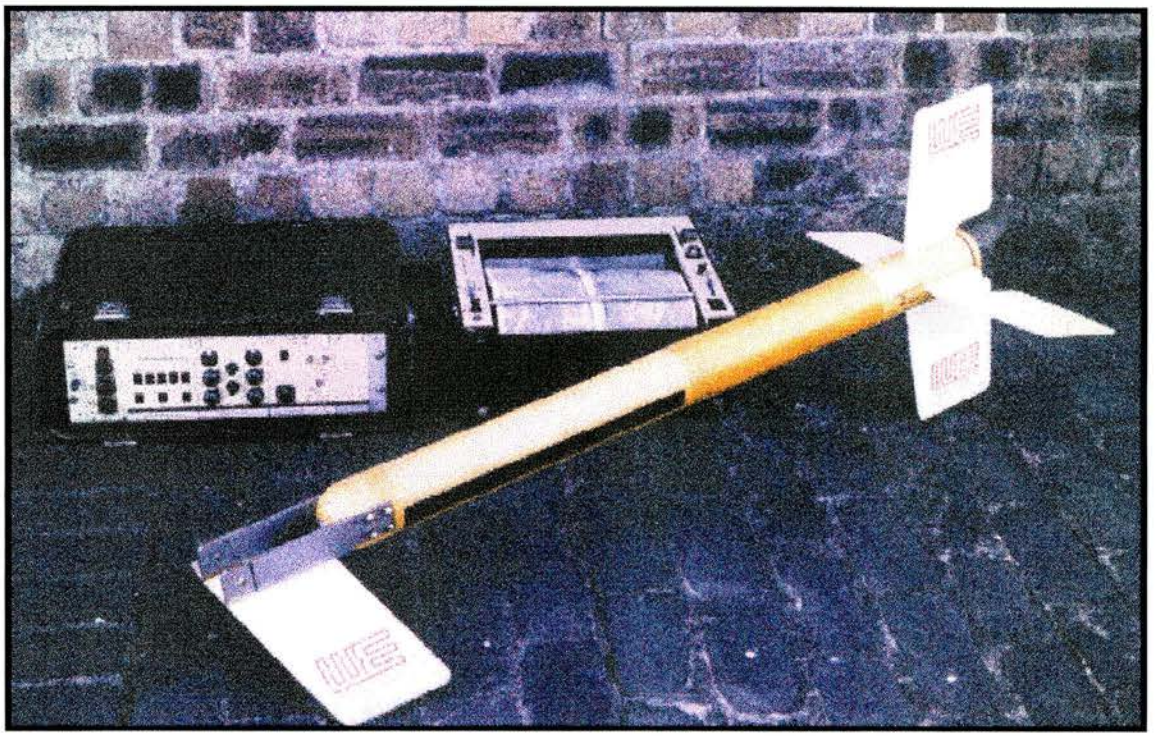

Plate 3.3: The Waverley Sonar 3000 (side-scan sonar system).

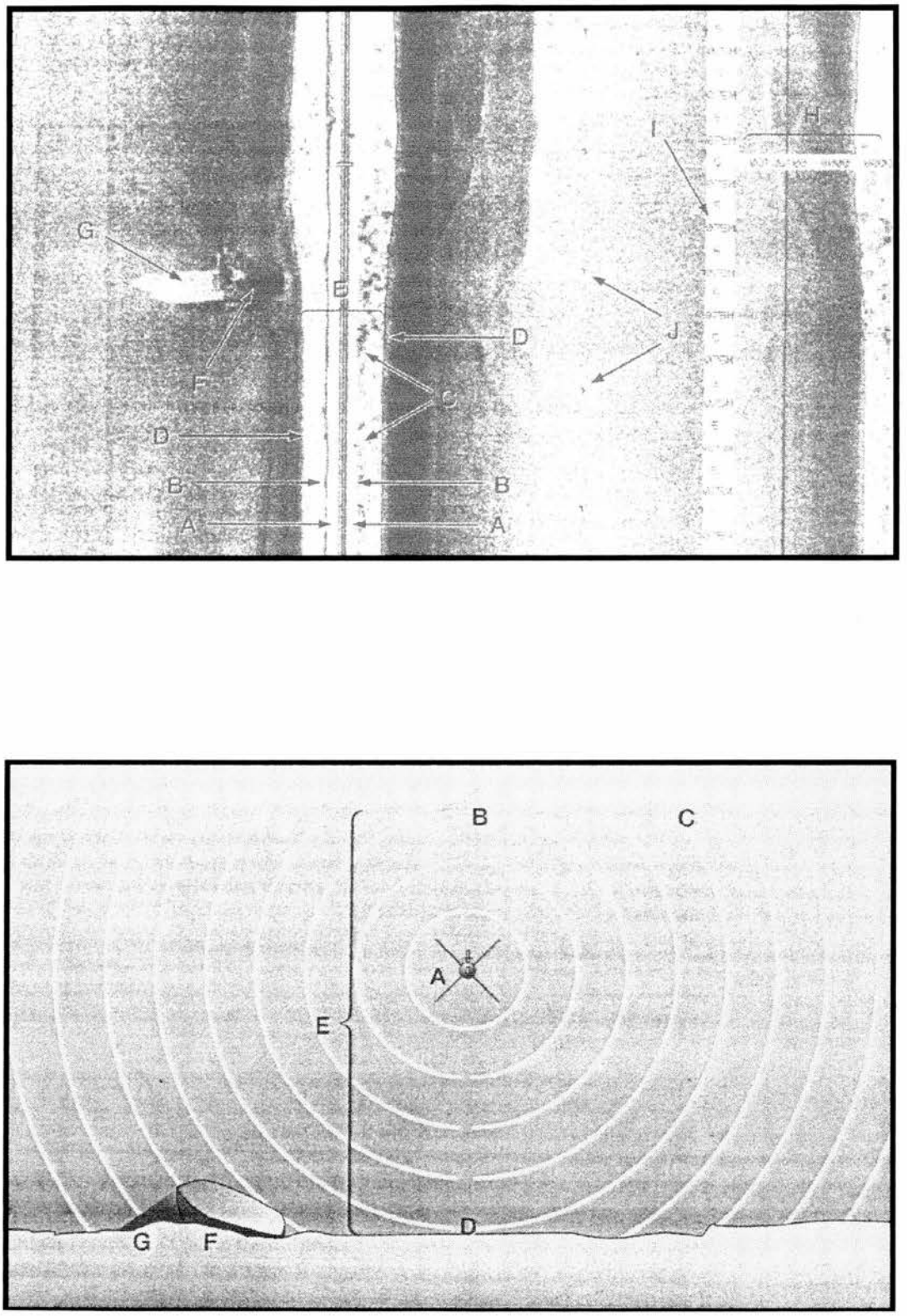

Fig. 3.12: Side-scan sonar record with corresponding sketch describing the conditions under which the record was made. A: trigger pulse, B: first surface return, C: sea clutter, D: first bottom return, E: water column, F: sunken vessel, G: shadow, H: data channel, I: system operational settings, J: 25m scale marks (after Fish and Carr, 1990).

signal is known variously as the emission signal (Leenhardt, 1974) or the trigger pulse (Fish and Carr, 1990). Depending on the depth position of the tow fish in the water column, the first recorded echo may be either the first surface return or the first bottom return (Klein, 1985). The white area between the dark marks of the trigger pulse and the first return is known as the water column. The first surface return is usually a good indication of the tow fish depth which can be scaled using the scale marks printed by the recorder (depending on the system distances between the scale lines are 15m, 25m or more). The first bottom return is almost always a strong reflector and a good indication of tow fish height (Leenhardt, 1974; Fish and Carr, 1990). The first bottom return will be followed by returns from the sea floor at successively greater distances from the tow fish. The recorder will print them at correspondingly increasing distances. These distances do not represent the true range across the sea bed but the slant range from the tow fish to the various features on the bottom (Anonymous, 1967). Large objects projecting above the sea floor will prevent sound from insonifying the bottom beyond the object thus producing an acoustic shadow. This will leave a white patch on the paper and its width and position relative to the fish can be used to calculate the object's height (Flemming, 1976). However, a simple target will not appear identical if viewed from different angles or track line distance or if insonified with a different acoustic system at a different frequency (Johnson and Helferty, 1990).

3.2.2.3 Design details

The general nature and essential features of side-scan sonar have already been discussed. This section will explain the design features in greater detail and will look at the transmitted energy level, length of sound pulses, shape of the acoustic beam, resolution and the importance of frequency selection as well as interference.

Source level

The energy transmitted into the water is defined as an acoustic source level (*SL*). The value is given in decibels (dB) and expresses the intensity (I) of the sound relative to that of a plane wave of a reference intensity (I_r) at unit distance. The reference pressure is normally 1 micro Pascal (μPa)

and the distance is 1m for side-scan sonars. The relationship is expressed as:

$$SL = 10 log \frac{I}{I_r} \qquad (9)$$

after Klein (1985).

Pulse length

The pulse length is closely related to the resolution of the system. A short pulse will have a better resolution but a longer pulse would have a narrower bandwidth and therefore would be less sensitive to noise in the water. Typical pulse lengths for a 100kHz system are around 0.1millisecond. The physical extent of a pulse is determined by the speed of sound. When a pulse leaves the transducer the leading edge will have already travelled some distance before the trailing edge has left the face (Fig. 3.13). This distance or thickness (also referred to as the sonic "footprint" when the pulse has reached the sea floor) (T_{sf}) is the product of the pulse length (L_p) and the sound velocity (v)

$$T_{sf} = L_p \cdot v \qquad (10)$$

after Klein (1985)

and affects the across-track resolution.

Across-track (range) resolution

"Range resolution is the minimum distance between two objects perpendicular to the line of travel that will be displayed as separate objects. This is a function of the display system as well as the topography but more exactly, the pulse width of the sonar will determine the lower limit of detecting the objects as distinctly separate" (Flemming, 1976). Flemming (1976) assumes that a minimum spacing of 1mm on the recording paper is needed to plot two objects separately so that the range resolution (R_r) will be the ratio of the range (r) divided by the width of the paper per channel (W_{pc}) expressed as:

$$R_r = \frac{r}{W_{pc}} \qquad (11)$$

after Flemming (1976).

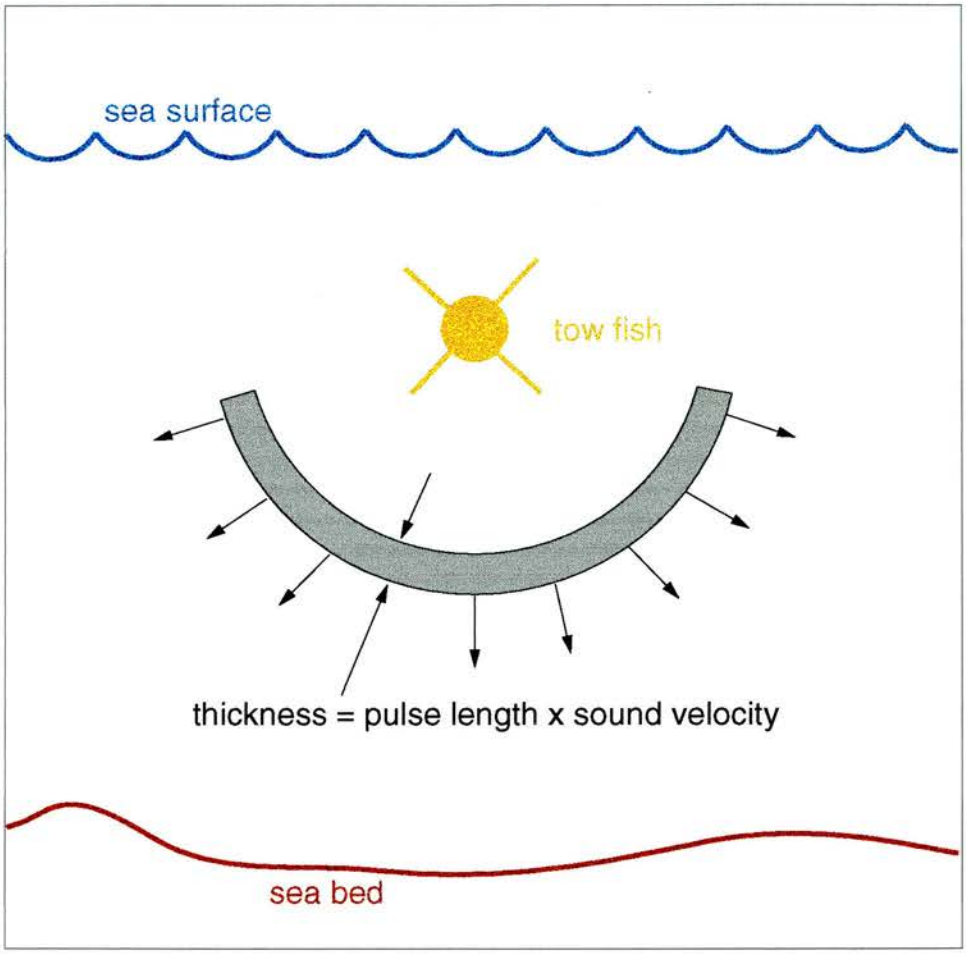

Fig. 3.13: Physical extent of acoustic pulse length (after Klein, 1985).

Resolution is the ability to resolve multiple targets as distinct and separate on the sea floor. The range resolution is mainly determined by the pulse length as well as the forward motion of the sonic footprint. When trying to resolve two objects, one closer and one farther from the tow fish, a shorter pulse will first insonify the closer target and then travel beyond it to the further one recording them as two distinct targets (Fig. 3.14). A long pulse might encompass both objects at the same time and record them as one target. An acoustic pulse forms an arc in the water resulting in a larger footprint in the near ranges and a smaller footprint in the far ranges (Fish and Carr, 1990). This implies that the across-track resolution is better farther away from the sonar.

Beam pattern and directivity

The side-scan sonar beam is carefully formed to provide a high resolution image of the sea floor. It has the highest energy level in a very narrow section in the horizontal view which is the main lobe of the pulse that propagates out across the sea floor (Fig. 3.15). The vertical beam width is very different due to the wide angle which provides near and far sea floor coverage (Fish and Carr, 1990) (Fig. 3.16). The main axis of the beam is angled between 10° and 20° down from the horizontal towards the sea floor.

Along-track (transverse) resolution

"Transverse resolution is the minimum distance between two objects parallel to the line of travel that will be displayed on the sonar as separate objects. This minimum distance is equivalent to the beam width (which widens with distance from the tow fish) at any particular point" (Flemming, 1976).

Transverse resolution (R_t) is a function of range setting (r) and the horizontal beam width (B_{ha})

$$R_t = (\sin B_{ha})r \qquad (12)$$

after Flemming (1976).

The range can be controlled by the operator unlike the horizontal beam width. If two objects are separated by a distance which is less than the spread of the sonar beam at that range they will appear as one object. If

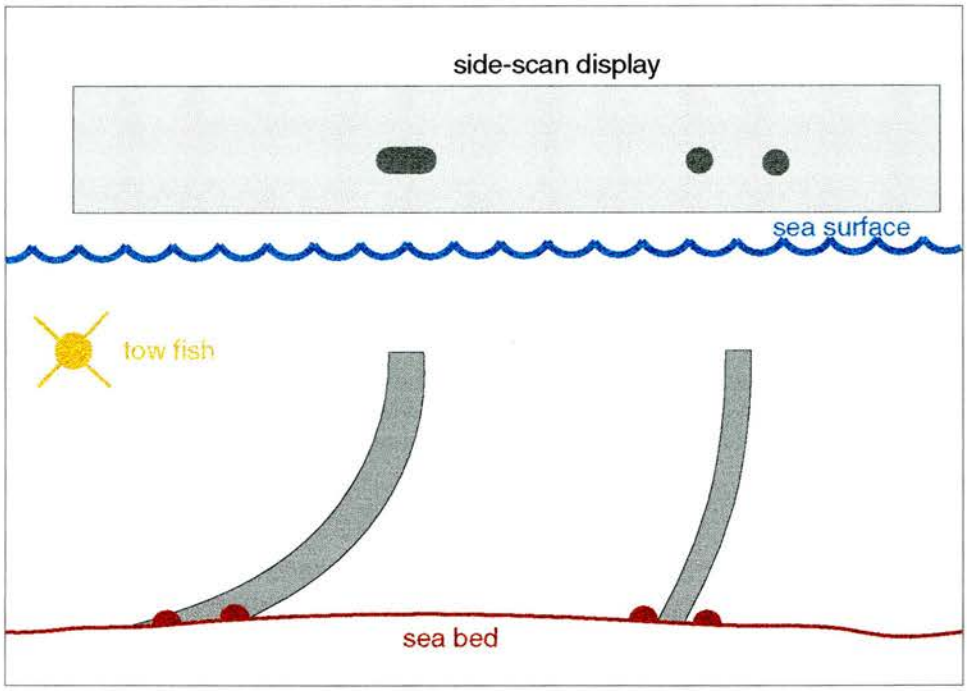

Fig. 3.14: Relationship between range resolution and sonic "foot-print" (after Klein, 1985).

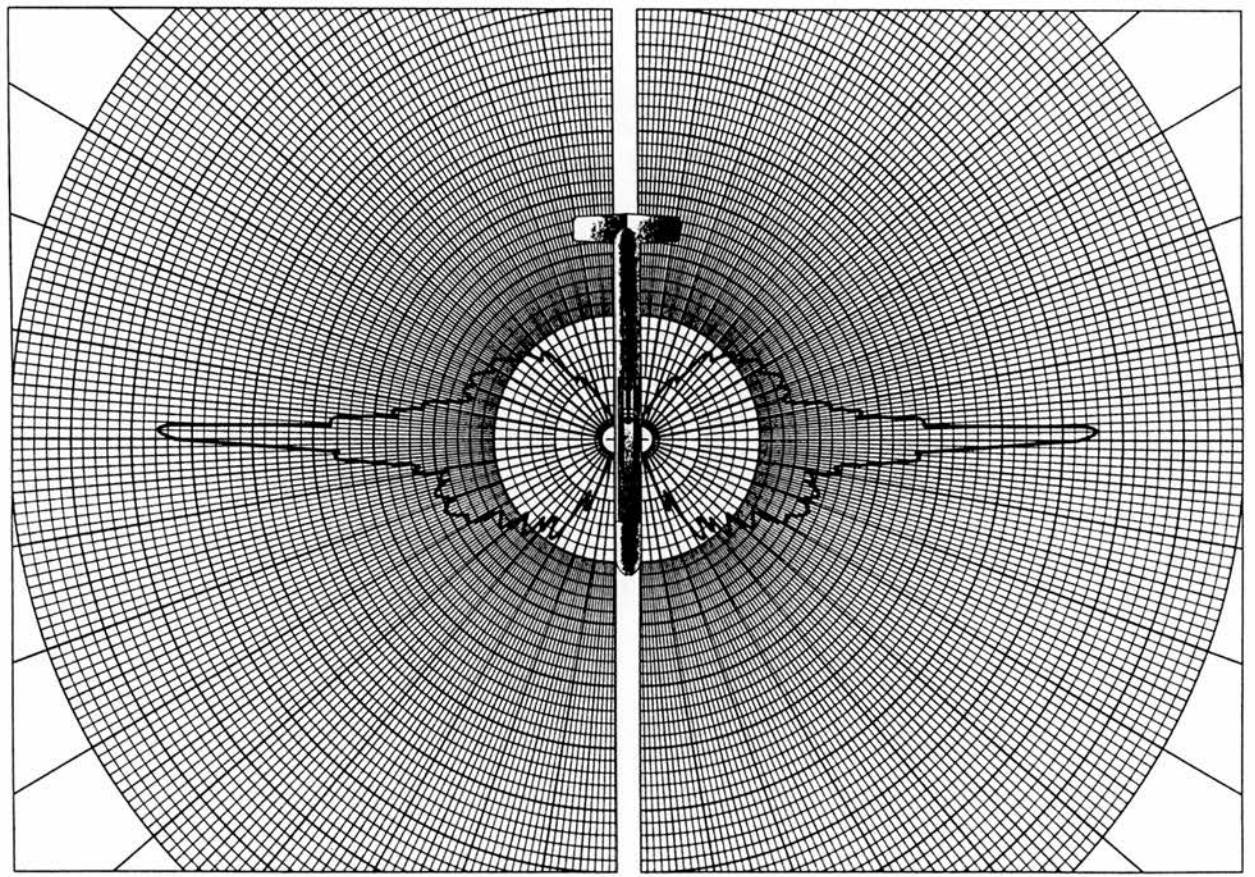

Fig. 3.15: As viewed from above, the side-scan sonar beam has the highest energy level in a very narrow section. This is the main lobe of the sonar pulse that propagates out across the sea bed (after Fish and Carr, 1990).

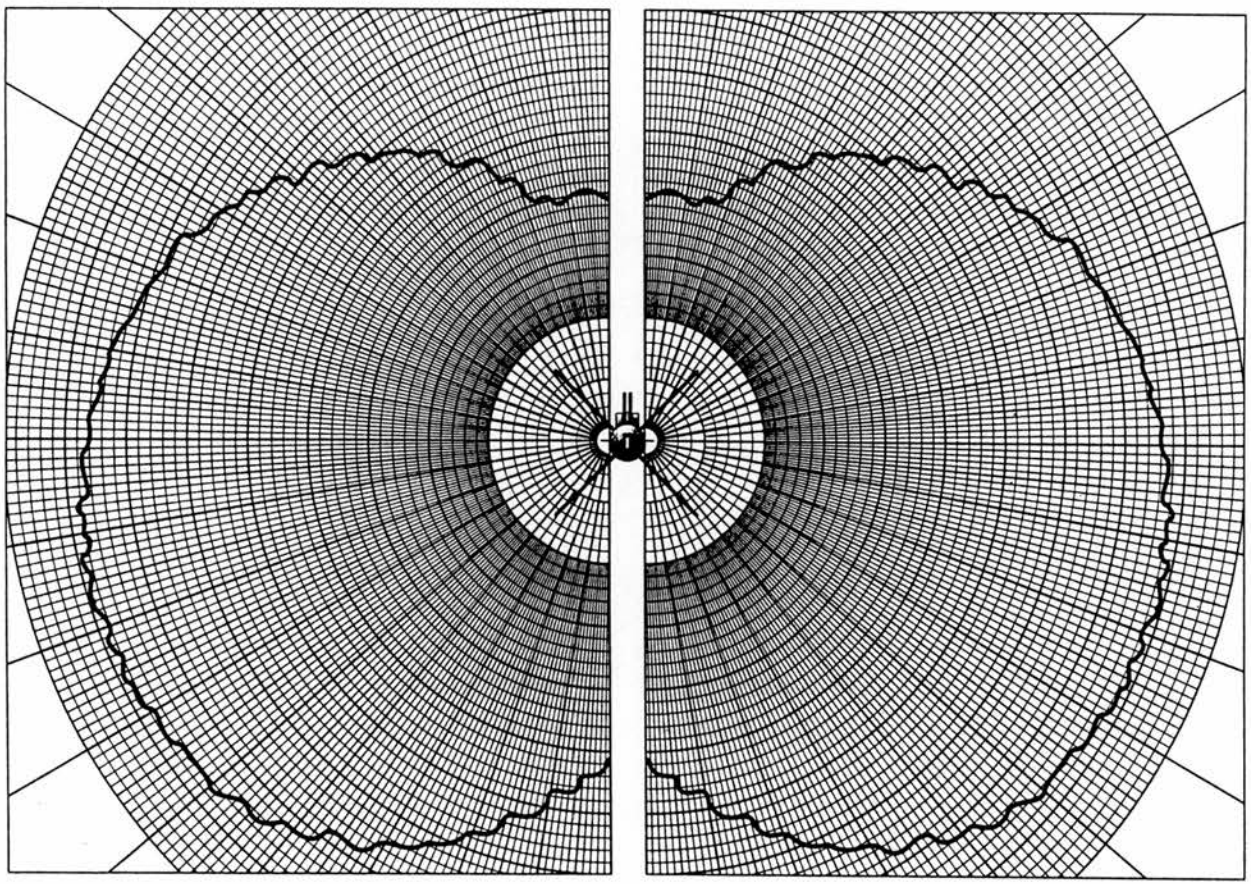

Fig. 3.16: The side-scan sonar beam as viewed from the front or back of the tow fish is very wide. This provides near and far sea floor coverage (after Fish and Carr, 1990).

the same two objects were in the closer range where the beam is narrower they would be resolved as two separate targets (Fig. 3.17). Hence, the along-track resolution is better at close range.

Time varied gain (TVG)

Absorption, spreading and scattering of the acoustic pulse weakens the strength of the returning signal. Since the display of the sonar data should look alike for any given bottom type over a chosen range, the returned signal must be amplified to counteract the occurred losses over the travelled distance. The TVG correction assumes a constant speed of sound in water and an appropriate reduction in the returning echoes with range. The gain is increased along a predetermined curve (Fig. 3.18).

Frequency

The operating frequency is closely related to the range and resolution. At higher frequencies there can be a shorter pulse length and narrower beam, resulting in a better resolution but, as mentioned in Section 3.2, the range will decrease due to attenuation in the water. A lower frequency can cover longer ranges but will decrease the resolution. Side-scan sonar frequencies commonly lie in a range between 5kHz and 500kHz (McQuillin and Ardus, 1977; D'Olier, 1979).

Interference

The reflection of the transmitted pulse is not the only sound received and recorded. "'Noise' in terms of underwater measurement, is defined as the signal which we don't want" (Fish and Carr, 1990). Much of it is recognisable as interference patterns. Noise sources fall into two categories: self-made and ambient. Self-made noise sources are other acoustic instruments such as echo-sounders and sub-bottom profilers as well as the ship's engines. Ambient noise sources include wave motion at the sea surface including wave breaking, rain as well as biological noise created by marine animals.

Another false trace, less common with towed fish transducers, in shallow water conditions, is the Lloyd's Mirror effect. This appears only in exceptionally calm weather when the water surface can act as a mirror

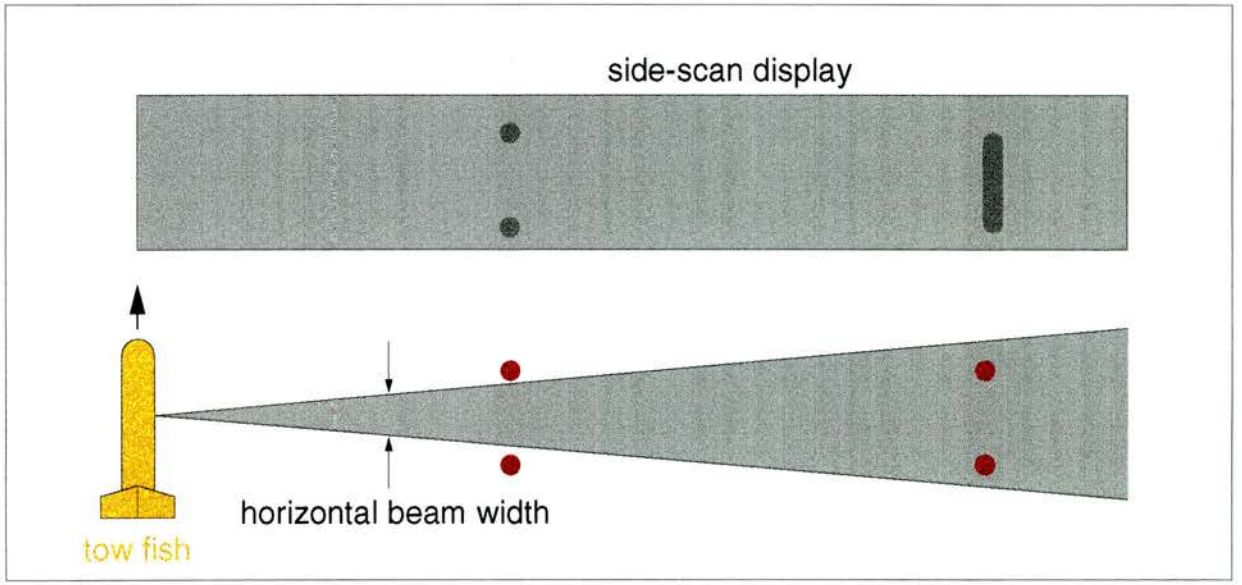

Fig. 3.17: Along-track (transverse) resolution depending on horizontal beam width and range (after Klein, 1985).

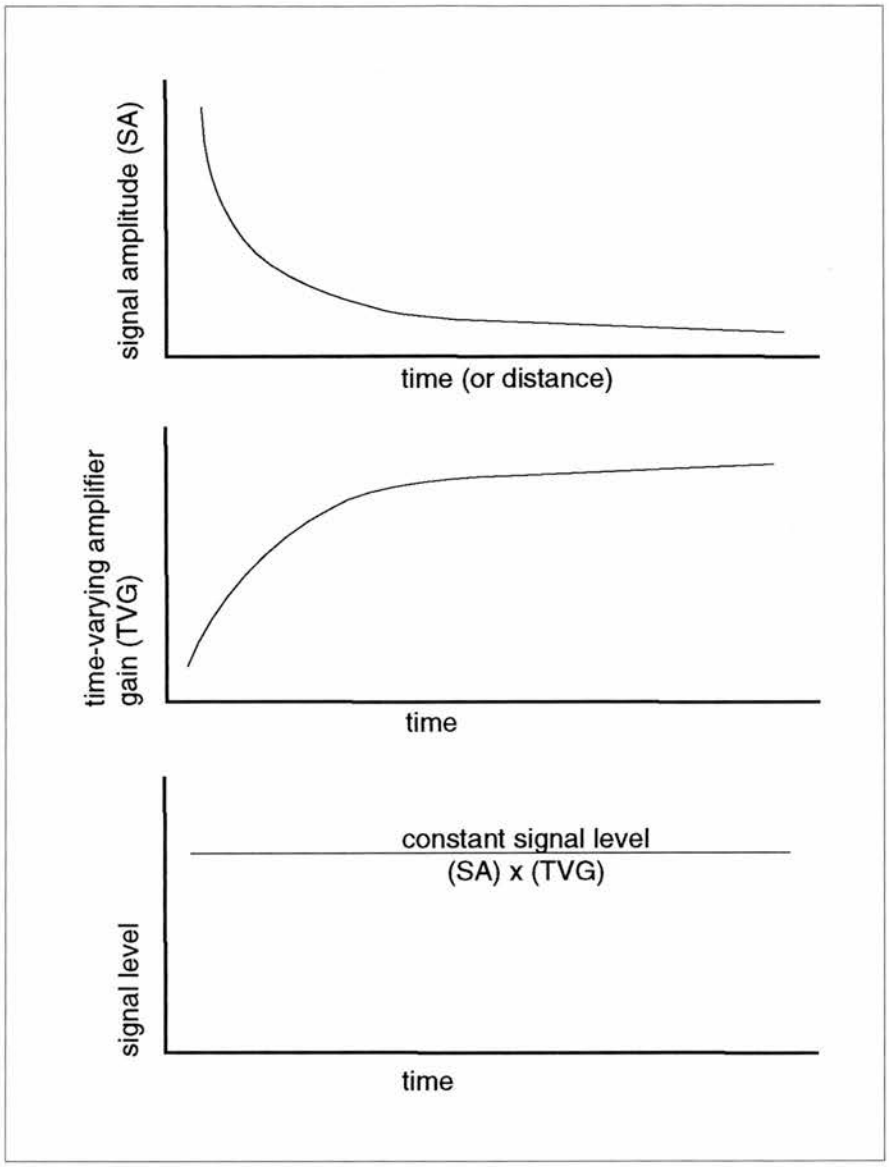

Fig. 3.18: Application of time-varying gain (TVG) amplification to a nonconstant signal (after Johnson and Helferty, 1990).

(Top) The natural decrease with time of a returned acoustic signal that decays because of geometric spreading and absorption. Since the actual signal is a rapidly varying function, this curve is just the upper envelope of the amplitude curve. If this side-scan signal were displayed without correction, the image would be too strong in the near-fish returns and too weak in the far-field returns. (Middle) The systematic increase in amplification of the TVG. The increase in amplification with time is designed to compensate for (and deconvolve) the decrease in amplitude in the signal due to geometric spreading and absorption. (Bottom) The ideal, correct TVG applied to the signal. In this case the TVG exactly compensates for the signal losses, and the signal level presented in the image is range-independent. Backscatter amplitudes in this ideal case now depend on the properties of the seafloor material, not distance from the side-scan fish.

and results in dark and light interference fringes (Morang and McMaster, 1982; Werner, 1982). These Lloyd's Mirror bands run approximately parallel to the ship's track across the sonograph. Towed fish transducers reduce this effect since only the weaker side lobes of the beam reach the water surface (D'Olier, 1979).

3.2.2.4 Record interpretation

Skill in interpreting sonar records can come only from experience. But even the most experienced operator can be fooled at times. Interpretation remains a thoroughly qualitative and tedious process. For accurate interpretation the operator must use the entire record as well as any available data recorded from previous surveys such as ground observations from divers, video recordings, sediment samples etc. for calibration.

The side-scan method produces a plan view of the shape and texture of the surface of the sea floor (Belderson *et al.*, 1972). However, the side-scan sonar image is not a representation of how the sea floor would look if the water were somehow removed. Instead it is a graphical presentation of how the sea floor interacts with acoustic energy. This conversion from how the sea floor "sounds" to how our models tell us the sea floor should look, can be a major pitfall for the interpreter of the images (Johnson and Helferty, 1990). In site investigation studies side-scan sonar is often used as a "fill-in" between bathymetrical lines to ensure that there are no anomalies in relief (Sly, 1981).

Distortion

Features recorded by side-scan sonar are not normally presented in their true proportions. The main factors causing distortions are the variations in survey speed affecting the along-track direction and the slant range distortion affecting the across-track direction. This causes major difficulties in the interpretation of side-scan sonar records (Mudie *et al.*, 1970). A solution to the problem of scale correction for distorted sonographs is provided by using a photographic technique which cannot correct for heading variations or slant range effects but only for distortion in the along-track direction (Kelland and Hopkins, 1972) or by the

application of digital image processing techniques (Sly, 1981) if the signals are recorded in digital form and the facilities are available.

Speed distortion

Distortion will occur in the along-track direction due to variable ship speeds during the survey. Slow traverse speeds produce visual distortions on uncorrected sonographs so that objects will appear larger. Travelling too fast on the other hand minimises the opportunity for reflections to be detected and decreases the dimensions of targets in the direction of traverse (Flemming, 1976) (Fig. 3.19).

Slant range distortion

As noted earlier the side-scan recorder shows the slant range from the tow fish to the various features on the sea bottom (Anonymous, 1967) and not the true range. If an object is detected and it is required to make a precise measurement of its size and position relative to the fixed position of the ship, corrections for slant range distortion should be applied. This can be done by using the Pythagorean theorem with the tow fish height (H_f) forming one side of the right-angled triangle, the measured slant range (R_s) the hypotenuse and the horizontal offset (R_h) the other side (Fig. 3.20):

$$R_h = \sqrt{R_s^2 - H_f^2} \qquad (13)$$

after Klein (1985).

Acoustic shadows and backscatter

Acoustic shadows are of extreme importance in the interpretation of sonographs. Their position, shape and intensity give clues to the actual conditions of the insonified sea bed. Objects such as rocks, sand waves or ship-wrecks will cast a clear, harsh shadow while other targets such as a gentle upward localised slope will only cause a light shadow on the record. The cause for lighter areas on a sonar record are grouped into three general categories (after Fish and Carr, 1990):

1) shadow zones that have been blocked from the sonar beam by an acoustically opaque object

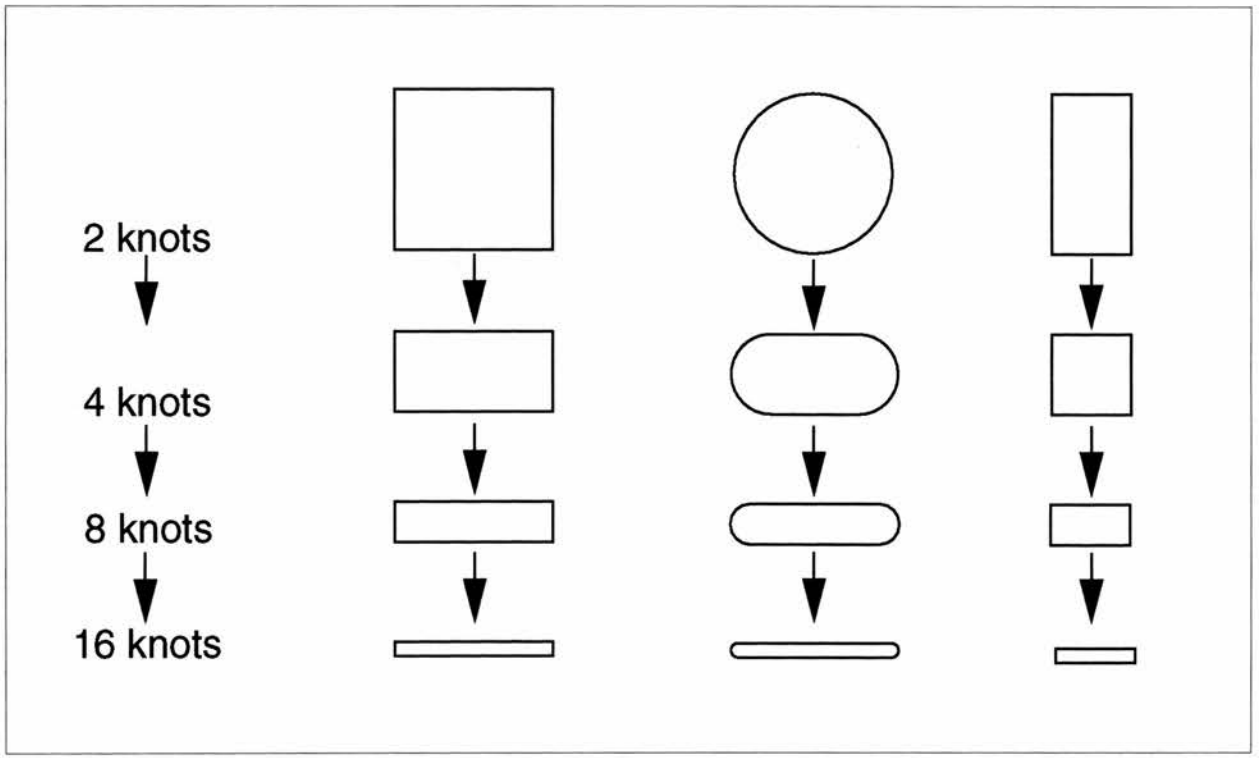

Fig. 3.19: Distortion effects on some common shapes parallel to the line of travel caused by various ship speeds (after Flemming, 1976).

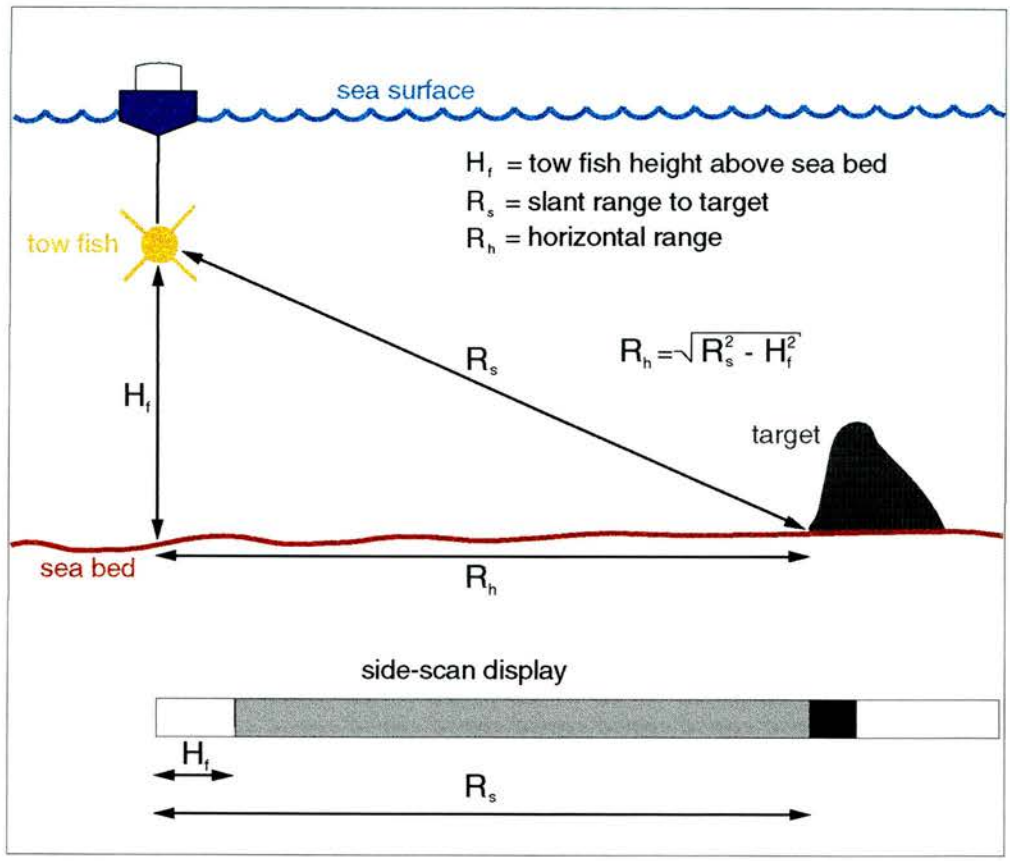

Fig. 3.20: Side-scan sonar geometry for horizontal range calculation (after Klein, 1985).

2) areas of topography that provide less backscattering of the sonar beam
3) areas that are oriented in such a way as to provide less backscatter, such as an area inclined away from the tow fish.

The shape of a shadow on a sonograph is directly related to the shape of the object casting it. Therefore the shape of the shadow is helpful in determining the physical conditions of the object. The geometry of the sonar slant range (Fig. 3.21) can be used to determine the height of a target as follows:

$$H_t = \frac{L_s \times H_f}{L_s + R_s} \qquad (14)$$

after Klein (1985)

with H_t - target height
L_s - shadow length
H_f - height of the tow fish above sea bed
R_s - slant range to the target.

The same formula can also be applied for target depth calculations if the target is a negative feature as shown in Fig. 3.22. This is only possible if the sonograph shows a shadow zone followed by a zone of strong reflection which is provided when the angle of the incoming ray (φ) is smaller than the angle of the slope (δ) closer to the transducer. However, it is not possible to calculate target depth on the basis of a low tonal colour zone (Fig. 3.23) when the angle of the incoming ray (φ) is greater than the angle of the slope (δ). Therefore height calculations for negative targets are only possible if the steep slope is closer to the transducer and the gentle slope farther away hence producing the required acoustic shadow for the measurements.

It may be difficult to determine the exact position of the target casting the shadow so that care must be taken. Side-scan sonar geometry can also prevent a target from casting a shadow on the sea bed. This may occur if the target is in the water column at a similar height as the tow fish so that the shadow would be beyond the displayed range. Also targets above the tow fish in the water column will be displayed on the record but will not cast a shadow on the sea bed.

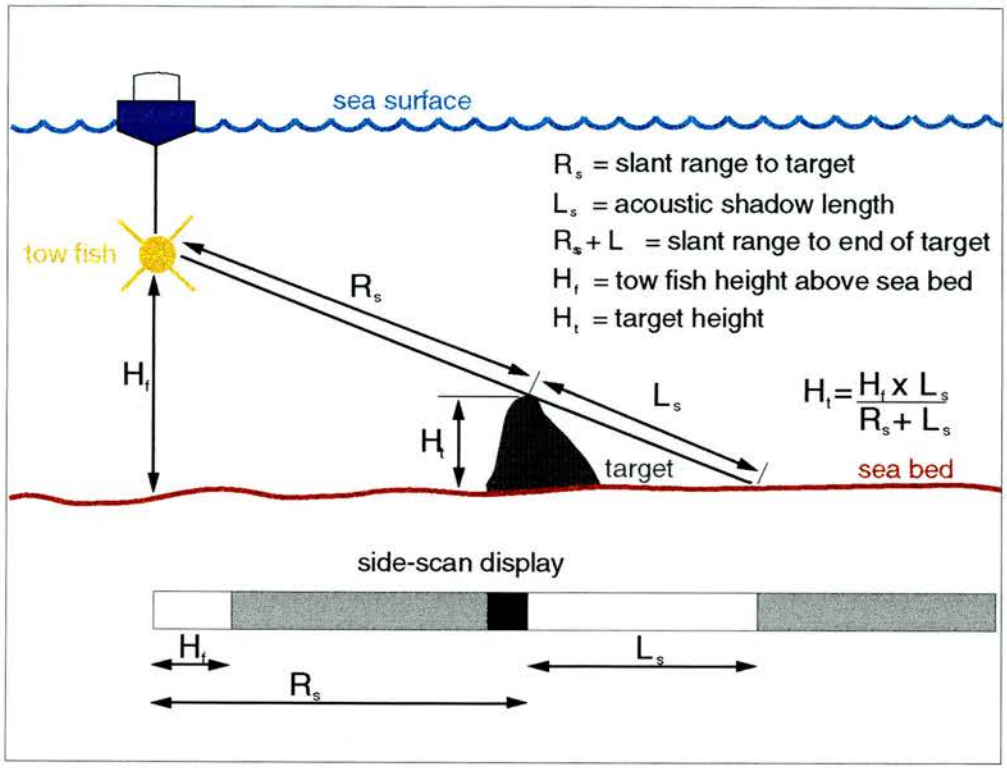

Fig. 3.21: Side-scan sonar geometry for target height calculation based on acoustic shadow (after Klein, 1985).

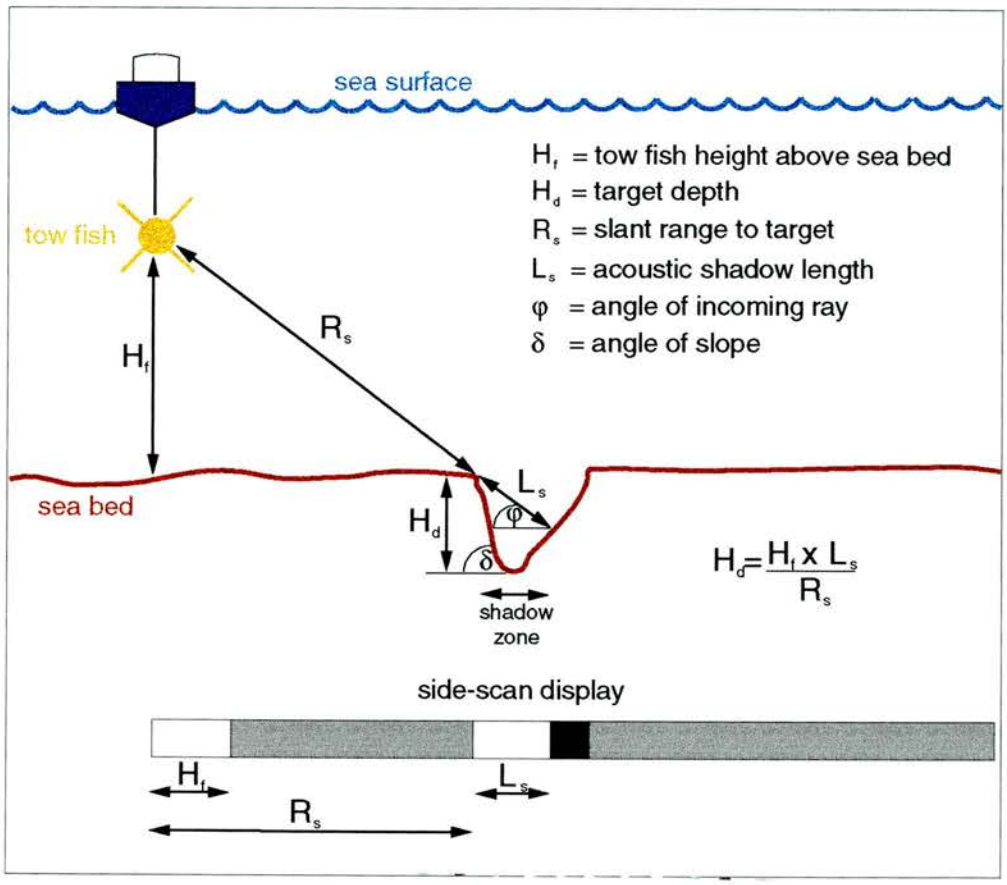

Fig. 3.22: Side-scan sonar geometry for target depth calculation based on acoustic shadow (after Dix, 1995).

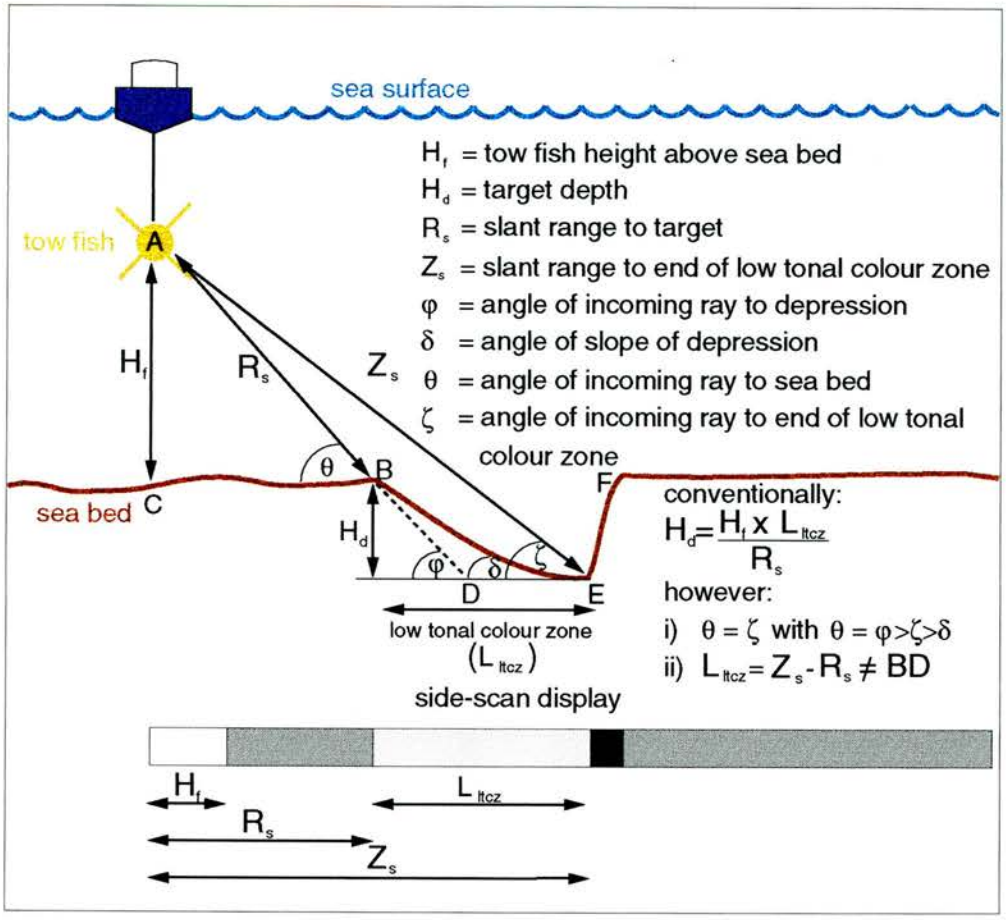

Fig. 3.23: Side-scan sonar geometry showing the impossibility of calculating target depth on the basis of a low tonal colour zone (after Dix, 1995).

Geology and topography

Side-scan sonar is an ideal tool for determining the configuration of the sea bed over a large scale. When the sonar signal is transmitted part of it is attenuated and scattered as it travels through the water. Further energy losses occur when the pulses strike the sea floor. The intensity of the returning signal will determine the tonal shading on the sonograph and largely depends on the composition and porosity of the sediment on the sea bed as well as the bottom topography (McQuillin and Ardus, 1977).

According to Williams (1982), relationships between tonal intensity and sediment characteristics are not yet fully understood but, in general, the denser and coarser the sediment, the greater the reflectivity and consequently the darker the tone on the sonograph. Almost half a century ago Lafond *et al.* (1950) found the character of sound reflection to be specific for mud, stones, sand and rock. Hence, outcrops of rock will have a very high reflectivity and will appear darkest on sonographs, gravel patches will be darker than sand and sand will be darker than fine-grained muddy sediments (Flemming, 1976; Hunter *et al.*, 1982). Williams (1982) has found an inverse relationship between acoustical impedance and sediment porosity. High porosity sediments like clay have a relatively low impedance and low reflectivity and therefore appear light on a sonograph, whereas low porosity material like well packed medium sand has a higher impedance and higher reflectivity and therefore appear in darker tones.

Topographic features of the sea floor also affect the reflectivity and may cause effects on the record similar to changes in sediment composition and porosity. The slopes of sand waves and ridges facing the transducer reflect sound waves better than surfaces lying oblique to the sound beam and will consequently result in darker tonal intensities on sonographs (Chesterman, 1968; Flemming, 1976; Rothwell *et al.*, 1991). Depending on their height they may also produce a pronounced acoustical shadow on the far side where no signal is reflected and a white area is produced (Williams, 1982). The patterns produced by the strong reflection and the acoustic shadow can reveal not only the presence of sand waves but also their shape and asymmetry, thereby providing evidence of the direction of sediment transport - a technique widely applied by various

scientists (Langhorne, 1973; Swift and Freeland, 1978; Caston, 1979; McCave and Langhorne, 1982; Goedheer and Misdorp, 1985).

Even though side-scan sonar has become a widely employed instrument in marine sciences it is not always possible to distinguish between natural phenomena and anthropogenic structures. Therefore the technique should only be used as a reconnaissance tool and in no way as a substitute for on-site investigations by divers (Duck and McManus, 1987). However, the technique has revealed the true extent of the complexity of surficial sediment relationships. It has also demonstrated the inadequacy of areal bottom classification based only on spot sediment samples (Bennett *et al.*, 1992).

3.2.2.5 Klein Hydroscan Model 401

The side-scan sonar system employed during the first field season of this project was the Klein Hydroscan Model 401 operating at a frequency of 400kHz. It is a dual-channel system with its transducers housed in a streamlined tow fish. The port and starboard transducers send out pulses with large vertical beam angles of 160° but narrow horizontal beam angles of 0.75°. The main axis of the beam is angled 10° down from the horizontal so that most of the energy is directed toward the sea floor.

The high frequency of 400kHz and the short pulse width of 100µs provide a high resolution. As described in Section 3.2.2.3 resolution is the minimum distance between two objects that will be displayed as separate objects on the record. Since side-scan sonar is a three-dimensional technique, resolution has to be described for the across-track or range (R_r) as well as the along-track or transverse (R_t) dimension. The theoretical range resolution is determined by the thickness of the sonic footprint described in equation (10) as

$$T_{sf} = L_p v$$

and therefore has the value of T_{sf}=0.15m for the Klein Hydroscan with L_p=100µs and an average sound velocity through water of v=1500m/s. The detectability of an object is determined by a different concept though, namely the actual dimensions of the sonograph. According to equation (11) the real range resolution (R_r) depends upon the chosen range

setting (r) and the width of the paper record per channel (W_{pc}). To plot two objects separately on the recording paper a minimum spacing of 1mm is needed giving the limit of detection as 1/125 of the range scale as the width of the paper trace per channel is 125mm. Since the chosen range was set at 75m per channel throughout the surveys, the real range resolution can be calculated as

$$R_r = \frac{75}{125} = 0.6m$$

The transverse resolution (R_t) is the minimum distance between two objects parallel to the line of travel that will be displayed as separate objects and hence depends on the range setting (r) as well as the horizontal beam angle (B_{ha}) as mentioned in equation (12). The horizontal beam angle of the system is given as 0.75° and at the range setting of 75m per channel during these surveys the transverse resolution is

$$R_t = (\sin 0.75)75 = 0.98m$$

At a closer range the horizontal beam width is narrower which will result in better resolution. Hence at a range of only 10m the R_t value would be 0.13m. This is only a theoretical value though, since the sonographs do not show the true distance values. As mentioned in Section 3.2.2.4 distortion in the along-track direction of a sonograph is affected by the variations of the speed of the survey vessel over the ground as well as the paper speed of the recorder.

3.2.2.6 Waverley Sonar 3000

The side-scan sonar system employed during the second and third field season was the Waverley Sonar 3000 operating at a lower frequency of only 100kHz. Like the Klein Hydroscan it is a dual-channel system with its transducers housed in a tow fish. The depression angle of the transducers is 10° and the beam has a horizontal angle of less than 1.5° and a vertical angle of higher than 50°. The pulse length is 100µs. As in Section 3.2.2.5 the theoretical range resolution (T_{sf}) can be calculated as

$$T_{sf} = 100\mu s \cdot 1500m/s = 0.15m$$

resulting in the same value as for the Klein Hydroscan. The real range resolution (R_r) is of a different value due to another paper width. The paper width of the thermal linescan recorder of the Waverley Sonar 3000 is 152.5mm per channel. For the same range setting of 75m per channel the real range resolution is therefore as follows

$$R_r = \frac{75}{152.5} = 0.49m$$

The transverse resolution (R_t) also has a different value due to its different horizontal beam angle which is twice the width of the Klein Hydroscan system. The transverse resolution (R_t) of the Waverley Sonar 3000 system with a beam angle of 1.5° at a range setting of 75m is therefore

$$R_t = (sin 1.5)75 = 1.96m$$

which shows that a narrower beam angle results in a better transverse resolution. At a range of only 10m the R_t value for this system would still be only 0.26m.

3.2.3 Position-fixing

Any measurement or observation made for any kind of study must be located with reference to a defined map co-ordinate system. Accurate position-fixing is essential to make it possible to return to a previously identified site and to compile observations made at different sites into maps/charts showing their correct spatial relationships (McQuillin and Ardus, 1977).

3.2.3.1 Global Positioning System (GPS)

The method of position fixing used in this project is the Global Positioning System (GPS) which depends on the reception of signals from a group of satellites operated by the US Government (McQuillin and Ardus, 1977), Department of Defence, with its master control station situated in Colorado Springs. The system has been primarily designed for the US military but also provides instantaneous navigation/position information to anyone with a GPS receiver. The system consists of 24

satellites working in six orbital planes (Magellan, 1990) (Fig. 3.24). Each satellite is in a fixed orbit and circles the Earth twice daily at a height of about 20,200km above the Earth's surface (Kumm, 1993) and an inclination of 55° from the equator (Magellan, 1990). The satellite orbits were chosen so that the signal of at least four satellites can be received anywhere on the Earth at any time (Kumm, 1993). Most receivers give a two-dimensional (2-d) or three-dimensional (3-d) mode. The 2-d mode needs a minimum of three satellites in direct view of the unit's antenna to give a position fix in latitude and longitude. The 3-d mode needs to receive the signal of four satellites in order to give a position fix of not just latitude and longitude but also altitude (Ardö and Pilesjö, 1992).

The satellites emit two carrier waves at f1=1575.42MHz and f2=1227.60MHz (Rogowski, 1995) which are modulated with two types of code. The generally accessible code is the C/A-code (clear or coarse acquisition) and is transmitted on f1. The P-code (protected or precise) is transmitted on both carrier waves but is reserved for military use. The C/A-code consists of 1000 bits and is transmitted in one microsecond giving it a code length of 300km at the speed of light. Both carrier waves also transmit navigation information (1500 bits) which consist of

- corrections of the satellite clock
- Almanac data
- Ephemeris data of each satellite.

Each satellite has its own nuclear clock/timer which runs on GPS-Time but even these show slight variations between all 24 satellites and therefore corrections have to be sent to the receiver. The Almanac data contain the approximate location of every satellite in the system and are necessary to quickly locate them as well as to do pre-calculations. The Ephemeris data are essential for the GPS receiver to obtain the exact position of each satellite. These data are updated by each satellite computer as well as by the master control station (Kumm, 1993). If, for any reason, a satellite is not operating properly, it will be marked as "unhealthy" by a ground control station and will then be ignored by receivers (Magellan, 1990). The Department of Defence also has the ability to degrade the satellite signal. This is called SA for Selective Availability and is operated for the C/A-code. During the Gulf War the US did not have enough military GPS receivers to use the P-code. Therefore,

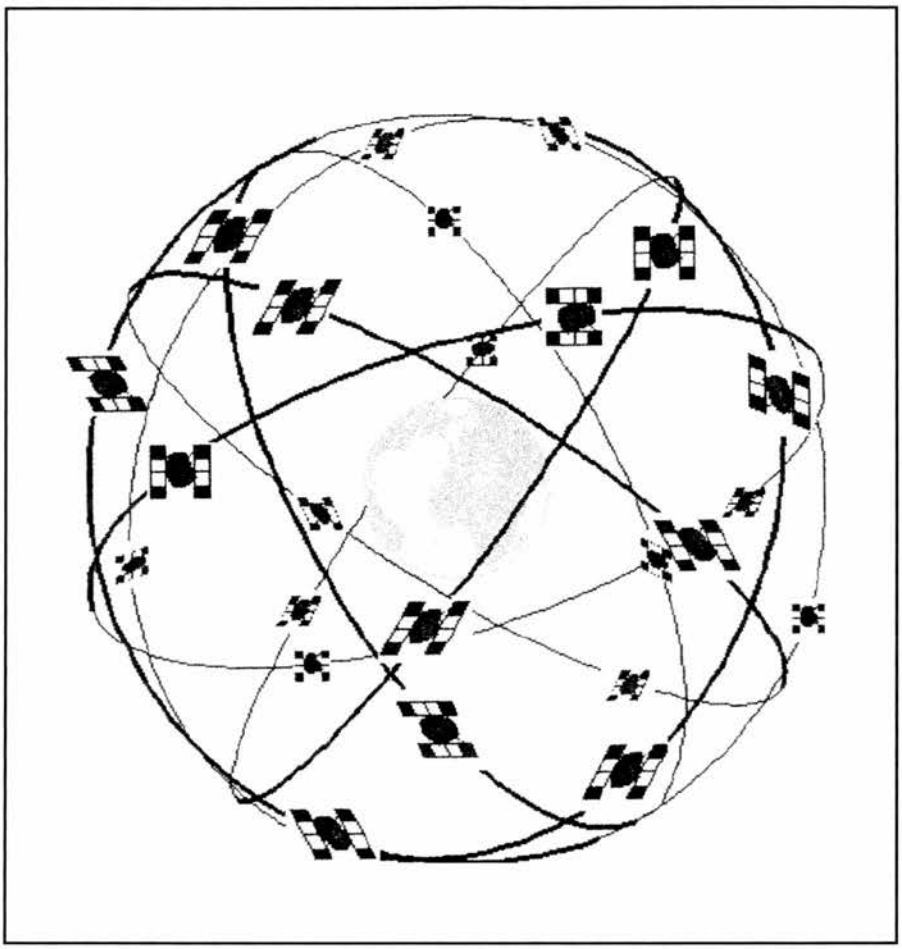

Fig. 3.24: Orbital configuration of the 24 GPS satellites consisting of four satellites in each of the six orbital planes (after Kumm, 1993).

the SA degradation was switched off resulting in a higher accuracy (Kumm, 1993).

3.2.3.2 Magellan NAV 1000 PLUS GPS receiver

The Magellan NAV 1000 PLUS is a hand held unit and therefore easily transportable (Plate 3.4). For continuous operation it can be connected to a standard 12 volts DC battery making it an ideal position fixing equipment for the surveys conducted for this project.

To obtain a 2-dimensional position fix the GPS receiver gathers information from an Almanac of one satellite to locate the other two required satellites. The receiver will search first for satellites at a minimum of 10° above the horizon (Fig. 3.25) and, if there are not enough satellites available, it will automatically search as low as 5° near the horizon. Still there may be times when low elevation satellites are blocked, e.g. by mountains or buildings, from the unit (Fig. 3.26). If the receiver has trouble locating three satellites, it may be switched to a different mode which lists all satellites 5° above the horizon and then the user may determine if those satellites are being blocked by obstructions. It takes approximately 2.5 minutes for the receiver to search for the signal of three satellites (Magellan, 1990). The receiver then determines the time of transmission and reception of the signal of each satellite. The difference in these times is then multiplied by the speed of light to obtain the satellites' distance from the receiver. To determine a position fix in degrees of latitude and longitude the calculated distance and the calculated orbital position of each satellite is used. In the continuous mode the Magellan receiver automatically updates the position every three seconds (Magellan, 1990).

The accuracy of a position fix is affected mainly by the signal quality (SQ) and the geometric quality (GQ). The signal quality gives an indication of the carrier to noise ratio (C/No) of the satellites' signals being used. The SQ level ranges from 0 (lowest quality) to 9 (highest quality). According to Magellan (1990) an SQ of at least 4 is high enough not to cause reliability problems. The GQ is based on the Position Dilution of Precision (PDOP) and is a measurement of the geometry of the satellites used for triangulating the position. The more spread out the satellites are, the better the accuracy of the position fix. Like the SQ the level of the GQ

Plate 3.4: The Magellan NAV 1000 PLUS Global Positioning System (GPS) receiver.

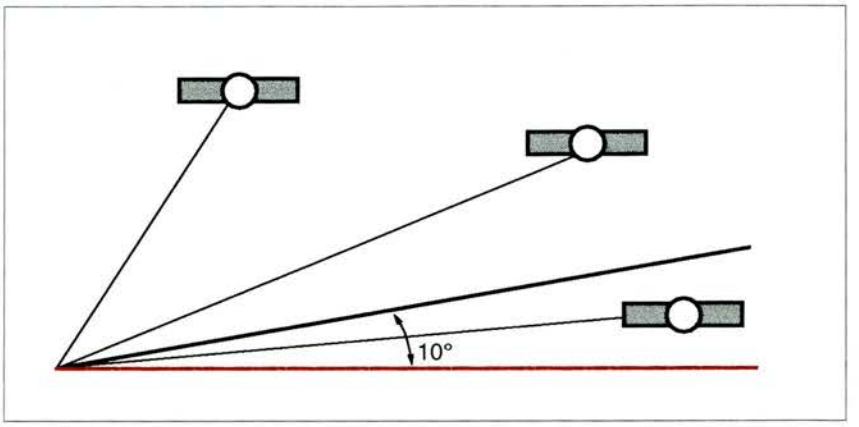

Fig. 3.25: Satellite coverage available for position fixes (after Magellan, 1990).

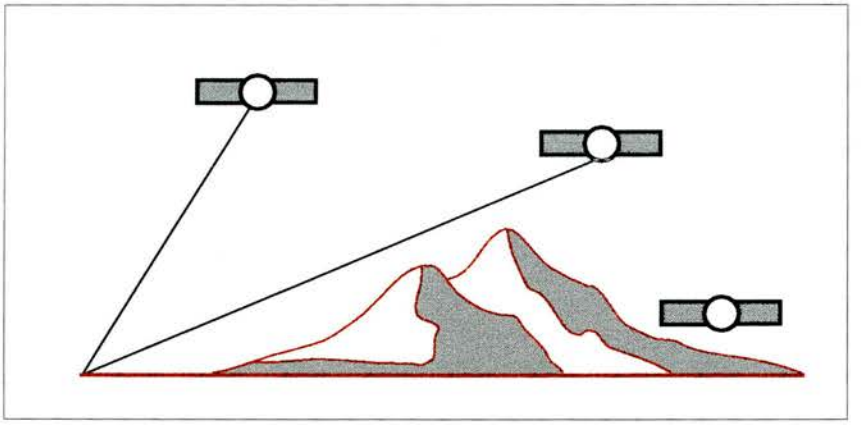

Fig. 3.26: Low elevation satellite blocked by obstruction (after Magellan, 1990).

ranges from 1 to 9 with a GQ of at least 7 indicating that the PDOP is such that the geometry should not be a cause of accuracy problems. If the quality levels fall below the value 4, a warning symbol appears on the display implying that the position fix should not be used for navigating (Magellan, 1990). Ardö and Pilesjö (1992) tested the Magellan GPS NAV 1000 receiver for accuracy and found that the largest error (total error=44m) in 2-d mode of 50 measurements had a signal as well as geometric quality of 9. They also found that a signal quality of less than 4 did not influence the error. The results of their study indicate that no systematic errors are connected with the Global Positioning System using a Magellan GPS NAV 1000 receiver. Magellan (1990) gives an accuracy of 25m or better in the C/A-code, while Lorimer (pers. comm., 1992) has found the accuracy to be of the order of ±8m.

Chapter 4

TRANSVERSE SEDIMENTARY STRUCTURES IN ESTUARIES

4.1 Introduction

Lack of agreement on classification and nomenclature of sedimentary bedforms in fluvial, intertidal and marine environments has led to some confusion. This chapter aims to define and describe the bedforms recorded in this project by side-scan sonar. Due to the resolution of the equipment only so called large-scale subaqueous bedforms will be examined.

According to Ashley (1990) all large-scale transverse bedforms (excluding ripples and antidunes) occupy a similar position in the lower-flow-regime sequence between ripples and upper plane bed. The wide variety of forms reflects the various hydrodynamic conditions as well as sediment type. Naturally occurring bedforms do not fall into specific size classes but form a continuum with wavelengths (crest to crest spacings) of between less than 1m to over 1000m.

Unlike the terms *sand wave* or *megaripple* which have been used for many different sedimentary configurations by various authors, the term *dune* has been used by researchers at the beginning of this century (Ashley, 1990) to document the position of large bedforms within the flow regime context. Therefore she suggests that these sedimentary bedforms should be termed dunes, a term which is then modified by primary descriptors of shape and size and the adjective subaqueous to distinguish them from aeolian dunes.

4.2 Classification

The new classification after Ashley (1990) which has been accepted by many workers such as Harris *et al.* (1992), Kostaschuk *et al.* (1995) and Dalrymple and Rhodes (1995) is shown in Table 4.1 and is based on a morphological classification scheme. According to Ashley (1990) sedimentary structures left by migrating bedforms should be described according to their morphology which is directly linked to flow regime.

Table 4.1: Classification of dunes (after Ashley, 1990, and after Dalrymple and Rhodes, 1995).

First-order descriptors:

size	term	small	medium	large	very large
	spacing (m)	0.6-5.0	5-10	10-100	>100
	height (m)	0.05-0.25	0.25-0.5	0.5-3.0	>3
shape	2-d: relatively straight crested, lacking scour pits				
	3-d: sinuous to lunate, with scour pits				

Second-order descriptors:

superposition	simple - lacks superimposed dunes
	compound - bears smaller, superimposed dunes
sediment characteristics	grain size and sorting

Third-order descriptors:

bedform profile (stoss and lee slope lengths and angles)
fullbeddedness (fraction of bed covered by bedforms)
flow structure (time-velocity characteristics)
relative strength of opposing flows
dune behaviour and migration history
orientation: transverse, oblique, longitudinal

Therefore, the first order descriptors are size and shape which divide the dunes into categories of *small*, *medium*, *large* and *very large*, as well as into 2-dimensional (2-d) and 3-dimensional (3-d) forms. The latter is viewed from the standpoint of the water flow: some bedforms can be treated as 2-d since only two coordinates are needed to describe them on one transect parallel to the flow. This type of bedform usually has a length or breadth which is large compared to its height (Allen, 1968) and is relatively straight crested (Dalrymple and Rhodes, 1995). Three-d forms on the other hand are characterised by sinuous to lunate crests with scour pits in their troughs and curved lee faces (Dalrymple *et al.*, 1978; Ashley, 1990; Dalrymple and Rhodes, 1995). The second order descriptors include superposition and sediment type while the third order descriptors describe the details of bedform morphology, bedform behaviour and flow characteristics. Table 4.2 gives a summary of the most commonly used

names for sedimentary bedforms of various sizes and shapes as well as their new terms after Ashley (1990).

Table 4.2: Previously used bedform names and their new terminology (after Ashley, 1990).

old term	reference	new term
large scale ripple sand wave	Allen (1968) Belderson *et al.* (1982)	dune
megaripple	Boothroyd & Hubbard (1975) Dalrymple *et al.* (1978)	small to medium, simple dune
type 1 megaripple linear megaripple low-energy sand wave	Dalrymple *et al.* (1978) Boothroyd & Hubbard (1975) Boothroyd (1985)	small to medium, simple, 2-d dune
type 2 megaripple cuspate megaripple sinuous megaripple	Dalrymple *et al.* (1978) Boothroyd & Hubbard (1975) Boothroyd (1985)	small to medium, simple, 3-d dune
rippled sand wave	Dalrymple *et al.* (1978)	large to very large, simple dune
sand wave megarippled sand wave high-energy sand wave	Langhorne (1973) Dalrymple (1984) Dalrymple *et al.* (1978) Boothroyd (1985)	large to very large, compound dune

4.3 Distribution

Dunes form under a broad range of conditions and are therefore extensively developed in many estuaries. Numerous examples of dunes have been described in tide-dominated estuaries and tidal inlets, including the Thames Estuary, UK (Langhorne, 1973), Parker and Essex Estuaries, USA (Boothroyd and Hubbard, 1975), Long Island Sound, USA (Bokuniewicz *et al.*, 1977), Westerschelde Estuary, Netherlands (Boersma and Terwindt, 1981), Doboy Sound, USA (Zarillo, 1982) and Bristol Channel and Severn Estuary (Harris and Collins, 1985).

Generally the distribution of dunes is controlled by the hydrodynamics and sediment characteristics. Channels with sand-sized beds tend to develop a wide range of bedforms which have been extensively studied in attempts to link flow conditions with bedform type (Reid and Frostick, 1994). Bedform phase diagrams (Fig. 4.1) show the combinations of mean flow speed and mean grain size as well as mean flow speed and flow depth (Harms *et al.*, 1975; Leeder, 1982; Allen, 1983). However, most of these diagrams rely on data derived from experiments and cannot necessarily be applied to natural conditions where flows vary dramatically with location and state of the tide (Reid and Frostick, 1994). In general, dunes form and migrate at a minimum current speed of approximately 0.5m/s which depends on water depth and grain size (Dalrymple and Rhodes, 1995). Dalrymple and Rhodes (1995) suggest a minimum mean grain size of approximately 0.13mm or 2.9phi independent of water depth which is near the lower limit of fine sand while Reid and Frostick (1994) indicate an upper limit of 0.51mm. The major requirement is the presence of enough cohesionless sediment to form the dunes. Bokuniewicz *et al.* (1977) found an absence of dunes in areas where the silt content of the sediment reached approximately 10% but they also state that dunes were absent in areas where the coarse fraction (>1mm) of the sand was greater than about 12%. The distribution of bedforms in their study in Long Island Sound indicates, however, that the dune height is independent of water depth although they have found that the water depth imposes an upper limit on the height of the dunes. Therefore, dunes seem to exist only in areas of certain sediment grain size.

4.4 Size

The wavelength and height of dunes is a complex function with the main variables being water depth, current speed and sediment grain size. Water temperature, sediment availability and age, or rather time-history, also influence the size of dunes, although Allen (1976) notes that bedform dimensions exhibit random variability even under the steady, equilibrium conditions of his experimental study.

Measurements of height and wavelength of dunes in various environments have shown a positive relationship with water depth despite considerable scatter (Dalrymple and Rhodes, 1995). It is suggested that the scale of current ripples depends on grain size whilst that of dunes depends on flow

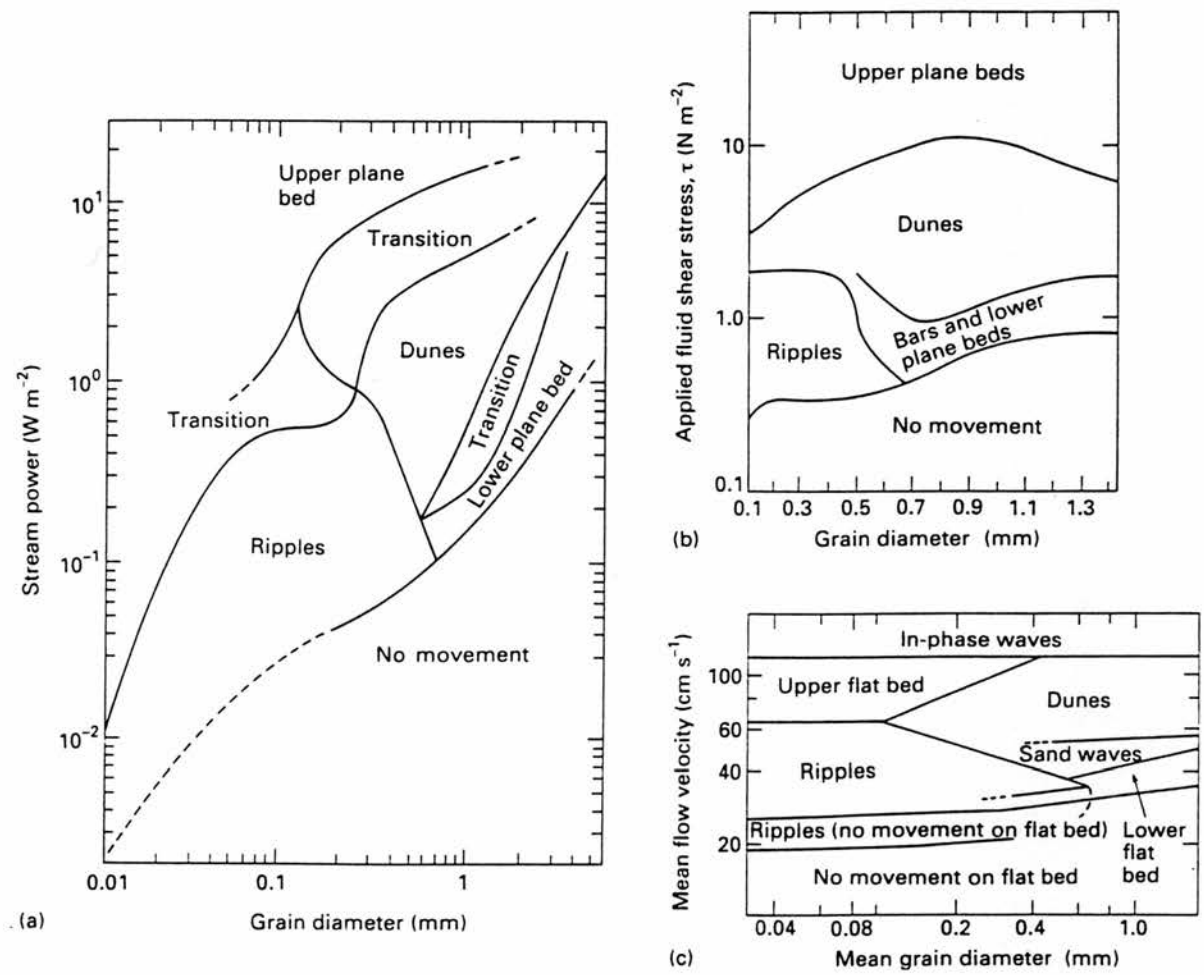

Fig. 4.1: Bedform phase diagrams: (a) after Allen (1983), (b) after Leeder (1982) and (c) after Harms *et al*. (1975).

depth (Dyer, 1972). Therefore, large to very large dunes generally occur in deep channels while the smaller dunes can be found on intertidal flats (Boothroyd and Hubbard, 1975; Dalrymple *et al.*, 1990). But, as mentioned in Section 4.3 Bokuniewicz *et al.* (1977) have not found a unique relationship between water depth (d) and dune height (H) and note that the formula suggested by Allen (1970)

$$H = 0.086 d^{1.19}$$

only gives an upper limit to dune height. However, Yalin (1964) suggested a contradictory relationship between water depth (d) and dune height (H) of

$$H = 0.167 d$$

and between water depth (d) and wavelength (L) of

$$L = 6 d$$

on the basis of laboratory and field measurements of mobile dune systems.

Current speed or rather flow strength has a major influence on bedform size. If the other variables are constant, dune height increases with increasing current speed, up to a maximum value, before decreasing as the speed reaches antidune conditions (Dalrymple and Rhodes, 1995). Near the upper-flow-regime boundary the height of dunes is thought to be low due to an increase of suspended sediment and a planing-off of the dune crest (Boothroyd and Hubbard, 1975). In contrast with the generally accepted idea of a positive correlation between flow strength and bedform dimensions, Goedheer and Misdorp (1985) have found the largest bedforms, in their side-scan sonar study of a subtidal channel at the mouth of the Oosterschelde (Netherlands), in the shallowest parts, associated the smallest current velocities and varying current directions. They point out that this may be due to the fact that the area was in a subtidal environment rather than intertidal and it may be an isolated case. In nature flow conditions change continuously so that bedforms do not remain in equilibrium. However, it takes finite time to transport the sediment volume needed to change dune morphology so that bedforms lag behind the change in flow condition (Dalrymple and Rhodes, 1995). Therefore it is

difficult to determine a specific set of hydraulic conditions responsible for bedforms. A reasonable approximation to these "effective" conditions is obtained by assuming that the major bedforms are produced by the peak flow during the dominant half of the tidal cycle (Dalrymple *et al.*, 1978). According to Allen *et al.* (1994) the cross-sectional area of a dune is broadly proportional to the square of the wavelength and therefore its ability to respond to a given change must decline with an increase in size. Generally less sediment needs to be moved to raise or lower the height of a dune than to change its wavelength so that dune heights vary much more rapidly than their wavelengths. Hine (1975) found a positive relationship between height and wavelength for small dunes only and not for dunes with wavelengths over 50m.

Grain size seems to be another important variable influencing bedform size but the relationship is poorly understood. So far field studies have reported a positive correlation only between dune wavelength and grain size (e.g. Cook and Gorsline, 1972) while flume data have indicated a negative correlation according to Dalrymple and Rhodes (1995).

Fullbeddedness, as termed in Ashley's (1990) classification, influences dune height because an insufficient amount of transportable sediment would produce only relatively low dunes if any. The limiting amount of sediment needed to form dunes is not known (Dalrymple and Rhodes, 1995).

Dune size is thus dependent on a complex association of processes involving water depth, current speed, sediment grain size, water temperature, sediment availability and flow history, and cannot be related to one variable only.

4.5 Shape

When examining dune shape two aspects need to be considered:

1) the vertical profile shape and
2) the shape in plan view (Fig. 4.2).

Plots of dune height against wavelength for bedforms in natural conditions show a good positive correlation. However, as dunes become larger they tend to become flatter (Dalrymple and Rhodes, 1995). Most estuarine

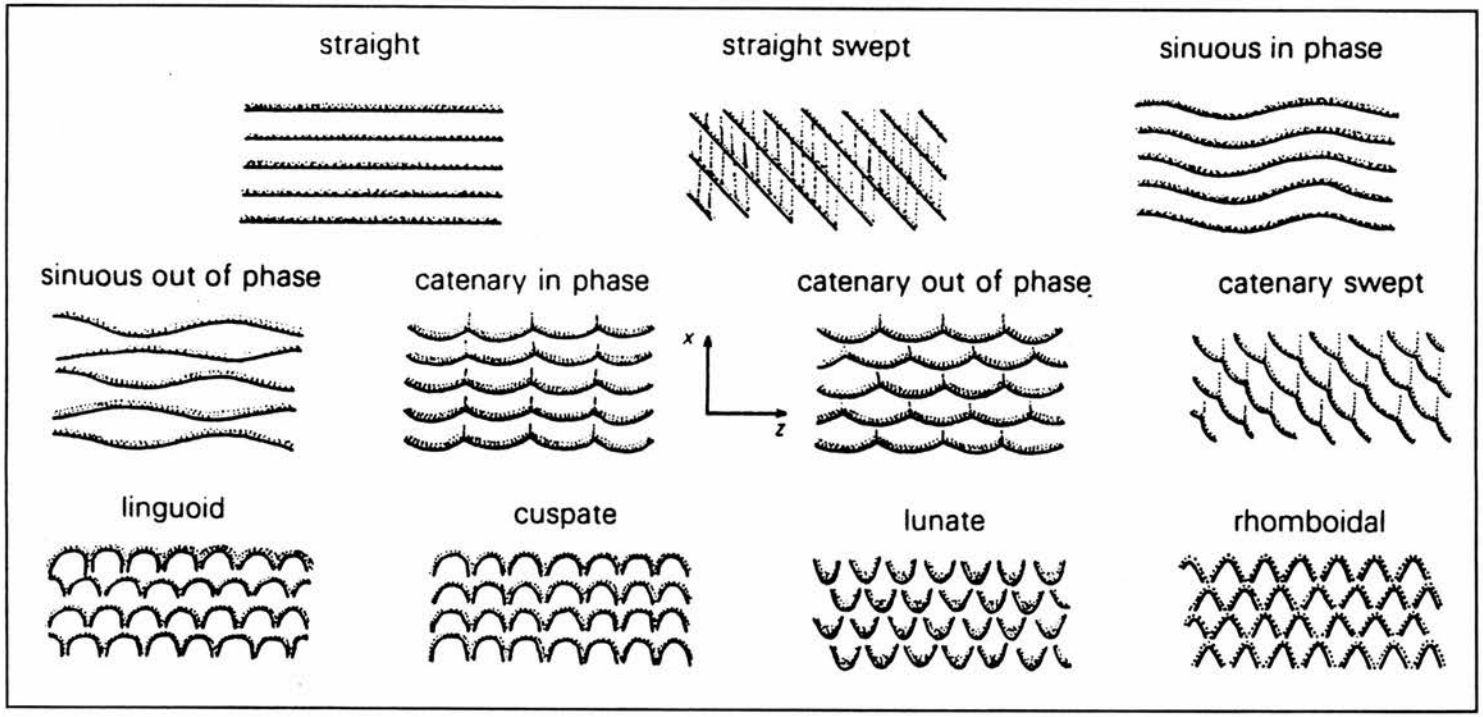

Fig. 4.2: Descriptive terms of plan patterns used for subaqueous bedforms (after Collinson and Thompson, 1989).

dunes have an asymmetric profile with a steep lee side and a gentle stoss side produced by an asymmetrical time-velocity profile of tidal currents (deVries Klein, 1970). The lee side faces in the direction of net sediment transport. The shape mainly depends on the strength of the dominant and subordinate currents and the orientation of the dune relative to the net transport direction, as well as on the presence or absence of superimposed dunes. Small to medium simple dunes have lee-side slope angles in the range of 15°-25° and stoss-side slopes of between 2°-5° (Dalrymple and Rhodes, 1995). Depending on the state of the tide dunes change their profile shape. Especially when viewed after the subordinate tide, small to medium dunes commonly exhibit partially reversed forms. Average slope angles for lee faces of larger and compound dunes are typically less than 10° but may be as low as 1°-2°. Stoss side slope angles for large and very large dunes are in the range of 1°-3°. Generally larger dunes have lower angles than smaller dunes (Dalrymple and Rhodes, 1995). Symmetrical forms indicate areas of zero net sediment transport (McCave and Langhorne, 1982) or where neither tide dominates the other.

Boothroyd and Hubbard (1975) and Dalrymple *et al.* (1978) have shown that the plan shape of dunes changes in a predictable manner according to the increase in current speed. Two-d dunes with nearly straight crests and lee faces and a uniform height along their length are formed at low current speeds (Open University, 1993). With increasing current speed 3-d dunes are formed with sinuous lee faces and scour pits. Three-d forms are the most widely developed type of dune in the small and medium size classes (Dalrymple and Rhodes, 1995).

4.6 Orientation

Bedform orientation is commonly used to estimate the direction of sediment transport. In most estuaries the confinement of the tidal currents by channel banks produces rectilinear flow, therefore most tidal dunes should be nearly transverse to ebb and flood flow. Various studies of estuaries (Langhorne, 1973; Boothroyd and Hubbard, 1975; Dalrymple, 1984) have found large-scale dunes of oblique orientation to the dominant current or residual sediment transport direction and not of perpendicular orientation as widely assumed. If the local situation is influenced by channel bends and irregular shorelines, the orientation may change and oblique or longitudinal bedforms may form (Dalrymple and Rhodes, 1995).

Hine (1975) measured bedform orientation in the flood-tidal delta of Chatham Harbor Estuary, Massachussetts, and plotted the orientations in a rose diagram which revealed a trimodal trend. The three modes were interpreted as reflecting the distinct bedform responses to the three different directions of flood flow in the estuary. Field observations showed that the current changes direction during mid-flood and at a second time during late flood while bedforms were unmodified by the small ebb flow. Hence, estimation of sediment transport direction should not be entirely based on bedform asymmetry but should also be supported by current direction data.

4.7 Superimposed dunes

Most larger estuarine dunes act as platforms for smaller dunes. These superimposed small dunes commonly occur on both the stoss and lee sides of the larger ones (Dalrymple and Rhodes, 1995). Langhorne (1973) found smallest superimposed dunes on the crests of the larger dunes. A common observation is the oblique orientation of superimposed dunes relative to the larger form (Langhorne, 1973; Boothroyd and Hubbard, 1975; Dalrymple, 1984) suggesting a secondary flow regime. The most logical explanation for this phenomenon would be that the near-bed current which forms the smaller superimposed dunes has a different direction than the main flow which forms the larger platform dunes (Dalrymple and Rhodes, 1995). McCave and Geiser (1979) presume that this oblique orientation reflects the ebb runoff flow. Using superposition to classify bedforms would imply a fundamental difference between simple dunes and dunes with superimposed forms. According to Ashley (1990), large-scale bedforms with superimposed ripples and dunes form wherever flow conditions are appropriate and space and time for growth and migration is available. Therefore, superposition is used only as a second order descriptor in her classification. However, it is important to record the dimensions of both small and large bedforms as well as the orientation of the smaller structures related to the larger ones and to note whether the smaller forms are confined to certain areas of the larger ones (such as stoss side, lee side or crest) (Collinson and Thompson, 1989).

4.8 Migration

Langhorne (1973), Bokuniewicz *et al.* (1977), Dalrymple (1984) and Kostaschuk *et al.* (1989), as well as others, have recorded migration rates for dunes. These values cover a large range from 0 to >5000m/yr and vary greatly within and between areas. Generally the migration rate decreases as the bedform height increases. Small dunes migrate a lot faster (100-300m/yr) than larger dunes (25-75m/yr) and very large dunes may even migrate for only a few decimetres per year (Dalrymple and Rhodes, 1995). Due to these differences in migration rates, the smaller superimposed dunes migrate faster than the larger "platform" dunes, "moving up the stoss side and onto the lee side where they are partially or completely "absorbed" by deposition as they migrate downward into areas with lower current speeds and sediment transport rates" (Dalrymple and Rhodes, 1995). In areas with nearly equal flood and ebb tidal flow dunes are stationary or migrate only slowly while in areas with a clear ebb or flood dominance they migrate faster. Migration rates of dunes are mainly controlled by the time-velocity pattern of bottom-current velocities during a tidal cycle and water depth (deVries Klein and Whaley, 1972). Boothroyd and Hubbard (1975) give an estimate of the minimum current velocity (0.60m/sec) for small to medium dune migration. Even though 3-d dunes are higher they migrate faster than 2-d dunes which are formed by slower currents (Dalrymple and Rhodes, 1995). Boersma and Terwindt (1981) have reported variations of migration rates of dunes depending on the neap-spring tidal cycle, indicating the importance of current speed. Langhorne (1973) has also measured dune migration which indicated movement at an unsteady rate. In his study of the Outer Thames Estuary, Great Britain, it appears that parts of dunes slowed in movement and then stabilised while further movement occurred elsewhere on the bedform.

4.9 Summary

Dunes are widely developed in the estuarine environment. Individual bedforms change in size, shape, position and orientation as the local currents remodel them with time. Through their own morphological changes, they influence the local flow patterns and strength of flow over the bed. Not only do individual bedforms change once established but new bedforms are formed to replace those being destroyed. Dune size, shape, distribution, orientation, superposition and migration rate depend on flow

strength, dominant flow direction, sediment characteristics, water depth, water temperature and sediment availability. Werner and Newton, as long ago as 1975, concluded that large-scale subaqueous bedforms are inadequately known in respect to their classification, composition and geometry as well as the hydrodynamics of their formation and more field studies are needed in order to combine theory with natural occurrence. Although a large amount of literature on subaqueous dunes now exists, many important aspects of their morphology and their response to changing conditions remain unsolved.

Chapter 5

SEDIMENTARY BEDFORMS RECORDED BY SIDE-SCAN SONAR

5.1 Introduction

The data gathered in this study refer to the sedimentary bedforms of the middle reaches of the Tay Estuary. Side-scan sonar was employed to investigate the bottom of this section of the estuary. Since the technique is based on acoustic remote sensing, it can provide only an indirect indication of the variability of the sea bed and its materials and may be used as a reconnaissance tool. Sonographs are often difficult to interpret and ideally require on-site verification to avoid mistakes. Therefore, echo-sounding was employed, sediment samples were collected and current measurements taken, the results of which are presented in the following three chapters. In addition, the bedforms identified from sonographs were statistically analysed to establish correlations between their various geometrical parameters and water depth, following similar studies by Allen (1970), Yalin (1977), Dalrymple *et al.* (1978), Zarillo (1982), Flemming (1988) and Berné *et al.* (1993) and several others.

5.2 Data collection

A systematic approach was taken to the collection of side-scan sonar data. Fieldwork started in August 1993 when nine traverses were run parallel to the Railway Bridge. The distance between traverses was about 100m. Throughout all surveys the side-scan sonar systems employed were set to a range of 150m, i.e. scanning 75m to either side of the transducer and hence giving a good overlap. The side-scan system employed for the first two days of fieldwork, on 27.08.93 and 26.10.93, was the Klein Hydroscan Model 401. A description of the system is given in Section 3.2.2.5. On 26.10.93 a further six traverses were run parallel to the Railway Bridge continuing coverage towards the east. Starting in February 1994 a different system was employed, namely the Waverley Sonar 3000, already described in Section 3.2.2.6. Trial runs were carried out along the Railway and Road Bridges on 10.02.94 with two traverses along the line of each bridge. Data collection then proceeded parallel to the Road Bridge with the Waverley system with three traverses on

20.05.94, six traverses on 02.06.94, seven traverses on 03.06.94 and five traverses on 02.11.94, progressing from east to west. The strong currents in the estuary often prevent the running of straight traverses and, although an overlap of data was achieved on the northern side due to some of the runs being parallel to the Railway Bridge and some parallel to the Road Bridge, an uncovered area still existed in the southern section of the fieldwork area. Therefore, short traverses were run on 14.03.95 to fill in the few remaining gaps.

5.3 Bedform geometries as recorded by side-scan sonar

Apart from a few minor gaps full coverage of the fieldwork area was obtained (Fig. 5.1). Overall, 43 lines were run, mainly in a general north-south direction. Although the sonographs were of varying quality, due to the use of two different systems and changing weather conditions, a general interpretation of the estuary floor was made. Sonographs from surveys carried out during different years were used in this analysis. However, this is deemed justifiable on the grounds that sonographs of the bed at the same locality, but obtained at different times, revealed a very close similarity of bedform geometries and distribution, as illustrated in Fig. 5.2.

A detailed interpretation of the sedimentary bedforms revealed by side-scan sonar was carried out. Without exception all bedforms observed were various types of dunes, according to the classification of Ashley (1990). These were analysed according to the following:

1) crest to crest spacing/wavelength
2) height
3) length along dune crest
4) crest shape/sinuosity
5) superposition
6) asymmetry
7) crest orientation.

Apart from length along the dune crest and sinuosity the above descriptors are based on the classification of Ashley (1990), as summarised in Chapter 4, while the other two parameters are described in Sections 5.3.3 and 5.3.4 respectively.

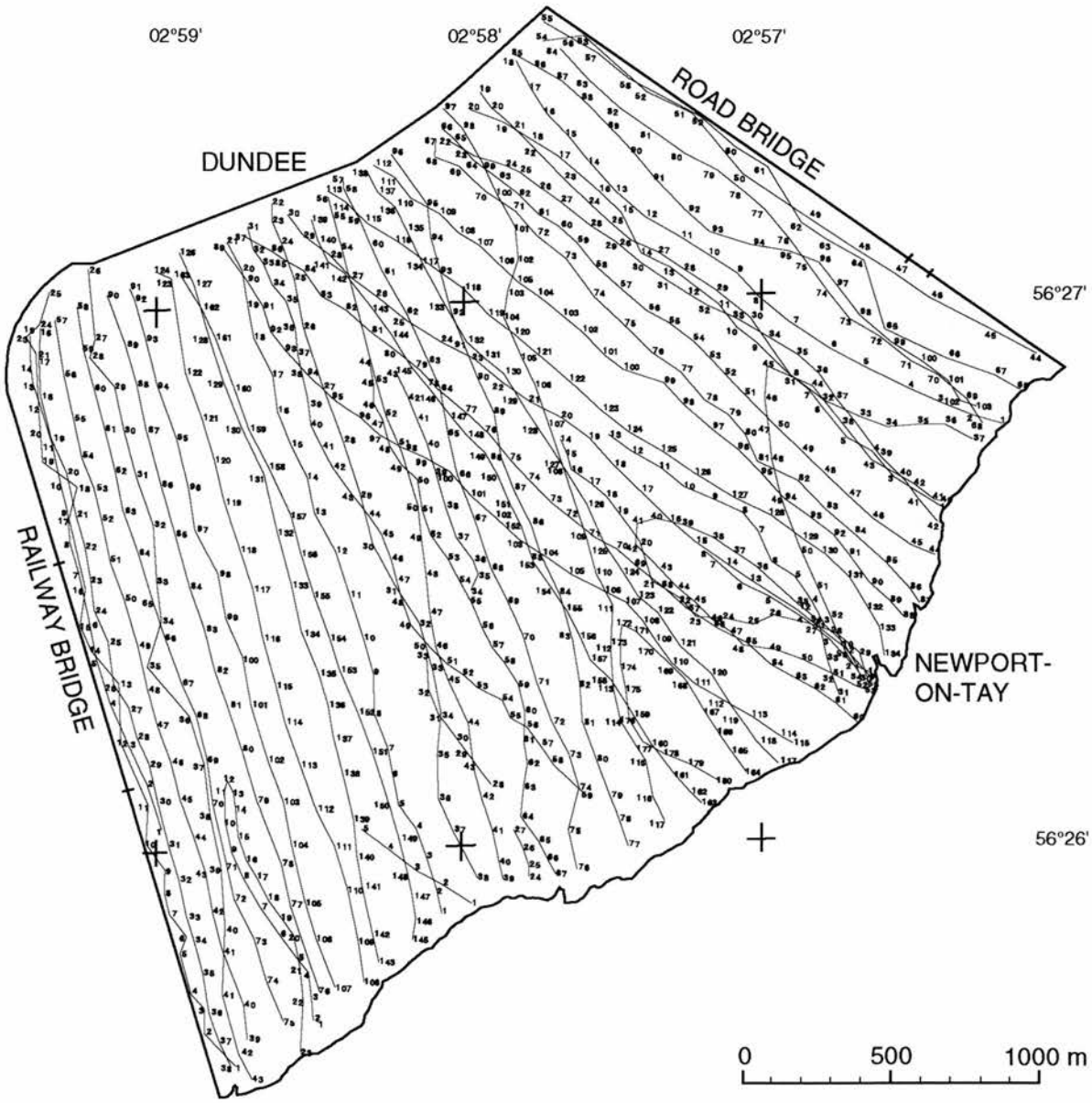

Fig. 5.1: Traverses of the side-scan sonar surveys. Numbers denote position fixes.

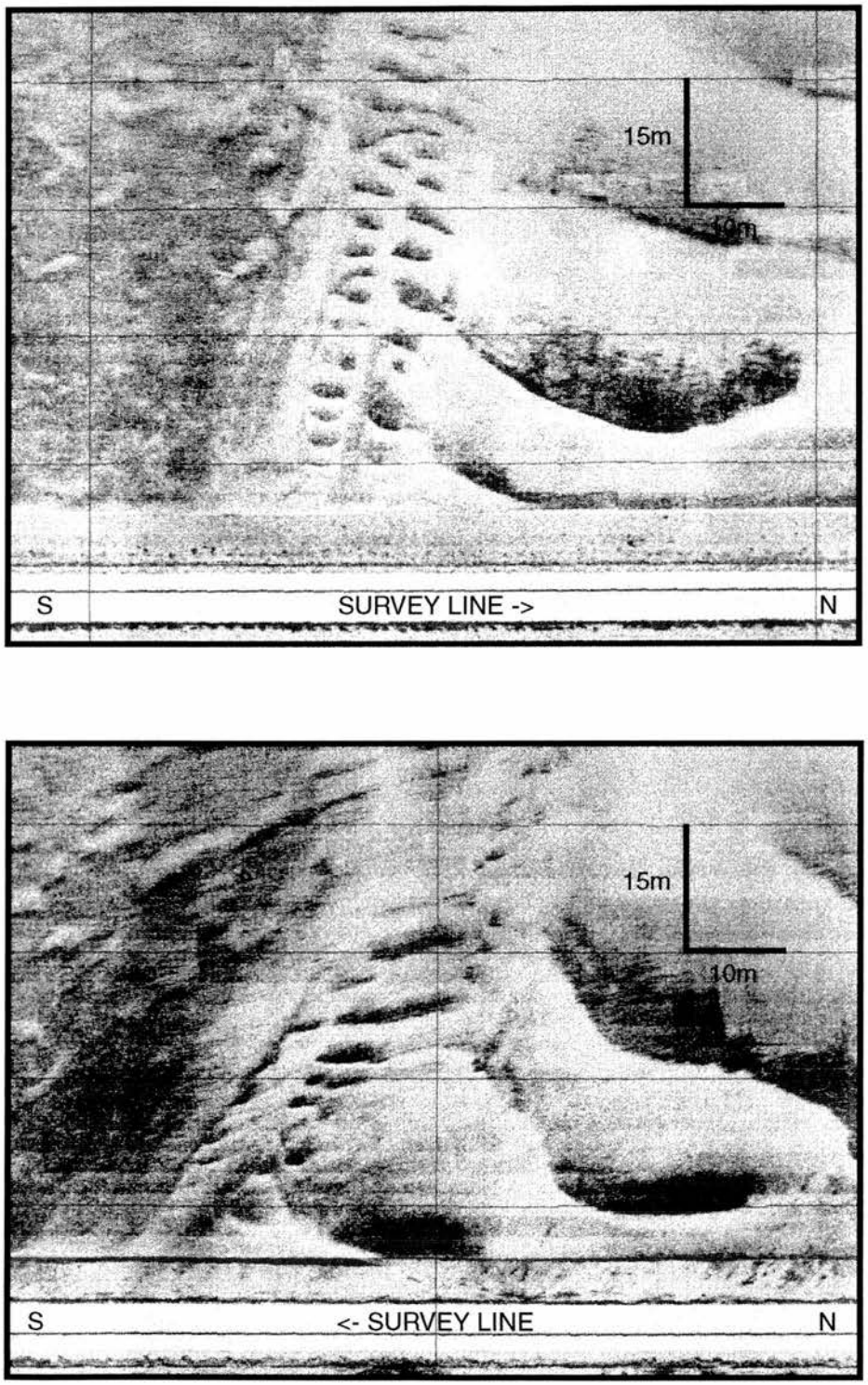

Fig. 5.2: Sonographs of bedforms recorded at the same locality (shown in Fig. 5.33) obtained on 03.06.94 (upper) and 14.03.95 (lower).

Since the geometry of some dunes tends to change between ebb and flood tidal conditions, the data were separated depending on the state of the tide at the time of recording. Therefore, one ebb and one flood map was drawn for each of the seven descriptors. The surveys were generally carried out over high slack water in order to have access to the full fieldwork area of which some dries out during low slack water. Consequently more lines were run during flood and slack tidal conditions than during the ebb tide when the water depth became too shallow to continue the survey. No traverses were recorded during low slack water. The areas not covered can be seen in Fig. 5.3 and Fig. 5.4 which show the traverses recorded during flood and slack tidal conditions or ebb, respectively, and are marked with question marks on the interpretation maps. Dotted lines were drawn on borders between two different bedform categories where no exact boundary could be interpreted from the sonographs. The white patches on all maps (Figs. 5.7, 5.9, 5.11, 5.13, 5.15, 5.16, 5.19, 5.22, 5.25, 5.26, 5.28, 5.29, 5.30, 5.31) indicate areas where no sedimentary bedforms exist or where they are too small to be detected by side-scan sonar as shown in the sonograph of Fig. 5.5 which was recorded on Middle Bank. Some sonographs show slight variations in tone which infer bedforms but, due to the resolution, they could not be measured.

5.3.1 Wavelength

Dune wavelength, also called crest to crest spacing, is the distance between the crests of adjacent bedforms. Due to the geometry of the acoustic pulse travelling through water and its reflection, the dune wavelength is generally easy to measure especially when a relatively large dune field is recorded. Commonly one channel of the sonograph allows a better interpretation when giving a good reflection from the steep lee side facing the outgoing pulse (appearing dark on the sonograph) followed by its acoustic shadow appearing as a blank area on the trace. The other channel will record the gentler stoss slope appearing in a lighter tone on the sonograph which does not always produce a distinct acoustic shadow. Slopes facing away from the transducer give only light reflections and may not be detectable (Fig. 5.6). Therefore, dune fields observed on both channels were easily detected while small individual dunes may have been overlooked. The morphological classification of dunes after Ashley (1990) divides crest to crest spacing into four classes: small - 0.6 to 5.0m,

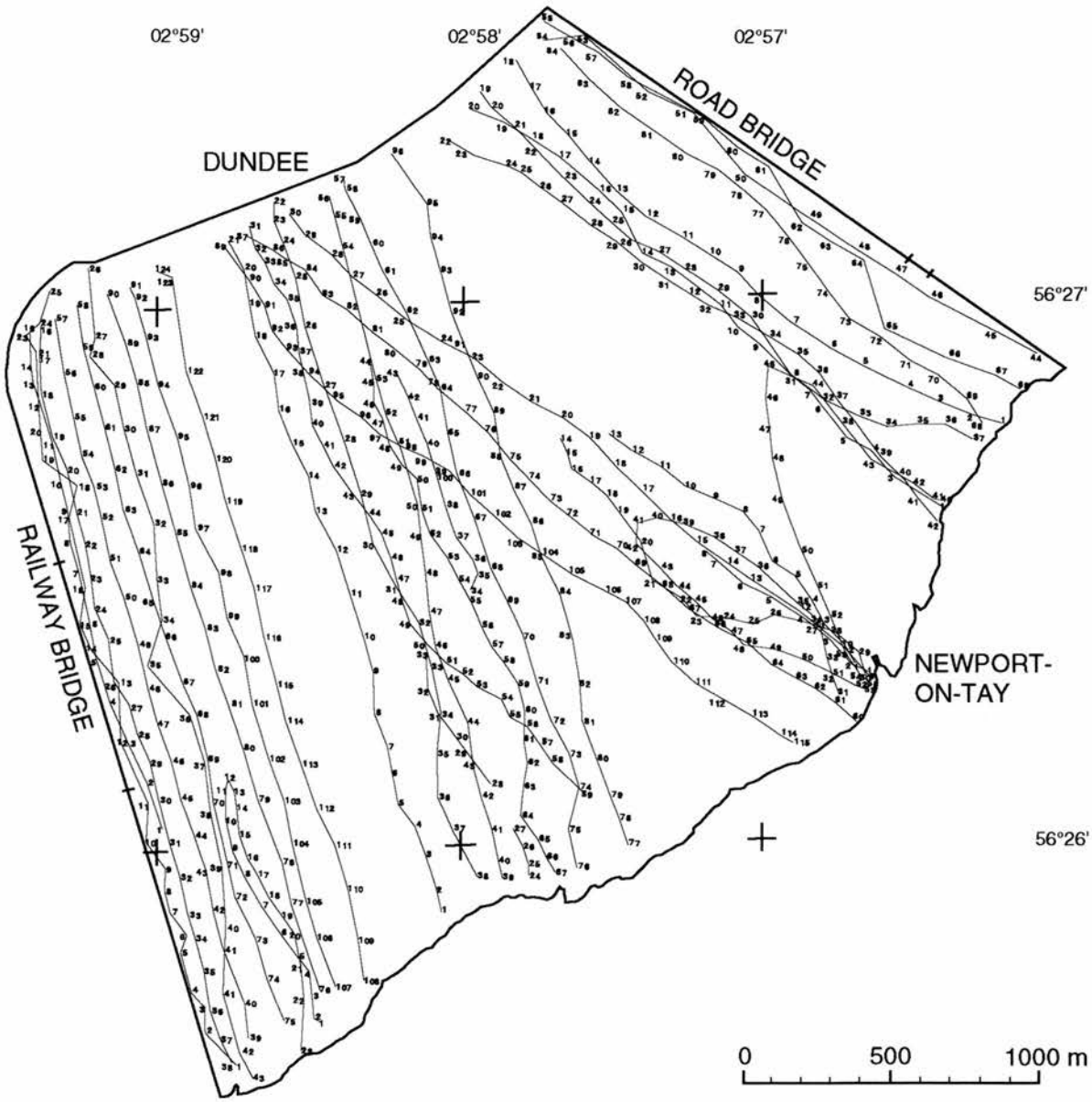

Fig. 5.3: Sonographs recorded during flood and slack tidal conditions. Numbers denote position fixes.

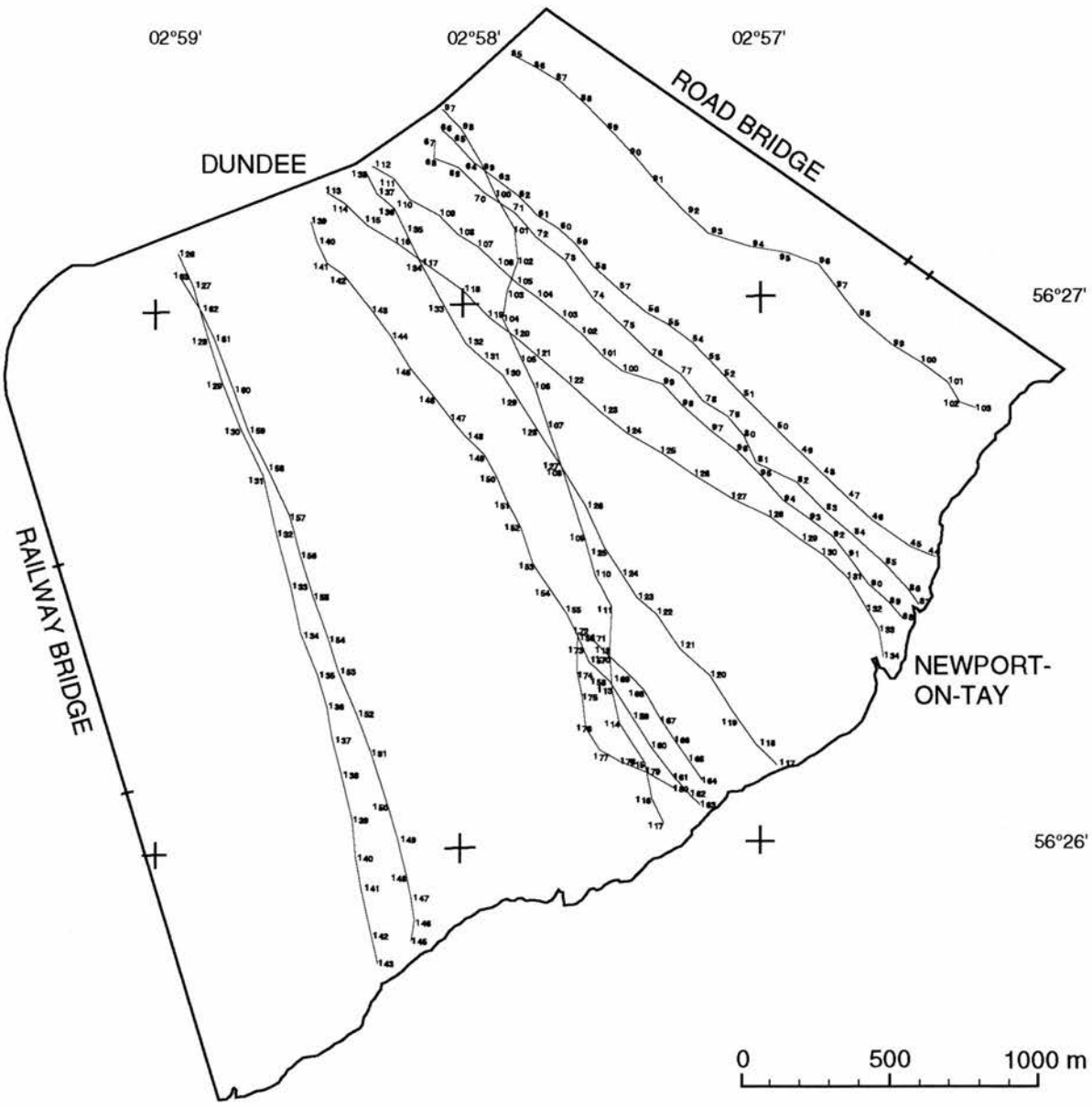

Fig. 5.4: Sonographs recorded during ebb tidal conditions. Numbers denote position fixes.

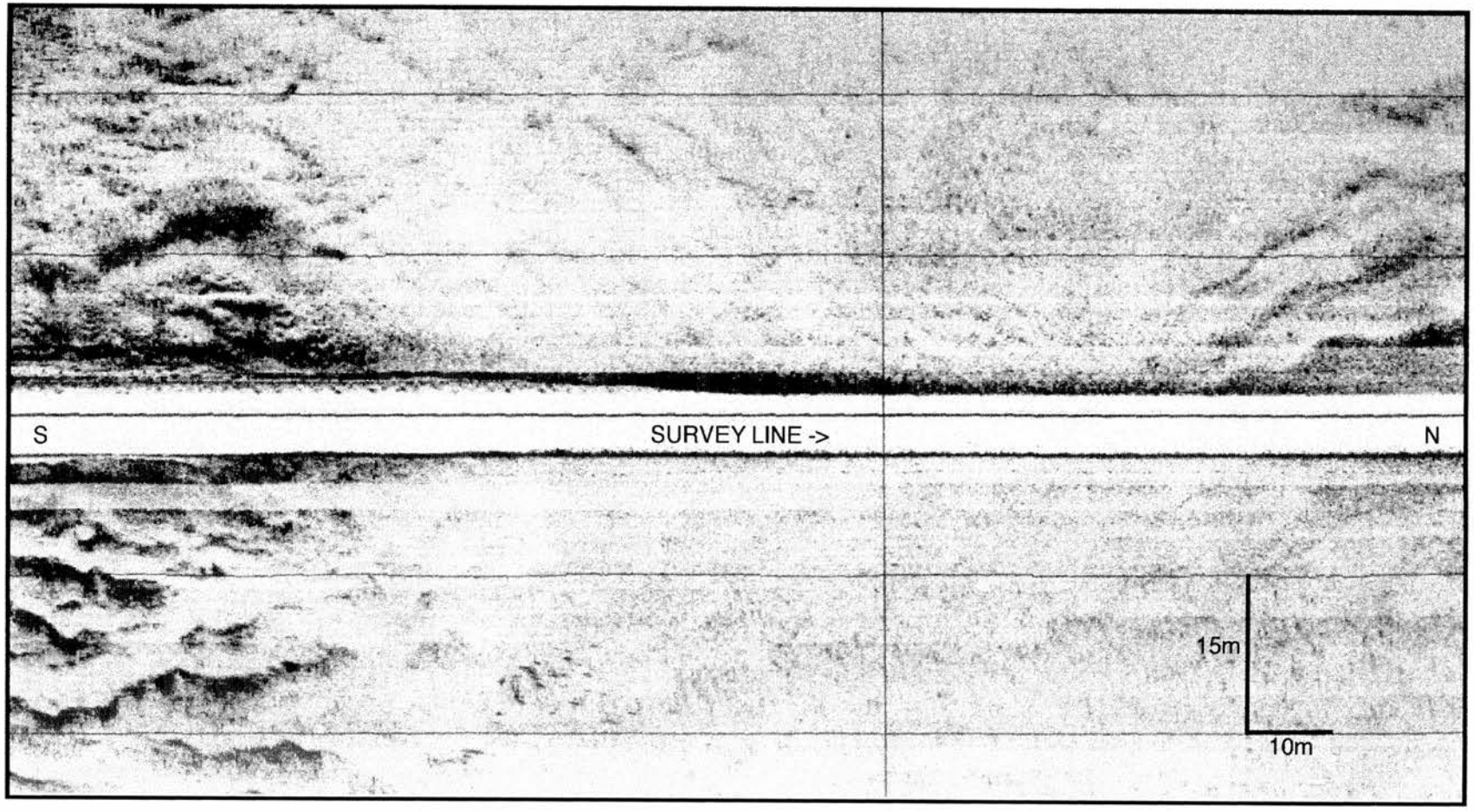

Fig. 5.5: Sonograph recorded on Middle Bank where no dunes could be detected in the east-central section. Location of record shown is shown in Fig. 5.33.

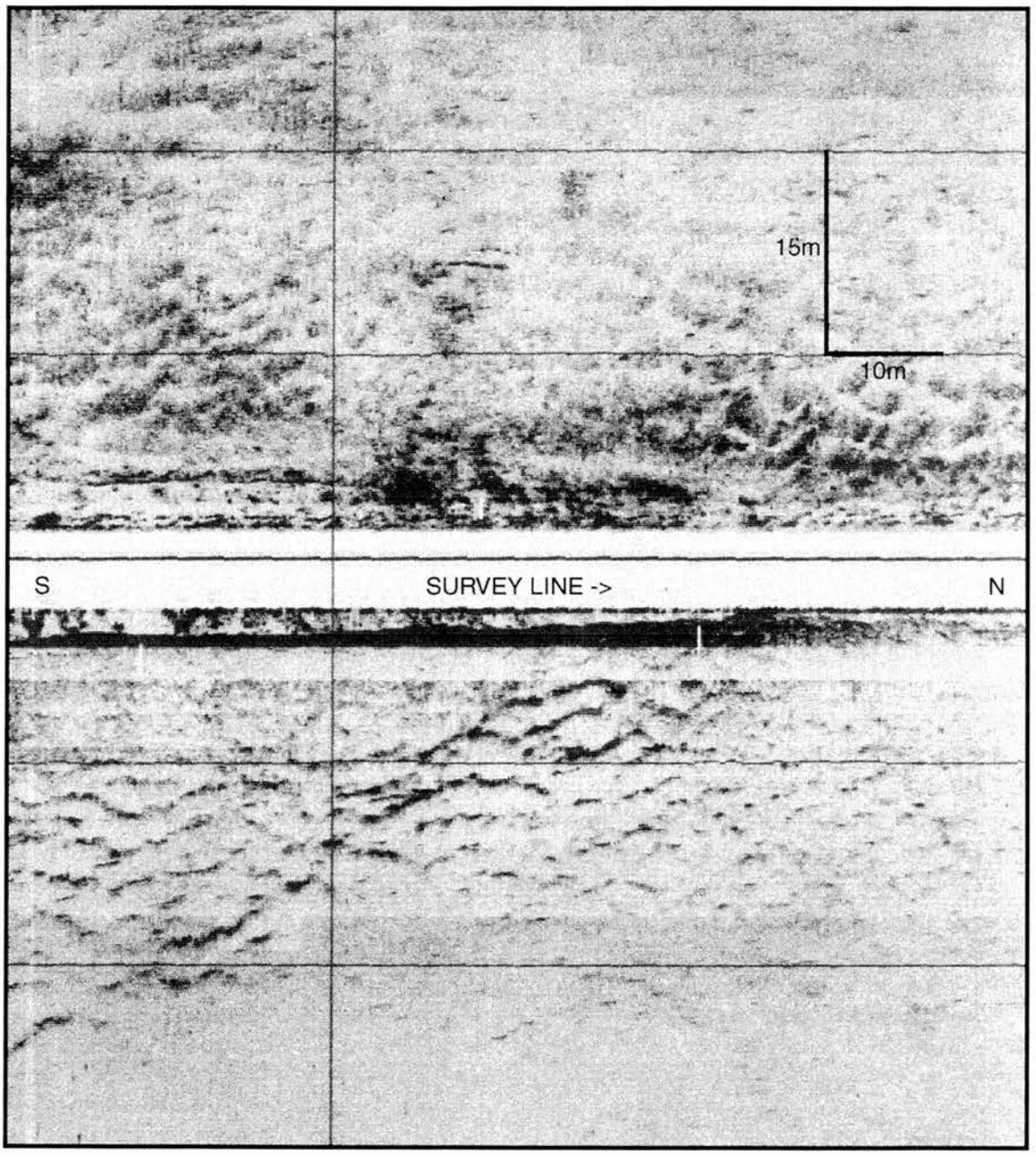

Fig. 5.6: Good reflections from the steep, lee slopes of small dunes (wavelength 0.6-5.0m; classification after Ashley, 1990) are shown in the lower half of the sonograph. Location of record is shown in Fig. 5.33.

medium - 5.0 to 10.0m, large - 10.0 to 100.0m and very large - over 100.0m. No dunes of very large wavelength were identified in the study area.

Flood

The dominant wavelength of dunes observed during flood tidal conditions (Fig. 5.7) was of the smallest class (0.6 to 5.0m). Such dunes occupy the deep areas of the Southern Channel, the main Navigation Channel and Queen's Road Channel. Sonographs recorded in Queen's Road Channel (Fig. 5.8) revealed that the areas where dunes occur are interspersed by ribbons of darker tonal intensities characteristic of cohesive silts and fine sands which are colonised by *Mytilus* beds as detected by Wewetzer and Duck (1996) along the Tay Road Bridge. Where the Navigation Channel swings from the south-east towards the middle of the estuary an area of dunes characterised by medium to large wavelengths was observed. The dunes on Middle Bank appear to have mainly medium wavelengths except in the centre area where large wavelength dunes occur just east of a region of small wavelength dunes. The latter region of small crest to crest spacings correlates with the bathymetrical changes of Middle Bank which are not shown on the Admiralty Chart due to the age of the survey data. Middle Bank was last surveyed by Dundee Port Authority in 1985 (Admiralty Chart, 1994). However, these bathymetrical changes can be seen on Plate 5.1, taken at low water on 30.08.96. This photograph clearly reveals a separation of Middle Bank into two or rather three sections. The shallower regions along the northern shore reveal a mixture of small, medium and large wavelength dunes.

Ebb

Fewer traverses were run on the ebb tide. The most dominant dune wavelength is of the small class and occupies all deeper parts of the study area (Fig. 5.9). Also during ebb tidal conditions medium and large dunes were observed where the Navigation Channel swings from the south-east towards the middle of the estuary while sonographs recorded in Queen's Road Channel, especially in the eastern part, revealed abrupt changes between areas of flat sea bed and areas of small dunes (Fig. 5.10). Middle Bank is covered by dunes of mainly medium wavelengths with far smaller

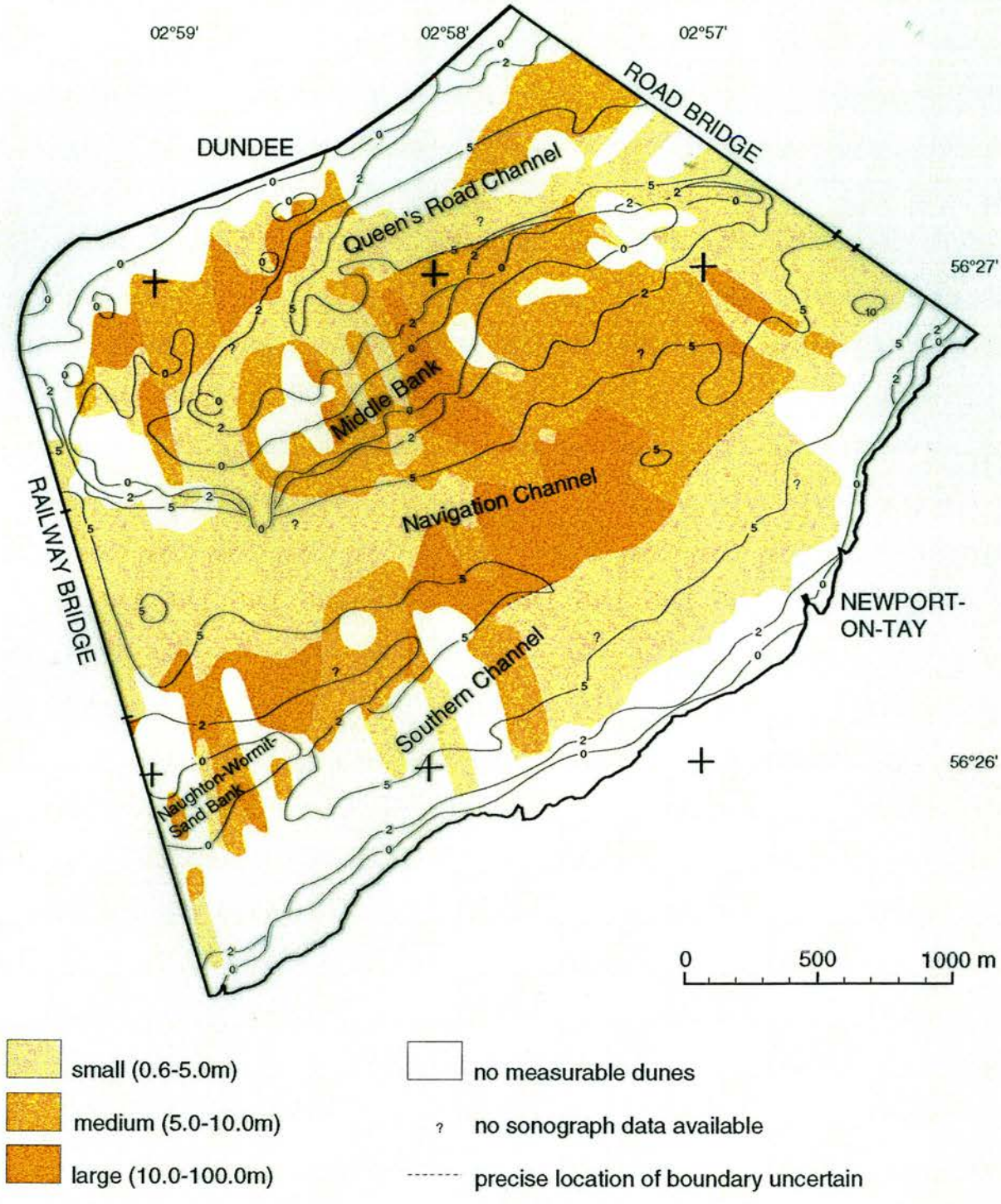

Fig. 5.7: Dune wavelength during flood and slack tidal conditions as interpreted from side-scan sonographs. Classification after Ashley (1990).

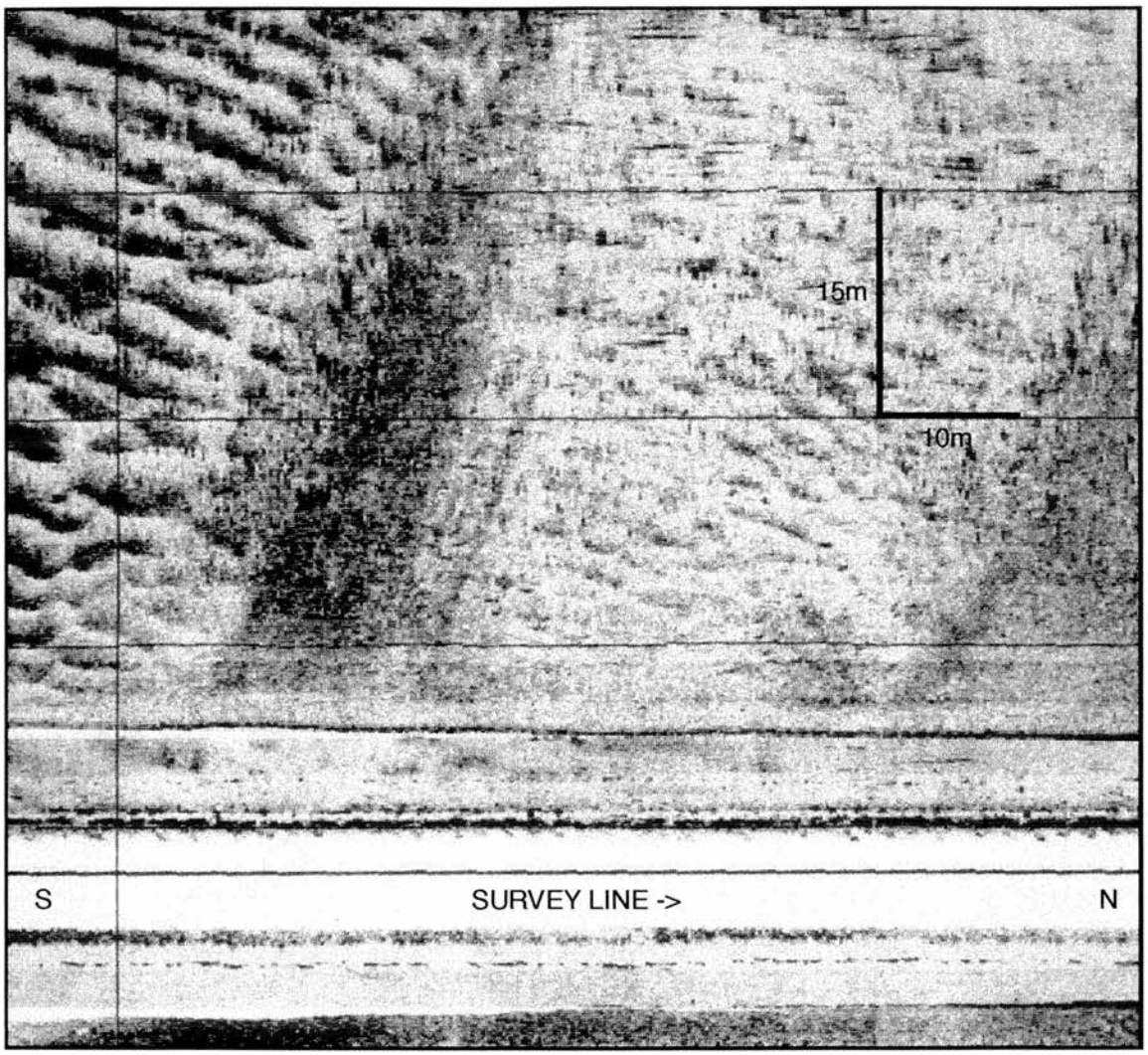

Fig. 5.8: Sonograph recorded in Queen's Road Channel showing dunes interspersed by ribbons of darker tonal intensities characteristic of cohesive silts and fine sands colonised by *Mytilus* beds. Location of record is shown in Fig. 5.33.

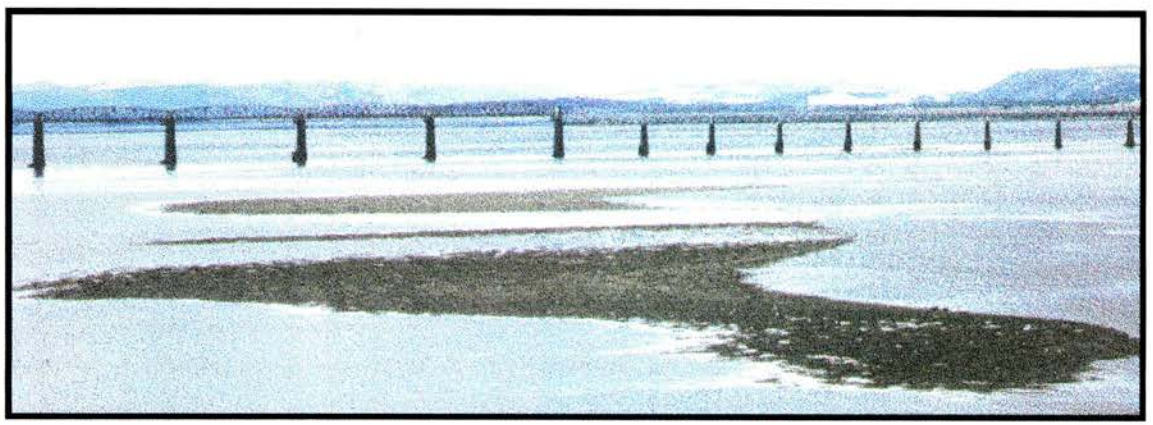

Plate 5.1: Photograph of Middle Bank at low water on a spring tide showing the subdivision into three small banks.

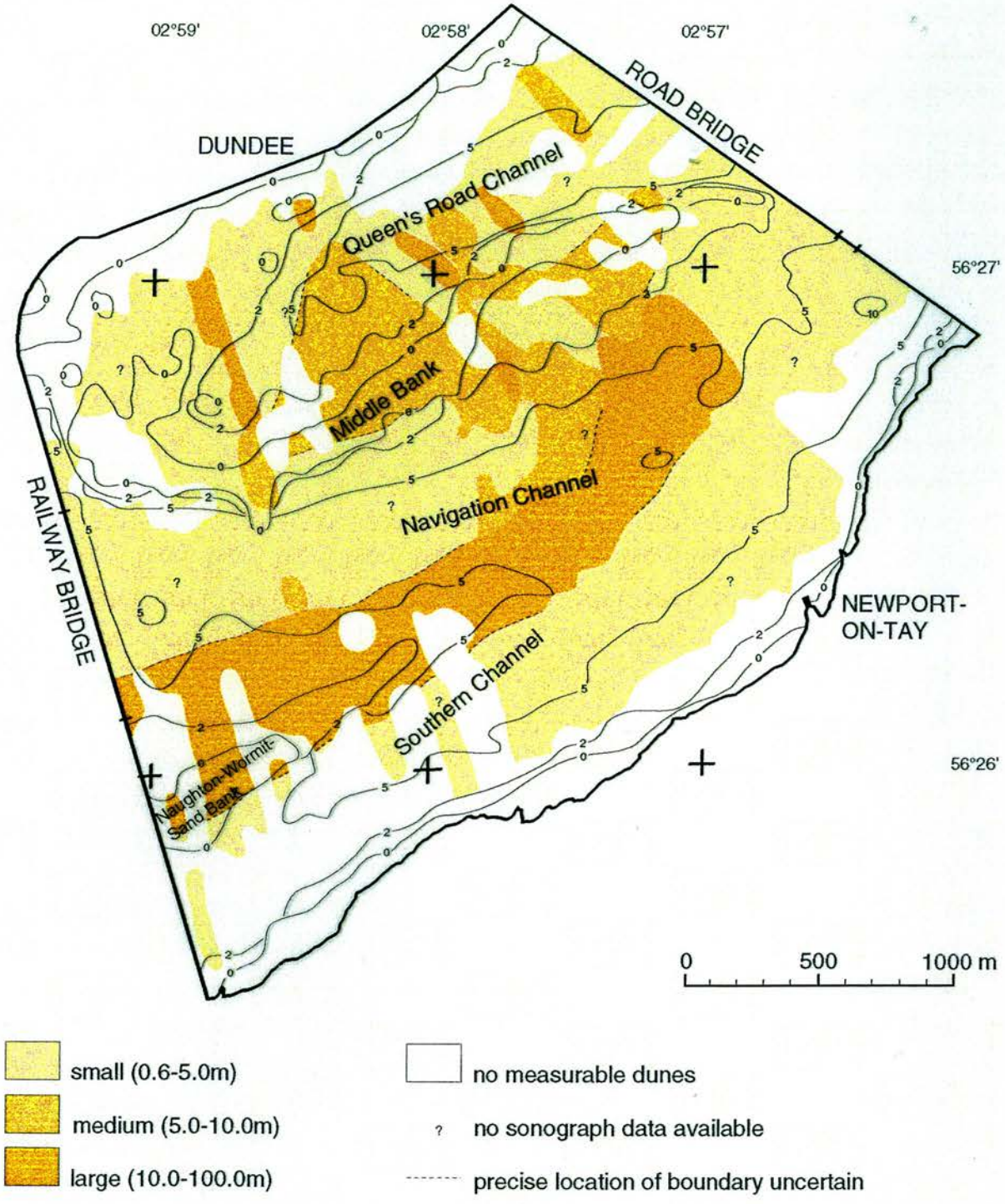

Fig. 5.9: Dune wavelength during ebb tidal conditions as interpreted from side-scan sonographs. Classification after Ashley (1990).

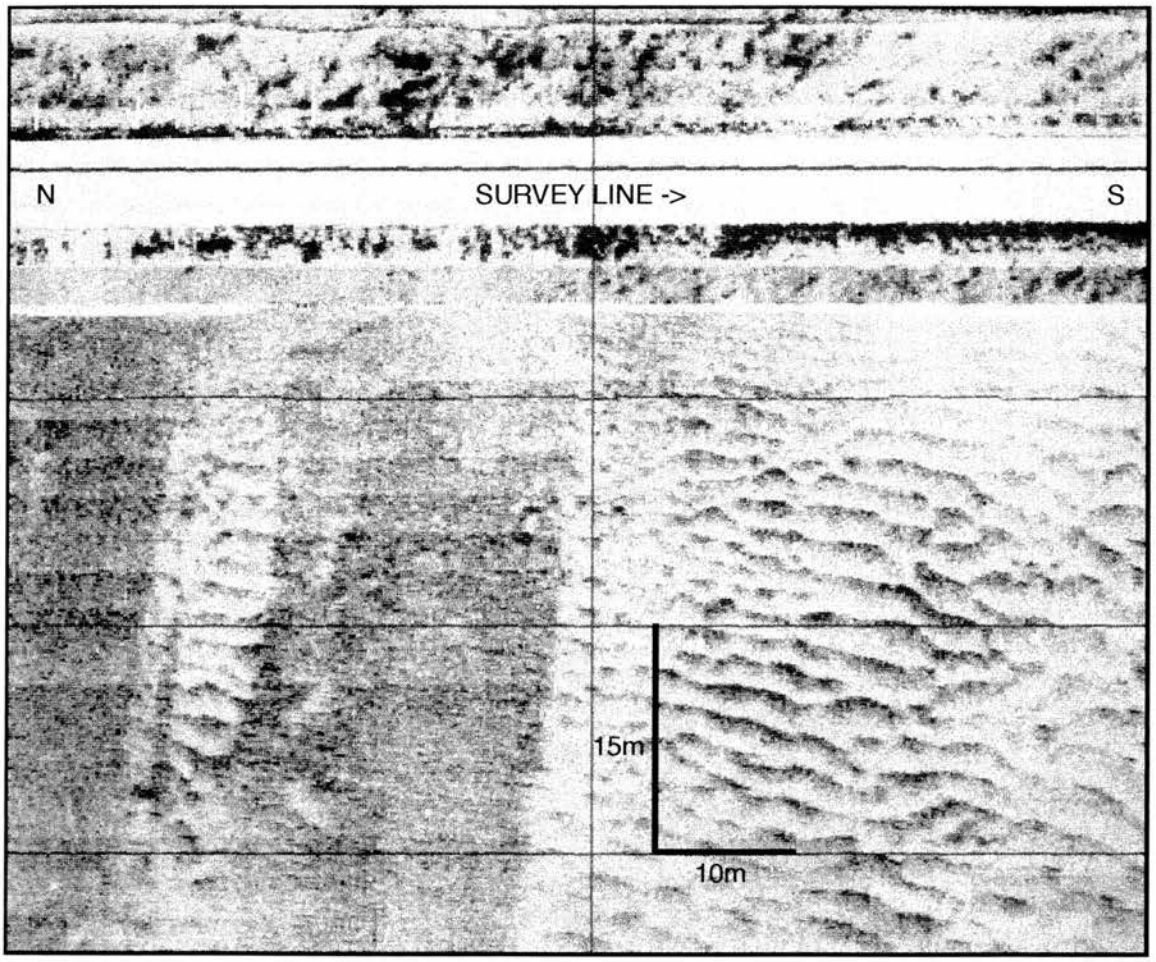

Fig. 5.10: Sonograph showing abrupt changes between areas of flat bed and areas of small dunes. Location of record is shown in Fig. 5.33.

areas of large and small dune wavelengths. All dunes along both northern and southern shorelines display only small wavelengths.

Comparison

The most dominant class of dune wavelengths in the study area is small i.e. crest to crest spacings of between 0.6 and 5.0m. Such dunes are mainly found in the deeper regions such as the Southern Channel, the main Navigation Channel and Queen's Road Channel. The centre part of the Navigation Channel displays dunes of medium and large wavelengths during both tidal states, although with a different distribution. Middle Bank reveals all three classes of crest to crest spacings but the section of small wavelength dunes where the "channel" divides Middle Bank into two main sections with a third, lower sand bank in between (Plate 5.1), could be detected only during flood tidal conditions. Different distributions of wavelength sizes were found in the sediments along the shorelines but especially along the southern one small wavelengths dominate the dunes.

5.3.2 Height

Dune height is the vertical distance between the trough and the crest of a dune. It is not possible to directly measure the height of dunes from sonographs. One has to measure the acoustic shadow produced by an object or bedform, the height of the tow fish above the sea bed as well as the slant range from the tow fish to the target. With the aid of these three measurements the height of an object or bedform may be calculated, as described in Section 3.2.2.4. The computed results should be carefully examined since not all of the measurements can be made with exact precision due to the resolution of the sonograph thermal linescan print-out and the sometimes indistinct acoustic shadow. Therefore, the results should be regarded as estimates rather than precise measurements. Ashley (1990) divides this descriptor into four classes: small dunes - 0.05 to 0.25m, medium - 0.25 to 0.50m, large - 0.50 to 3.00m and very large - over 3.00m. No very large dune heights were calculated from acoustic shadows recorded on the sonographs.

Flood

The majority of the dunes in the study area, including the channels and Middle Bank, are of medium height (Fig. 5.11). A major section of dunes of large height stretches from the Road Bridge towards the centre of the estuary. This covers the middle section of the main Navigation Channel. A few small patches of dunes of large height are also found in the south-western corner close to the Railway Bridge. Dune heights along the shorelines where the waters are shallow belong to the smallest class. The centre section revealed a remarkably abrupt transition from small height dunes in the northern and southern shore areas to large heights towards the middle of the estuary. These abrupt changes can be seen in Fig. 5.12.

Ebb

During ebb tidal conditions the most dominant dune height (Fig. 5.13) is within the range of the medium class. Such dunes cover most of the channel areas while a large part of Middle Bank exposes only small height dunes along its full length from east to west. North of Middle Bank is a relatively big region characterised by large height dunes which lie within the deeper waters of Queen's Road Channel. In the eastern part of the Navigation Channel, from close to the Road Bridge up to its southern point in the centre section, dune heights of the large class are present. This bears a close correlation with the bathymetry of the channel.

Comparison

The dominant dune height calculated from the sonographs is of the medium class, in the range between 0.25 and 0.50m. During flood tidal conditions the dunes along the shorelines revealed small heights while during ebb tidal conditions they revealed medium heights. However, the opposite happened to dunes on Middle Bank. On the flood tide the calculated height was mainly between 0.25 and 0.50m (medium) while the height decreased to the range of 0.05 to 0.25m during the ebb tide. During both tidal states large dune heights were recorded south of Middle Bank in parts of the main Navigation Channel but on the flood tide this area covers a far larger part of the estuary (Fig. 5.11) which stretches as far north as the eastern section of Queen's Road Channel. On both tides dunes of large heights were recorded north-west of Middle Bank. Once again,

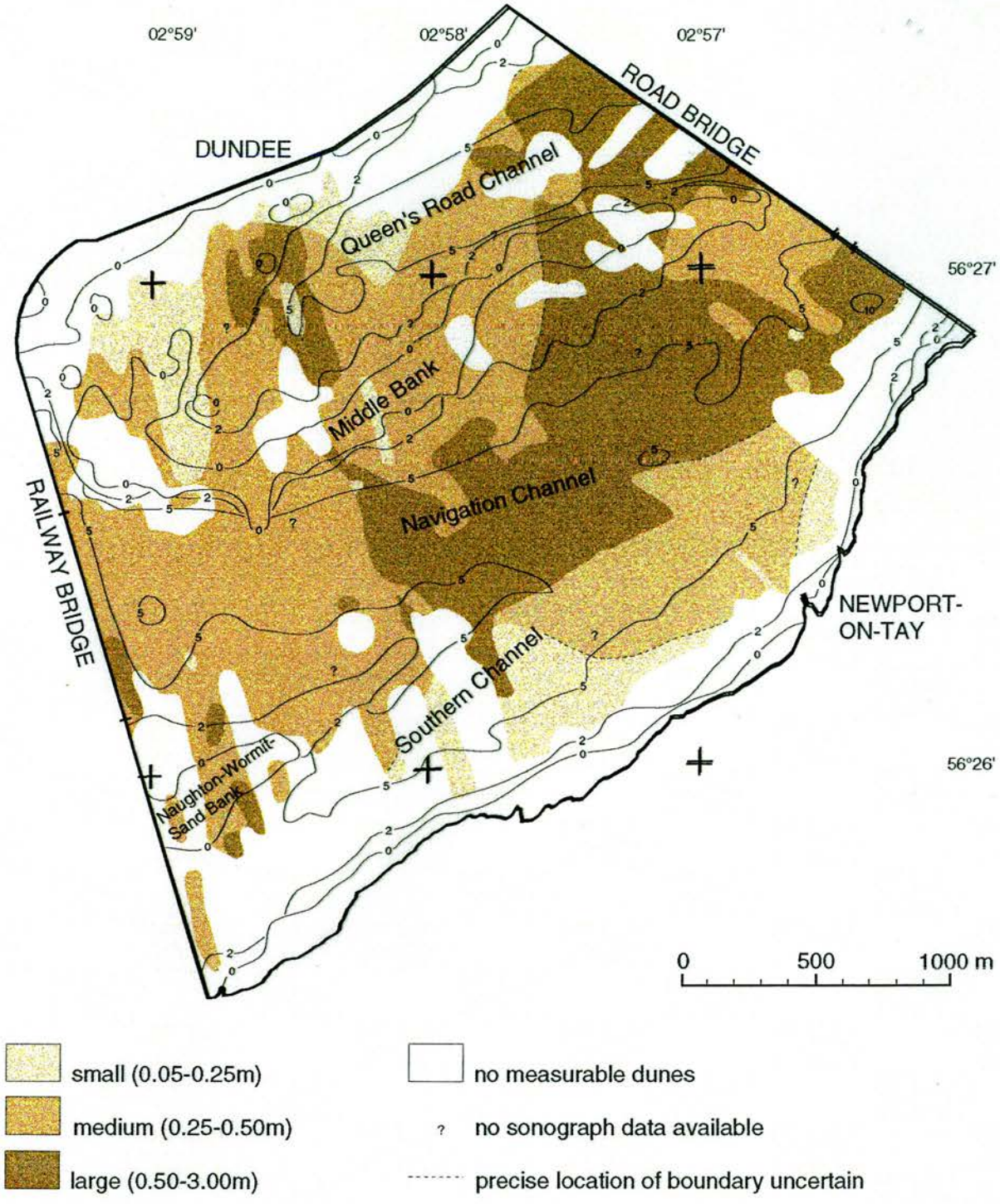

Fig. 5.11: Dune height during flood and slack tidal conditions as interpreted from side-scan sonographs. Classification after Ashley (1990).

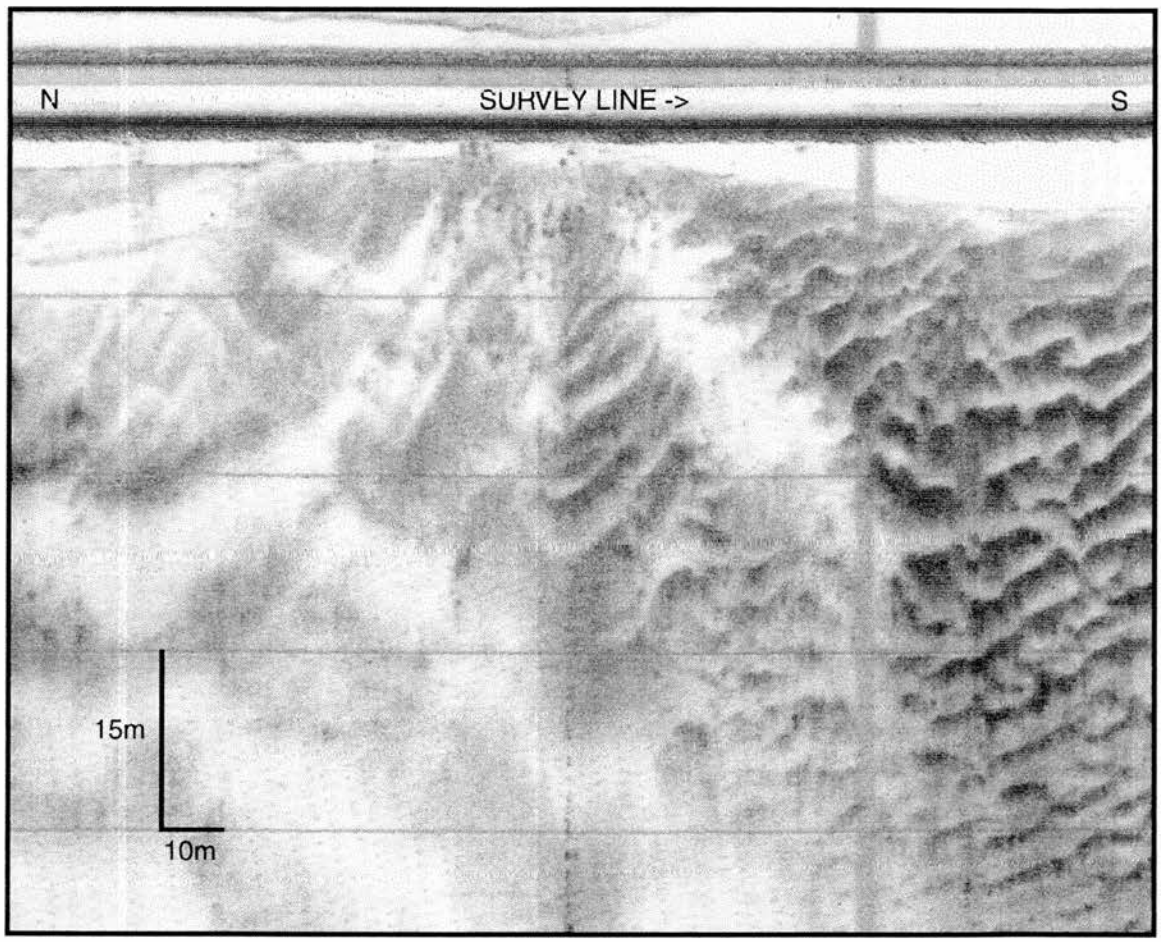

Fig. 5.12: Abrupt changes in dune wavelength and height recorded in Queen's Road Channel showing large dune wavelengths and heights on the left and small dune wavelengths and heights on the right. Location of record is shown in Fig. 5.33.

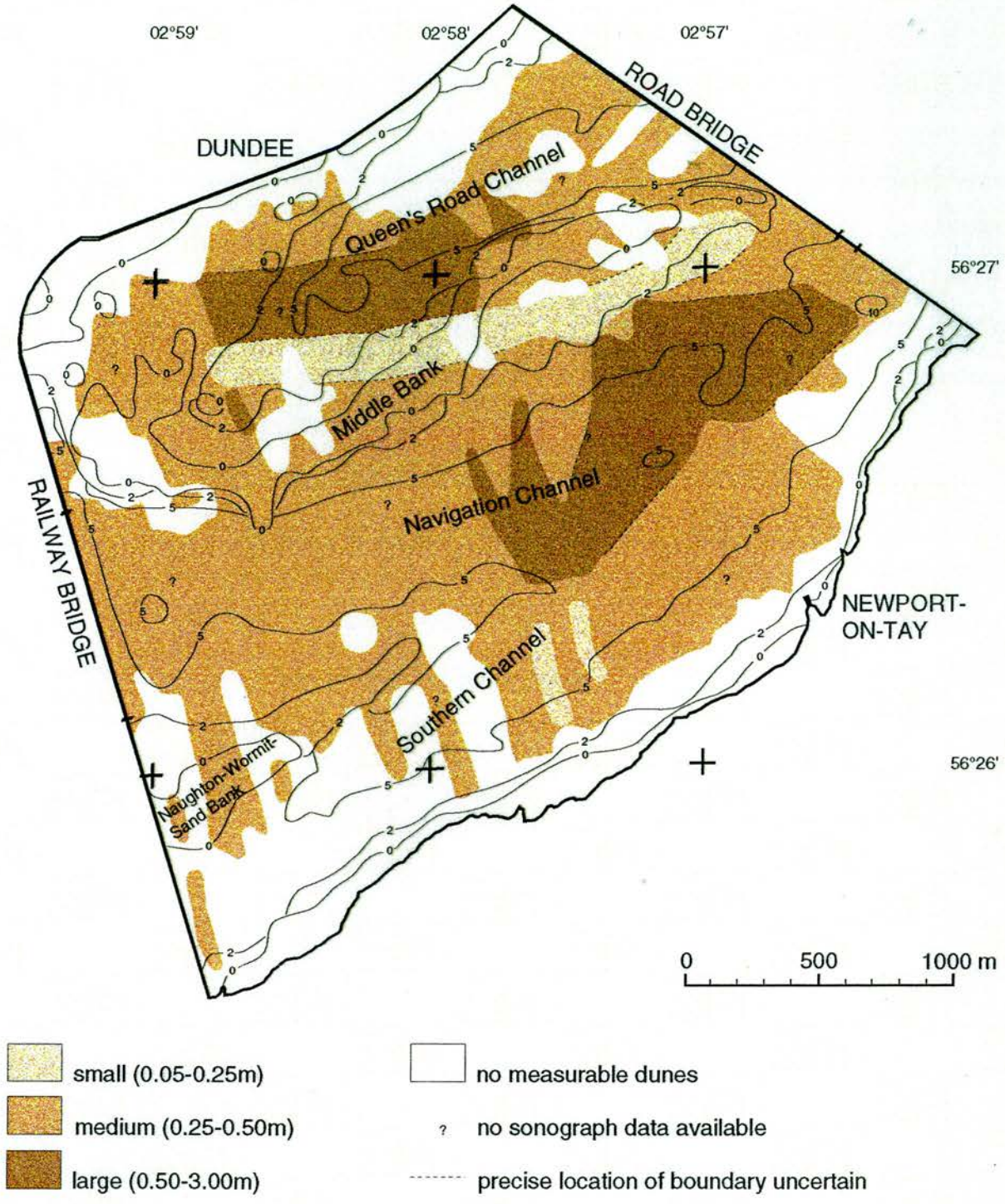

Fig. 5.13: Dune height during ebb tidal conditions as interpreted from side-scan sonographs. Classification after Ashley (1990).

abrupt transitions from small to large heights were revealed although the distribution was quite dissimilar between the two states of the tide.

5.3.3 Length along dune crest

The descriptor "length along dune crest" is not included in the classification of Ashley (1990). This is because it is a very subjective measurement and may vary depending on how it is measured. It was chosen in this study in order to establish a correlation between dune dimensions and was defined as the length along dune crest of a good reflection from the steep, lee side of a dune recorded on a sonograph. An example is shown in Fig. 5.14. The descriptor was divided into seven classes as can be seen on the interpretation maps in Figs. 5.15 and 5.16.

Flood

A major part of the study area on the flood tide was covered by dunes with lengths of between 20 and 50m (Fig. 5.15). Such dunes can generally be found in the centre area of the estuary, namely in Queen's Road Channel, on Middle Bank and in the northern part of the Navigation Channel. In the Southern Channel, as well as where the Navigation Channel passes underneath the two bridges, the lengths along dune crests were of smaller dimensions (10-20m). Very small areas only were found to have the shortest lengths along dune crests of under 10m. These were discovered in the south-western corner of the study area close to the Railway Bridge, the largest area just off the TERC pier towards the north-west and a few smaller patches along the southern edge of Middle Bank. In the main Navigation Channel larger lengths along dune crests were recorded in patches ranging throughout all four larger classes but still with the dominant length between 20 and 50m.

Ebb

During ebb tidal conditions the dominant length along dune crests recorded was in the range of 20 to 50m (Fig. 5.16). This covers basically the whole study area from the southern shore to the border between the Navigation Channel and the Southern Channel. The lengths along dune crests decrease in the Southern Channel and are mainly in the range of 10 to 20m just off Newport-on-Tay and under 10m further to both the east and

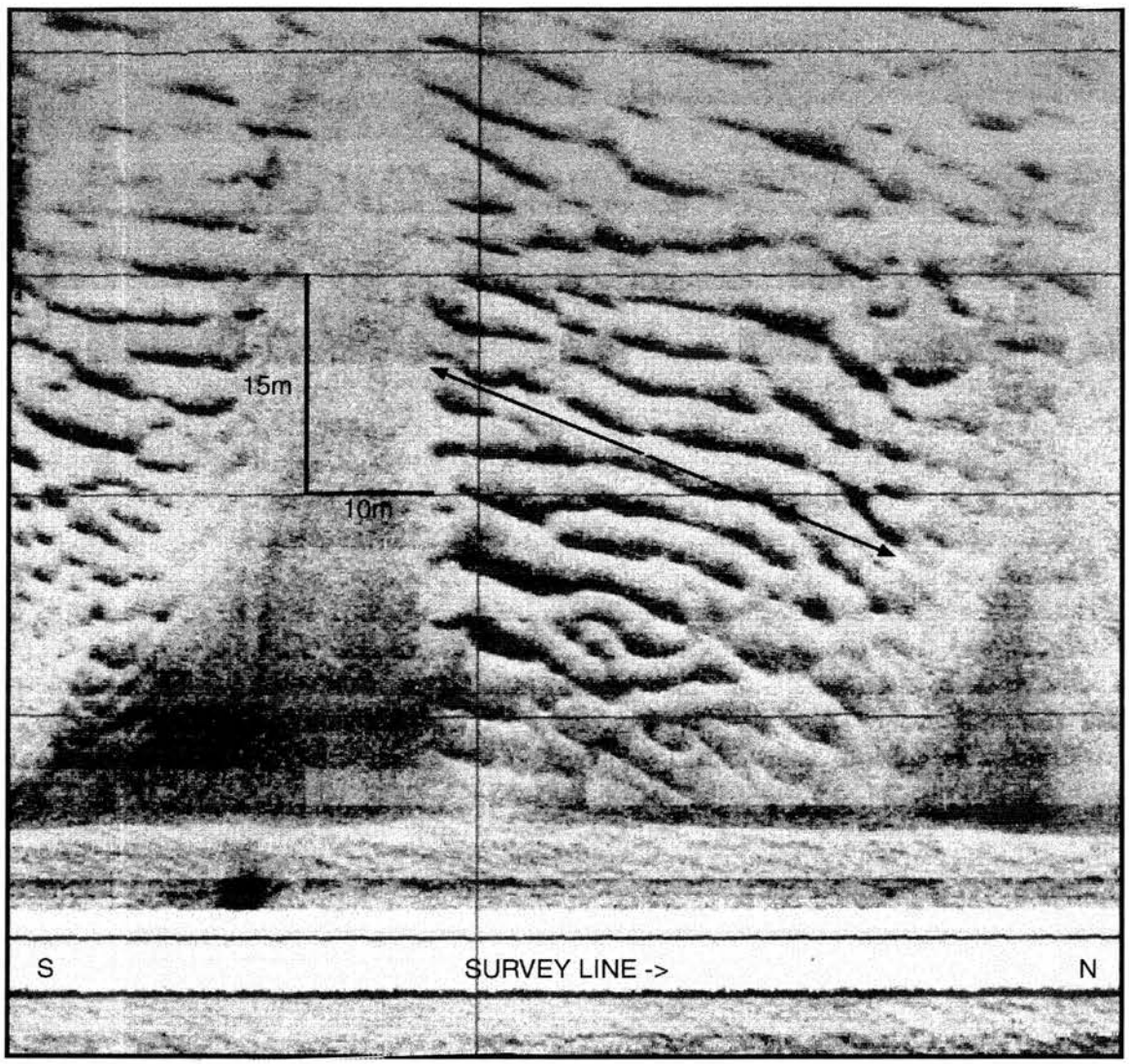

Fig. 5.14: Length along dune crest (see arrow) is defined in this thesis as the length of a good reflection from the steep, lee slope of a dune recorded by side-scan sonar. Location of record is shown in Fig. 5.33.

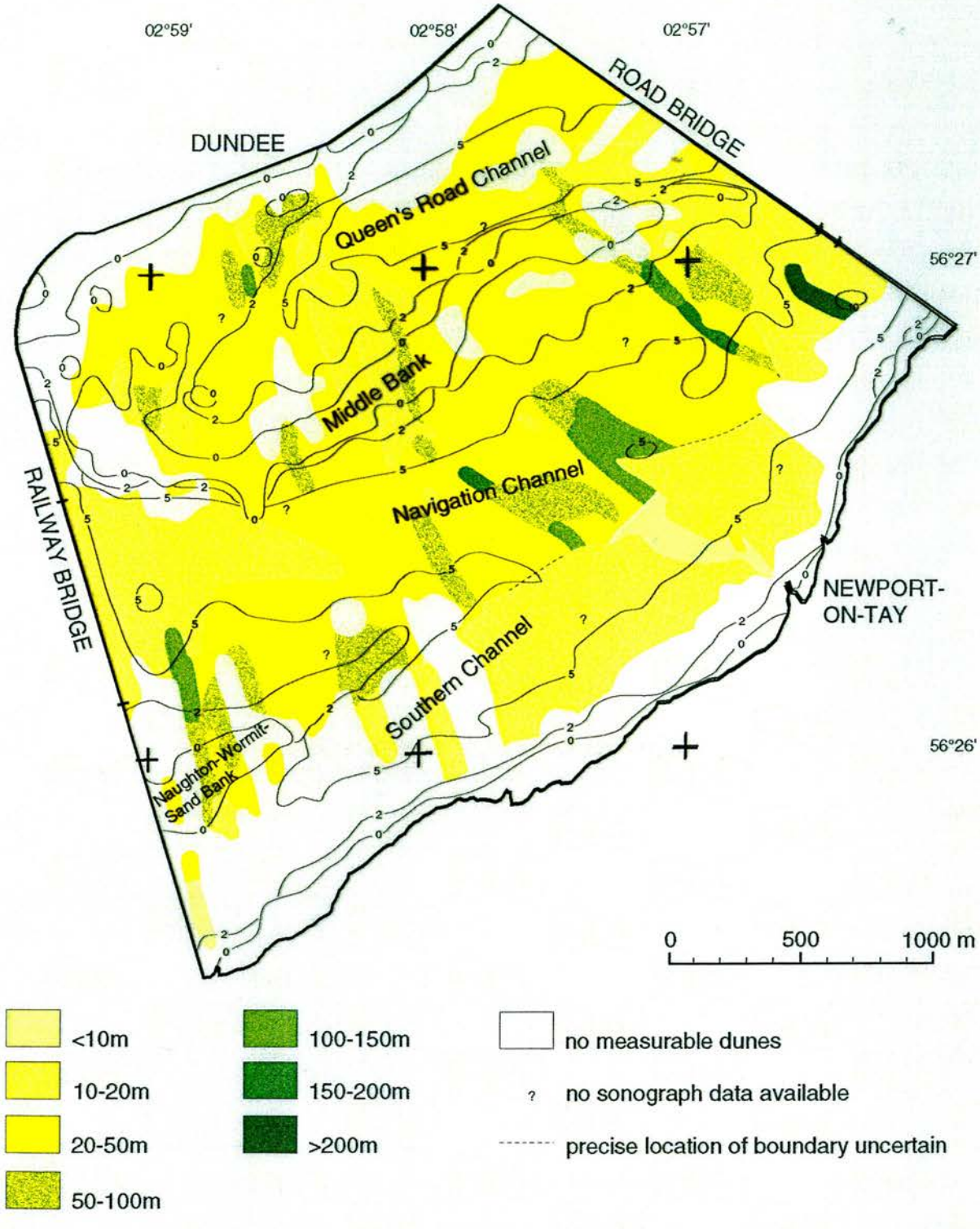

Fig. 5.15: Length along dune crest during flood and slack tidal conditions as interpreted from side-scan sonographs.

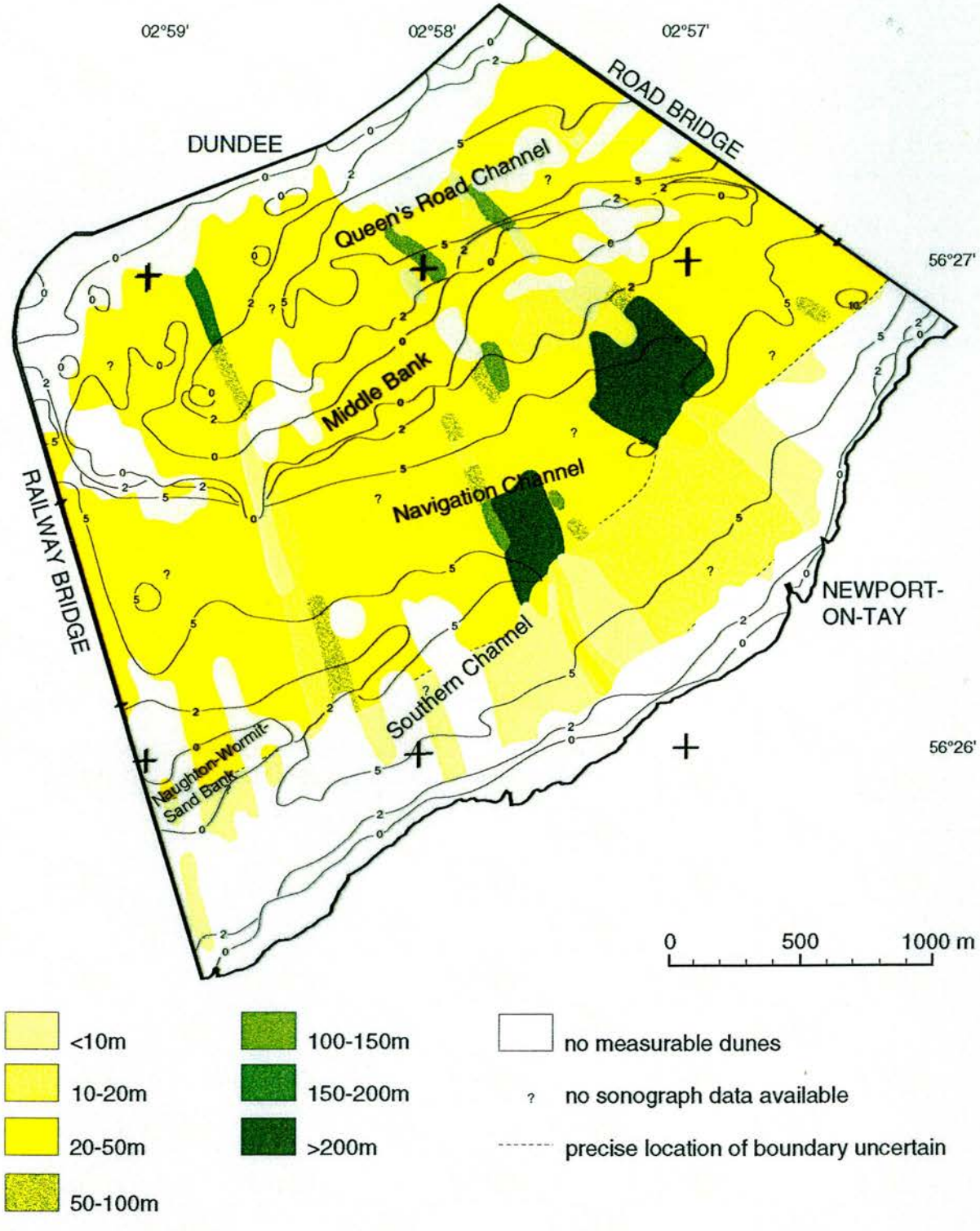

Fig. 5.16: Length along dune crest during ebb tidal conditions as interpreted from side-scan sonographs.

west. A few small areas in Queen's Road Channel revealed larger lengths along dune crests of up to 200m. Longest overall lengths along dune crests, of over 200m, were recorded during ebb tidal conditions in two areas in the centre and eastern parts of the Navigation Channel.

Comparison

Although most dunes have lengths along their crests in the range of 20 to 50m both on the ebb and flood tide, the general distribution is quite different during the two tidal conditions. During the flood tide, greater areas of large lengths along dune crests were revealed, especially in the Navigation Channel. In addition, the lengths along dune crests in the Southern Channel appear to be longer during the flood tide. However, the longest dune crests of over 200m were recorded in the Navigation Channel during ebb tidal conditions.

5.3.4 Sinuosity

Sinuosity describes the shape of a dune crest in plan view. It is described in Section 4.5. However, two patterns were recorded during the side-scan sonar surveys additional to those shown in Fig. 4.2. The two shapes, not formerly described, are "interference" and "patchy, discontinuous". Examples of the two are shown in Figs. 5.17 and 5.18. Interference patterns in symmetrical dunes result from at "least two probably coexisting wave sets" (Collinson and Thompson, 1989). Patchy, discontinuous patterns were found mainly in the channels. This name is rather a description than a generally used term but no similar feature has been described in the literature. It is not clear from sonograph data alone if these bedforms consist solely of sediment or if their shape is due to a cover of mussels and pebbles. This point is addressed further in Section 6.3.5.

Flood

Most of the dunes recorded in the study area on the flood tide had a sinuous crest shape and were out of phase (Fig. 5.19). Sinuous shapes are usually asymmetrical which relates to a dominant current direction. Only small areas of sinuous in phase shapes were revealed which were distributed over the whole study area. Such an area is shown in Fig. 5.20.

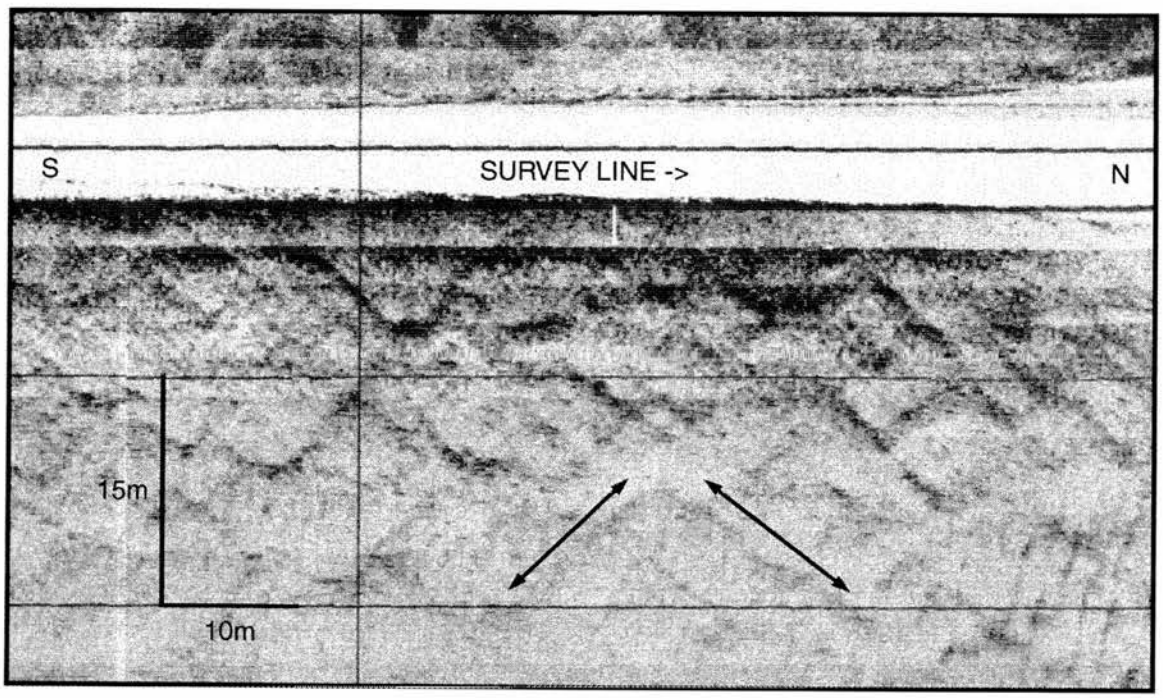

Fig. 5.17: Dune interference pattern recorded on Middle Bank by side-scan sonar. Arrows indicate the crest orientations. Location of record is shown in Fig. 5.33.

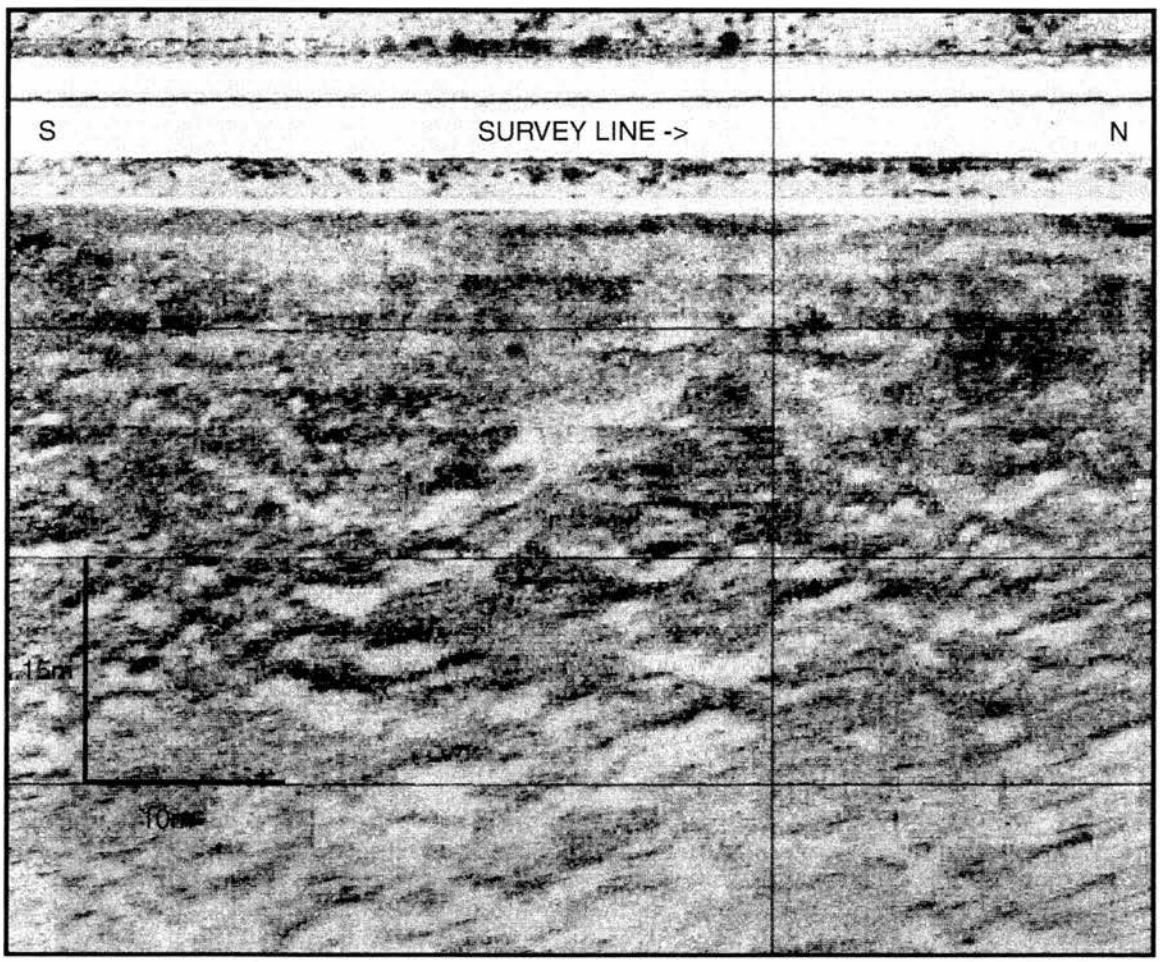

Fig. 5.18: Patchy, discontinuous signature recorded in the channels by side-scan sonar. Location of record is shown in Fig. 5.33.

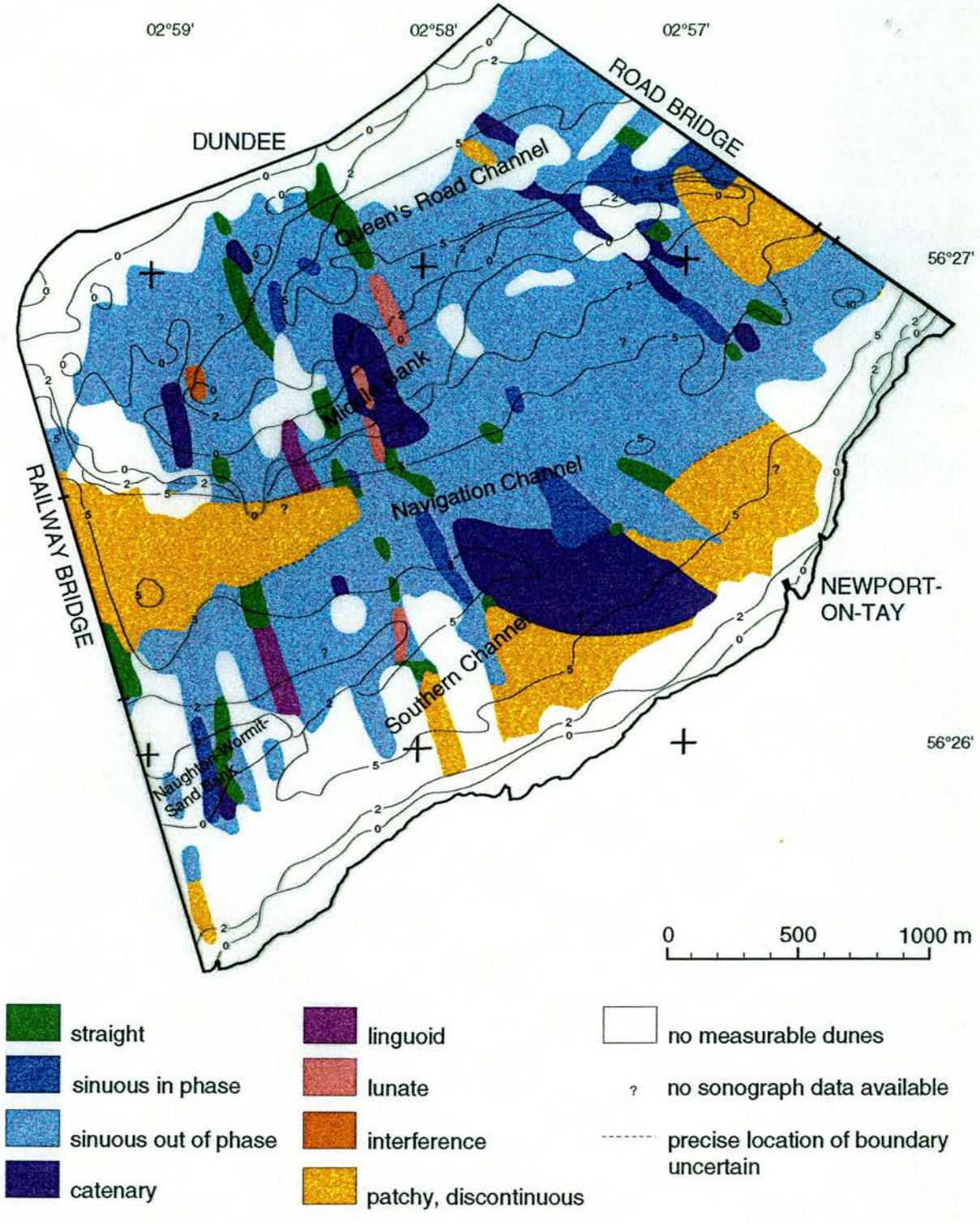

Fig. 5.19: Dune sinuosity during flood and slack tidal conditions as interpreted from from side-scan sonographs. Classification after Collinson and Thompson (1989).

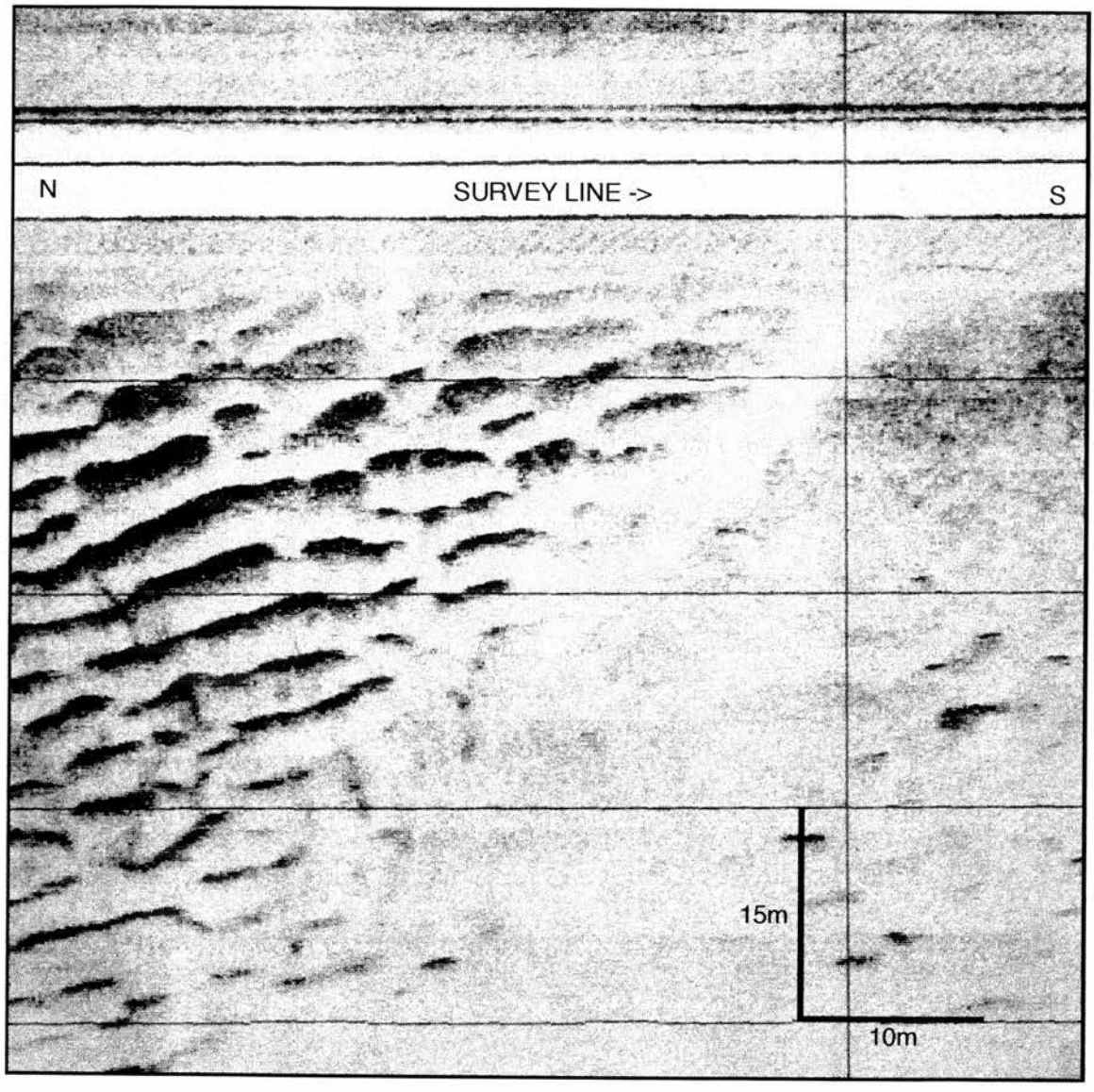

Fig. 5.20: Sonograph showing an area of dunes of generally sinuous in phase shape and a region where no dunes were detected. Location of record is shown in Fig. 5.33.

This sonograph was recorded along the northern edge of Middle Bank and shows the border between an area of dunes of generally sinuous in phase shape and a region where no dunes were detected. According to Collinson and Thompson (1989), straight crested dunes are associated with wave action. This would explain their occurrence in the vicinity of Middle Bank but a different explanation would have to be found for their occurrence in deeper regions. Sinuous to lunate shapes belong to the 3-d dune forms (Dalrymple and Rhodes, 1995). While relatively straight crested dunes lack scour pits, and therefore have 2-d shapes, scour pits are often found in the lee side of sinuous to lunate forms. The occurrence of 2-d and 3-d forms is also closely related to flow strength (Collinson and Thompson, 1989) and flow duration (Allen, 1968). Therefore it is remarkable that catenary and lunate crest shapes were found on Middle Bank during the flood tide. It is suggested that this is related to the draining of waters off the emerging Middle Bank during low slack water and a variety of current directions forming the dunes. Interference dunes were found at the western end of Middle Bank. Patchy, discontinuous patterns were restricted to the deeper waters of the Southern Channel and the eastern and western end of the Navigation Channel where they are present beneath the bridges. Abrupt changes of dune sinuosity were recorded especially along the northern border of the Southern Channel where dune sinuosity changes first from "patchy, discontinuous" to straight and then to sinuous in phase within a distance of between 15-70m as shown in Fig. 5.21.

Ebb

The dominant dune sinuosity type on the ebb tide is also of the category of sinuous out of phase (Fig. 5.22). Two relatively large areas of sinuous in phase dune shapes were recorded in the eastern half of the Navigation Channel. Small areas of catenary, linguoid and cuspate forms were found mainly in the vicinity of Middle Bank. Interference dunes are more widely distributed especially in the centre of Middle Bank but also towards its south-western tip, as well as close to the north-eastern end of Naughton-Wormit Sand Bank. Their occurrence is not entirely surprising since the sonographs were recorded at the early stages of ebb tide when forms produced by flood currents had not yet been totally remodelled. The centre of Middle Bank displays dune crests of rhomboidal shapes which are asymmetrical. Patchy, discontinuous forms line the bottom of the western

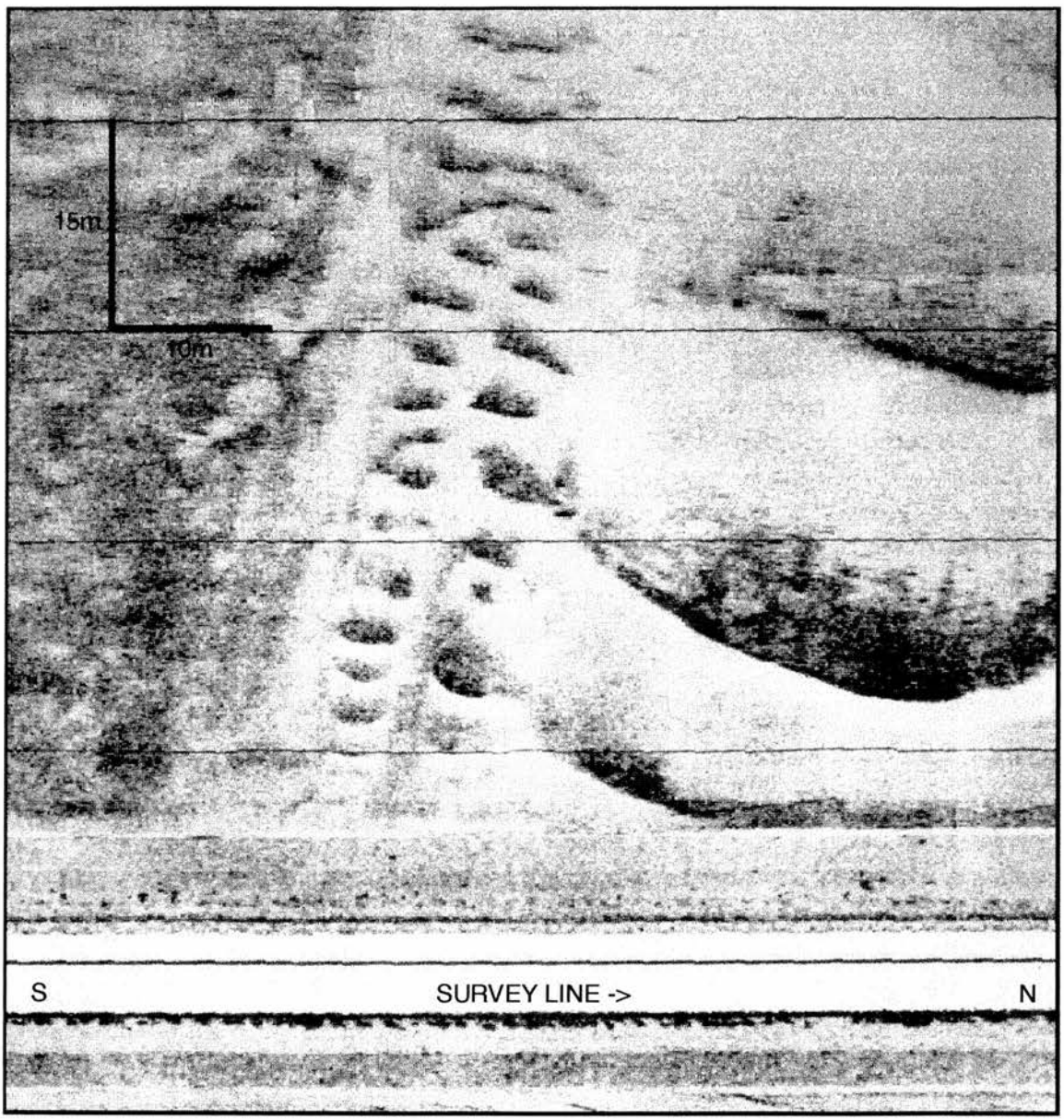

Fig. 5.21: Abrupt changes of dune height, wavelength and sinuosity from "patchy, discontinuous" to straight and then to sinuous in phase (from south to north) at the northern edge of the Southern Channel as recorded by side-scan sonar. Location of record is shown in Fig. 5.33.

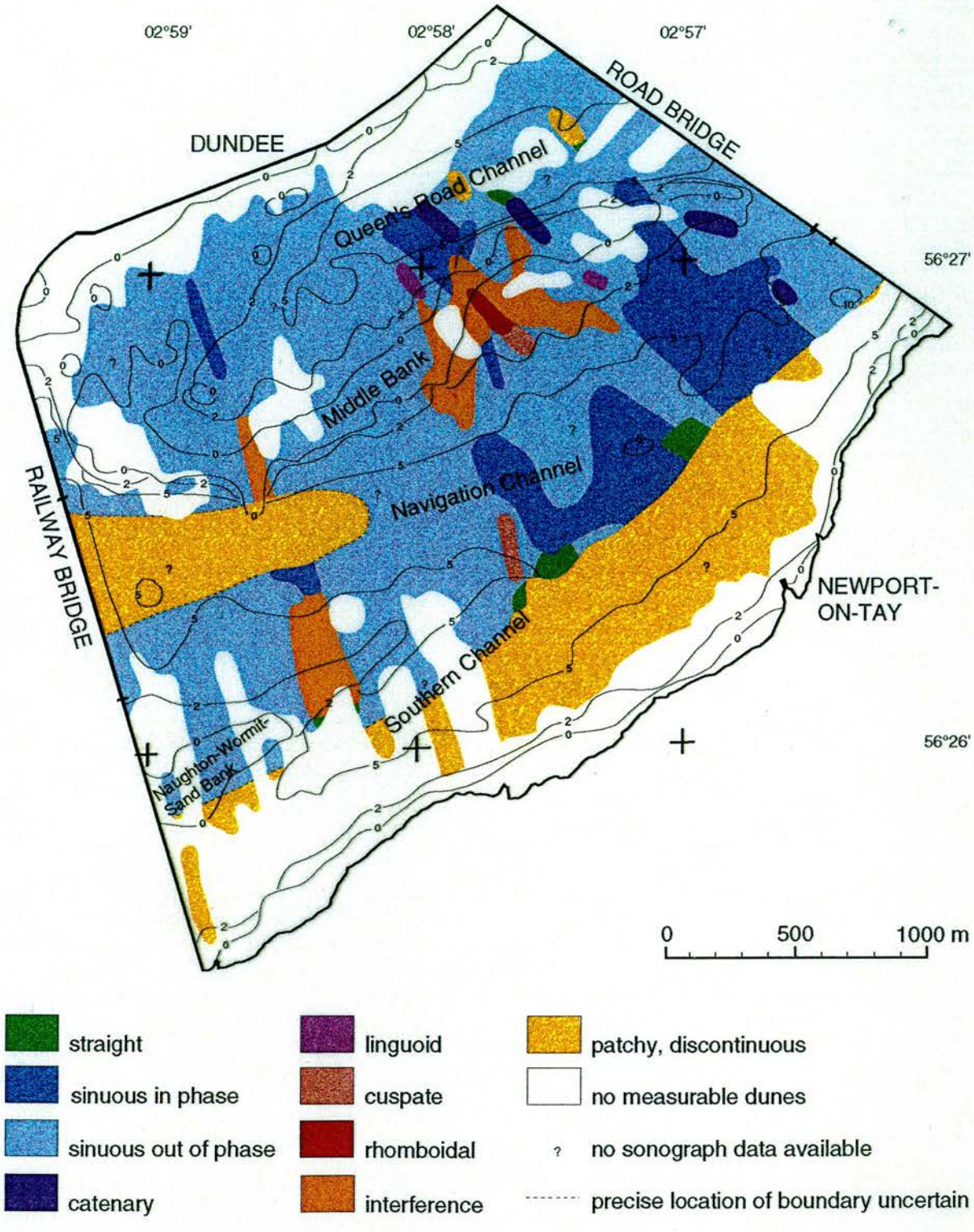

Fig. 5.22: Dune sinuosity during ebb tidal conditions as interpreted from side-scan sonographs. Classification after Collinson and Thompson (1989).

part of the Navigation Channel as well as the Southern Channel. Only two small areas of patchy, discontinuous dunes were found in Queen's Road Channel.

Comparison

During both tidal stages the dominant dune crest shape recorded in the estuary is sinuous out of phase. The deeper channel areas are lined with patchy, discontinuous dunes. All other forms occur in relatively small areas and do not appear to have the same distribution during both tidal states. In particular, the regions of interference dunes recorded on the ebb tide were not recorded during flood tidal conditions which suggests changes in crest form between the two tidal states.

5.3.5 Superposition

Dune superposition is divided into two categories, after Ashley (1990). Simple dunes lack superimposed dunes while compound dunes bear smaller, superimposed dunes. Examples of simple dunes and compound dunes as recorded by side-scan sonar are shown in Figs. 5.23 and 5.24.

The distribution of simple and compound dunes in the study area is very similar on both stages of the tide (Figs. 5.25 and 5.26). Generally the bed of the Southern Channel, Queen's Road Channel and the western part of the Navigation Channel consists of simple dunes while the centre region of the estuary displays compound dunes. The larger number of small areas of simple dunes, revealed during the flood tide, is believed to be a reflection of the greater number of survey lines.

5.3.6 Asymmetry

Most dunes have an asymmetric vertical profile (see also Section 4.5). The gentle stoss side faces the dominant current direction and the steep lee side faces the direction of sediment transport. Asymmetrical dunes therefore indicate the dominant direction of sediment transport. Symmetrical forms occur where no net sediment transport exists or where neither tide dominates. The recording of symmetrical dunes depends on the time of the survey which should preferably be carried out during slack water conditions. The category of mixed asymmetries was chosen for

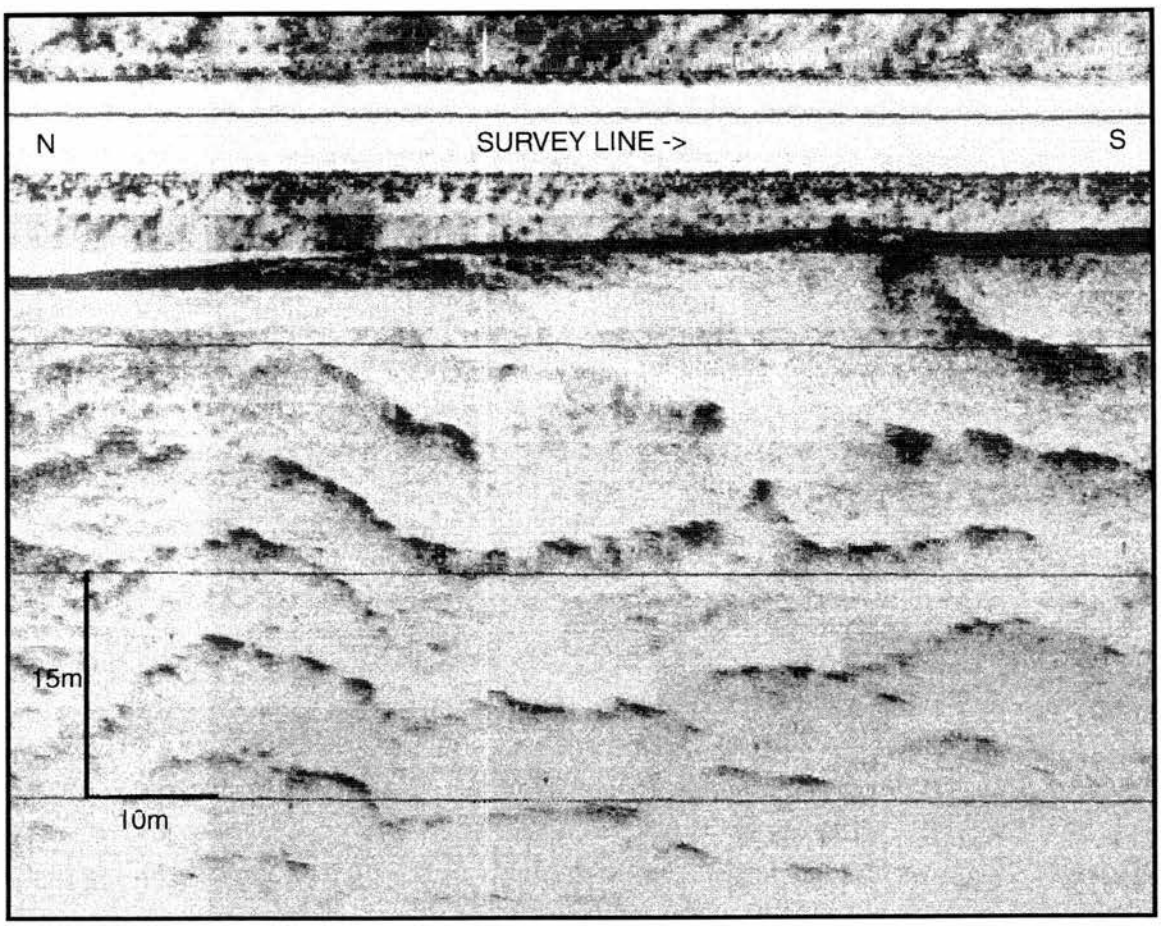

Fig. 5.23: Sonograph showing simple dunes of medium wavelength as defined by Ashley (1990). Location of record is shown in Fig. 5.33.

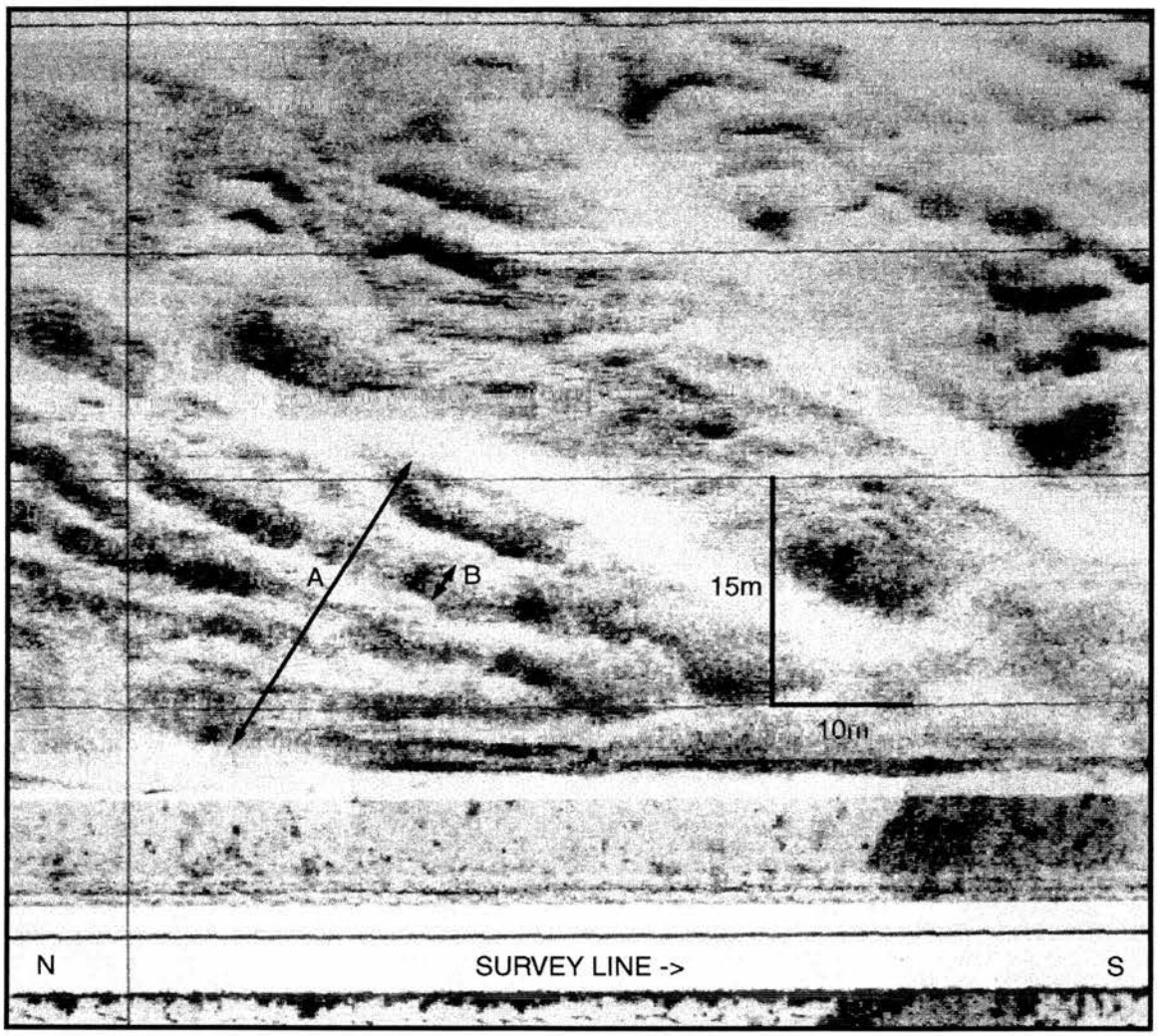

Fig. 5.24: Sonograph showing compound dunes: A - platform dune, B - superimposed dune. Location of record is shown in Fig. 5.33.

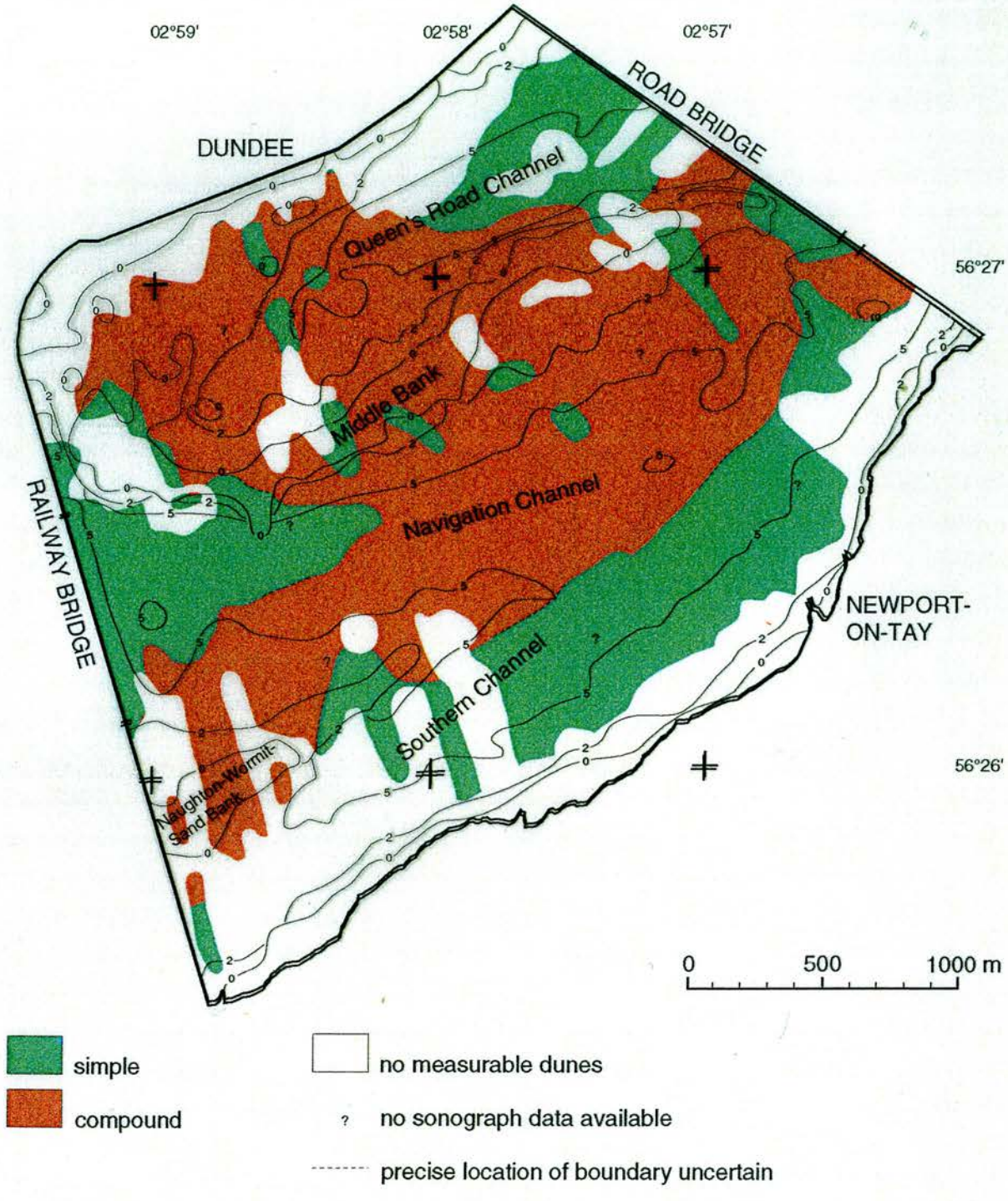

Fig. 5.25: Dune superposition during flood and slack tidal conditions as interpreted from side-scan sonographs. Classification after Ashley (1990).

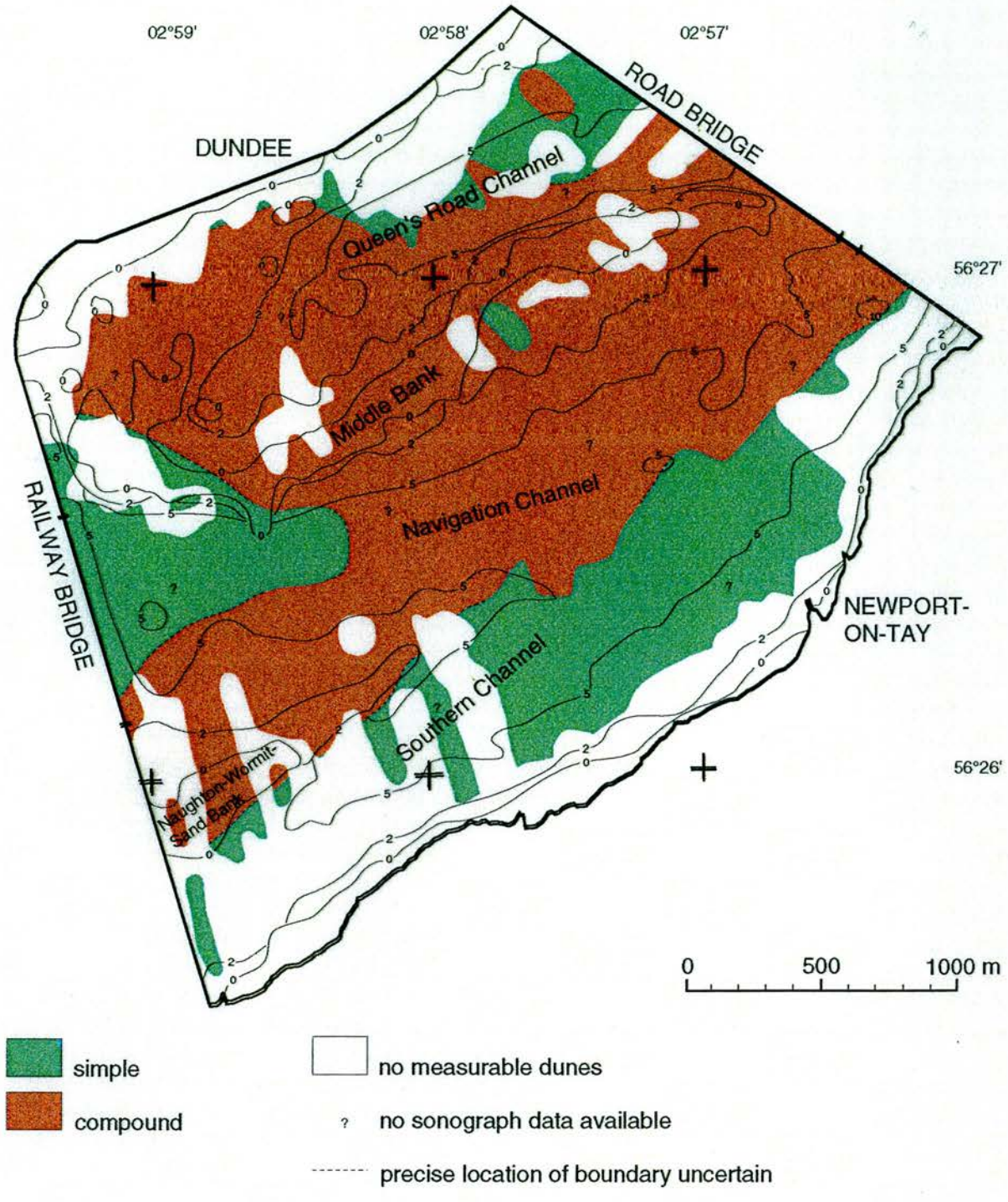

Fig. 5.26: Dune superposition during ebb tidal conditions as interpreted from side-scan sonographs. Classification after Ashley (1990).

areas where asymmetric dunes exist, of which some are indicative of the dominance of flood currents while others suggest ebb dominant currents. Dune asymmetries are readily detected on sonographs by examination of the relative proportions of a good reflection from a dune and its acoustic shadow (Fig. 5.27).

Flood

Most dunes recorded on the flood tide in the study area have an asymmetry suggesting the dominance of flood currents, hereafter referred to as flood dominant dunes (Fig. 5.28). Larger areas of dunes with an asymmetry indicative of the dominance of ebb flows, hereafter referred to as ebb dominant dunes, were found in the western half of the Navigation Channel, the western end of Queen's Road Channel and the southern centre part of Middle Bank. Smaller areas were revealed in other regions of the channels. Only a very small field of mixed asymmetric dunes was detected at the western end of Middle Bank. Symmetric dunes were widely distributed in the estuary but restricted to small areas.

Ebb

Dune asymmetries recorded on the ebb tide (Fig. 5.29) were dominated by the flood tide. Flood dominant dunes cover most channels, the only exception being the centre part of Queen's Road Channel where dunes display an ebb dominant asymmetry. Dunes of mixed asymmetries were recorded on most regions of Middle Bank. This is probably related to the change of the tide shortly before the recording of the sonographs. Symmetric dunes were revealed along the edges of the Navigation Channel as well as within the area of ebb dominant dune asymmetries in Queen's Road Channel.

Comparison

The obvious dominant current direction detected from dune asymmetries is the flood tide flowing from the north-east through the Road Bridge. Dune asymmetries indicative of flood dominant flows are especially common in most parts of the channels. Areas of ebb dominant dunes generally change position and distribution with the tide. Large parts of the Navigation Channel which were ebb dominant on the flood tide revealed a

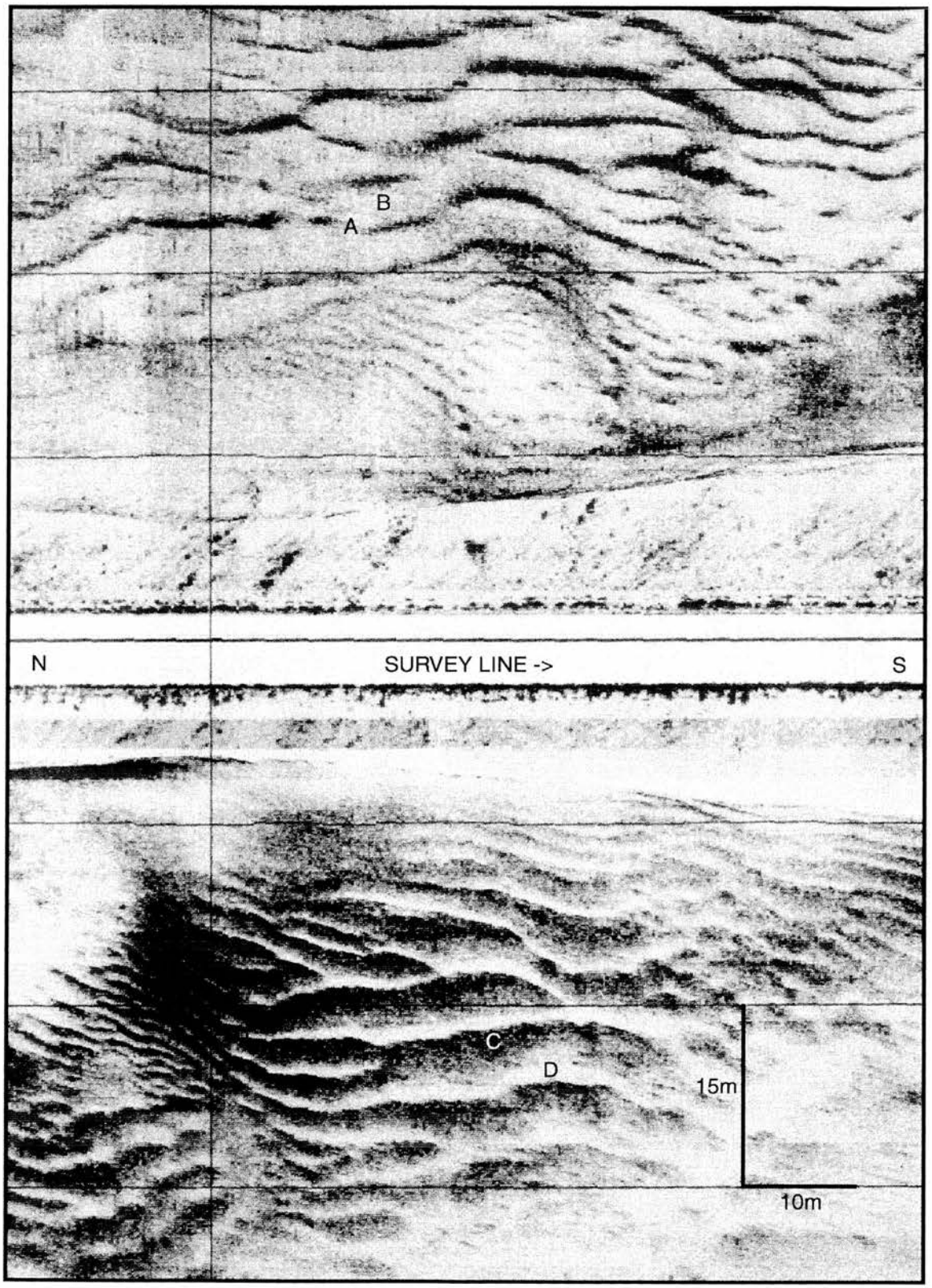

Fig. 5.27: Sonograph showing asymmetric dunes: A - steep, lee slope facing the transducer giving a strong reflection on the port channel, B - gentle, stoss slope facing away from the transducer on the port channel, C - gentle, stoss slope facing the transducer on the starboard channel, D - acoustic shadow of the dune on the starboard channel. Location of record is shown in Fig. 5.33.

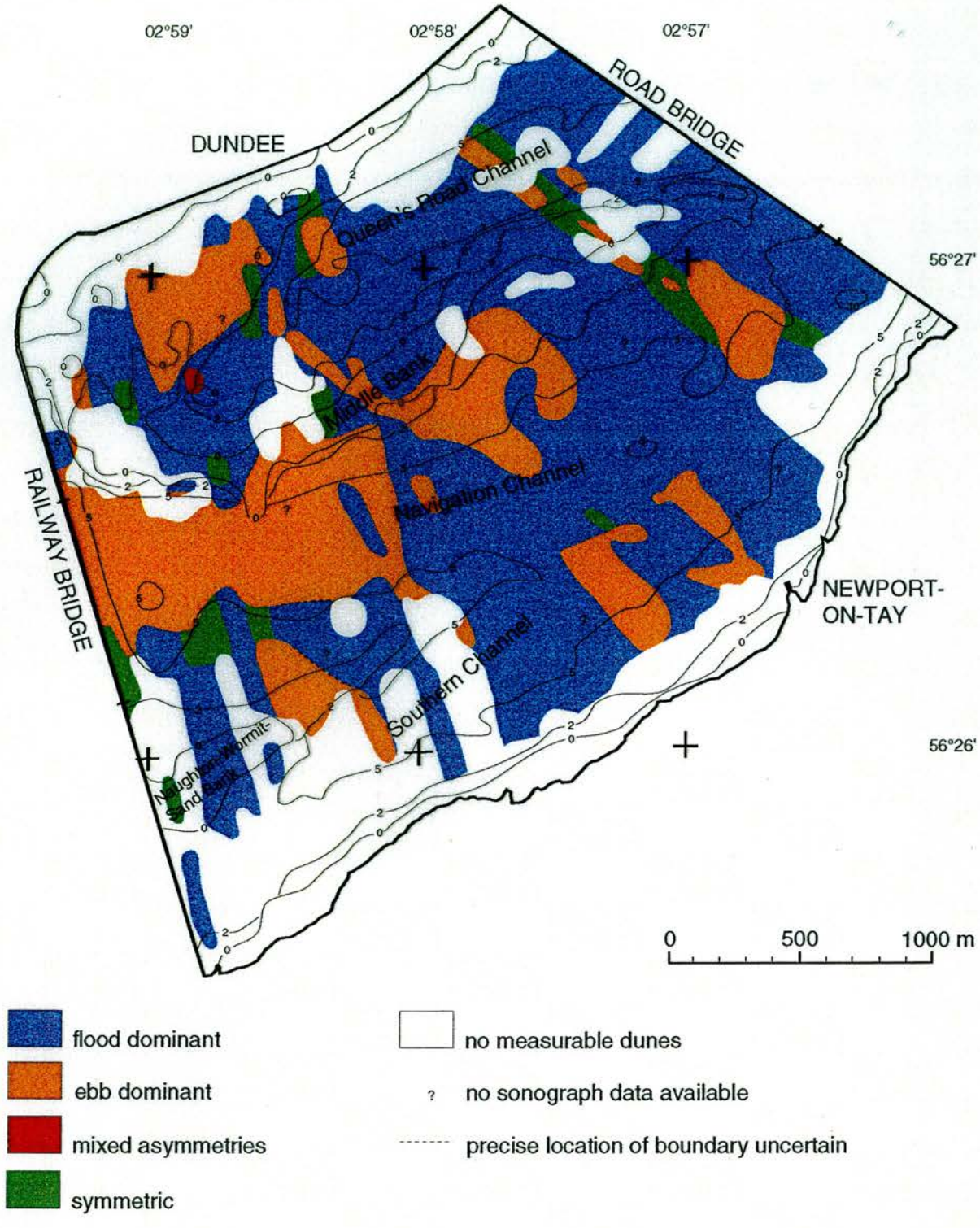

Fig. 5.28: Dune asymmetry during flood and slack tidal conditions as interpreted from side-scan sonographs.

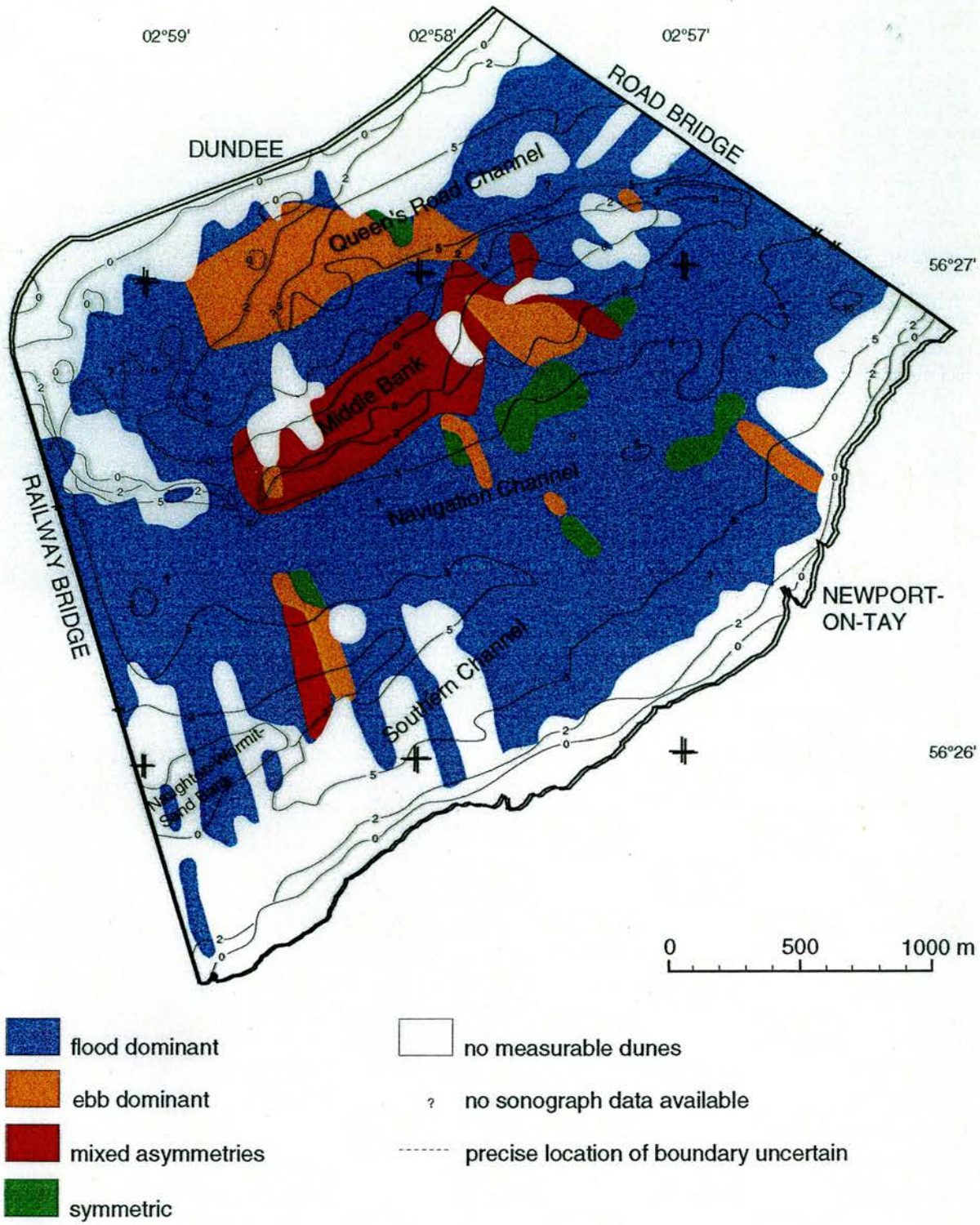

Fig. 5.29: Dune asymmetry during ebb tidal conditions as interpreted from side-scan sonographs.

flood dominance on the ebb tide. This is a remarkable result since the sonographs were recorded towards the end of the flood tide and the beginning of the ebb tide. Flood dominant areas and ebb dominant areas on Middle Bank during flood tidal conditions generally blend to a mixture of asymmetries on the ebb tide. Areas of symmetric dunes varied in position on the flood and ebb tide. The majority of symmetric dunes recorded on the flood tide were recorded as flood dominant dunes at the beginning of the ebb tide. Therefore, a change from symmetric to flood dominant dunes seems to take place at the end of the flood tide. Only a small area of symmetric dunes recorded on Middle Bank during the flood tide occurred in the region of mixed asymmetries during ebb tidal conditions. Areas in which symmetric dunes were recorded during ebb tidal conditions showed a variation of ebb and flood dominant dunes on the flood tide.

5.3.7 Crest orientation

As already mentioned in Section 4.6 dune crest orientation in conjunction with asymmetry is commonly used to estimate the direction of sediment transport. It is assumed that the dominant current or the sediment transport direction would be perpendicular to the crest orientation of the dunes. As also stated in Section 4.6 this is not always the case and estimation of sediment transport direction should be supported by current direction data. However, McManus (pers. comm.) has occasionally found currents to be oblique to the crests of dunes on Middle Bank. Therefore the following measurements of crest orientation give only an indication of bed sediment transport.

Flood

Most dune crests have a general south to north orientation (Fig. 5.30). Close to the Railway Bridge dune crest directions vary slightly from a south-south-east to north-north-west tendency. In Queen's Road Channel, as well as on and around Middle Bank, dune crest orientations vary between south-south-east to north-north-west, south-east to north-west and even south-west to north-east. A similar variation of crest orientations was recorded in the Southern Channel just off the TERC pier. Dunes in the eastern area of the Navigation Channel close to the Road Bridge also revealed deviations, although the majority of crests were oriented in a south-east to north-west direction.

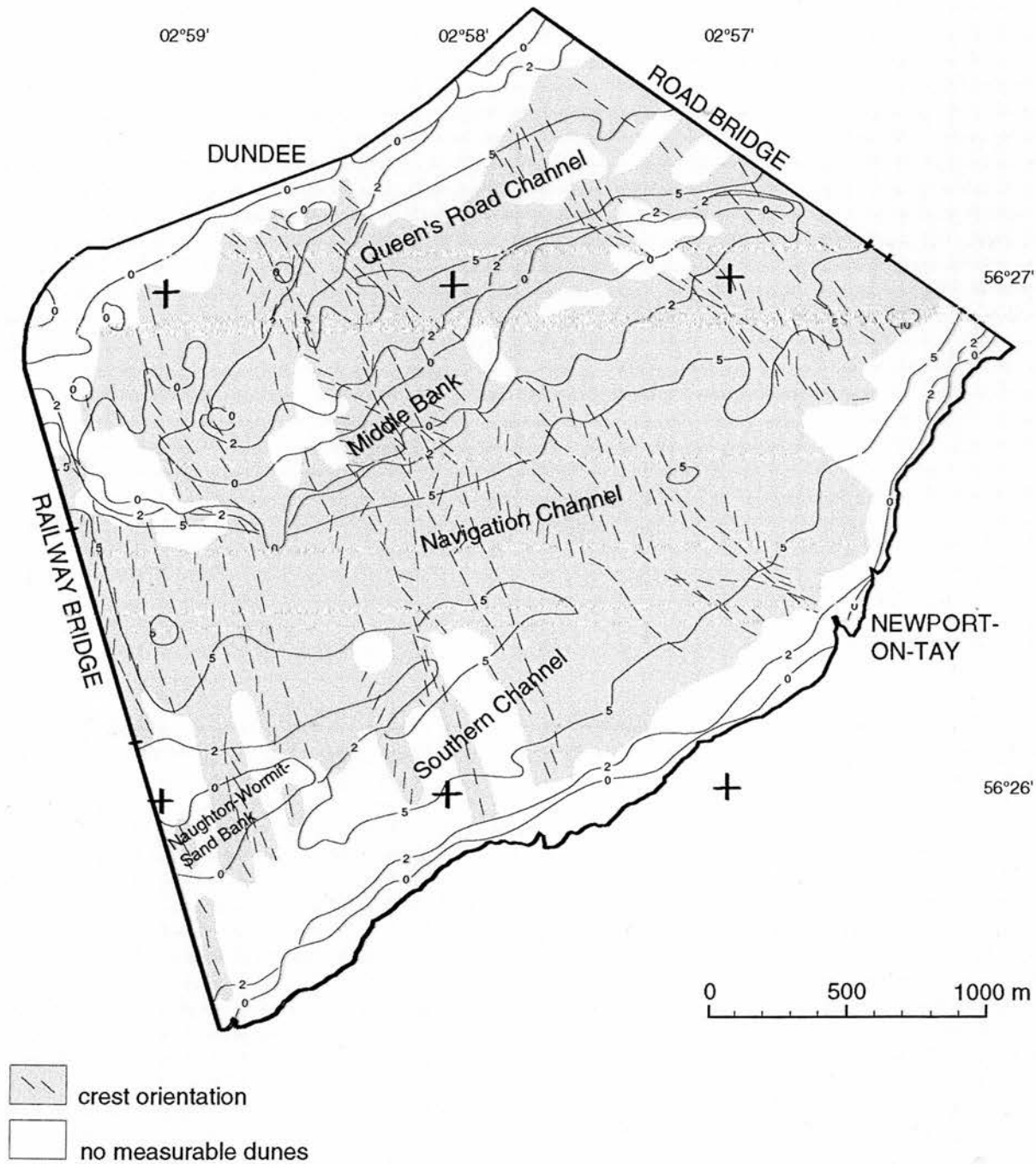

Fig. 5.30: Dune crest orienation during flood and slack tidal conditions as interpreted from side-scan sonographs.

Ebb

Crest orientations recorded during ebb tidal conditions (Fig. 5.31) displayed a prevalent south-north direction. In the western section of Queen's Road Channel an abrupt change in crest orientation from south-east to north-west, in the south, to south-west to north-east was revealed. This is also shown in the sonograph in Fig. 5.32. Another remarkable mixture of crest orientations was recorded in the centre part of the Southern Channel.

Comparison

Far more lines were run during flood tidal conditions than ebb during the various surveys. This may have caused some confusion when interpreting dune orientations because tides are never the same and small changes in current direction might also change crest orientations. The possibility of the tow fish streamlining at a slight angle to the boat is relatively high due to the strong currents in the estuary. The recorded (GPS) positions relate to the boat and not the tow fish so that slight variations cannot be ruled out. Nevertheless, the results show a general tendency of crest orientations lying in a north-south direction with deviations to either side but never turning east-west.

5.3.8 Summary of the interpretation of sonographs

Side-scan sonar surveys were carried out on seven days between August 1993 and March 1995. The recorded sonographs were analysed for geometrical parameters of dunes, namely: wavelength, height, length along dune crest, sinuosity, superposition, asymmetry and crest orientation, of which most are based on the classification by Ashley (1990).

The majority of the dunes recorded had small wavelengths of between 0.6 and 5.0m on both the flood and ebb tide. Dunes of small and medium heights were recorded in most areas of the channels and on Middle Bank while dunes of large heights were revealed in parts of the Navigation Channel and Queen's Road Channel. Most dune crests were between 20 and 50m long. In the Navigation Channel under the bridges lengths along dune crests decreased to 10-20m while the longest dune crests of over

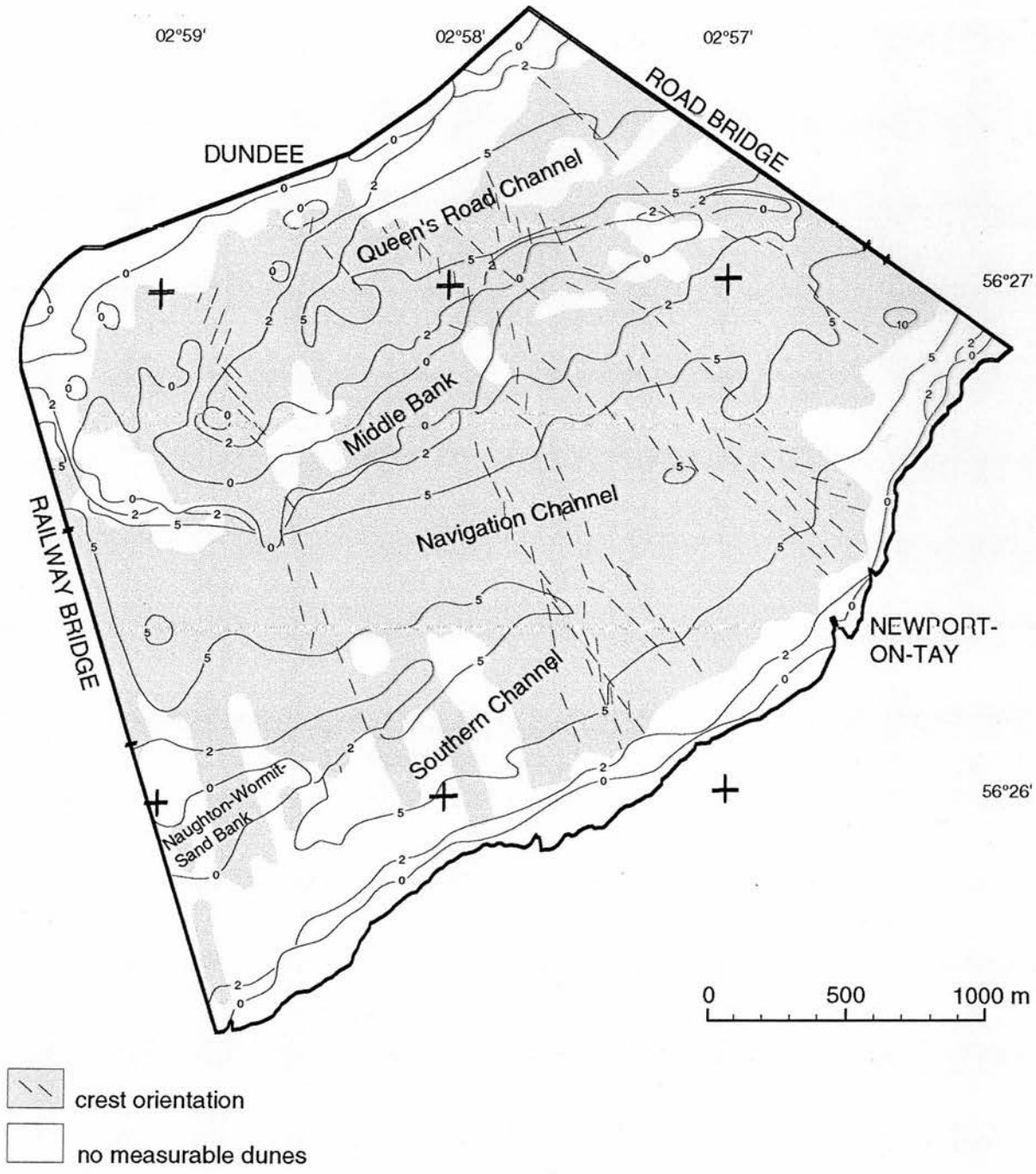

Fig. 5.31: Dune crest orientation during ebb tidal conditions as interpreted from side-scan sonographs.

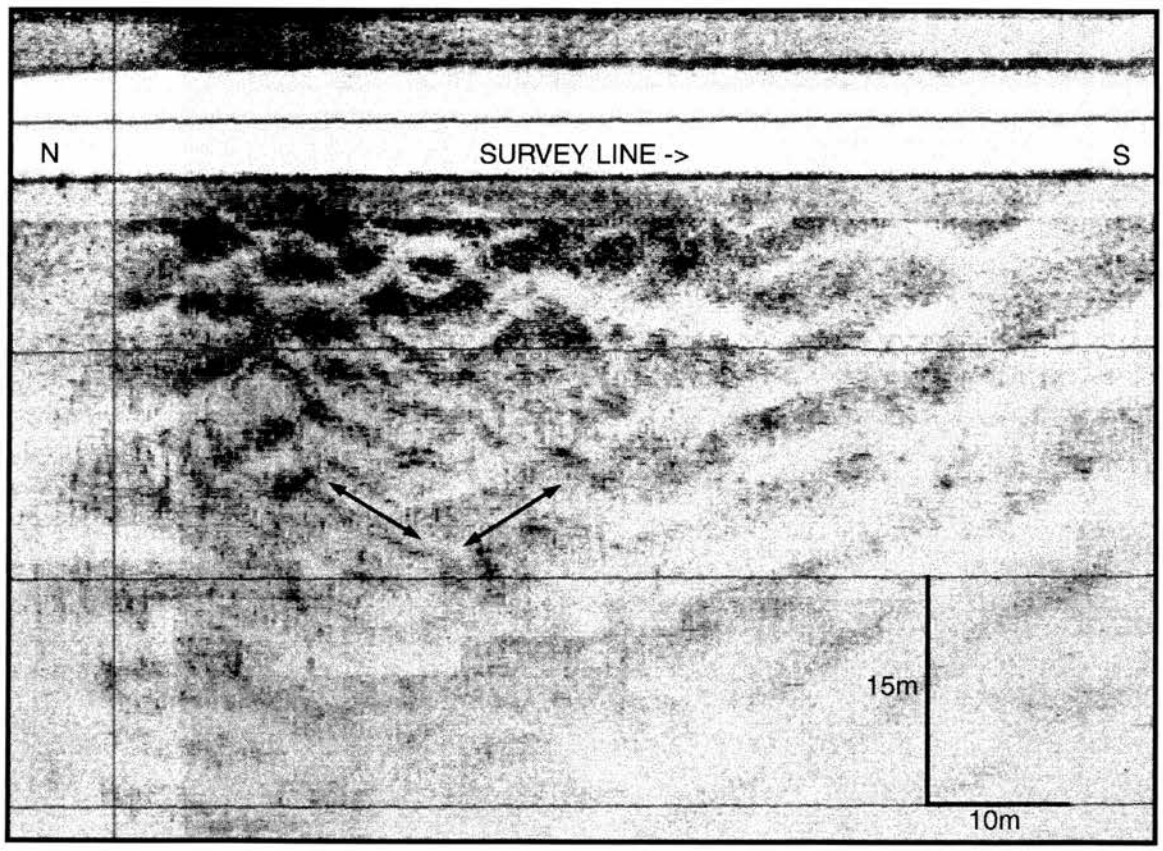

Fig. 5.32: Abrupt change of dune crest orientation (indicated by arrows) recorded in Queen's Road Channel. Location of record is shown in Fig. 5.33.

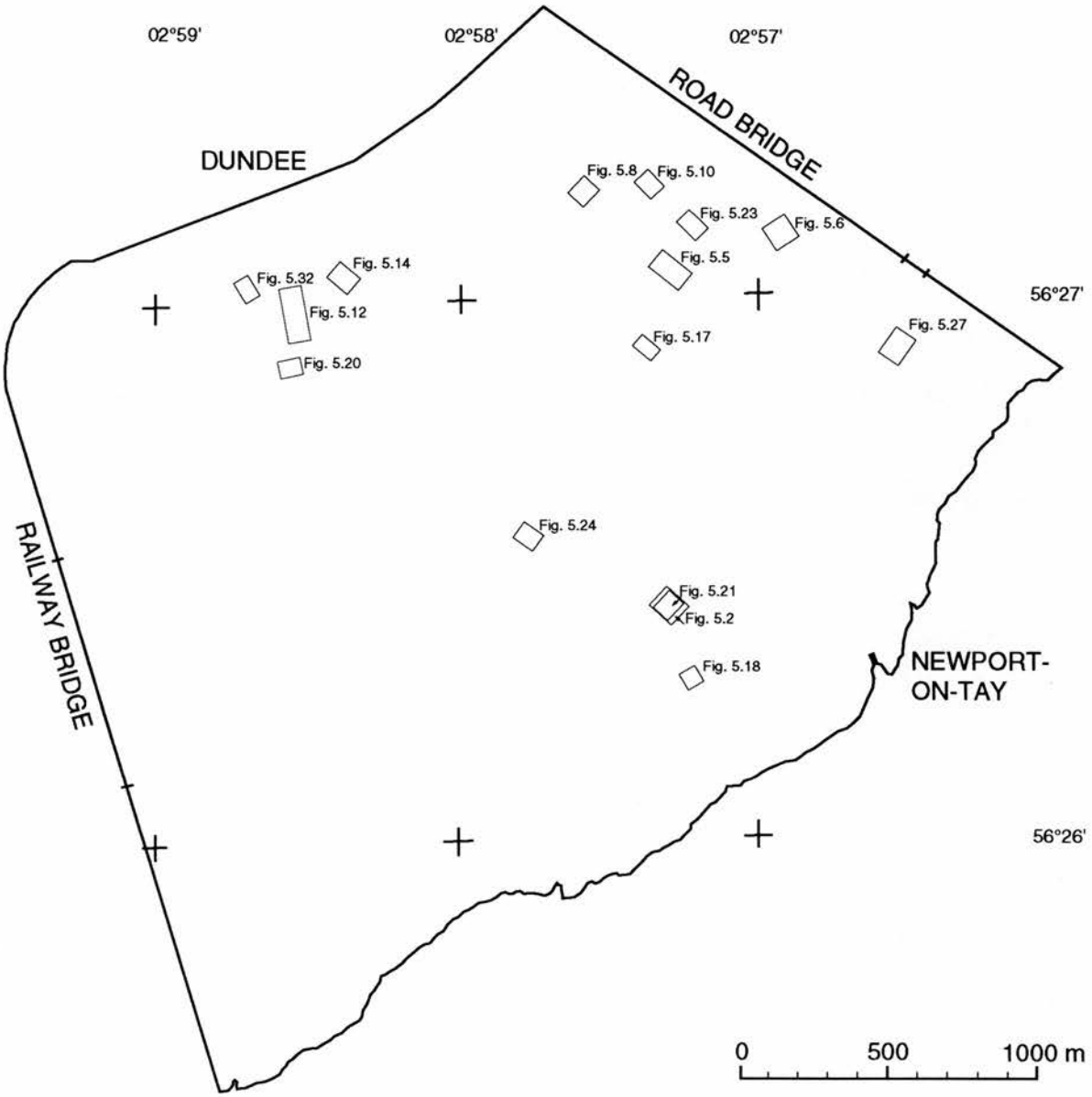

Fig. 5.33: Locations of sonographs shown in Figs. 5.2, 5.5, 5.6, 5.8, 5.10, 5.12, 5.14, 5.17, 5.18, 5.20, 5.21, 5.23, 5.24, 5.27 and 5.32.

200m were found in the eastern and central section of the Navigation Channel on the ebb tide. "Sinuous out of phase" was the dominant category of dune sinuosity for both tidal stages. "Patchy, discontinuous" crest shapes were restricted to the channels. Interference dunes were recorded during the ebb tide on Middle Bank as well as in the western half of the study area, north and south of the Navigation Channel. Compound bedforms occupied all shallower areas while simple bedforms lined the channels and deeper waters. Dunes are dominated by flood currents revealing strong asymmetries. Areas of mixed asymmetries were mainly found on Middle Bank during ebb tidal conditions. Generally the positions of ebb dominant areas change with the tides. Crest orientations were found to be south to north with a variety of deviations to either side but never turning east-west.

5.4 Geometrical parameters of dunes

Many researchers have investigated the relationships between dune wavelength and height and their occurrence at certain water depths. The present state of knowledge of intertidal bedforms is far greater than that of subtidal bedforms which are difficult to observe visually. Zarillo (1982), Goedheer and Misdorp (1985), Harris and Collins (1985), Ashley (1990), Berné *et al.* (1993) and Dalrymple and Rhodes (1995) have conducted research on subtidal dune morphology in tidal environments using side-scan sonar. Dalrymple *et al.* (1978), Dalrymple (1984) and Allen *et al.* (1994), as well as many others, have investigated intertidal bedforms. All of these authors investigated the relationships between dune morphology and water depth. In view of the analysis of the above workers a subdivision of dunes into subtidal and intertidal classes has been made.

In this section dune morphologies recorded in the study area of the Tay Estuary by side-scan sonar are examined in terms of intercorrelations of wavelength, height, length along dune crest and water depth. The data were analysed for the whole study area, then divided into intertidal and subtidal as well as into ebb and flood tidal data sets. Table 5.1 shows the results of statistical analysis using the Pearson Product-Moment Correlation Coefficient (r_{cc}). Highest correlation coefficients were computed for linear regression analysis but analysis for non-linear regression, such as exponential and logarithmic regression, was also carried out. However, these computed values were in the very low range

of around r_{cc}=0.000 and were therefore not investigated further apart from for comparable purposes with the results of other authors.

The Product-Moment Correlation Coefficient (r_{cc}) can vary between -1.000 and 1.000 with a value of 0.000 indicating no correlation. A value of 1.000 indicates a perfect positive correlation while a value of -1.000 indicates a perfect negative correlation. Table 5.1 shows that a strong positive correlation (r_{cc} close to 0.800) was found between dune wavelength and length along dune crest for the whole data set (Fig. 5.34) as well as for dunes recorded during the ebb and flood tide and for subtidal dunes during ebb and flood tidal conditions, but not for intertidal dunes. A strong negative correlation of r_{cc}=-0.844 (Table 5.1 and Fig. 5.35) was computed between height and wavelength of intertidal dunes recorded during ebb tidal conditions. This was the only strongly negative correlation found in all data sets. Values close to 0.000, indicating no or minimal correlation, were computed for the whole data set between water depth and wavelength as well as water depth and length along dune crest.

Table 5.1: Correlation coefficients (r_{cc}) computed for linear regression analysis of geometrical parameters of dunes and water depth.

a) all recorded dunes

	wavelength	height	length along dune crest
height	0.567		
length along dune crest	0.813	0.566	
water depth	-0.009	0.252	0.006

b) dunes recorded during flood and **ebb** tidal conditions

flood / **ebb**	wavelength	height	length along dune crest	water depth
wavelength		**0.604**	**0.827**	**-0.018**
height	0.508		**0.673**	**0.301**
length along dune crest	0.788	0.428		**0.020**
water depth	0.004	0.267	0.006	

c) intertidal and **subtidal** dunes

intertidal / **subtidal**	wavelength	height	length along dune crest	water depth
wavelength		**0.576**	**0.825**	**-0.041**
height	0.084		**0.575**	**0.214**
length along dune crest	0.283	0.243		**-0.031**
water depth	-0.166	0.614	0.220	

d) intertidal dunes recorded during flood and **ebb** tidal conditions

flood / **ebb**	wavelength	height	length along dune crest	water depth
wavelength		**-0.844**	**0.520**	**-0.550**
height	0.149		**0.596**	**0.583**
length along dune crest	0.270	0.244		**-0.318**
water depth	-0.095	0.648	0.220	

e) subtidal dunes recorded during flood and **ebb** tidal conditions

flood / **ebb**	wavelength	height	length along dune crest	water depth
wavelength		**0.606**	**0.827**	**-0.050**
height	0.524		**0.673**	**0.285**
length along dune crest	0.818	0.442		**-0.022**
water depth	-0.023	0.222	-0.021	

A commonly accepted (Ashley, 1990; Dalrymple and Rhodes, 1995; Kostaschuk et al, 1995; and others) correlation between dune height (H) and crest to crest spacing (L) for subtidal dunes was determined by Flemming (1988) as

$$H = 0.0677L^{0.8098}$$

while Zarillo (1982) found that maximum dune wavelengths were of the order of $2\pi H$ or

$$H = \frac{L}{6.283}$$

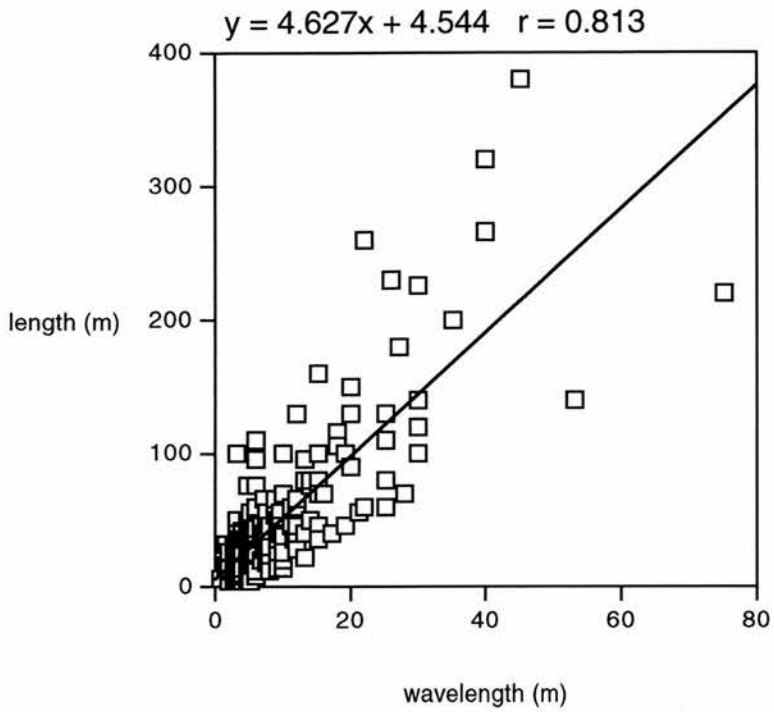

Fig. 5.34: Plot of dune wavelength versus length along dune crest as measured from sonographs (total data set).

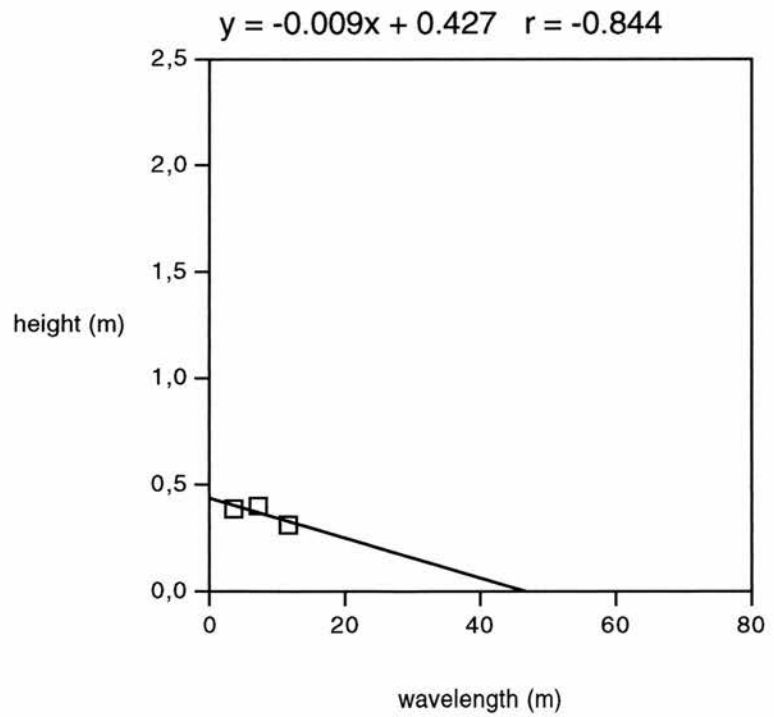

Fig. 5.35: Plot of intertidal dune wavelength versus dune height as measured from sonographs recorded during ebb tidal conditions.

in a tide-dominated salt estuary in Georgia. Dalrymple *et al.* (1978) found varying relationships between dune heights and wavelengths in intertidal environments depending on the type of dune measured (Table 5.2).

Table 5.2: Intertidal bedform size and morphological characteristics (after Dalrymple *et al.*, 1978; dune type after Ashley, 1990).

dune type	wavelength (m)	height (m)	characteristic
small to medium, simple, 2-d dune	0.1-25.0	0.05-0.50	-straight to smoothly sinuous -lack scour pits -height constant along crestline -wavelengths and heights poorly correlated: $H=0.0947L^{0.346}$ (r=0.462 for n=70)
small to medium, simple, 3-d dune	0.05-14.0	0.05-0.70	-sinuous to lunate in plan -scour pits -height variable along crestline -wavelengths and heights well correlated $H=0.0865L^{0.787}$ (r=0.788 for n=255)
large to very large, compound dune	10.0-215.0	0.15-3.4	-straight to sinuous in plan -lack scour pits -height constant along crestline -wavelengths and heights moderately correlated $H=0.0635L^{0.733}$ (r=0.791 for n=58)

A correlation between dune height (H) and wavelength (L) of dunes measured from sonographs in this study was computed to be

$$H = 0.247L^{0.375}$$

with the correlation coefficient being r_{cc}=0.591. The analysis of subtidal dunes revealed a similarly positive correlation between dune wavelength and height. The value of the correlation coefficient is r_{cc}=0.576 (Table 5.1 and Fig. 5.36) for a linear regression and r_{cc}=0.614 for an exponential regression giving a relationship between dune height (H) and wavelength (L) of

$$H = 0.246L^{0.384}$$

for subtidal dunes. No good correlation was found between dune wavelength and height for intertidal dunes recorded by side-scan sonar. The value of the correlation coefficient of the linear regression analysis was as low as r_{cc}=0.084 (Table 5.1 and Fig. 5.37) but slightly higher for the exponential regression (r_{cc}=0.220) giving a relationship between dune height (H) and wavelength (L) of

$$H = 0.313L^{0.154}$$

for intertidal dunes. A further division of the intertidal data set into the three types of dunes as described by Dalrymple *et al.* (1978) (Table 5.2) was made. Type 1 of the intermediate dune type scale revealed no correlation with the coefficient being r_{cc}=0.001 but only two dune groups of this type had been recorded. The correlation coefficient computed for dunes of type 2 of the intermediate scale was r_{cc}=0.000 although 19 dune groups of this type had been recorded in the intertidal environment. For the large scale dune types only one group was recorded and no further analysis was possible.

As already mentioned in Section 4.4, measurements of dune height and wavelength in previous studies have shown a positive relationship with water depth (Dalrymple and Rhodes, 1995). Allen (1970) suggested the formula

$$H = 0.086d^{1.19}$$

for the relationship between dune height (H) and water depth (d). Yalin (1977), however, suggests that dune height should be approximately 17% of the water depth or

$$H = 0.167d$$

based on a combination of theory and empirical observations and wavelength (L) and water depth (d) are related to each other as

$$L = 6d$$

as mentioned in Section 4.4. In common with the findings of Bokuniewicz *et al.* (1977) (see Section 4.4) no perfect correlation between dune height

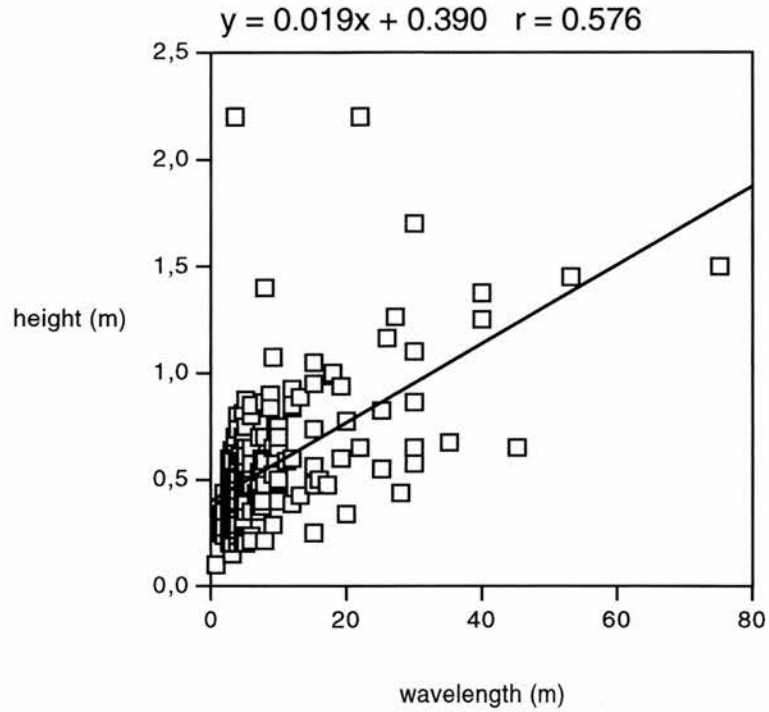

Fig. 5.36: Plot of subtidal dune wavelength versus dune height as measured from sonographs.

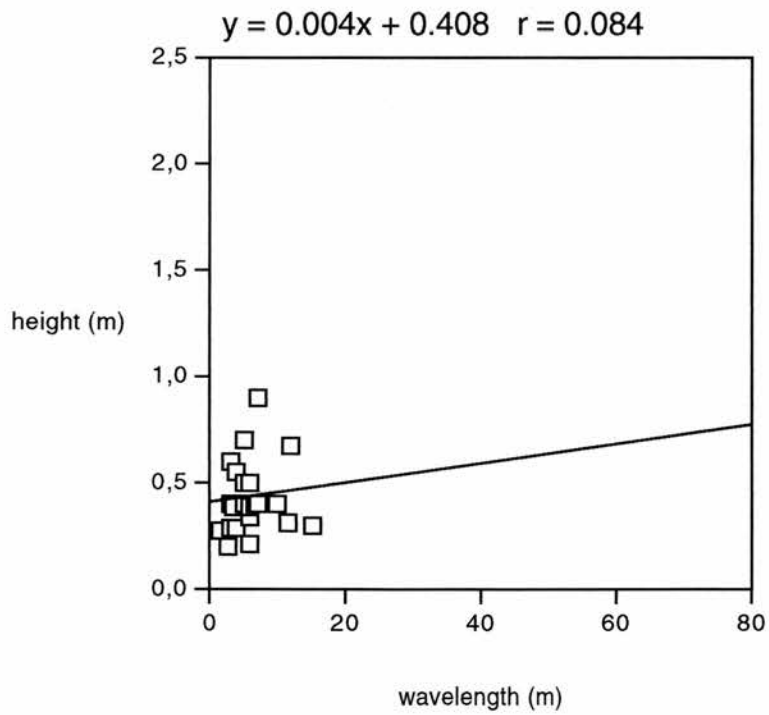

Fig. 5.37: Plot of intertidal dune wavelength versus dune height as measured from sonographs.

and water depth or dune wavelength and water depth was found in this study (Table 5.1, Figs. 5.38 and 5.39). It is questionable how closely related these two parameters are in natural environments. Water depth changes with the tidal state, especially in estuaries, and varies in the study area between 4 and 6m (see Section 2.3.2.1). For the following computations the water depth was derived on the basis of the first bottom return on the sonographs (see Section 3.2.2.2). Exponential regression analysis of the data collected suggests a relationship between dune height (H) and water depth (d) of

$$H = 0.113d^{0.623}$$

with the correlation coefficient being r_{cc}=0.335. Intertidal dunes showed a stronger correlation between dune height (H) and water depth (d) with the coefficient being r_{cc}=0.636 for a relationship of

$$H = 0.044d^{1.099}$$

while dune height (H) and water depth (d) of subtidal dunes were not as strongly correlated (r_{cc}=0.295) with a relationship of

$$H = 0.122d^{0.589}$$

Most values of the linear correlation coefficient (r_{cc}) were between r_{cc}= -0.550 and r_{cc}=0.004 for dune wavelength and water depth. An exponential relationship between dune wavelength (L) and water depth (d) was computed as

$$L = 8.679d^{-0.186}$$

for all dunes recorded by side-scan sonar but the correlation coefficient showed no correlation being close to zero (r_{cc}=0.078). Similar results were computed for intertidal and subtidal dunes with correlation coefficients being close to 0.000. Linear correlation coefficients (r_{cc}) for dune height and water depth were between r_{cc}=0.214 and r_{cc}=0.301 with higher values of up to 0.648 for intertidal dunes as well as for intertidal dunes recorded during ebb or flood tidal conditions.

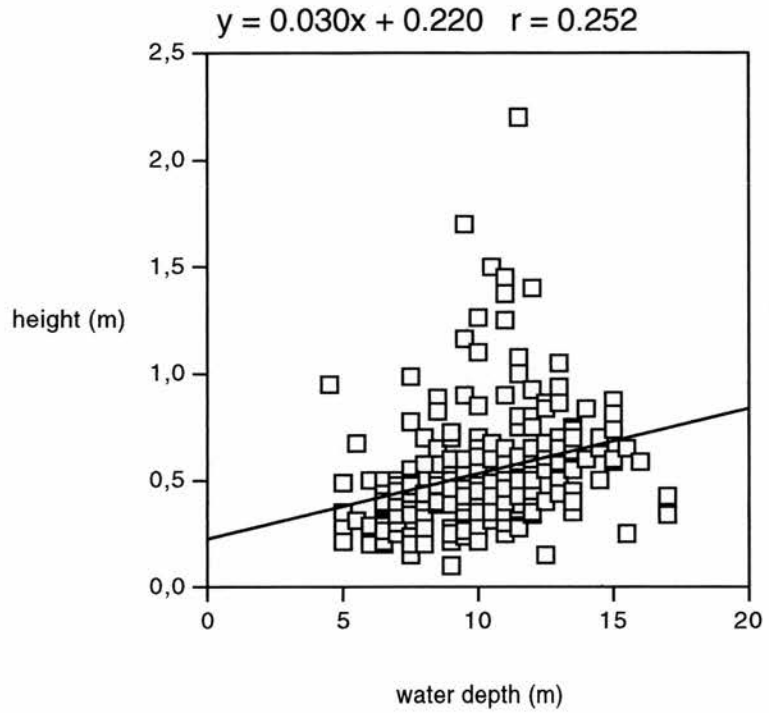

Fig. 5.38: Plot of water depth versus dune height as measured from sonographs (total data set).

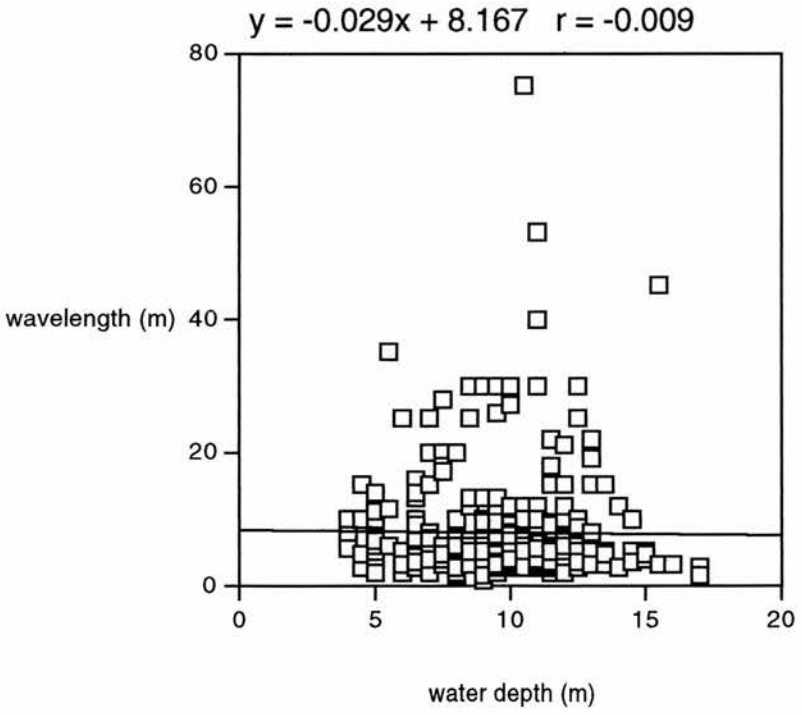

Fig. 5.39: Plot of water depth versus dune wavelength as measured from sonographs (total data set).

5.5 Conclusions

Many different shapes and sizes of dunes were recorded during the side-scan sonar surveys of this project. However, such a remote sensing technique can give only an indication of the findings on the sea bed and an element of doubt exists in the interpretation of side-scan sonographs. In 1980 Morang and McMaster, for example, interpreted sand wave bedforms from sonographs off the coast of Rhode Island, U.S.A., which were subsequently shown by Cook (1982) and Werner (1982) to be acoustical interference patterns. Therefore, additional data to support sonograph interpretation is required. This was achieved by means of echo-sounding (see Chapter 6), current measurements (see Chapter 8) and sediment sampling (see Chapter 7). The former allows a more precise measurement of bedform height, although it is also an acoustic remote sensing technique. The latter yields important ground information.

The great variety of relationships computed between dune height and wavelength, dune height and water depth and dune wavelength and water depth suggest that these parameters do not just depend on one another but are part of a far more complex system. Many authors have tried to establish relationships between the above examined parameters. Dalrymple *et al.* (1978), Zarillo (1982) and Flemming (1988) established positive relationships between dune height and dune wavelength but with different formulae. Flemming's (1988) formula has been accepted and used in studies where dune height could not be measured but had to be calculated for sediment transport predictions (Ashley, 1990; Kostaschuk *et al.*, 1995). Yalin (1964, 1977, 1987), similarly to Allen (1968), used a combination of theory and empirical observation to establish relationships between dune height and water depth unlike Goedheer and Misdorp (1985) who investigated dunes solely in natural environments and were not able to establish a relationship between dune height and water depth but recorded the highest dunes in their area of study, Oosterschelde (south-west Netherlands), in the shallowest waters. However, Goedheer and Misdorp (1985) studied a small part only of the Oosterschelde, namely one of the subtidal channels, the Schaar van Colijnsplaat. Similar to the Tay Estuary a semidiurnal tide occurs in this subtidal channel but the tidal amplitude ranges from about 2.3m at neap tide to about 3.0m at spring tide only, unlike the tidal range of 4.0-6.0m in the Tay Estuary. Bokuniewicz *et al.* (1977) also found no strong correlations between dune

height and water depth nor dune wavelength and water depth when studying sedimentary bedforms in the eastern Long Island Sound, U.S.A.. Although semidiurnal tides also occur in the Long Island Sound, this estuary is far larger than the Tay Estuary being 150km long and up to 40km wide compared with 50km in length and up to 4km wide. The results of the regression analysis carried out in this project show that the relationships between dune height and wavelength, dune height and water depth and dune wavelength and water depth vary considerably and that general formulae should be used only for rough estimations. The influence of more variables such as flow strength and sediment characteristics as well as sediment availability needs to be investigated before more generally acceptable formulae can be established although Dalrymple and Rhodes (1995) state that these variables have an important influence on dune occurrence, sizes and shapes and migration.

Chapter 6

BEDFORM GEOMETRIES RECORDED BY ECHO-SOUNDING

6.1 Introduction

Sonographs do not permit exact measurement of bedform dimensions but only give a good indication. Echo-sounders on the other hand can be used to measure bedform dimensions with a higher accuracy. However, echo-sounders give a two-dimensional profile of the bedform and do not produce a plan view of an area like side-scan sonar. Therefore, echograms may be used to measure crest to crest spacing, bedform height, superposition and asymmetry. The results of the echo-sounding survey were compared with those of the side-scan sonar survey. The accuracy, especially when measuring bedform height, depends on the water depth and the chosen scale of the print-out giving a different resolution to the side-scan sonar system. A description of the echo-sounder employed in this project, the Lowrance X-16, can be found in Section 3.2.1.5.

6.2 Data collection

The aim of the echo-sounding surveys was to collect data in areas where bedforms could not be clearly identified or measured from the sonographs. The side-scan sonar systems were not able to produce good records in the shallow waters over Middle Bank. Therefore, echo-sounding was concentrated mainly in this area.

An inexplicable pattern was recorded in most parts of the channels (see Section 5.3.4). Patchy, discontinuous patterns recorded by side-scan sonar needed to be identified as it was not certain whether they were produced by bedforms or by material changes on the bed, for example by areas of mussels and gravel alternating with sand. In consequence, echo-sounding traverses were carried out in channel areas where this signature was characteristically recorded on sonographs.

On 10.05.95 three echo-sounding traverses were run during flood tidal conditions - one along the Railway Bridge from south to north, one along

the northern edge of Middle Bank from west to east and one along the middle section of the Road Bridge from north to south. Data from another six traverses were recorded on 25.05.95. All six traverses ran over and along the edges of Middle Bank. The first three were recorded before high tide during flood tidal conditions, while the other three were recorded after high tide during ebb tidal conditions. During the flood tide two traverses extended from east to west and one from west to east, while during the ebb tide two lines were recorded from west to east and one from east to west (Fig. 6.1).

In July 1996 a survey was conducted during flood and slack tidal conditions consisting of a grid of six lines in the Navigation Channel at the Railway Bridge, with three lines running in a north-south direction and the other three running in an east-west direction. One longer line was also recorded in the Southern Channel (Fig. 6.1).

6.3 Bedform geometry

The echo-sounding data were analysed for dune wavelength, height, superposition and asymmetry and were, in common with the sonograph data (Chapter 5), separated into data recorded on the flood and the ebb tide. As in Chapter 5 all bedforms observed were dunes according to the classification of Ashley (1990). Small sections of the echo-soundings could not be interpreted either because of their poor quality or because of necessary changes of range scale during which no data were recorded. These sections are shown in the maps (Figs. 6.2, 6.3, 6.11, 6.12) as the black traverse lines and are not coloured as the interpreted data. Measurements of wavelength and asymmetry could be made only where the echo-sounding lines were run perpendicular to the crest orientations of the dunes. Therefore lines which were run parallel to the crest orientations are not included in Figs. 6.2, 6.3, 6.11 and 6.12.

6.3.1 Wavelength

The dune wavelength or crest to crest spacing recorded by echo-sounding has to be measured in a different way than from sonographs. The first step is to calculate the distance travelled between two adjacent GPS fixes and relate this distance to the corresponding fix marks on the echograms to determine the wavelength. Therefore the accuracy of the calculated

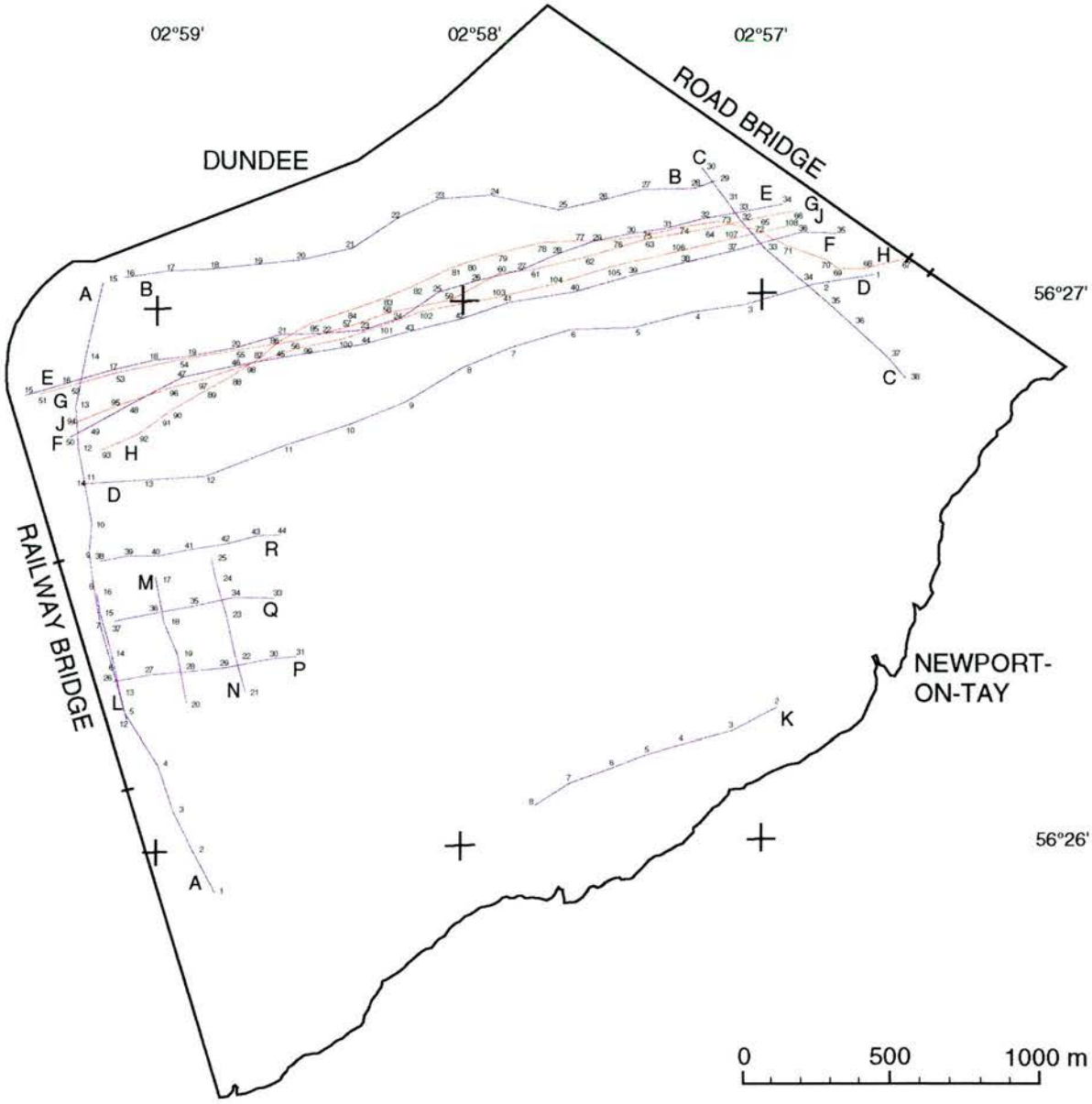

Fig. 6.1: Echo-sounding traverses recorded during ebb and flood and slack tidal conditions. Numbers denote position fixes and letters indicate traverse start and end points.

wavelength depends on the accuracy of the GPS system employed (see Section 3.2.3.2). Crest to crest spacing is divided into four classes: small - 0.6 to 5.0m, medium - 5.0 to 10.0m, large - 10.0 to 100.0m and very large - over 100.0m. Dunes with wavelengths of all four classes were recorded during both flood and ebb tidal conditions.

Flood

Dune wavelengths recorded during flood tidal conditions are shown in Fig. 6.2. No class dominates although very large wavelengths were recorded in only relatively small areas. The echogram from the Southern Channel (traverse K) displays small dunes with wavelengths of approximately 3m in its eastern part which increase to 14m (large) in the centre section before decreasing again to 7m (medium) and once more increasing to 15m (large) at its western end. Dune wavelengths in the Navigation Channel close to the Railway Bridge (traverses P, Q and R) were between 6m (small) and up to 130m (very large) in length. Along the southern edge of Middle Bank (traverse D) dunes of medium and large wavelengths (between 5.5 and 23.0m) were recorded on the eastern and western ends of the traverse while the centre section revealed dune wavelengths of less than 5m. The two traverses E and F on Middle Bank recorded dunes with wavelengths mainly of the large class with two sections of very large crest to crest spacings (up to 120m) in the western half and dunes with small wavelengths (just under 5m) at the eastern end. The northern line B recorded dunes with wavelengths of between 7 and 14m in its western half which decrease to under 5m in its eastern half.

Ebb

Large wavelength dunes were found at the western end of Middle Bank (Fig. 6.3) with crest to crest spacings of between 19 and 40m. On the centre traverse G wavelengths increased to 150m (very large), while on the southern traverse J and northern traverse H wavelengths decreased to 6m (medium class). The centre section displayed dune wavelengths of the large class before decreasing to medium and small wavelengths at the eastern end of the traverses towards the Road Bridge.

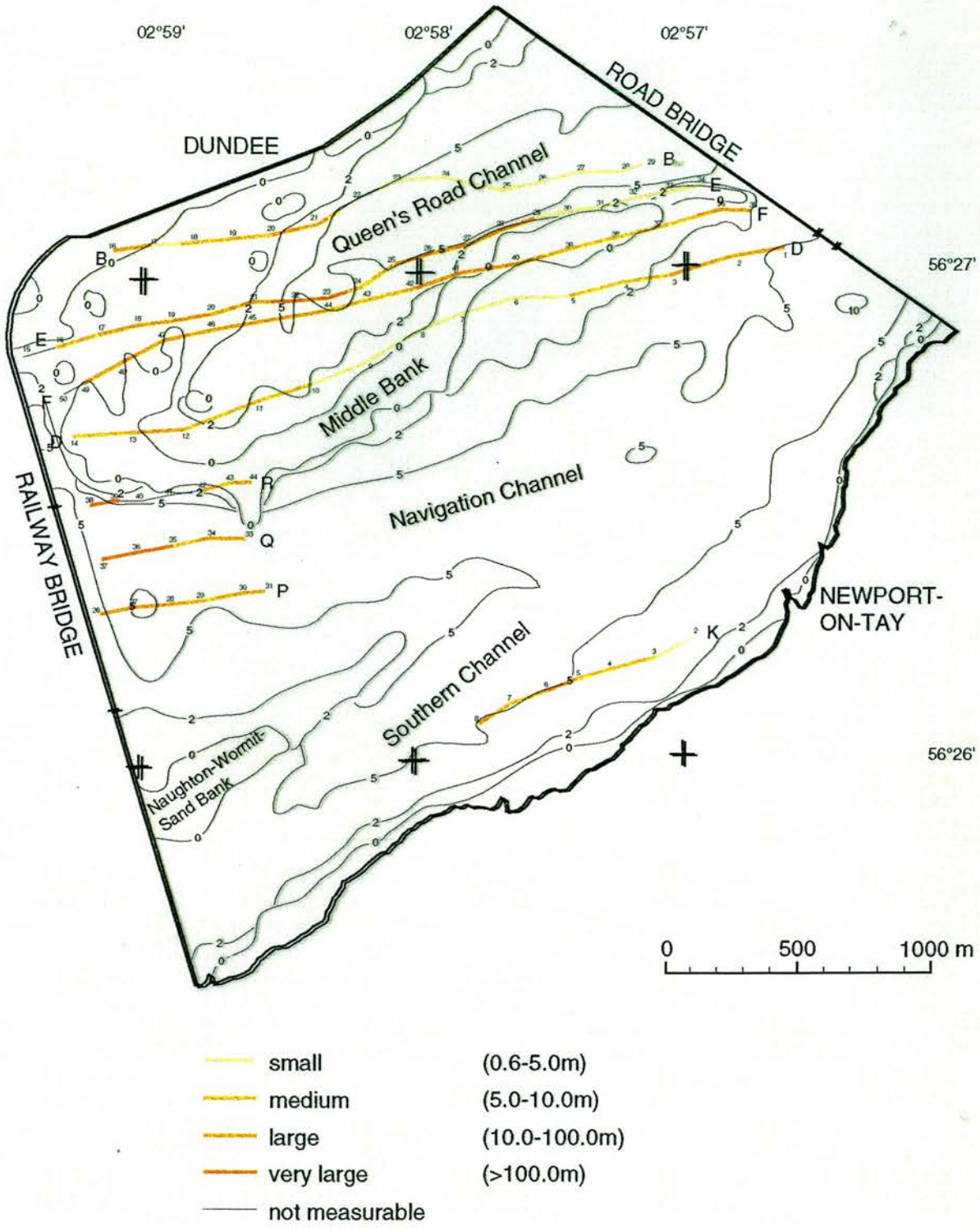

Fig. 6.2: Dune wavelength during flood and slack tidal conditions as determined by echo-sounding. Classification after Ashley (1990). Numbers denote position fixes and letters indicate traverse start and end points.

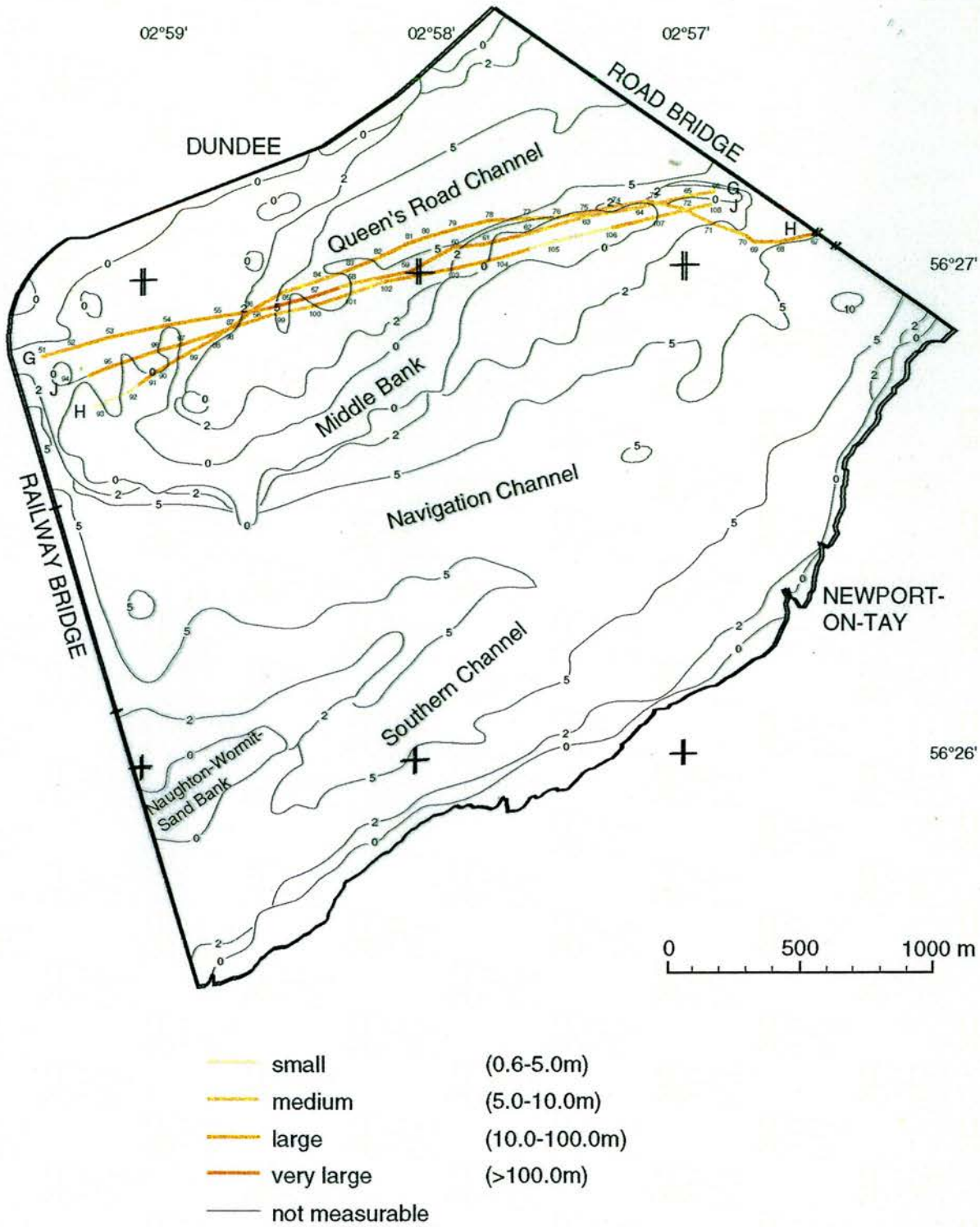

Fig. 6.3: Dune wavelength during ebb tidal conditions as determined by echo-sounding. Classification after Ashley (1990). Numbers denote position fixes and letters indicate traverse start and end points.

Comparison

During both stages of the tide dunes characterised by very large wavelengths, of up to 150m, were recorded just west of the centre of Middle Bank. The western ends of the traverses as well as the centre sections display large crest to crest spacings but with high variations of between 16 and 96m. Towards the Road Bridge, at the eastern end of the traverses, dune wavelengths decrease to medium and small lengths.

6.3.2 Height

It is relatively straightforward to measure bedform heights from echograms. However, the accuracy of such measurement depends on the range scale chosen on the print-out. During the echo-sounding surveys in summer 1995 the echo-sounder was set to a range scale of either 0-15m or 0-20m, recording on a paper width of 9cm. This does not permit accurate measurement of bedform heights of less than 0.25m. Therefore, it was necessary to combine the category of small dune heights with that of the medium class. Nevertheless, flood and ebb tidal echograms recorded a variety of dune heights. The same classification of Ashley (1990), as described in Sections 4.3 and 5.3.2, is applied, although the small and medium classes were grouped as one: small to medium - 0.05 to 0.50m, large - 0.50 to 3.00m and very large - over 3.00m.

Flood

Dunes of small to medium height dominate the study area (Fig. 6.4). An irregular distribution of dunes with large heights was recorded in the channel as well as along the edges of Middle Bank, alternating with dune heights of the small and medium class. A very short line of less than 100m revealed dune heights of over 3m at GPS fix 35 of traverse F, the highest dunes found in the study area in this project.

Ebb

During ebb tidal conditions mainly large dunes were recorded on the three traverses G, H and J (Fig. 6.5). The western ends of all traverses displayed dunes of small and medium heights, as well as the north-eastern ends of traverses G and J, while dunes with large heights were

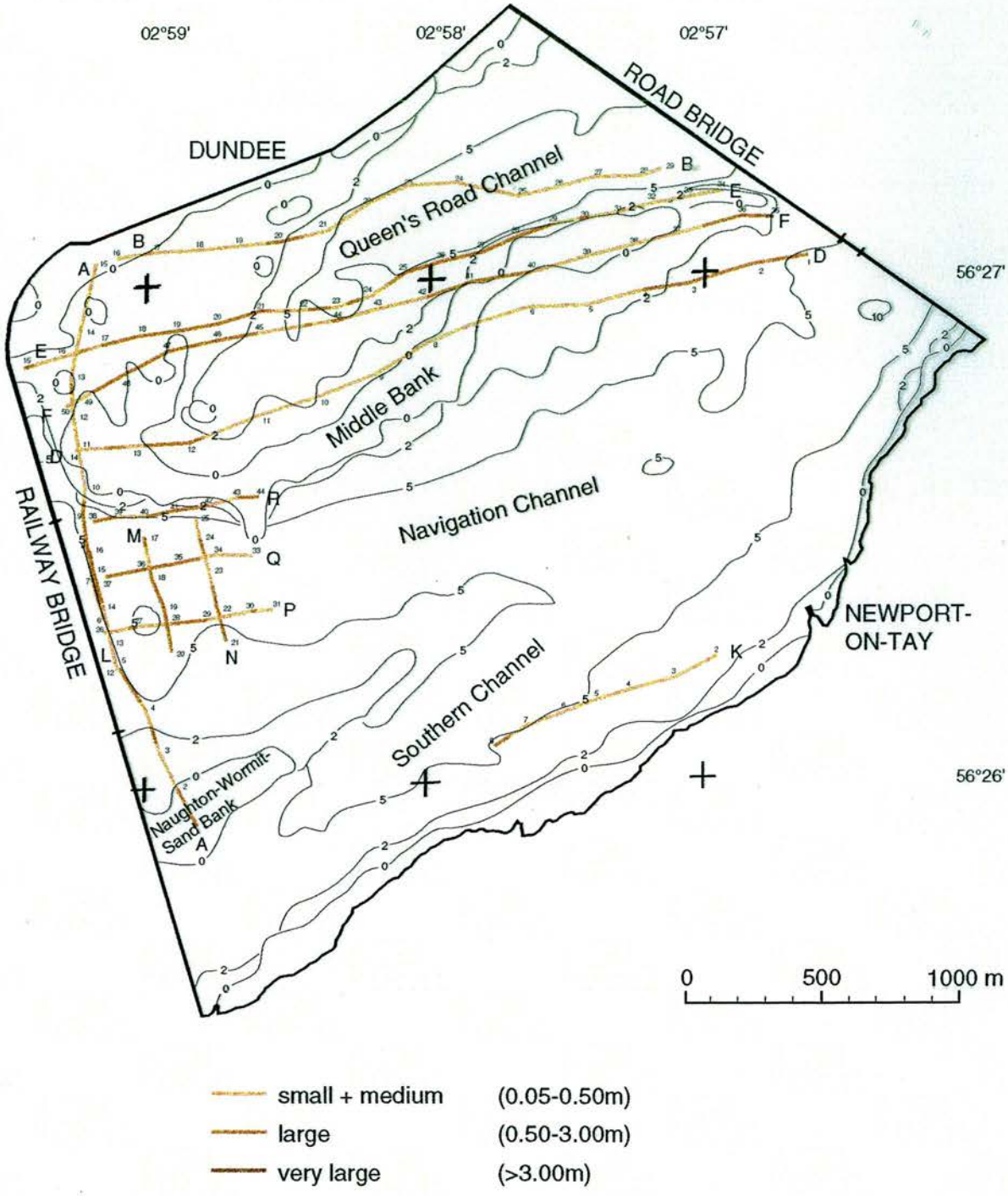

Fig. 6.4: Dune height during flood and slack tidal conditions as determined by echo-sounding. Classification after Ashley (1990). Numbers denote position fixes and letters indicate traverse start and end points.

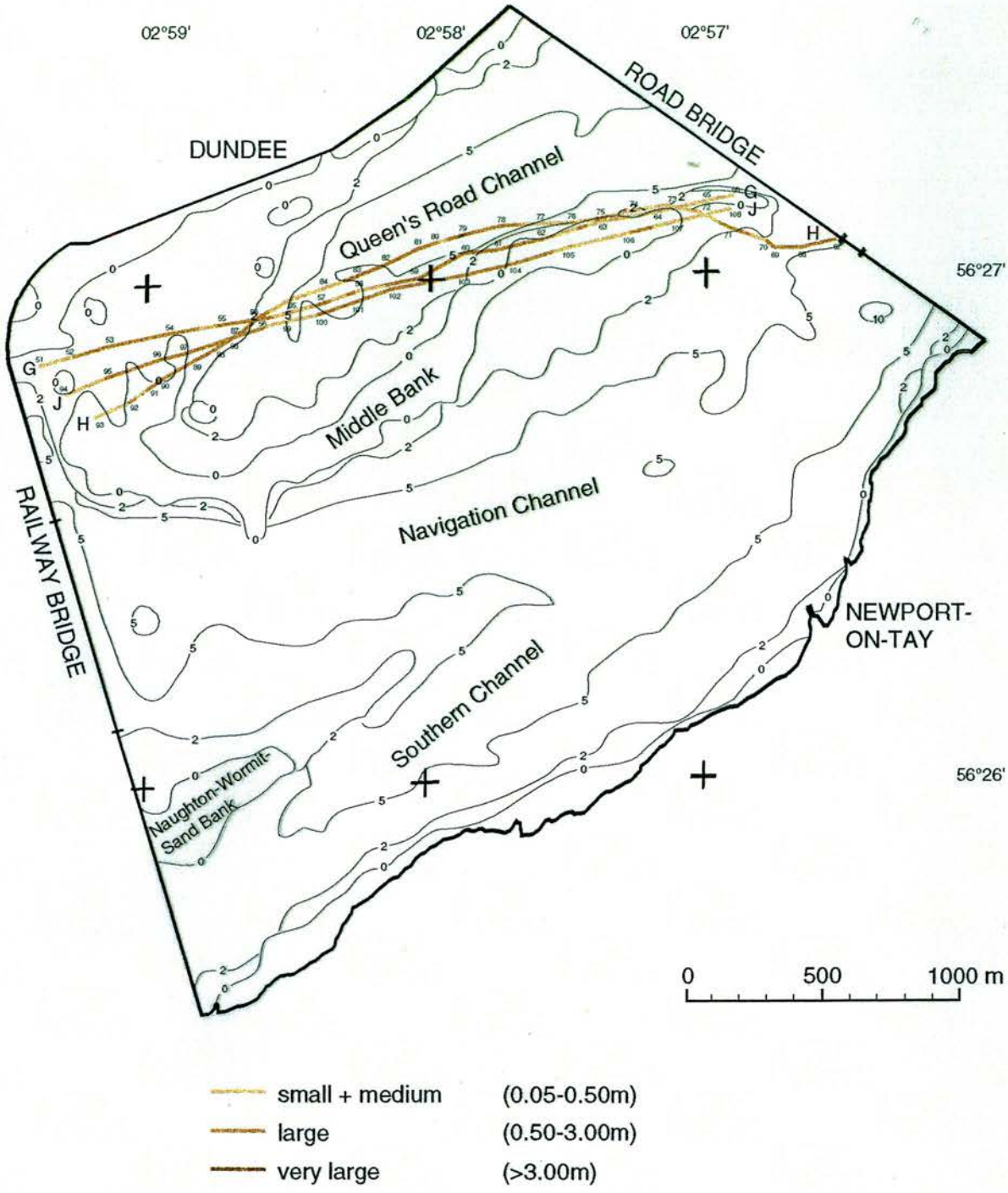

Fig. 6.5: Dune height during ebb tidal conditions as determined by echo-sounding. Classification after Ashley (1990). Numbers denote position fixes and letters indicate traverse start and end points.

recorded on the south-eastern traverse H. One isolated very large dune with a height of over 3m was revealed at GPS fix 79 of traverse H (Fig. 6.5).

Comparison

Most dune heights recorded during flood tidal conditions belong to the small and medium class. Dunes on Middle Bank had various heights but, especially along the edges, small and medium heights dominate. Dunes in the channel also revealed big variations in height with no clear dominance. However, most areas of Middle Bank displayed dunes of large heights on the ebb tide although small and medium dune heights were also recorded, especially at the far western end as well as at the north-eastern end.

6.3.3 Superposition

Ashley (1990) divides bedform superposition into two categories: 1. simple dunes which lack superimposed dunes and 2. compound dunes which bear smaller, superimposed dunes. Echograms of simple and compound dunes are shown in Figs. 6.6 and 6.7.

Flood

Most sedimentary bedforms recorded by echo-sounding during the flood tide were compound dunes (Fig. 6.8). They were especially found on Middle Bank but also on four of the grid lines recorded in the Navigation Channel. The line K in the Southern Channel as well as the lines A and L running parallel to the Railway Bridge revealed mainly simple dunes. Simple dunes were also recorded on traverses B and E in the north-eastern section of the study area.

Ebb

The three lines (G, H and J) run during ebb tidal conditions revealed simple dunes at the eastern end of the traverses close to the Road Bridge (Fig. 6.9). Along 250m on the northern traverse H as well as 100m in the north-western area of traverse G simple dunes were recorded. The echograms of the remaining lines revealed compound dunes.

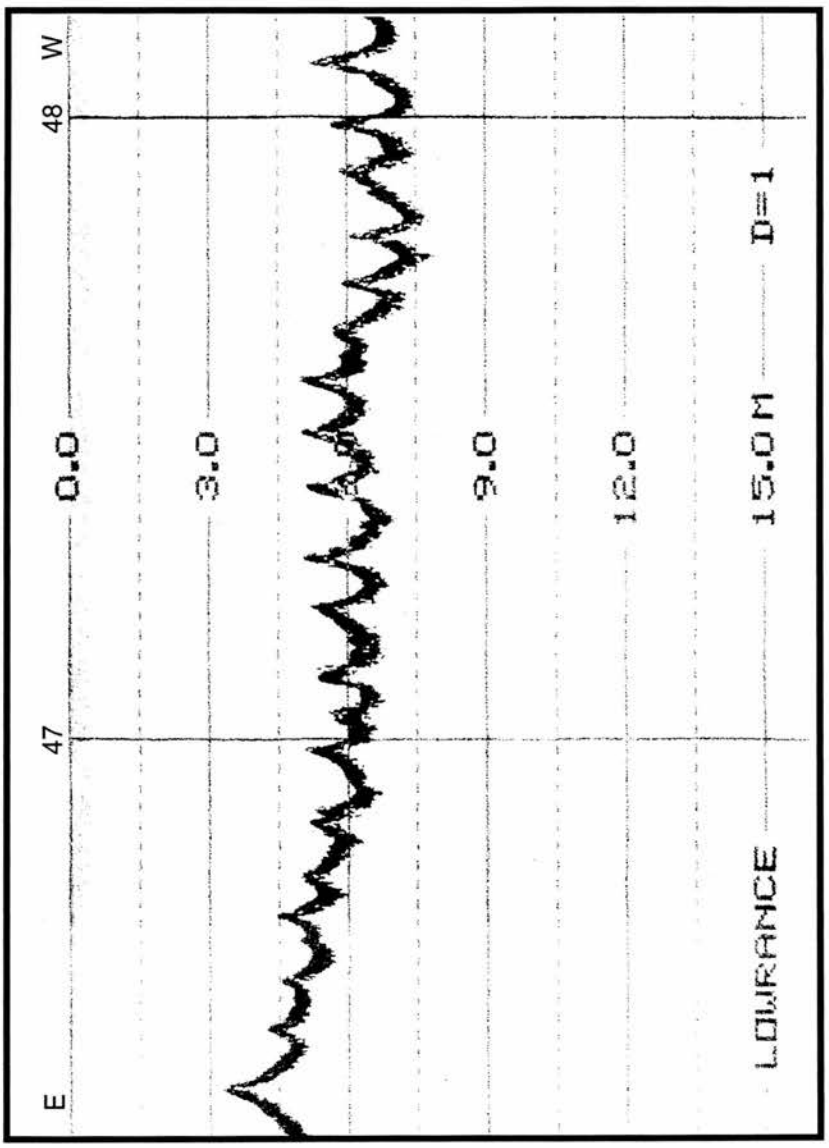

Fig. 6.6: Echogram of simple dunes recorded between GPS fixes 47-48 of traverse F. Vertical scale in metres.

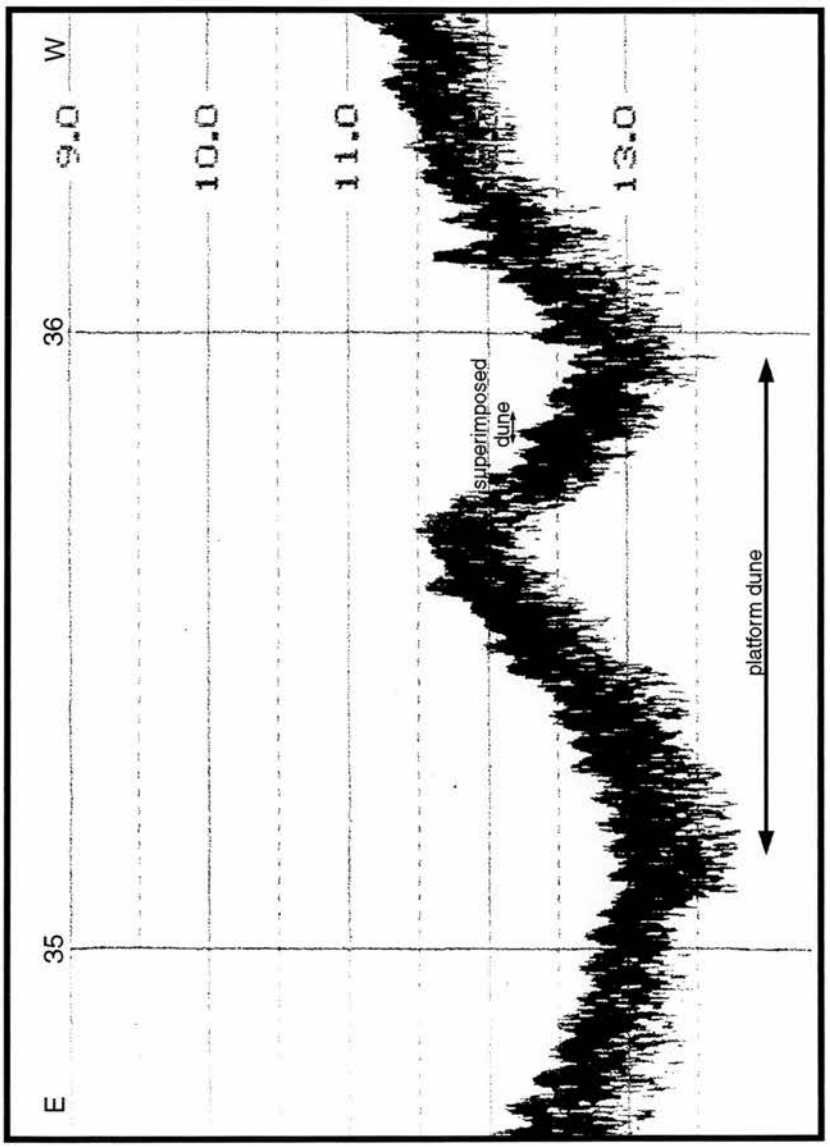

Fig. 6.7: Echogram of compound dunes recorded between GPS fixes 35-36 of traverse Q. Top of scale is 9.0m below the water surface.

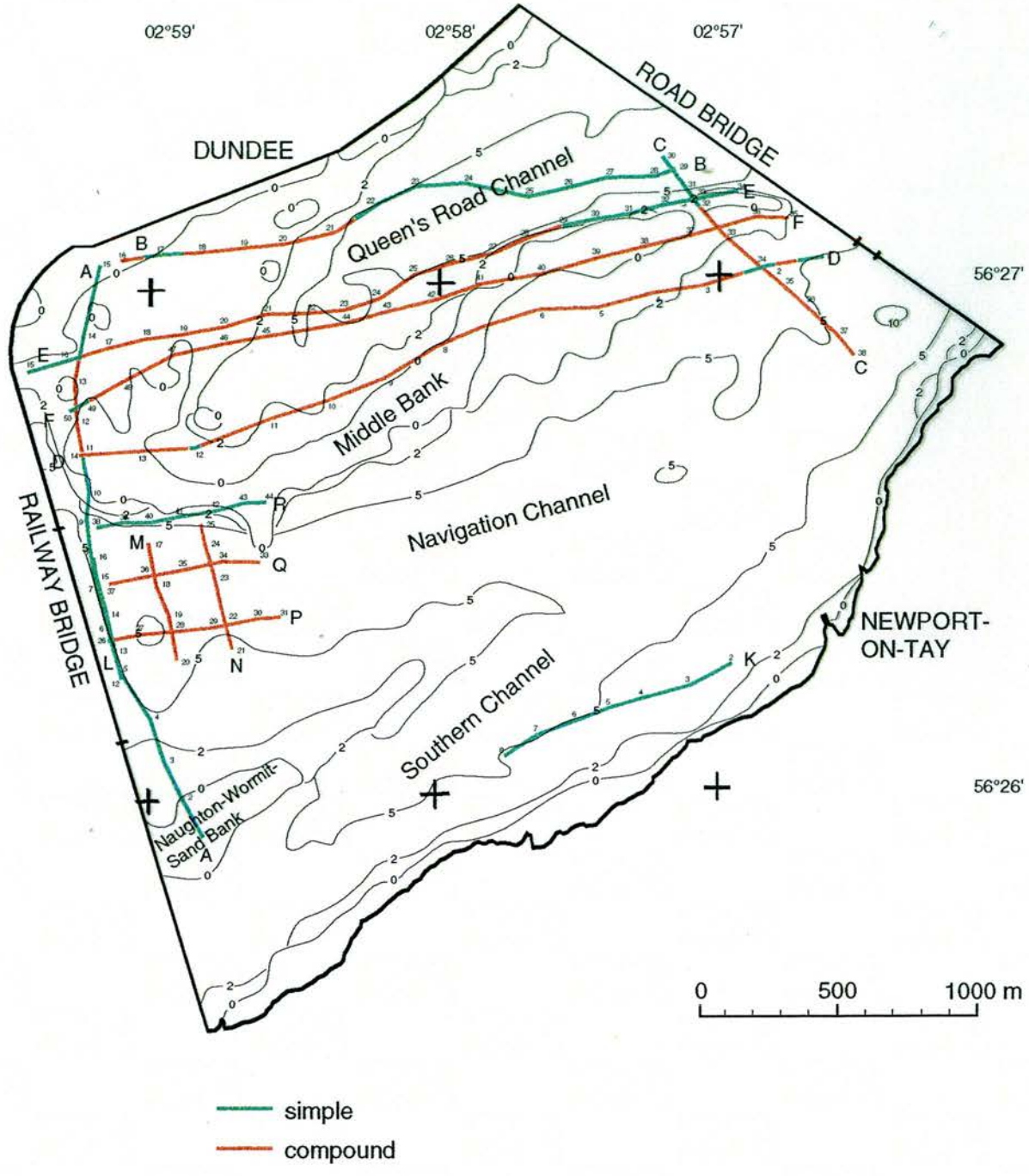

Fig. 6.8: Dune superposition during flood and slack tidal conditions as determined by echo-sounding. Classification after Ashley (1990). Numbers denote position fixes and letters indicate traverse start and end points.

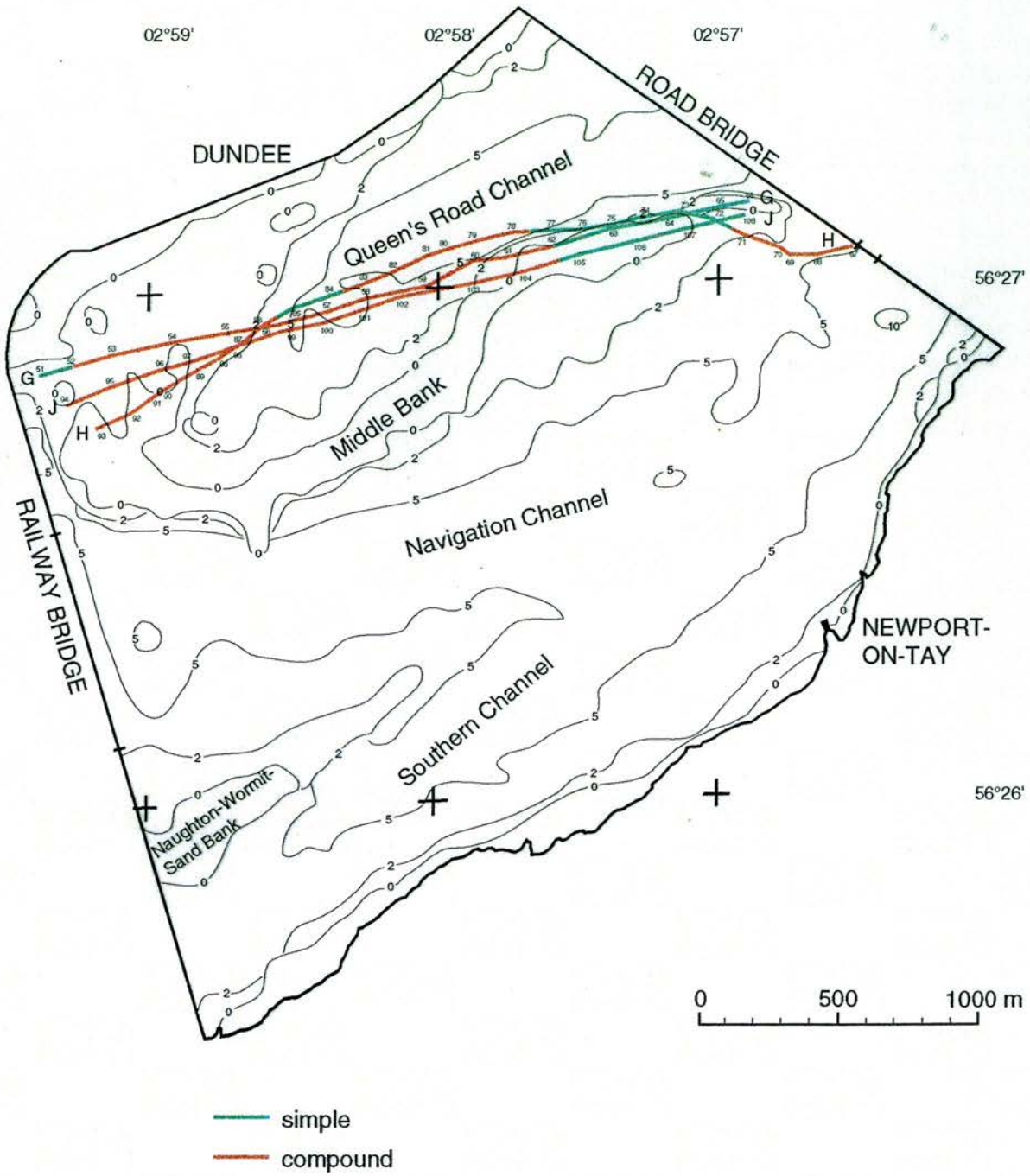

Fig. 6.9: Dune superposition during ebb tidal conditions as determined by echo-sounding. Classification after Ashley (1990). Numbers denote position fixes and letters indicate traverse start and end points.

Comparison

Compound dunes were recorded on most areas of Middle Bank during both tidal stages. Four lines (M, N, P and Q) of the grid of traverses in the Navigation Channel revealed compound dunes, while all other lines recorded in deeper waters displayed simple dunes. Simple bedforms were also found at the eastern end of Middle Bank especially during ebb tidal conditions.

6.3.4 Asymmetry

Echo-soundings can record dune asymmetry only when the traverse is run perpendicular to the crest orientation. Therefore, echograms from east-west trending lines only could be interpreted for dune asymmetry. As described in Section 5.3.6, asymmetrical dunes indicate the dominant direction of bed load transport. An example of a series of strongly asymmetric dunes is shown in Fig. 6.10. This echogram displays dunes the asymmetry of which is indicative of the dominance of flood tidal flows and was recorded close to the Road Bridge during flood tidal conditions.

Flood

The echograms recorded during the flood tides reveal both types of asymmetries as well as symmetric dunes (Fig. 6.11). The three east-west traverses (P, Q, and R) of the grid recorded in the Navigation Channel display flood dominant dunes at the western ends and ebb dominant dunes at their eastern ends. Only the northern traverse R reveals a section, of approximately 100m, of symmetric dunes. The line D along the southern edge of Middle Bank shows flood dominant dunes at its western end while the eastern end displays ebb dominant and symmetric forms towards the Road Bridge. Ebb dominant and symmetric bedforms were also located by the echo-sounder at the western and eastern ends of the southern traverse F running over Middle Bank, while the northern of the two, traverse E, revealed flood dominant dunes at the ends of the traverse but symmetric and ebb dominant bedforms in the centre. The traverse B running along the northern edge of Middle Bank could only be partly interpreted for asymmetry. Ebb dominant dunes were found at the eastern end of the line followed by symmetric forms which then graded into flood dominant bedforms in the centre section.

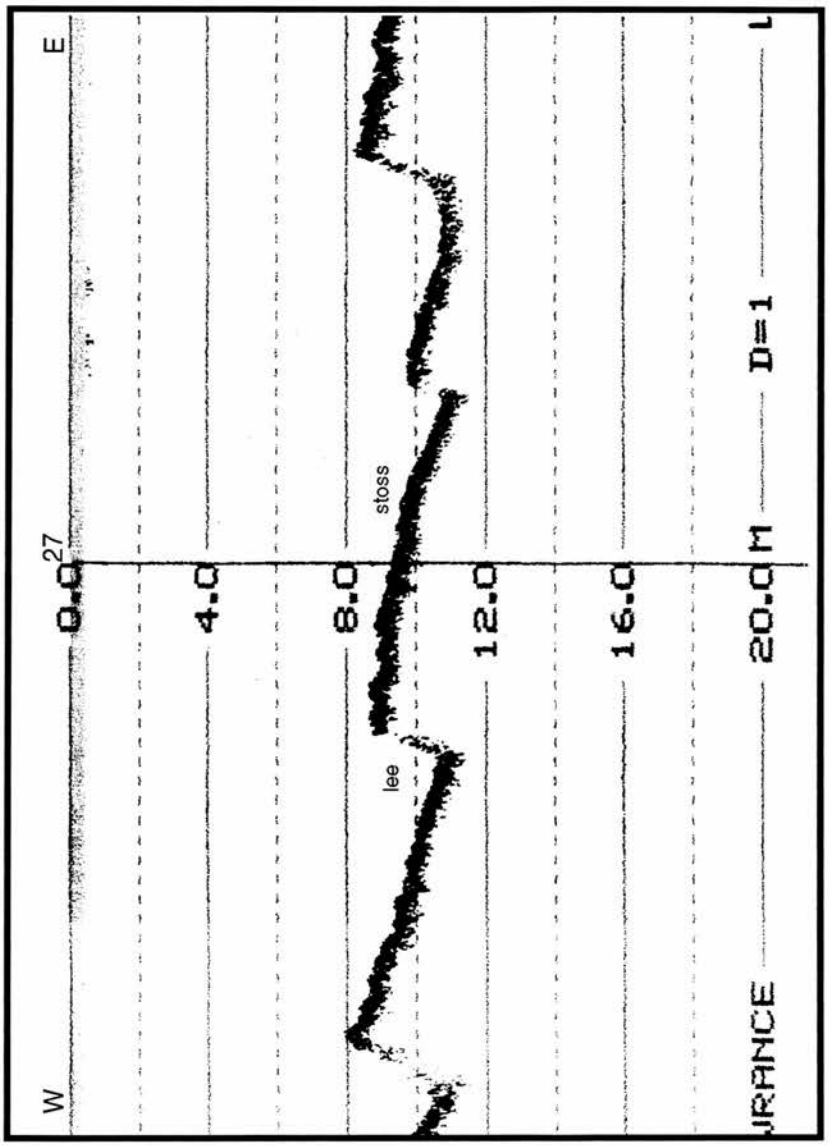

Fig. 6.10: Echogram of large flood asymmetric dunes recorded at GPS fix 27 of traverse E. Vertical scale in metres.

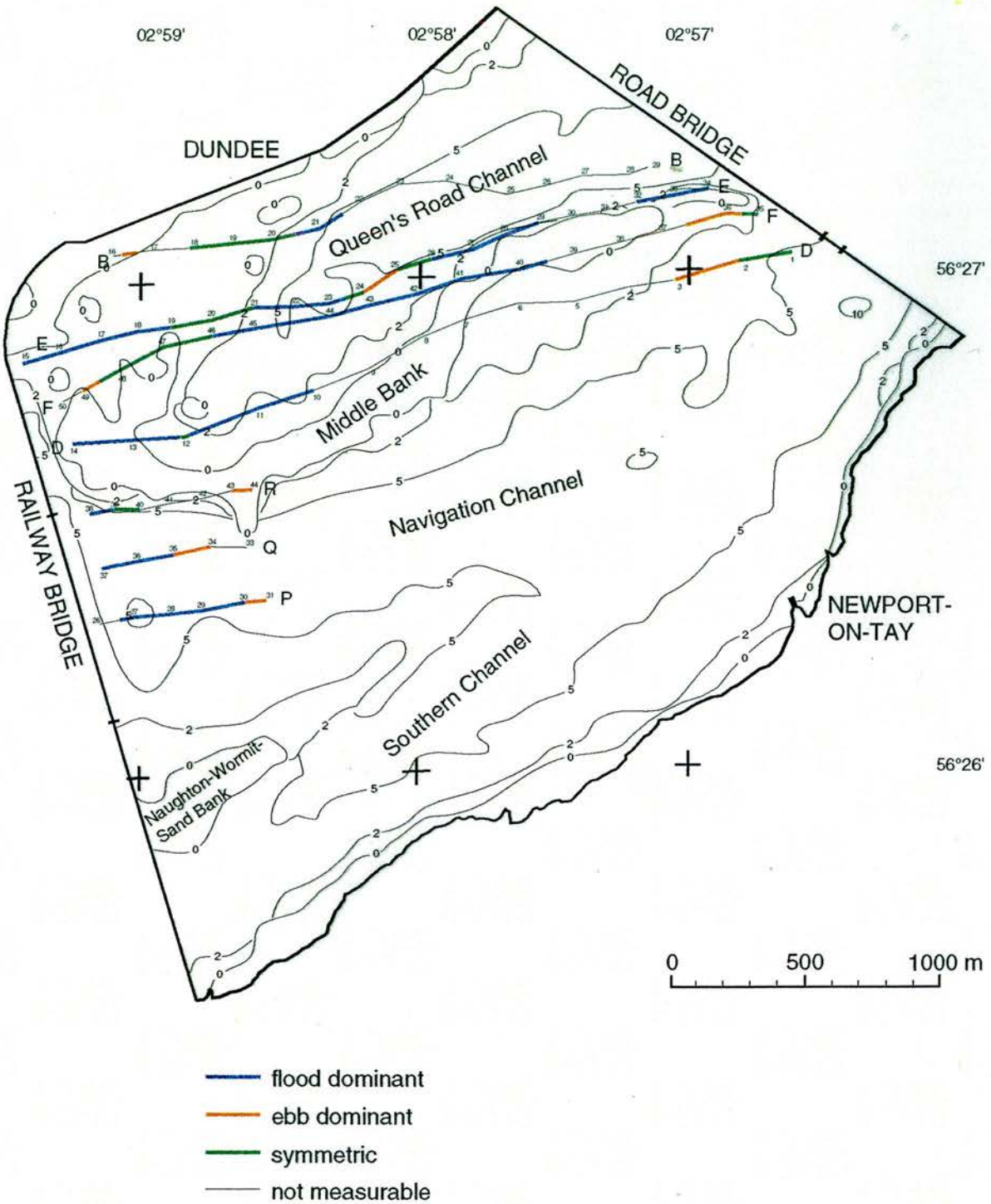

Fig. 6.11: Dune asymmetry during flood and slack tidal conditions as determined by echo-sounding. Numbers denote positions fixes and letters indicate traverse start and end points.

Ebb

Both types of asymmetries were also recorded during ebb tidal conditions (Fig. 6.12) but areas of certain dominances were more clearly identified. Flood asymmetric dunes dominated on all three traverses (H, G and J). Areas of symmetric forms were recorded on all three traverses in the centre of Middle Bank, halfway between the centre and the western end, as well as on the two southern traverses (H and J) at the extreme western end. Only two areas of ebb dominant dunes were recorded. One of approximately 100m length was close to the Road Bridge at GPS fixes 69-70 of traverse H, while a larger stretch of around 300m was recorded between GPS fixes 89-92 on traverse H towards the south-western end of Middle Bank.

Comparison

Both Figs. 6.11 and 6.12 show a dominance of flood asymmetric dunes in the study area. The echograms suggest that the dunes of the eastern and western ends of Middle Bank appear to maintain a constant direction of asymmetry, whereas the dunes in the central part of this major sand bank change in asymmetry according to the tidal state. During flood tidal conditions a zone of ebb dominant dunes was recorded but no such forms were found during ebb tidal conditions when only flood dominant and symmetric dunes were revealed.

6.3.5 Summary of the interpretation of echograms

A large variety of dune geometries was recorded by echo-sounding especially over Middle Bank where side-scan sonographs had not permitted a reliable interpretation of dune shapes and sizes. The largest wavelengths recorded in the study area were up to 150m in length, while the smallest measurable crest to crest spacings were as short as 4m. Shorter wavelengths could not be measured due to the along-track resolution which depends on the paper speed as well as the speed of the survey vessel. During flood tidal conditions dune heights of the small and medium class of under 0.5m dominate, while dunes during the ebb tide revealed large heights. Most recorded dunes during both tidal stages were of compound form with smaller superimposed dunes all of which were mainly flood dominant in asymmetry.

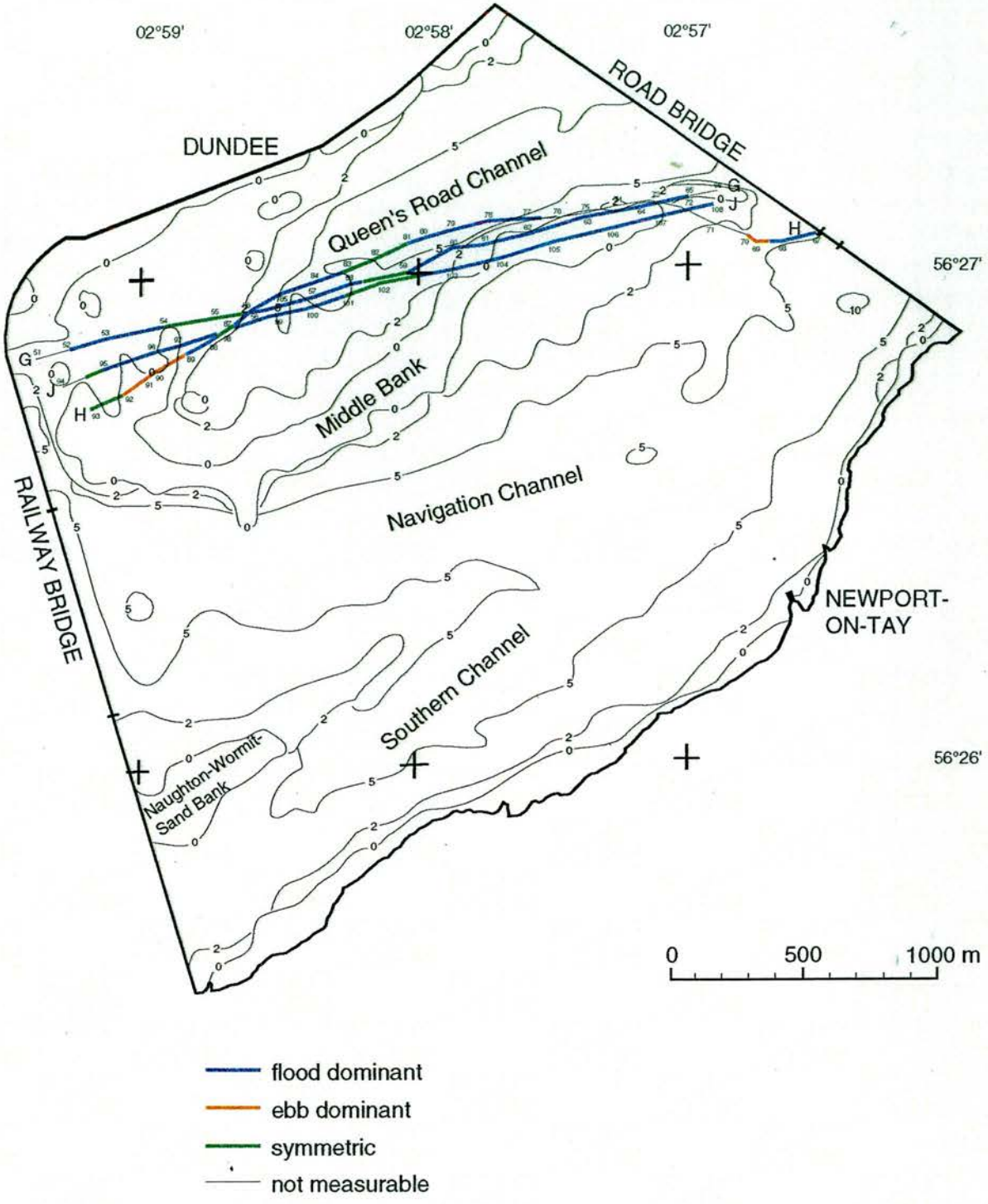

Fig. 6.12: Dune asymmetry during ebb tidal conditions as determined by by echo-sounding. Numbers denote position fixes and letters indicate traverse start and end points.

The formerly inexplicable patchy, discontinuous patterns which were recorded by side-scan sonar in most channel areas could be measured from the echograms. The recorded data suggest that these patterns are produced by small-scale sedimentary bedforms and not by changes of sea bed material.

6.4 Comparison of side-scan sonar and echo-sounding survey results

The main task of this project was to survey the area of the Tay Estuary between the two bridges by means of side-scan sonar to investigate the sedimentary bedforms, sediment types and facies variations. Full coverage was achieved by side-scan sonar but some sonographs did not permit detailed interpretation or needed more data to support their interpretation. Therefore, 16 traverse lines were run with an echo-sounder to gather more information. The data of both surveys were divided into ebb and flood data sets depending on the tidal state at the time of recording. As mentioned in Section 6.1, echograms can be used to measure only wavelength, height, superposition and asymmetry of sedimentary bedforms since they give a profile of the sea bed and not a plan view like side-scan sonar. These four descriptors are compared below, as detected by side-scan sonar and echo-sounding.

6.4.1 Wavelength

Dune wavelengths varied depending on whether they were measured from sonographs or echograms. Generally dune wavelengths were longer when measured on echograms than on sonographs and therefore often belonged to the next higher group. This discrepancy is probably due to the different resolution and acoustic beam geometry of the two systems. On the echograms dune wavelengths could be classified into four groups ranging from small (0.6-5.0m) to very large (>100.0m) while on the sonographs no very large dune wavelengths were detected. However, general distributions of dune wavelengths were similar revealing dunes of small wavelengths in channel areas and a variety of dunes of small, medium and large (even very large on the echograms) wavelengths on and around Middle Bank.

Flood

On the flood tide both echograms (Fig. 6.2) and sonographs (Fig. 5.7) revealed dunes of medium and large wavelengths in the middle region of the study area. This was especially the case for echo-sounding traverses E and F. On traverse D a long stretch of dunes of small wavelengths was recorded in its centre section while the sonographs revealed dunes with mainly medium and large wavelengths. Echo-sounding traverses P, Q and R, recorded in the Navigation Channel close to the Railway Bridge, displayed a higher variety of dune wavelengths, changing from medium to large and even very large, while the sonographs suggested the presence of dunes of small wavelengths in this area. During both side-scan sonar and echo-sounding surveys dunes with small wavelengths were recorded especially in the eastern part of Queen's Road Channel (traverse B of the echo-sounding survey). Along the northern shore wavelengths of dunes changed from small to medium and large in a distance of less than 150m recorded on the western part of traverse B. This was also recorded by side-scan sonar.

Ebb

Fewer side-scan sonar as well as echo-sounding traverses were run during ebb tidal conditions (Figs. 5.9 and 6.3). Therefore, only a small part of the study area can be compared during this tidal state. Similar areas of dunes with small, medium and large wavelengths could be detected but, as already mentioned, measured dune wavelengths were always longer on the echograms than on the sonographs. In particular the eastern end of the echo-sounding traverses (G, H and J) mainly revealed dunes with wavelengths of the medium and small class unlike the sonographs which recorded dunes with small wavelengths. On Middle Bank dune wavelengths varied between medium and large but were up to very large on echograms.

6.4.2 Height

Classes of dune height had to be altered slightly for the interpretation of the echograms due to the range scale on the print-out, as already mentioned in Section 6.3.2. Nevertheless, dune heights can be measured

directly from echograms and do not have to be calculated as from sonographs. The comparison revealed that dune heights measured from echograms varied between small and medium, large and very large on much shorter sections of the traverses, for example from large to small and medium and back to large in less than 200m, which could not be detected by side-scan sonar. However, measurements of this dune parameter should be accepted with care since an exact computation, especially from sonographs, is not always possible. When calculating dune heights from sonographs the acoustic shadow forms the basis of the calculation. Acoustic shadows seldom have an exact outline but are more often rather indistinct which results in deviations so that, for example, a dune which is actually 0.50m high could be estimated as 0.52m or as 0.48m high and would therefore be assigned to a different class.

Flood

Most dune heights computed from sonographs (Fig. 5.11) belong to the medium class (0.25-0.50m). Dunes of this category were recorded in the channels as well as in the shallower parts of the study area. No dunes of very large heights were detected on any of the sonographs. On the echograms (Fig. 6.4) the majority of the dunes recorded had heights of the small and medium (0.05-0.50m) class. A very short stretch of dunes with very large heights was recorded by echo-sounder at position fix 35 of traverse F but the sonographs suggested dunes of medium heights in this area.

Ebb

During ebb tidal conditions the dominant dune height computed from the sonographs (Fig. 5.13) also belonged to the medium class (0.25-0.50m) while dune heights measured on the echograms (Fig. 6.5) belonged to the large class (0.50-3.00m). However, the centre part of the echo-sounding traverses was recorded in the area of dunes of large heights as interpreted from sonographs. The associated echograms revealed a mixture of dunes of small, medium and large heights in the same area. The overall distribution of dune heights detected by echo-sounding varied from those detected by side-scan sonar with the latter being generally smaller.

6.4.3 Superposition

The majority of dunes recorded in the middle reaches of the estuary by side-scan sonar as well as echo-sounding were compound dunes. These were found especially in the centre regions of the study area while dunes recorded in the deeper waters of the channels, as well as in the shallower regions along the shore, belonged to the simple class. However, some areas of simple dunes as detected by side-scan sonar appeared to be of compound form when recorded by echo-sounding. This difference is probably related to the resolution of the two systems; as mentioned in Section 3.2.2.5 the real range resolution (R_r) of the side-scan sonar systems was 0.6m for the Klein Hydroscan and 0.49m for the Waverley with the transverse resolution (R_t) being 0.98m and 1.96m respectively. With this kind of resolution the detection of very small superimposed dunes depends on the geometry of the acoustic shadow on the sonograph. For example, a small superimposed dune might be detected on a sonograph if it is recorded at such an angle from the tow fish that the acoustic signal produces a shadow or that the slope of the dune facing the transducer gives a strong reflection followed by a lighter reflection from the slope facing away from the transducer. If no shadow or pattern of dark and lighter tones is produced on the sonograph, the superimposed dune will not be detected. On the echograms the resolution depends on the scale range chosen for the print-out, as mentioned earlier, and as shown in Fig. 6.7 superimposed dunes of only 15cm in height were detected by echo-sounding. However, the range scale chosen during most of the echo-sounding surveys was either 0-15m as in Fig. 6.6 or 0-20m as in Fig. 6.10. The asymmetric dunes shown in Fig. 6.10 display superimposed dunes on their stoss side but since they are less than 1mm high on the recording paper, they are too small to be measured precisely.

Flood

Overall, dune superposition was similar on the echograms (Fig. 6.8) as compared with the sonographs (Fig. 5.25). Small areas showed variations, for example on traverse D at position fixes 2 and 12, where echograms revealed simple dune shapes while those recorded by side-scan sonar were of compound form. It is remarkable that echo-sounding traverses M,

N, P and Q revealed compound dunes in the Navigation Channel close to the Railway Bridge while these areas clearly revealed simple dunes on the sonographs. As mentioned above, this is probably due to the resolution of the side-scan sonar systems as compared with the echo-sounder.

Ebb

Overall similarities of dune superposition were also recorded during ebb tidal conditions. Most dunes were of compound forms especially in the centre region of the estuary while simple forms were recorded in the channels and along the shores. Echograms (Fig. 6.9) of all three traverses (G, H and J) detected a relatively large area of simple dunes close to the Road Bridge (traverse G: fix 62-66, traverse H: fix 72-77, traverse J: fix 105-108) while sonographs (Fig. 5.26) revealed compound dunes. However, the centre section of this area revealed on the echograms covers a small area where no dunes could be measured on the sonographs. These dunes recorded by echo-sounding are of small and medium height and extend over a relatively large area.

6.4.4 Asymmetry

The majority of dunes have an asymmetrical profile with a steep lee side and a gentle stoss side depending on the dominant current direction. In the study area of the Tay Estuary most dunes have asymmetries indicative of the dominance of flood tidal currents as determined by both side-scan sonar and echo-sounding.

Flood

Sonographs revealed large regions of flood dominant dune asymmetries throughout the study area during flood tidal conditions (Fig. 5.28). Large sections of dunes with asymmetries indicative of ebb tidal flows were recorded by side-scan sonar but not always in the same locations as recorded by echo-sounding (Fig. 6.11). Larger areas of symmetrical dunes were recorded by echo-sounding than by side-scan sonar but were detected in different regions of the study area and no overall similar distributions could be detected.

Ebb

Most dunes recorded by echo-sounding (Fig. 6.12) and side-scan sonar (Fig. 5.29) during ebb tidal conditions indicate a flood dominant asymmetry. Echo-sounding revealed a centre section (approximately 250m in length) of symmetric dunes. In this area ebb dominant dunes were detected in the northern half and flood dominant dunes in the southern half when recorded by side-scan sonar. Just west of this area, but still in the region of ebb dominant dunes as detected by side-scan sonar, dunes changed from a flood dominant asymmetry to symmetric and back to flood dominant on the echograms (on traverse H within 100m and on traverse G within 300m). Two stretches of ebb dominant dunes were recorded by echo-sounding at the eastern and western ends of traverse H. Both of these areas showed dunes of flood dominance when recorded by side-scan sonar.

6.5 Conclusions

The aim of the echo-sounding surveys was to augment the results of the side-scan sonar surveys and to fill in the gaps where no detailed interpretation of the sonographs was possible. General similarities were detected on both surveys but the measurements of dune wavelengths and heights revealed higher values on the echograms than on the sonographs and the distribution also varied.

The interpretation of the two types of data sets has shown complex variations of the dunes in the middle Tay Estuary. Dune sizes, shapes and distributions varied depending on the tidal state and between the side-scan sonar and echo-sounding surveys but some general statements can be made. Dunes on Middle Bank and in the channels ranged from medium (5.0-15.0m) to large (10.0-100.0m) in wavelength. Dunes of small (0.6-5.0m) wavelengths were recorded closer to the shores. The dominant dune height recorded was of the medium class (0.25-0.50m) while dunes of large (0.5-3.0m) heights were detected in the eastern part of the Navigation Channel. Most dunes were of compound form with smaller dunes superimposed on the larger platform dunes while simple dunes were detected mainly in the deeper waters of the channels and close to the shore. During both surveys dune asymmetries revealed a flood

dominance apart from small areas on Middle Bank where ebb dominant dunes as well as a mixture of dune asymmetries were recorded.

The interpretation of dune asymmetry in the study area suggests a high input of bed load of marine origin supporting the findings of former studies (Buller and McManus, 1975; Buller *et al.*, 1975; McManus,1986b; Al-Dabbas and McManus, 1987). This result is probably related to the times at which the surveys were conducted. Surveys were carried out on well established flood tides (shortly before and during high water) while ebb tide surveys had to be carried out during the early stages of the ebb tide shortly after high water. This has possibly not allowed enough time for the "lag effect" to take place. As already mentioned in Section 4.4, bedforms lag behind the change of flow conditions since it takes a finite time to transport the sediment volume needed to change dune morphology (Dalrymple and Rhodes, 1995). Future work should therefore include surveys of the bed at the end of the tides for better comparison. This is not practical where sand banks dry out at low water but channel areas could be surveyed while the regions of the sand banks where changes are expected would not be accessible. This includes most regions where large dune fields occur in the study area. However, this is the first time that such a study has been carried out on the Tay Estuary and the side-scan sonar and echo-sounding surveys have improved our knowledge of the distribution of sedimentary bedforms, facies changes and variations which had so far been based on point sampling only.

Chapter 7

SEDIMENT SAMPLING AND ANALYSIS

7.1 Introduction

All surveys employing remote sensing techniques require the support of ground information. Although side-scan sonar has revealed in many cases the complexity of surficial sediment relationships and demonstrated the inadequacy of areal bottom classification based on spot sediment samples only (Bennett *et al.*, 1992), ground information is essential for calibration. Sonographs show only relative relationships between tonal intensities and sediment characteristics so that rock appears darkest, followed by gravel, then sand, while fine-grained muddy sediments appear in lighter tones (Flemming, 1976; Hunter *et al.*, 1982). Samples are therefore necessary for a more detailed interpretation of the sediment distribution patterns recorded by side-scan sonar.

The modern Tay Estuary deposits mantle a complex sedimentary fill as described in Chapter 2. The fieldwork area has been studied by various researchers, especially Buller and McManus (1975) who have found that it is dominated by sand, migrating sand banks and migrating channels. Buller *et al.* (1971) discovered that the sands become coarser towards the east with coarser sands in the channels than on the sand banks. In 1975 Buller and McManus published the results of a detailed study of the bottom sediments of the upper and upper middle reaches of the Tay Estuary. Since the area is known to be highly dynamic, the results of the present survey are compared with the 1975 data in order to detect any changes.

The sampling sites were chosen according to the spatial distributions of various tonal intensities recorded on the sonographs. The aim was to collect samples in each area of differing tonal intensity. Strong currents did not always permit sampling in the exact location determined by the recorded and interpreted sonographs but good overall coverage was obtained (Fig. 7.1).

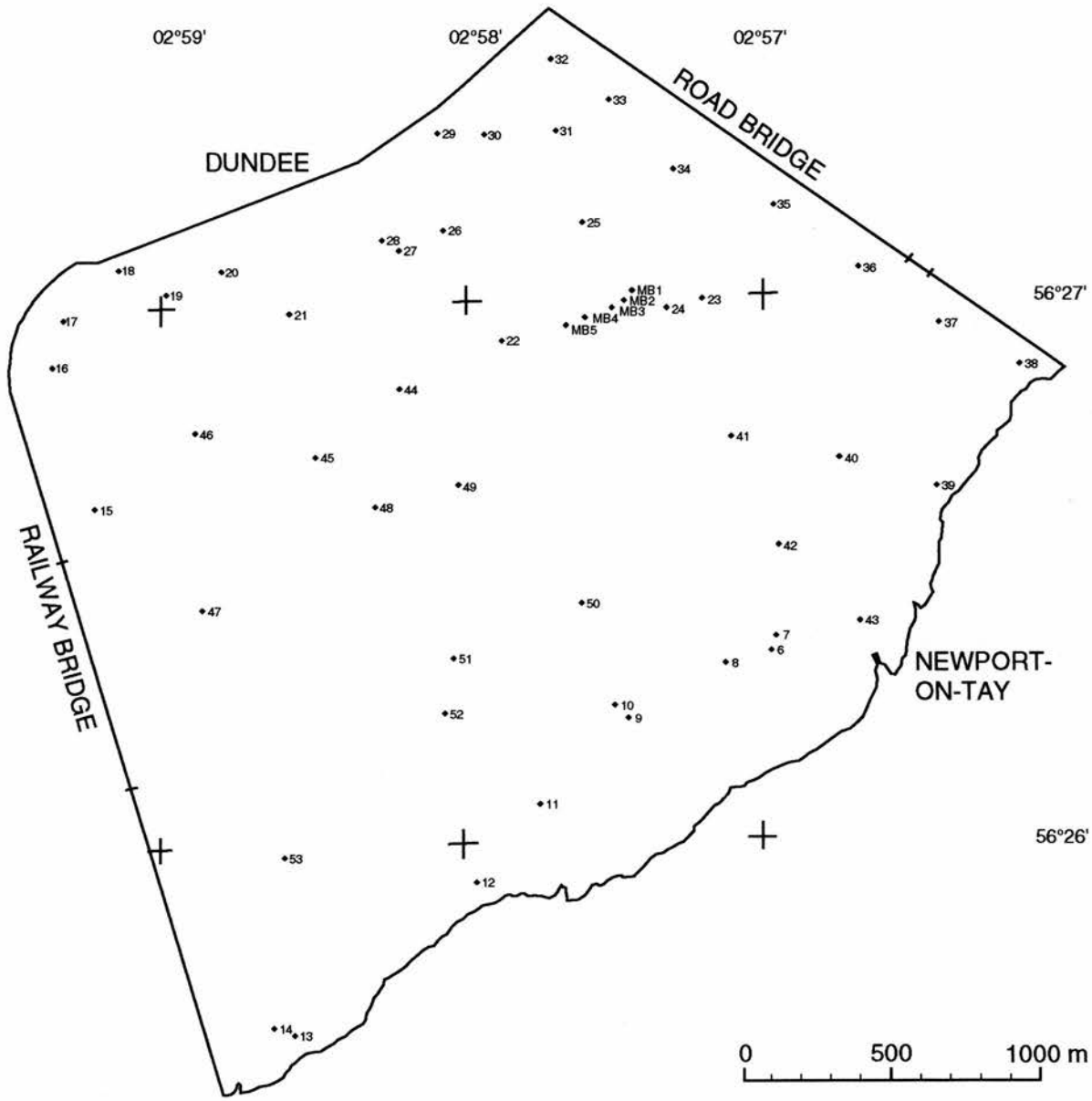

Fig. 7.1: Positions of collected sediment samples determined by side-scan sonograph interpretation.

7.2 Methodology

7.2.1 Sediment sampling

The technique of sediment sampling employed in an estuarine study varies according to the physical nature of the water body. Intertidal flats may be accessible during low tide and can therefore be sampled directly by hand or from a vessel when covered by water at high tide. All subtidal areas have to be sampled remotely, unless divers are employed.

Parts of the main sand bank of the study area, Middle Bank, are generally exposed at low water on spring tides. On July 17th, 1995, 20 samples of the surface deposits were collected by trowel; 4 samples each at 5 points from east to west (Fig. 7.1). All 20 samples were analysed and then averaged for further statistical analysis.

The 48 samples in the subtidal area (Fig. 7.1) were collected remotely by means of a modified van Veen grab. This sampler (Plate 7.1) consists of a set of jaws which shut when lowered to the surface of the bottom sediment. According to Mudroch and MacKnight (1991) the "van Veen grab is suitable for obtaining bulk samples ranging from soft, fine-grained to sandy material ... for studies in deep water and strong currents in the marine environment". In principle the grab is lowered through the water column until it settles on the bottom, then the lowering rope slackens and the hook on the release device rotates so that the short suspension chains fall free. When the lowering rope is slowly made taut, the suspension chains exert tension on the long arms of the grab and cause them to lift, dipping deeper into the sediment and trapping the material as they close tightly (Mudroch and MacKnight, 1991). The grab is then hauled up on to the sampling platform and the sample transferred into a labelled container for analysis in the laboratory.

Good samples were obtained in sandy areas of the estuary but some samples contained only mussels, isolated pebbles or seaweed. These were subjected to visual description but were disregarded for subsequent grain size analysis. Especially in areas of coarse sediment or mussels, the grab often had to be lowered several times in order to retrieve a sample.

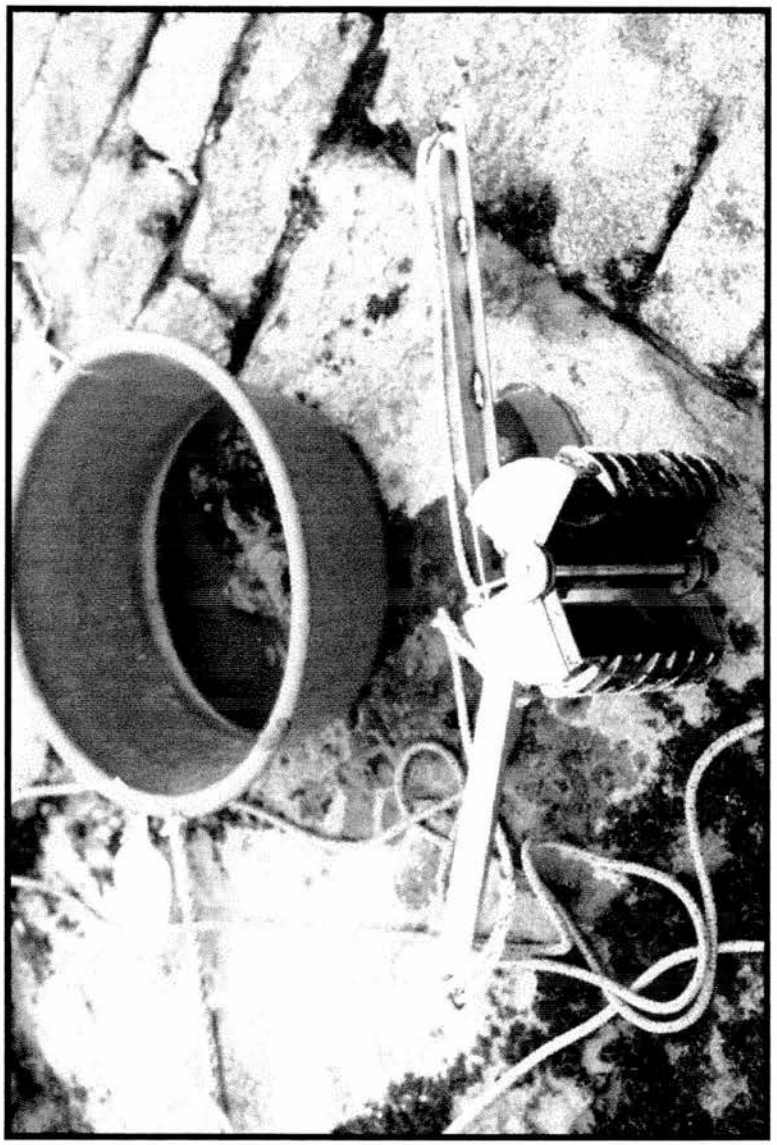

Plate 7.1: Photograph of van Veen grab modified with the addition of teeth.

7.2.2 Preparation of samples for analysis

All collected sediment samples were prepared for grain size analysis according to the standard procedure described by Buller and McManus (1979) and McManus (1988). Sediment samples derived from estuaries contain quantities of salt within their interstitial waters. Before drying the samples, these need to be removed since they would form a precipitate on the surface cementing adjacent particles together. A large proportion of the salt may be removed by repeatedly washing the sample in beakers of fresh water and decanting the clear liquid after settling of the sediment. During decantation care must be taken that no particles are lost. The samples were then placed in open evaporating basins and left to dry in a thermostatically controlled oven at a temperature of 90°C. Caking of fine particles in some samples was destroyed by gentle crushing between fingers.

7.2.3 Grain size analysis

The simplest and most widely used method of grain size analysis is dry sieving which was used in the size range between 4.00mm (-2.0phi) and 0.71mm (0.5phi). This is an effective and economical method of dividing sediment samples into different fractions containing particles of more or less similar size (Mudroch and MacKnight, 1991). The samples were weighed and then placed on top of a nest of six sieves, with mesh openings of 4.00mm (-2.0phi), 2.80mm (-1.5phi), 2.00mm (-1.0phi), 1.40mm (-0.5phi), 1.00mm (0.0phi) and 0.71mm (0.5phi), on a mechanical shaker. All samples were subjected to agitation for a period of 15 minutes. The material retained in each sieve was weighed and converted into a weight percentage of the sample. This method was employed only to measure the gravel and coarse sand content of the sample.

The analysis of the finer particles was carried out with a Coulter Counter LS-100. The Coulter Counter LS-100 is a laser diffraction grain size analyser, the operation of which is based on the interaction between light and particles. Particles of a given size scatter light through a given angle with the angle increasing with decreasing particle size (Loizeau *et al.*, 1994). This method is fast, reproducible and precise (Agrawal *et al.*, 1991) and provides a sophisticated and rapid way for routine analyses of

sediments (Stein, 1985). Although laser diffraction computes size distribution expressed in volume units while sieving results are obtained in weight units, Loizeau *et al.* (1994) have found that the two methods produce similar results. Therefore only the coarse contents of the samples were analysed by sieving, while the finer particles were analysed by the faster method namely the Coulter Counter. The data obtained by the Coulter Counter analysis had to be converted from volume percentage to weight percentage for statistical analysis.

7.2.4 Statistical analysis

There are two principal forms of statistical analysis of grain size data. One is called the Method of Moments which is a computational method of obtaining values. Since every grain in the sediment sample affects the measure, it gives a true picture of the grain size distribution within a sample. The other method involves plotting the cumulative grain size distribution curve of the sample and extracting the diameter values represented by various percentile values and entering these into established formulae (Folk, 1974; McManus, 1988). The values of the statistical parameters characterise the distribution curves and permit numerical comparisons between samples (McManus, 1988). Although the computational method is more accurate, for the purposes of comparison with the data of Buller and McManus (1975), the present statistical analysis was carried out after the graphic method.

Data obtained from grain size analysis may be plotted in various ways, the easiest and most accurate method for further statistical analysis being the cumulative curve with a probability ordinate (Folk, 1974). Grain size is commonly plotted as the x axis (abscissa) either in millimetres or phi with the latter being more convenient and accurate to read (Folk, 1974). The cumulative percentage is plotted as the y axis (ordinate). The size frequency distribution of most sediments tends to approach a normal probability curve indicating that the majority of particles cluster about a given size with progressively less material to either side. Since the probability scale is condensed in the middle and expanded at the ends of the scale, it straightens the curve and allows the reading of percentile values with much greater accuracy.

Once the cumulative curve is plotted, various percentile values and their corresponding grain size values may be read off the graph. The most common statistical parameters used to describe size frequency distribution curves are median (*Md*), mean (*M*), standard deviation (σ), skewness (*Sk*) and kurtosis (*K*). These measures are usually calculated after Inman (1952) or Folk (1974). Inman's (1952) parameters include only the 16, 50 and 84th percentiles and ignore the tails of the distribution. Many authors have criticised the use of such measures, especially Folk (1974) who proposed the use of the 5, 16, 25, 50, 75, 84 and 95th percentiles which therefore include the tails of the curves.

For the comparison of the results of the present study with the results obtained by Buller and McManus (1975), three statistical parameters were calculated. These three parameters were the median, standard deviation and skewness. Although Folk (1974) includes seven percentile values in his formulae (see Appendix I) and therefore obtains more all-embracing statistical values than Inman (1952) who includes only three (see Appendix I), the statistical parameters were calculated after Inman (1952) as chosen by Buller and McManus (1975). A brief description and the formulae of the statistical parameters are shown in Appendix I.

7.3. Results and discussion

7.3.1 Description and distribution of sediment types

The classification of the sediment samples is based on the proportions of gravel (>2mm), sand (0.0625-2mm) and mud (<0.0625mm) according to the triangular diagram presented by Folk (1974) (Fig. 7.2). The amount of gravel in a sample is highly significant due to its dependence on the maximum current velocity at the time of deposition while the ratio of sand to mud reflects the amount of winnowing at the site of deposition (Folk, 1974).

The textural classification map (Fig. 7.3) of the sediments sampled in the Tay Estuary resembles the bathymetric chart. The dominant sedimentary class found between the two bridges is slightly gravelly sand which covers most of the middle region. The deep areas are lined with coarser fractions such as pebbles, gravelly sand as well as mussels (mainly *Mytilus edulis*). The shipping channel beneath the Road Bridge is lined

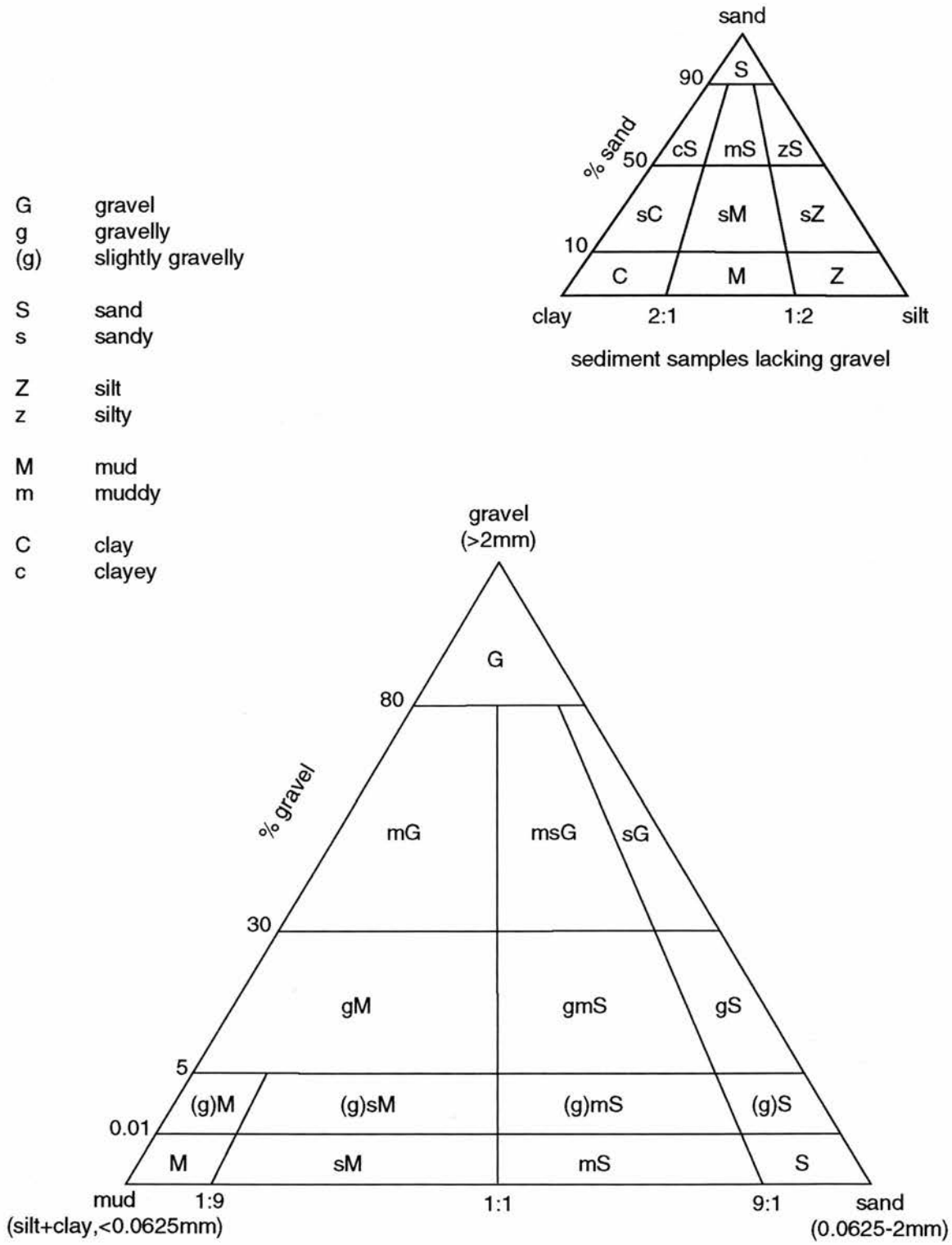

Fig. 7.2: Textural classification of sediments after Folk (1974).

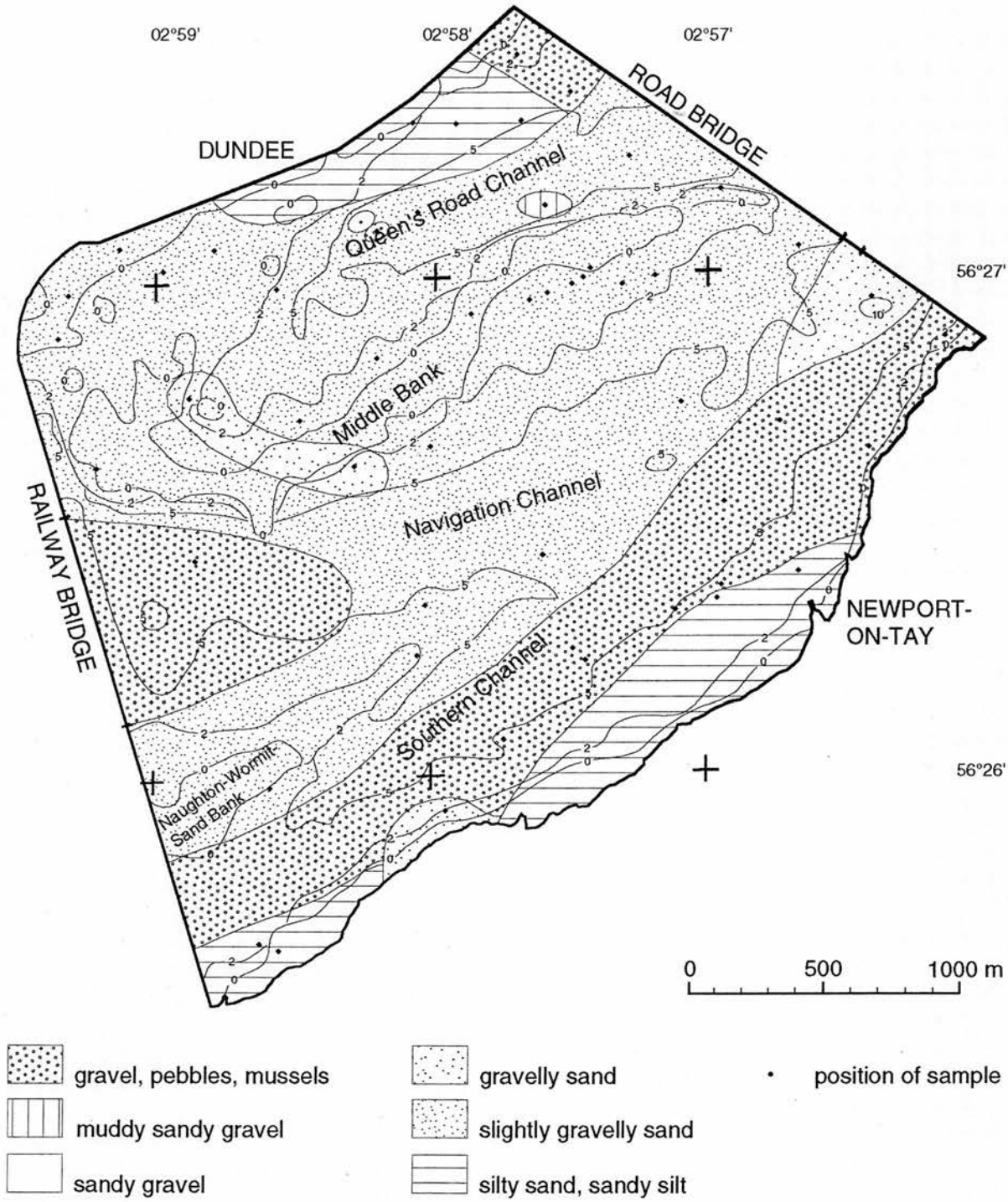

Fig. 7.3: Textural classification of sediments after Folk (1974). Distribution is based on sediment samples in correlation with side-scan sonographs.

with gravelly sand and mussels, then passes through an area of slightly gravelly sand in the middle of the estuary until it is lined again with mussels closer to the Railway Bridge. The sediments closer to the shore consist mainly of silty sand and sandy silt, some of which are exposed at low tide. Middle Bank, the main sand bank between the Navigation Channel to the south and Queen's Road Channel to the north, is composed of slightly gravelly sand, while to its western end an area of more gravelly sand occurs. Queen's Road Channel also traverses the area of slightly gravelly sand although it contains two patches of coarser material. The eastern one is described as muddy sandy gravel and the western one as sandy gravel. No connection between these two areas and the bathymetry is evident. Although most of the northern shoreline sediments are fine grained, the two samples (32 and 33) collected adjacent to the northern end of the road bridge were composed of mussels and broken shells only.

7.3.2 Statistical measures

For comparative purposes with the results of Buller and McManus (1975) the parameters chosen are the median, phi sorting and skewness. Although Folk (1974) strongly criticised the use of the median, Buller and McManus (1975) chose this parameter "because it can be directly taken from the cumulative frequency curves without extrapolation". The distribution of the median (Fig. 7.4a) is similar to the textural classification of sediment types (Fig. 7.3). The areas characterised by mussels, shells and pebbles are the same in all distribution maps since no statistical grain size analysis could be made from those samples. The study area is dominated by medium sand which veneers the middle part of the estuary. Finer sediments are found along the shorelines but vary from very fine sand to medium sand. The northern shore is lined with pebbles and mussels at its eastern end, neighbouring an area of very fine sand towards the west which is followed by medium sand grading into fine sand close to the Railway Bridge. Queen's Road Channel is clearly defined on the map being lined with coarse sand. Unlike the sediments of the northern shore, the sediments along the southern shore consist of very fine sand apart from where the mussel lined channel meets the shore and one small area of medium sand.

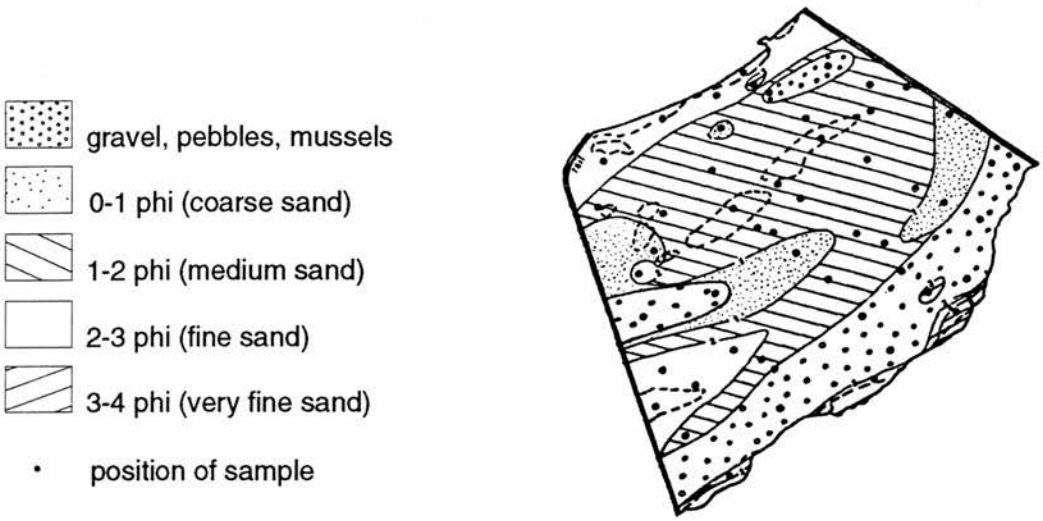

Fig. 7.4b: Distribution of median grain diameter after Buller and McManus (1975).

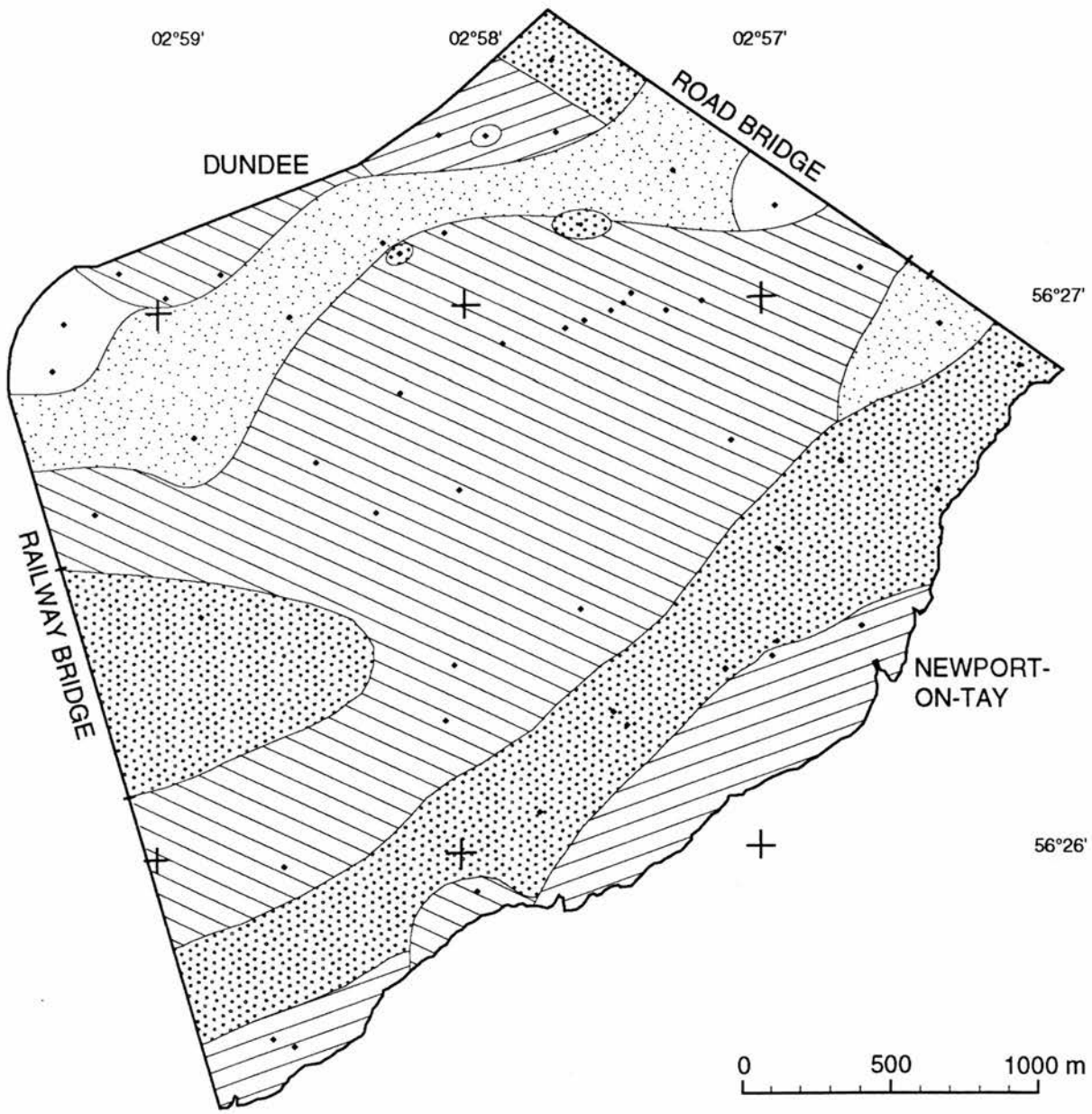

Fig. 7.4a: Distribution of median grain diameter based on sediment sampling in correlation with side-scan sonograph interpretation. Classification after Wentworth (1922).

The phi sorting distribution (Fig. 7.5a) shows no apparent similarity with that of the median diameter which is mainly due to their geometric independence. The overall phi sorting distribution pattern reveals a tendency for sorting to decrease towards the shore. The sediments of the middle regions are well or moderately well sorted while those along the shore are moderately or poorly sorted.

The final statistical parameter calculated in this study is phi skewness. It is a dimensionless measure and independent of sorting. Symmetrical cumulative curves have a skewness of *Sk*=0.00, asymmetrical curves with excess fine material have a positive skewness and those with excess coarse material have a negative skewness (Folk, 1974). Fig. 7.6a shows that most of the sediments have a skewness of around 0.00 in the middle region with those of the north-eastern part being slightly negatively skewed and those of the south-western part slightly positively skewed. The sediments along the southern shore are positively skewed which supports the findings of generally fine material. The values for the sediments along the northern shore also reveal a positive skewness although closer to a symmetric distribution.

The comparison of the results of Buller and McManus (1975) and those of this study revealed several problems. Buller and McManus had no previous information available to them for locating sampling sites and so distributed them evenly but randomly. In this study the sampling sites were chosen according to the findings of the sonographs. In both surveys a similar number of samples was collected; Buller and McManus collected 52 samples compared with 53 in the present study. When drawing maps it should be noted that any kind of contouring is subjective unless full coverage is obtained. Sediment sampling is point sampling and without the benefit of acoustic remote sensing the overall sediment distribution cannot be justified on the basis of so few samples in such a large area. The sampling strategy in this study was correlated with the side-scan sonar surveys and the contours of Figs. 7.3a-7.6a were drawn not only on the basis of the sediment grain size data but also of the sonograph interpretation. The field area is known to be highly dynamic and changes are to be expected. It was not possible to explain minor differences in results since they may stem from changes in time but also from imprecise positioning of the sampling points. Therefore, only a broad comparison is made.

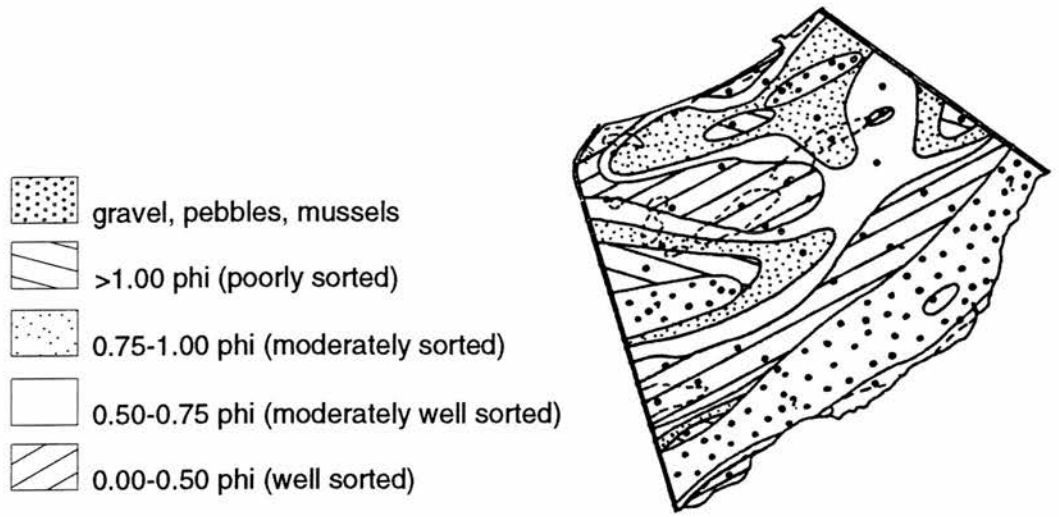

Fig. 7.5b: Distribution of sorting characteristics after Buller and McManus (1975).

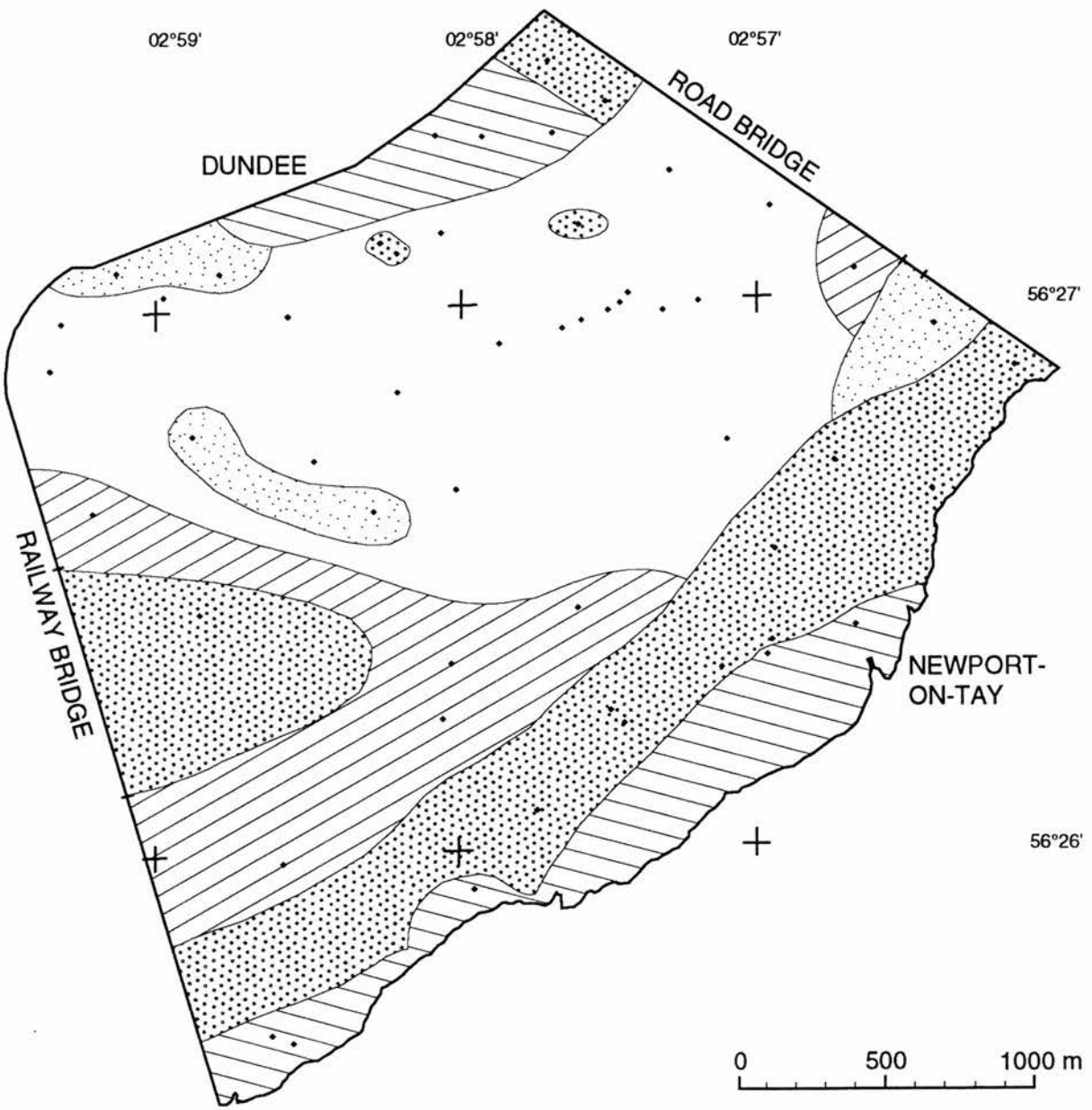

Fig. 7.5a: Distribution of sorting characteristics based on sediment sampling in correlation with side-scan sonograph interpretation. Classification after Buller and McManus (1975).

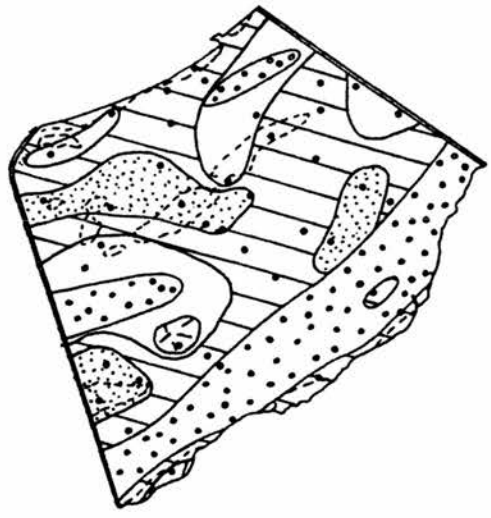

gravel, pebbles, mussels

<-0.4

-0.4 to -0.2

-0.2 to 0.0

0.0 to +0.2

+0.2 to +0.4

position of sample

Fig. 7.6b: Distribution of skewness variations after Buller and McManus (1975).

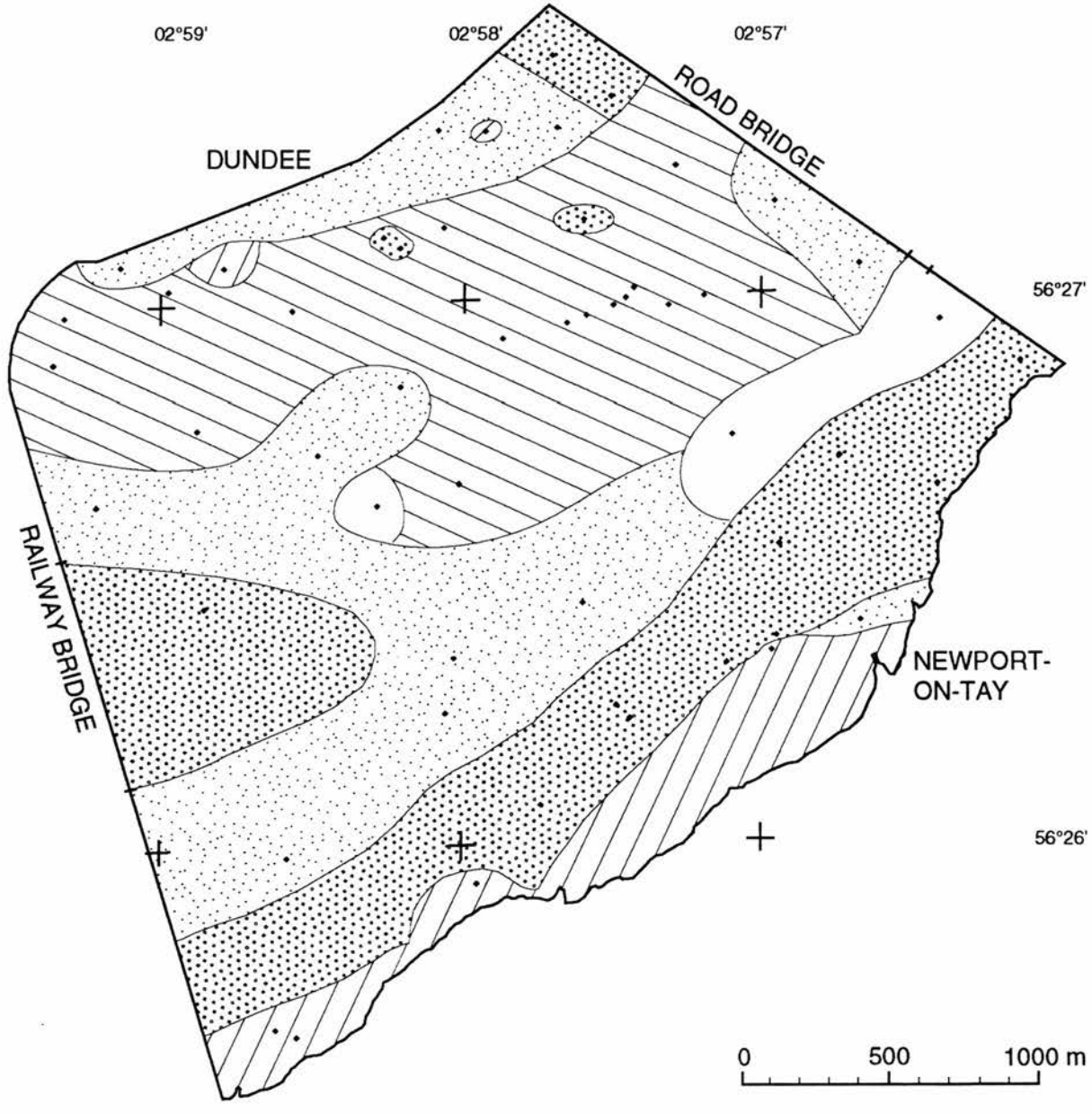

Fig. 7.6a: Distribution of skewness variations based on sediment sampling in correlation with side-scan sonograph interpretation. Classification after Buller and McManus (1975).

The overall sediment distribution pattern (Fig. 7.4a and 7.4b) of the median is the same in both surveys. Mussels and pebbles line the channels and medium sand dominates the middle region while finer sediment is found along the shores. The phi sorting plots (Fig. 7.5a and 7.5b) show slightly different results but the sediments have the general tendency of being well or moderately well sorted in the middle region. The samples collected by Buller and McManus reveal an overall better sorting than the sediments analysed in this study. The phi skewness maps (Fig. 7.6a and 7.6b) also show different results but a similar tendency towards symmetric to negatively skewed distribution curves. The dominant class in Buller and McManus' study lies between -0.2 and 0.0 closely followed by the class of -0.4 to -0.2 while the new phi skewness distribution map is dominated by the classes of 0.0 to +0.2 and -0.2 to 0.0 and therefore reveals a more symmetric distribution of grain sizes in the collected samples.

The results of the sediment sampling and analysis serve as ground information for the acoustic remote sensing surveys. They permit a more detailed interpretation of the sonographs and show a correlation of sediment type, bathymetry and tonal intensity recorded on sonographs. The overall distribution pattern of sediments has not changed significantly over the last 20 years. On the broad scale the bed sediment distribution pattern recorded in this survey is very similar to the results of Buller and McManus' (1975) survey especially for such a dynamic area.

Chapter 8

CURRENT MEASUREMENTS

8.1 Introduction

Bedform geometry and sediment transport in estuaries are closely linked to water movement, especially caused by tidal currents. In order to establish a simplified circulation model of the tidal waters between the Tay Railway and Road Bridges, current measurements were necessary and the results of this survey are described in this chapter. The objectives were to (1) establish sediment transport paths, (2) establish any relationships between sedimentary bedform dimensions, grain size and current velocities and (3) to estimate bed load transport. Objectives (1) and (2) are discussed in Chapter 9 while an estimate of bed load transport is presented in Section 8.5.

Since the collection of current data is extremely time consuming and heavily dependent on weather conditions, measurements were restricted to five locations. The positions (marked in red in Fig. 8.1) were chosen according to the results of the sonograph interpretations in conjunction with the newly established sediment distribution. The choice of positions was based on dune parameters (wavelength, height, length along crest, sinuosity, superposition and asymmetry), as described in Chapter 5, and sediment classification, as described in Chapter 7. Table 8.1 gives an overview of the variations of the dune parameters at all stations during ebb and flood tidal conditions as well as their associated bed sediment. The positions are mainly in the vicinity of Middle Bank because the dune crest orientation and geometries determined from sonographs in that zone did not clearly reveal a dominant current direction but rather variations. The measurements at the five positions were complemented by data acquired at three additional positions during earlier surveys. Two of these data sets (QRC, T2-T) were collected as part of a "Job Creation" project at TERC in 1977-78. These and a third data set are published in TERC Report No.8 (McManus, 1984). These three stations are shown in blue in Fig. 8.1. The data sets of these three stations (QRC, T2-T and NOM) were chosen on the same basis as the other five stations and are included in the overview in Table 8.1. However, Stations QRC and NOM are just on the border between areas where dunes could be measured from sonographs and the

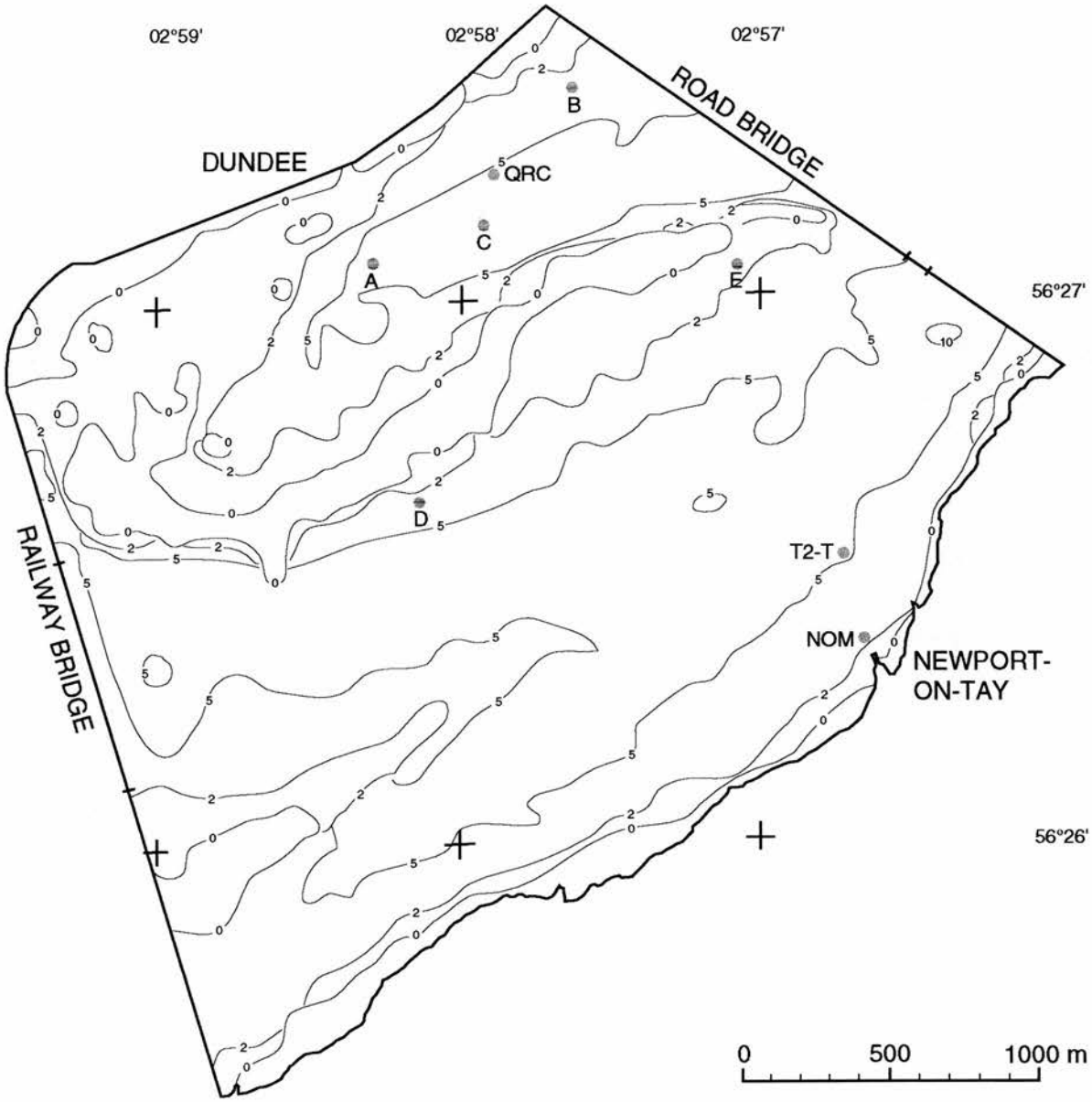

- A: 29.04.96, 23.07.96
  B: 06.06.96
  C: 24.05.96
  D: 07.05.96
  E: 21.05.96
- QRC: 11.05.78
  T2-T: 01.06.78
  NOM: 21.05.80

Fig. 8.1: Positions of current measuring stations.

Table 8.1: Variations of dune parameters (during flood and ebb tidal conditions) and sediment classification at current meter stations. Dune parameters are based on Ashley (1990) and sediment classification is based on Folk (1974).

dune parameter	tidal state	Station A	Station B	Station C	Station D	Station E	Station QRC	Station T2-T	Station NOM
wavelength	flood	small	medium	small	small	small	medium	small	small
	ebb	small	medium	medium	small	small	small	small	small
height	flood	small	medium	medium	small	medium	medium	medium	medium
	ebb	medium	medium	medium	medium	small	medium	medium	medium
length along crest	flood	20-50	20-50	20-50	10-20	10-20	20-50	10-20	10-20
	ebb	20-50	20-50	20-50	20-50	20-50	20-50	10-20	<10
sinuosity	flood	straight	sinuous out of phase	sinuous out of phase	catenary	straight	sinuous out of phase	patchy, discontinuous	patchy, discontinuous
	ebb	sinuous out of phase	sinuous out of phase	sinuous out of phase	sinuous out of phase	sinuous in phase	sinuous out of phase	patchy, discontinuous	patchy, discontinuous
super-position	flood	compound	simple	simple	compound	simple	simple	simple	simple
	ebb	compound	compound	compound	compound	compound	compound	simple	simple
asymmetry	flood	flood dominant	flood dominant	flood dominant	ebb dominant	flood dominant	flood dominant	flood dominant	flood dominant
	ebb	ebb dominant	flood dominant	flood dominant	mixed asymmetries	flood dominant	flood dominant	flood dominant	flood dominant
sediment		gravelly sand	gravel, pebbles, mussels	gravelly sand	gravelly sand	gravelly sand	silty sand, sandy silt	gravel, pebbles, mussels	silty sand, sandy silt

class of "no measurable dunes" as shown in the interpretation maps (Figs. 5.7, 5.9, 5.11, 5.13, 5.15, 5.16, 5.19, 5.22, 5.25, 5.26, 5.28, 5.29, 5.30, 5.31) in Chapter 5.

For the purposes of comparison with the acoustic data, current measurements had to be taken on days with similar tidal heights to those of the side-scan sonar surveys. For Stations A and C current data were collected on days of exactly the same predicted tidal height (according to the Tide Tables), while there were slight variations for Stations B, D and E (see Table 8.2). Tidal heights of the side-scan sonar survey days in the areas of Stations QRC, T2-T and NOM varied slightly from tidal heights of the days when current measurements were taken (Table 8.2). Full tidal cycle measurements in one day were taken at Stations B, C, D and E, while at Station A the measurements had to be split into two half tidal cycles of the same tidal height. Data sets for Stations QRC, T2-T and NOM were each collected during one tidal cycle.

Table 8.2: Comparison between tidal height of side-scan sonar surveys and current measurements

Station	tidal height of side-scan sonar survey (m)	tidal height of current measurement survey (m)
A	4.4	4.4 / 4.7 + 4.4
B	5.4	5.2 + 5.0
C	4.4	4.4 + 4.2
D	4.6 / 5.4	5.2 + 5.0
E	4.5	4.9 + 4.7
QRC	4.4/4.6	4.8+4.6
T2-T	4.4	4.6
NOM	4.9	4.4+4.2

8.2 Equipment and methods

The basic data requirements concerning horizontal water movement are the rate and the direction of flow (Ingham, 1975). To measure the surface and subsurface current speed and direction of flow, current meters have

been successfully employed for many years in estuarine environments (Kjerfve, 1979).

In this project two Braystoke MK 3, 5" Diameter Impeller current meters were used (Plate 8.1) to obtain surface and bottom measurements simultaneously. The sensor is a propeller, the rate of rotation of which increases with the current speed. The rate of flow was measured for 100 seconds and then converted into current speed in m/s by means of the Conversion Chart published in the Braystoke Operating and Maintenance Instruction Manual. The direction of the flow is measured by a built-in compass and is displayed as the flow towards the given bearing on the scale of 000°-350° in increments of 10°. Measurements were taken at 1m below the water surface (hereafter referred to as surface current) and 1m above the estuary bed (hereafter referred to as bottom current) at 20 minute intervals over full tidal cycles. The three "TERC" data sets were obtained using the Braystoke current meter as well as Plessey and Toho Dentan instruments. Measurements were taken at 0.5m above the seabed and 0.5m below the water surface, as well as within the water column, at 30 minute intervals.

8.3 Results

The results of the current measurements at all eight stations are presented individually in Figs. 8.3, 8.5, 8.7, 8.9, 8.11, 8.13, 8.15 and 8.17. The data are displayed in two types of graphs. The first type shows the difference between surface and bottom current velocities over a tidal cycle. Surface currents tend to have a higher velocity than bottom currents but variations have been recorded at the different stations. Assuming that the bottom currents principally influence the bedform geometry, their speeds and directions are plotted separately as rose diagrams. A summary of average and maximum current velocities for all eight stations is presented in Table 8.3.

Station A

As shown in Table 8.1 dune asymmetries recorded at Station A change with the tides, i.e. flood dominant dunes were recorded during flood tidal conditions and ebb dominant dunes during the ebb tide. The recorded dunes (Fig. 8.2) at this station were of small wavelength, small to medium

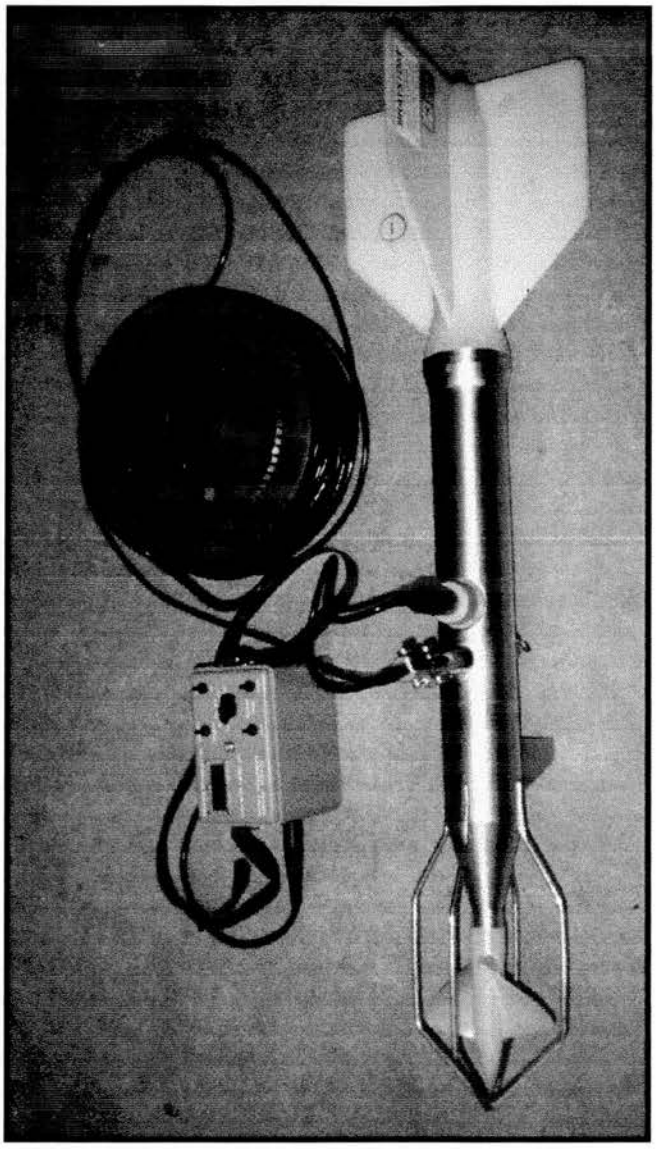

Plate 8.1: The Braystoke MK 3, 5" Diameter Impeller current meter.

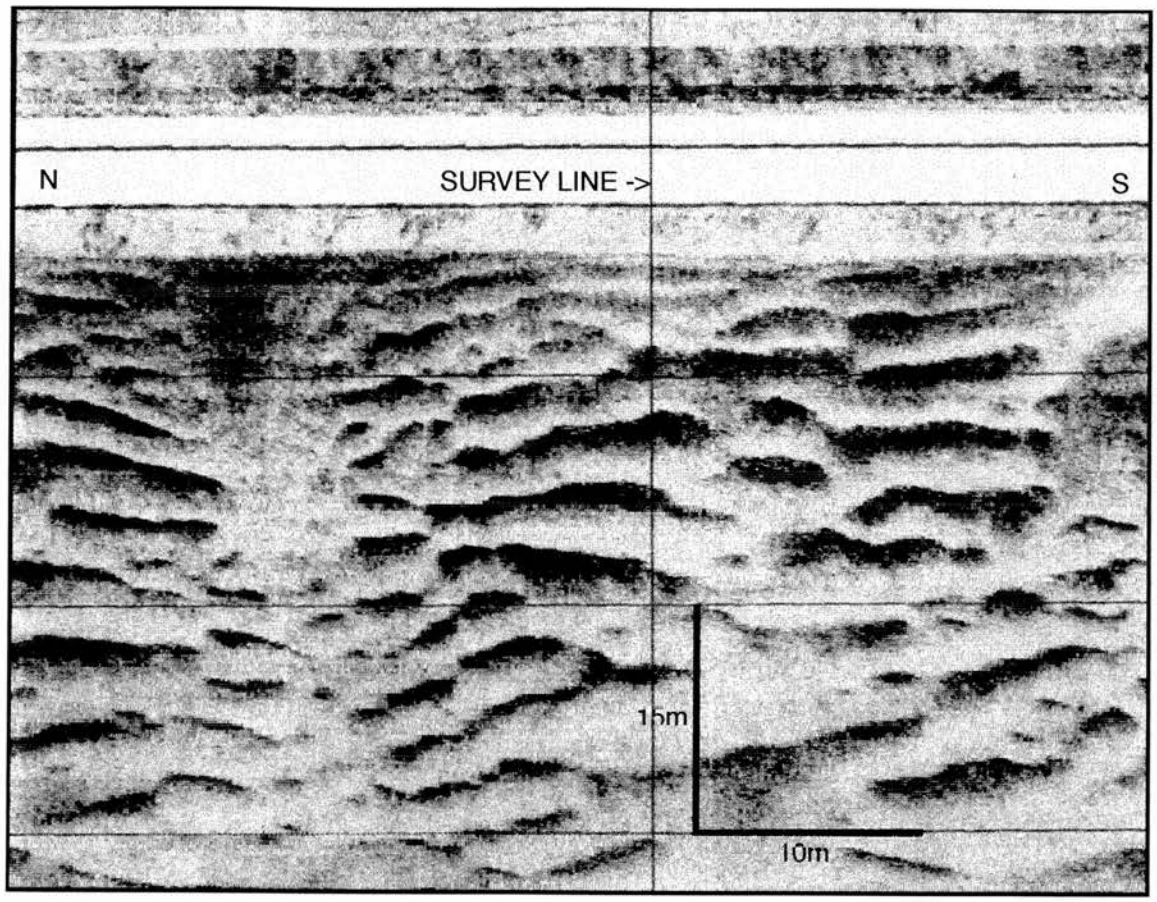

Fig. 8.2: Sonograph of the bed at Station A showing ebb dominant dunes recorded during ebb tidal conditions.

height and up to 30m in length along the dune crest. Although sinuosity varied between straight during flood tidal conditions and sinuous out of phase during ebb tidal conditions, dunes remained of compound superposition (superimposed dunes were of very small dimension) during both tidal states.

Table 8.3: Average and maximum current speeds and directions.

Station	tide	average speed (m/s)	average direction (°)	maximum speed (m/s)	direction of max. speed (°)
A	ebb	0.40	057	0.58	070
	flood	0.47	247	0.65	260
B	ebb	0.60	058	0.93	060
	flood	0.48	241	0.62	240
C	ebb	0.31	070	0.47	060
	flood	0.41	252	0.62	240
D	ebb	0.61	072	0.95	070
	flood	0.50	246	0.61	250
E	ebb	0.63	043	0.86	040
	flood	0.59	226	0.78	230
QRC	ebb	0.50	058	0.70	040
	flood	0.31	222	0.60	240
T2-T	ebb	0.60	045	0.98	046
	flood	0.45	238	0.60	227
NOM	ebb	0.38	036	0.45	030
	flood	0.28	269	0.45	260

Current speed and direction at Station A were measured for a period of 5 hours and 20 minutes on 29.04.96 (10:00-15:20) and for 8 hours on 23.07.96 (10:00-18:00), covering a full tidal cycle with an overlap at low water. Both sets of measurements were taken on days with a predicted tidal height of 4.4m. High tide was predicted at 13:05 on 29.04.96 and at 8:20 and 21:02 on 23.07.96. The time series plot of current velocities shows a systematic variation between ebb and flood tide with clear periods of slack water in between (Fig. 8.3a). The average velocities of the bottom current were 0.40m/s on the ebb tide and 0.47m/s on the flood tide (Table 8.3). However, the maximum flow strength on the ebb tide was

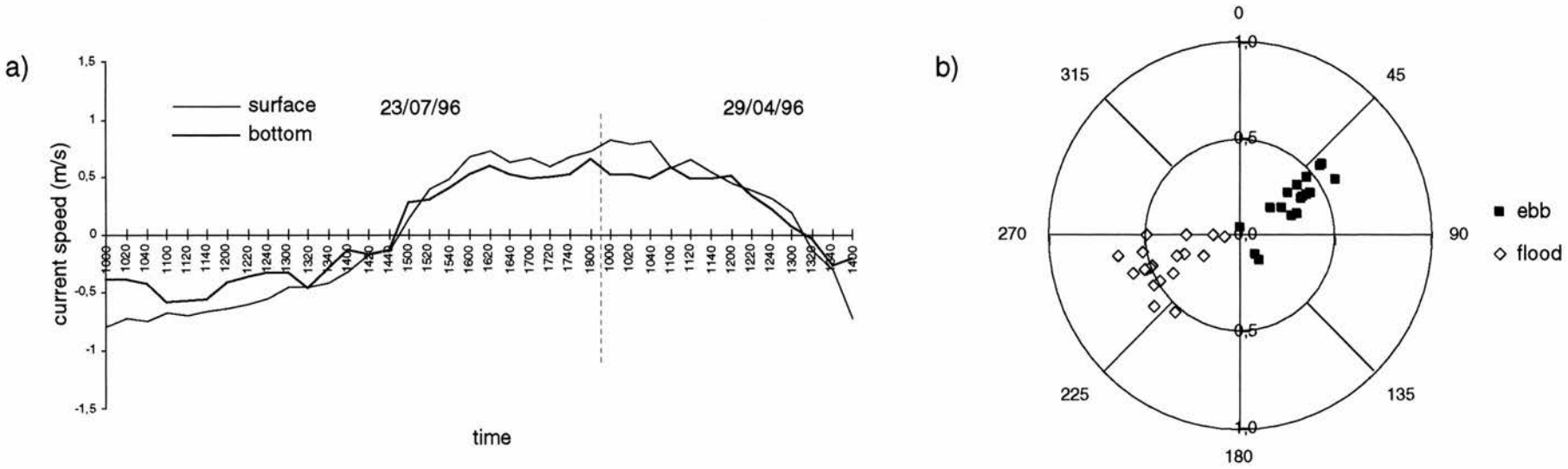

Fig. 8.3: Station A
a) time series plot of surface and bottom current velocities
b) speed and direction of bottom currents

0.58m/s and 0.65m/s on the flood tide. The strength of the current speed therefore suggests a clear flood dominance. It was necessary to choose a threshold value at which dunes form and migrate and with reference to the literature 0.5m/s is a good compromise value following Dalrymple and Rhodes (1995). However, a threshold value should be looked at as a range rather than a single value since it varies depending on water depth and grain size (see Section 4.3). During ebb tidal conditions this threshold was exceeded for 1 hour and 30 minutes compared with 4 hours and 20 minutes on the flood tide when currents speeds were mainly over 0.5m/s or just slightly under the threshold (Fig. 8.3a) supporting the flood dominance already suggested by the strength of the current speed. The rose diagram (Fig. 8.3b) of the bottom current speed and direction reveals only little variation in direction on the ebb tide in the range of 050°-070° with an average of 057°, with exceptions of 010° and 140° occurring only at the turn of the tide. The direction on the flood tide varied between 220° and 270°, with an average of 247°.

Station B

Dunes recorded at Station B by side-scan sonar were of similar dimensions and sinuosity as well as of flood dominant asymmetry during both tidal states (Table 8.1). Dunes varied only in superposition with simple dunes being recorded during the flood tide and compound forms during the ebb tide. The sediment sample of gravel, pebbles and mussels supports the side-scan sonar record (Fig. 8.4) which shows dark tonal intensities especially on the northern side indicating a dense material and supporting the suggestion of strong tidal currents.

Measurements at Station B were taken for a period of 12 hours and 20 minutes (9:00-21:20) on 06.06.96. The tidal height was predicted as 5.2m for high tide at 6:45 and 5.0m at 19:28. Periods of slack water can be seen on Fig. 8.5a which shows the time series plot of surface and bottom current velocities. On both tides the surface currents were slightly stronger than at the bottom. Bottom current speeds were, on average, 0.60m/s on the ebb and 0.48m/s on the flood tide. Maximum flow strength on the ebb tide was 0.93m/s and 0.62m/s on the flood. Average and maximum velocities suggest an ebb dominance of tidal currents. The threshold of 0.5m/s was exceeded on the ebb tide for 5 hours and on the flood tide for 2 hours and 40 minutes (including three measurements just below the

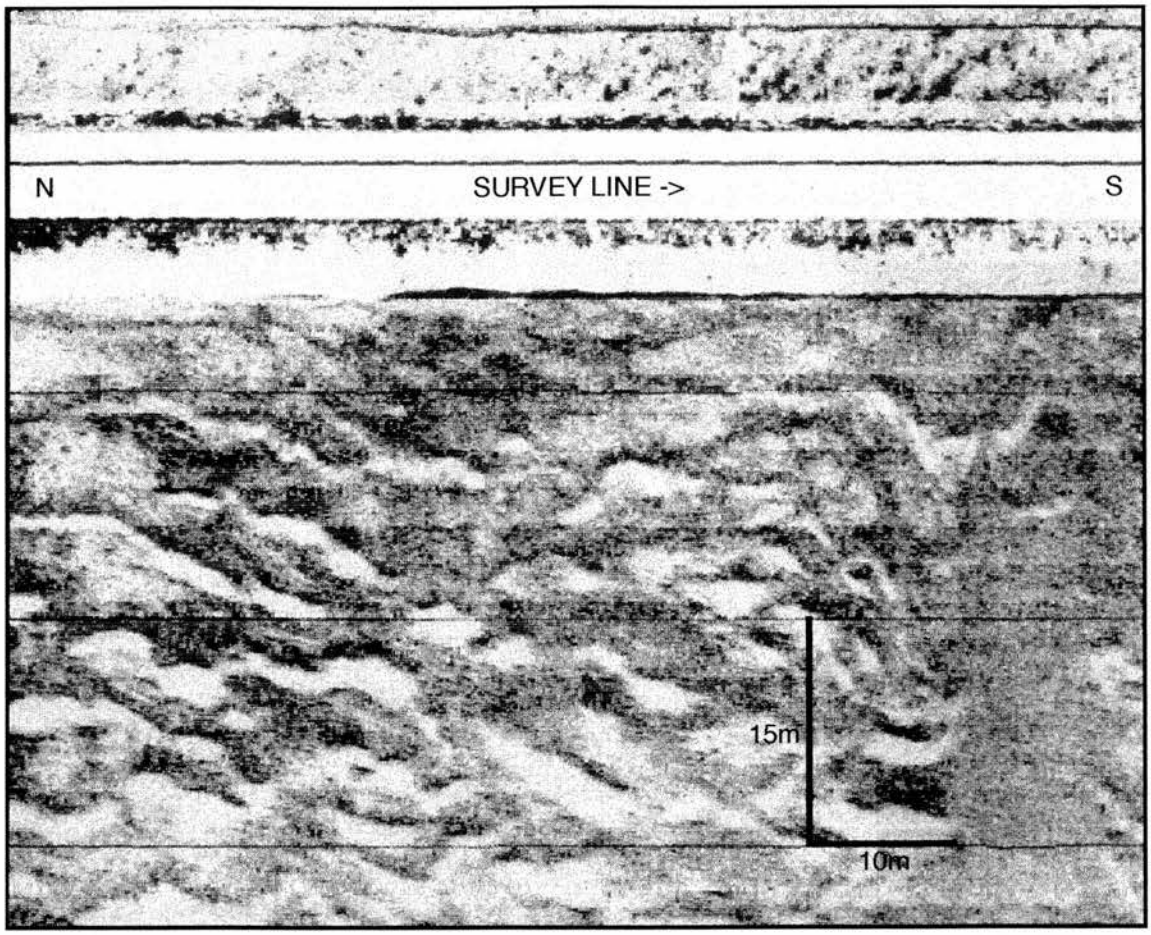

Fig. 8.4: Sonograph of the bed at Station B showing flood dominant dune asymmetries.

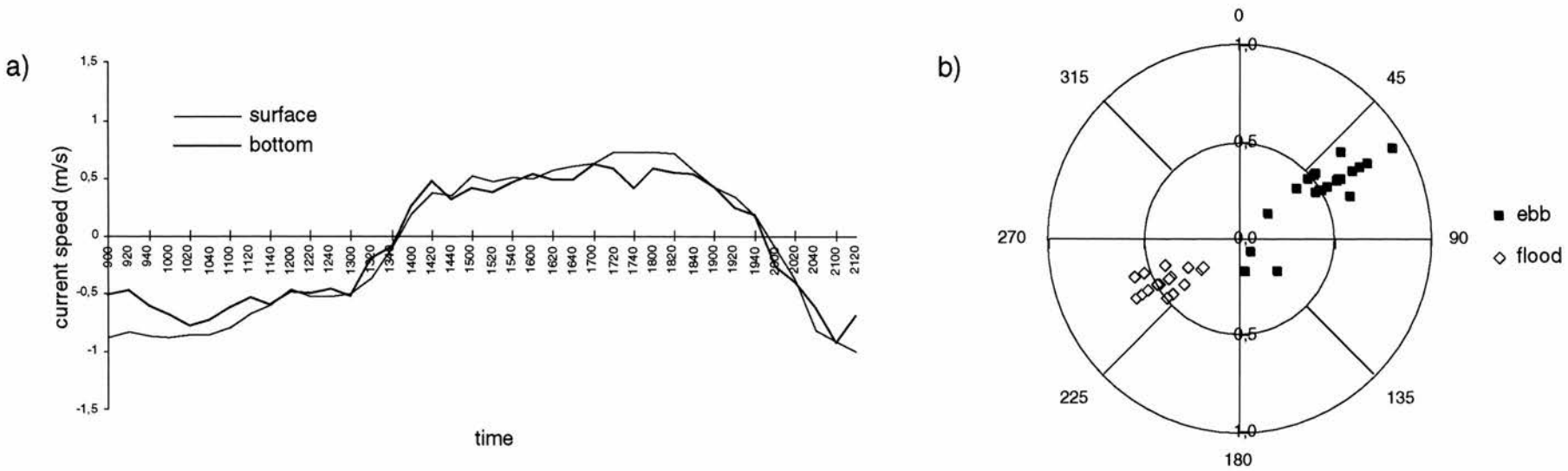

Fig. 8.5: Station B
a) time series plot of surface and bottom current velocities
b) speed and direction of bottom currents

threshold) also suggesting an ebb dominance (Fig. 8.5a). The rose diagram (Fig. 8.5b) shows that the ebb currents all lie within the range of 050°-070° with an average of 058°. The flood currents all flowed towards the west-south-west between bearings of between 230° and 250°, with an average of 241°.

Station C

The sonographs recorded at Station C revealed flood dominant dunes during both tidal conditions (Table 8.1). Similar to the dunes recorded at Station B, superposition varied between simple during the flood tide and compound during ebb tidal conditions. As shown on the sonograph (Fig. 8.6) dunes varied in height and wavelength in a relatively small area around the current station.

The data set collected at Station C on 24.05.96 covered a period of 12 hours and 40 minutes from 8:40-21:20. High tide was predicted at 7:51 and 20:29, with heights of 4.4m and 4.2m respectively. Fig. 8.7a shows that surface currents were stronger on both the ebb and on the flood tide than bottom currents. The average speed was 0.31m/s on the ebb and 0.41m/s on the flood tide, although maximum speeds were 0.47m/s on the ebb and 0.62m/s on the flood and therefore significantly higher. The data indicate that the flood tide dominates the water movement at this station. During ebb tidal conditions the currents never exceeded the threshold of 0.5m/s. On the flood tide the threshold was exceeded for 1 hour and 40 minutes only (Fig. 8.7a) which included two measurements when the currents were less than the threshold (0.46 and 0.45 m/s) but still suggesting a flood dominance. The average current directions were 070° on the ebb and 252° on the flood tide and occurred within the range of 050°-080° and 230°-280° respectively (Fig. 8.7b).

Station D

The side-scan sonar record shown in Fig. 8.8 displays dunes as described in Table 8.1 for Station D during ebb tidal conditions. Although dune wavelengths were small and dune superposition was compound during both tidal states, dune height, length along dune crest, sinuosity and asymmetry varied with the tidal condition. Ebb dominant dunes were recorded during the flood tide and dunes of mixed asymmetries during the

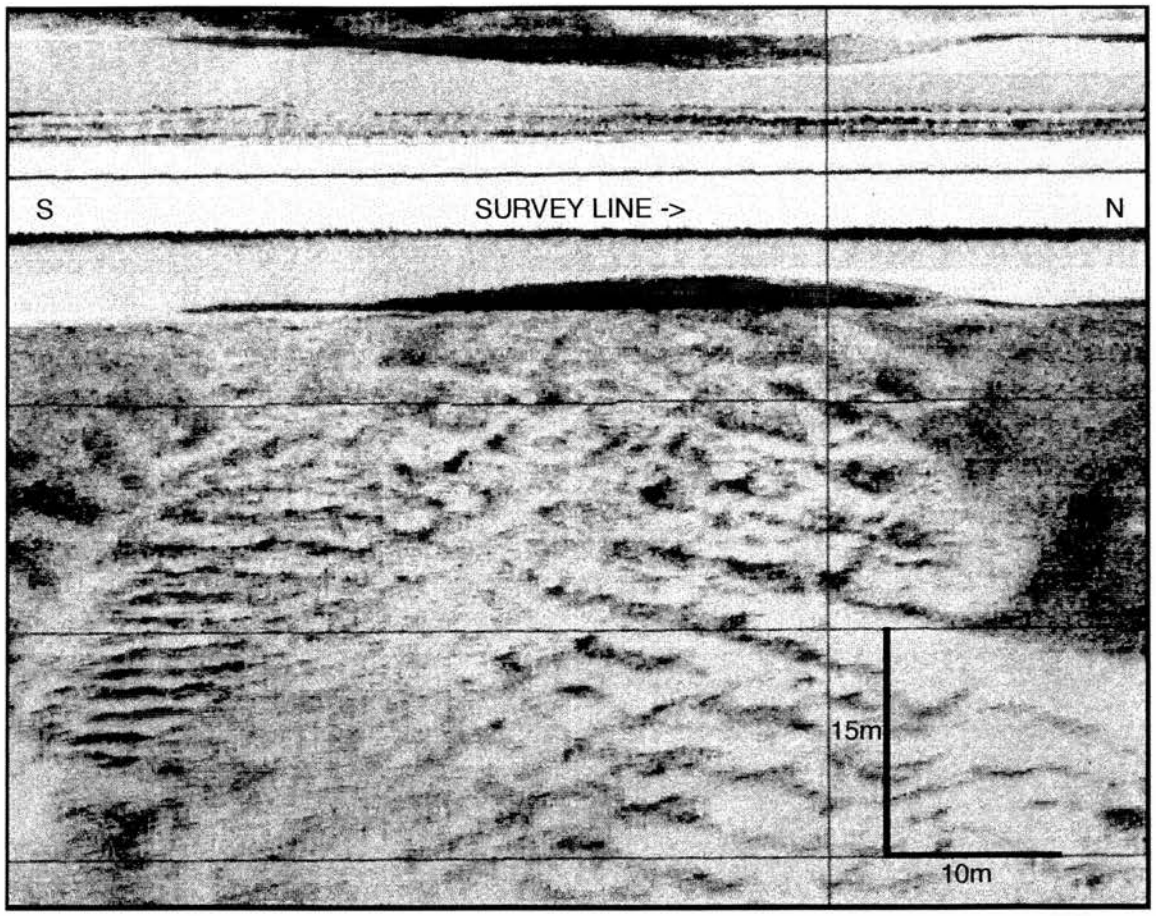

Fig. 8.6: Sonograph of the bed at Station C showing flood dominant dune asymmetries.

Fig. 8.7: Station C
a) time series plot of surface and bottom current velocities
b) speed and direction of bottom currents

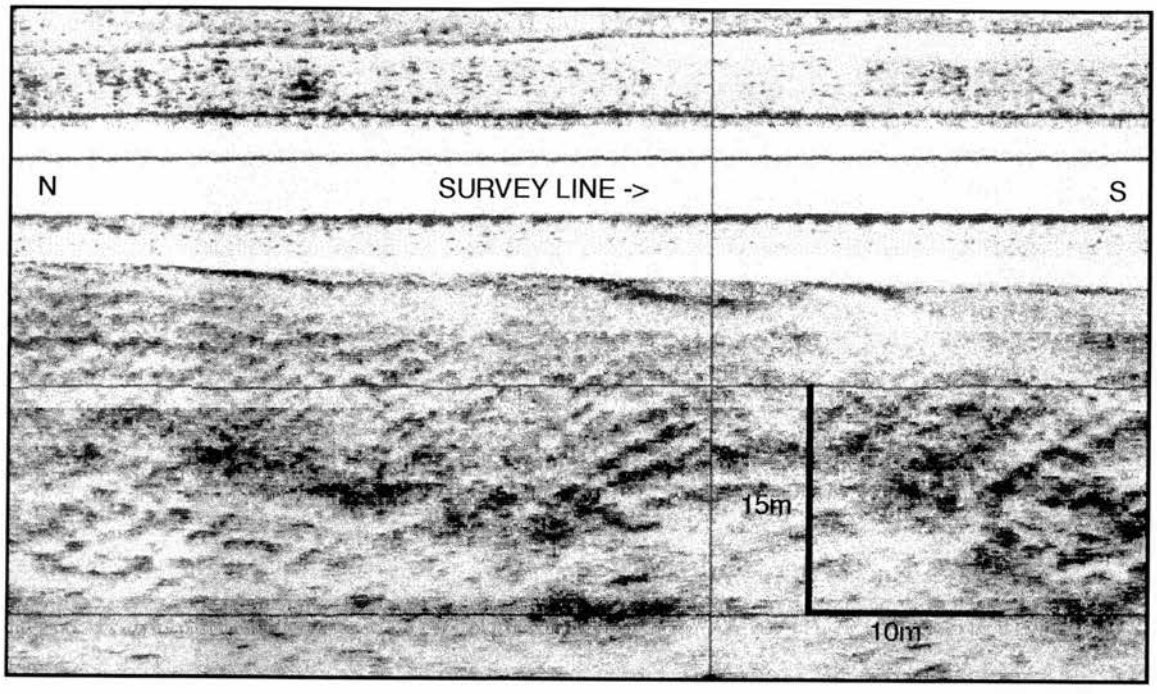

Fig. 8.8: Sonograph of the bed at Station D showing dunes of mixed asymmetries recorded during ebb tidal conditions.

ebb tide. The differences between the four geometrical parameters of dunes according to the tidal condition suggests a strongly varied tidal current regime at this station.

At Station D current speed and direction were measured from 9:00 until 20:40 covering 11 hours and 40 minutes, although a full tidal cycle is approximately 12 hours and 35 minutes. Predicted high tides and tidal heights for 07.05.96 were 5.2m at 6:11 and 5.0m at 18:46. Surface and bottom current speeds were very similar on the flood tide but varied on the ebb tide with the surface speeds being stronger (Fig. 8.9a). Average bottom current speeds were at 0.61m/s on the ebb tide and 0.50m/s on the flood tide. Maximum flow strength on the ebb tide was 0.95m/s and 0.61m/s on the flood tide. These measurements clearly suggest an ebb dominance. However, the threshold of 0.5m/s was exceeded for 4 hours both on the ebb and the flood tide (Fig. 8.9a) but during ebb tidal conditions the current strength was below the threshold for two measurements (0.42 and 0.45m/s). The current directions varied between 060°-080° (average 072°) on the ebb tide and 230°-270° (average 246°) on the flood tide, as shown in Fig. 8.9b.

Station E

Dunes recorded by side-scan sonar (Fig. 8.10) at Station E revealed a flood dominant asymmetry during both tidal conditions although dune height, length along crest, sinuosity and superposition varied as shown in Table 8.1.

On 21.05.96 12 hours were spent at Station E collecting current data. Predicted high tides were at 5:50 with a height of 4.9m and at 18:18 with a height of 4.7m. Surface currents were slightly stronger than bottom currents on the ebb tide (Fig. 8.11a). The average speeds were closely similar on the ebb and the flood tide, being 0.63m/s and 0.59m/s respectively, suggesting a slight ebb dominance. Maximum speeds revealed a flood dominance of 0.86m/s compared with 0.78m/s. However, the threshold of 0.5m/s was exceeded for 4 hours and 40 minutes during ebb tidal conditions and 4 hours during flood tidal conditions (Fig. 8.11a), hence suggesting an ebb dominance. The average direction of 043° was between 030°-070° showing the highest variation for the ebb currents recorded and 226°, between 210°-240°, for the flood currents (Fig. 8.11b).

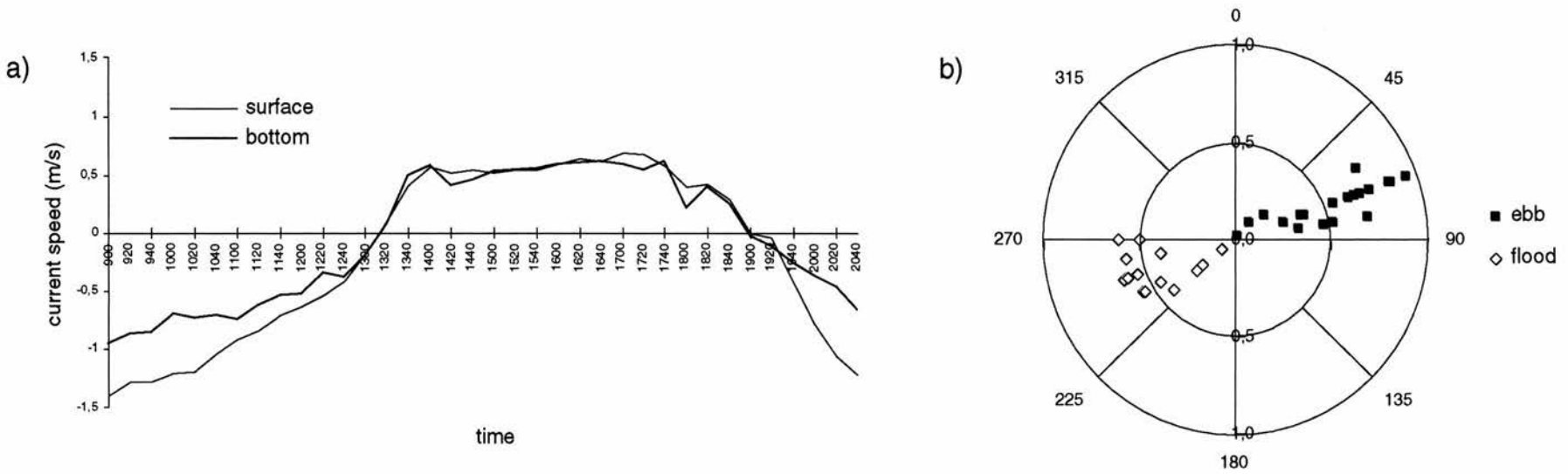

Fig.8.9: Station D
a) time series plot of surface and bottom current velocities
b) speed and direction of bottom currents

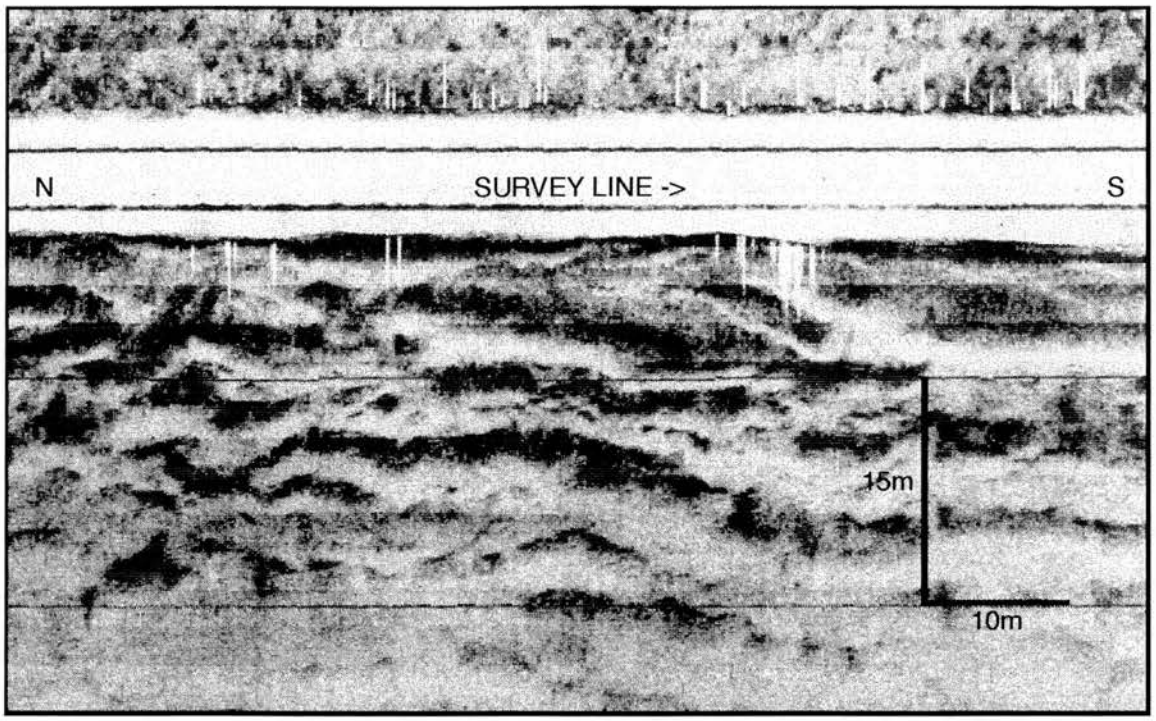

Fig. 8.10: Sonograph of the bed at Station E showing flood dominant dune asymmetries.

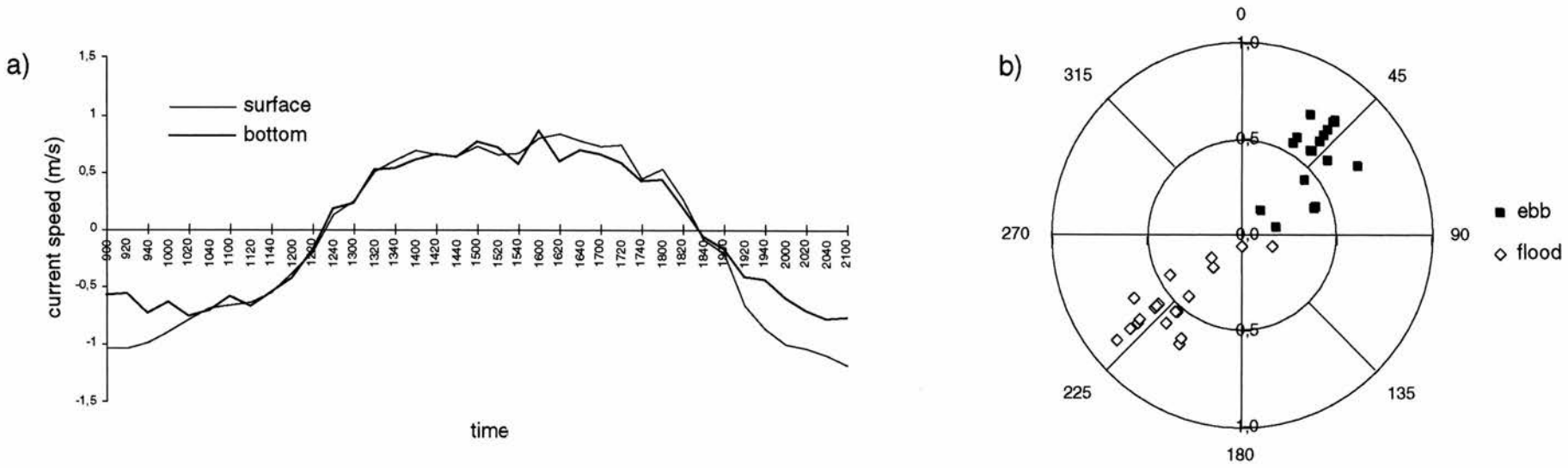

Fig. 8.11: Station E
a) time series plot of surface and bottom current velocities
b) speed and direction of bottom currents

Queen's Road Channel (QRC)

The light tonal intensities displayed in the sonograph (Fig. 8.12) recorded at Station QRC support the classification of the sediment sample analysis as being silty sand/sandy silt (Table 8.1). The current meter station was positioned at the northern border of the recorded dune field. Dunes were flood dominant during both tidal conditions according to the sonograph interpretation.

The measurements at this station were taken by M. Hope and J. Gillespie on 11.05.78. The data set covers a period of 12 hours and 20 minutes between 8:10 and 20:30. High tides were predicted at 5:57 and 18:23 with heights of 4.8m and 4.6m respectively. The surface currents in Fig. 8.13a are clearly stronger on the ebb than the bottom currents but closely similar on the flood tide. The data set shows a period of low slack water for approximately one and a half hours for the bottom currents but a far quicker transition for the surface currents. The average bottom current speed was 0.53m/s on the ebb and 0.27m/s on the flood, revealing an ebb dominance. However, the maximum flow strength was 0.60m/s during both ebb and flood tidal conditions. Few measurements of current speed exceeded the threshold of 0.5m/s at this station (Fig. 8.13a). During ebb tidal conditions the threshold was exceeded for 2 hours and 30 minutes with the current speed falling below the minimum for one reading (0.46m/s) while during flood tidal conditions the threshold was generally exceeded for 3 hours although the current speed was as low as 0.2m/s for one reading in this period. This suggests a flood dominance contrary to the average bottom current speed. The direction varied between 040°-070° with an average of 060° on the ebb tide and a surprisingly big variation on the flood tide of between 160°-340°, with an average of 240° (Fig. 8.13b).

TRB2-TERC (T2-T)

The position of this station is described as being midway between the former navigation buoy TRB2 and the TERC mooring (McManus, 1984). The side-scan sonar record (Fig. 8.14) coincides with the analysis of the sediment sample collected at Station T2-T (Table 8.1). The position of this station lies in the Southern Channel (Fig. 8.1) and the sonograph revealed the "patchy, discontinuous" pattern typical of most channel areas. Gravel,

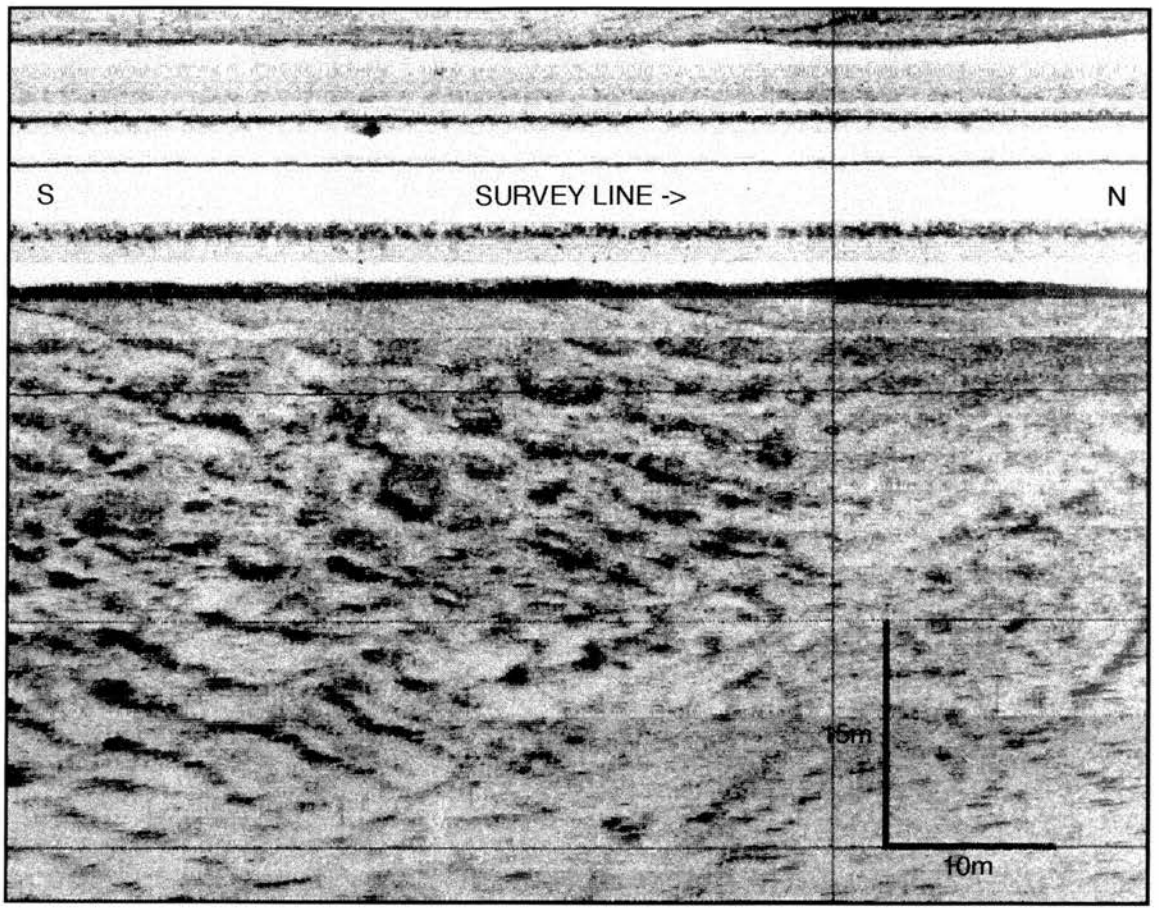

Fig. 8.12: Sonograph of the bed at Station QRC showing flood dominant dune asymmetries.

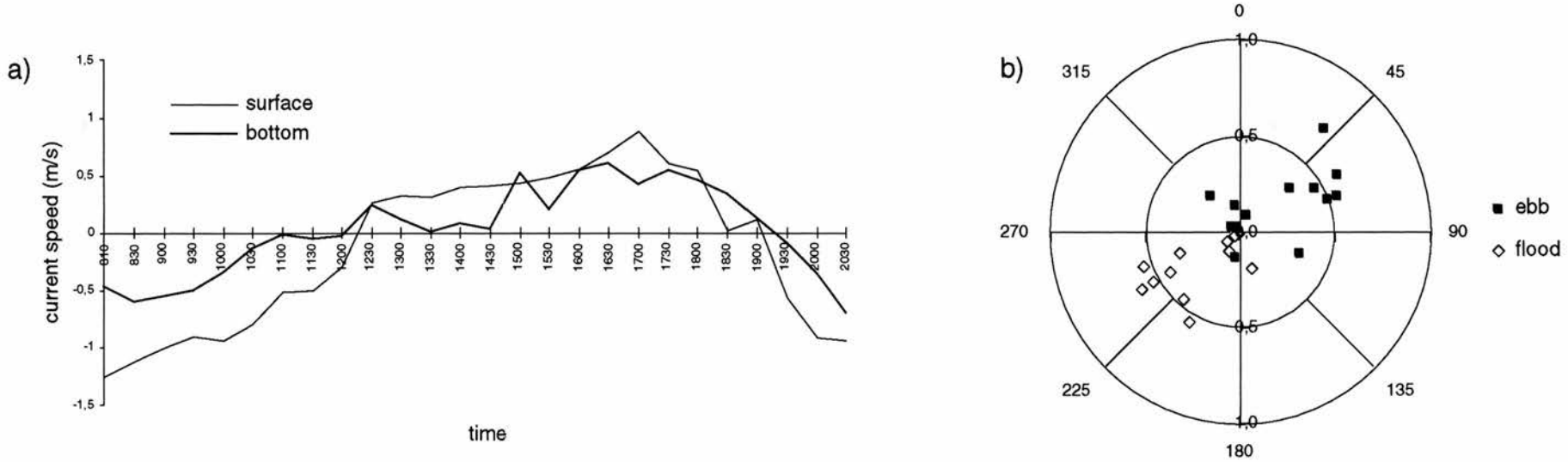

Fig. 8.13: Station QRC
a) time series plot of surface and bottom current velocities
b) speed and direction of bottom currents

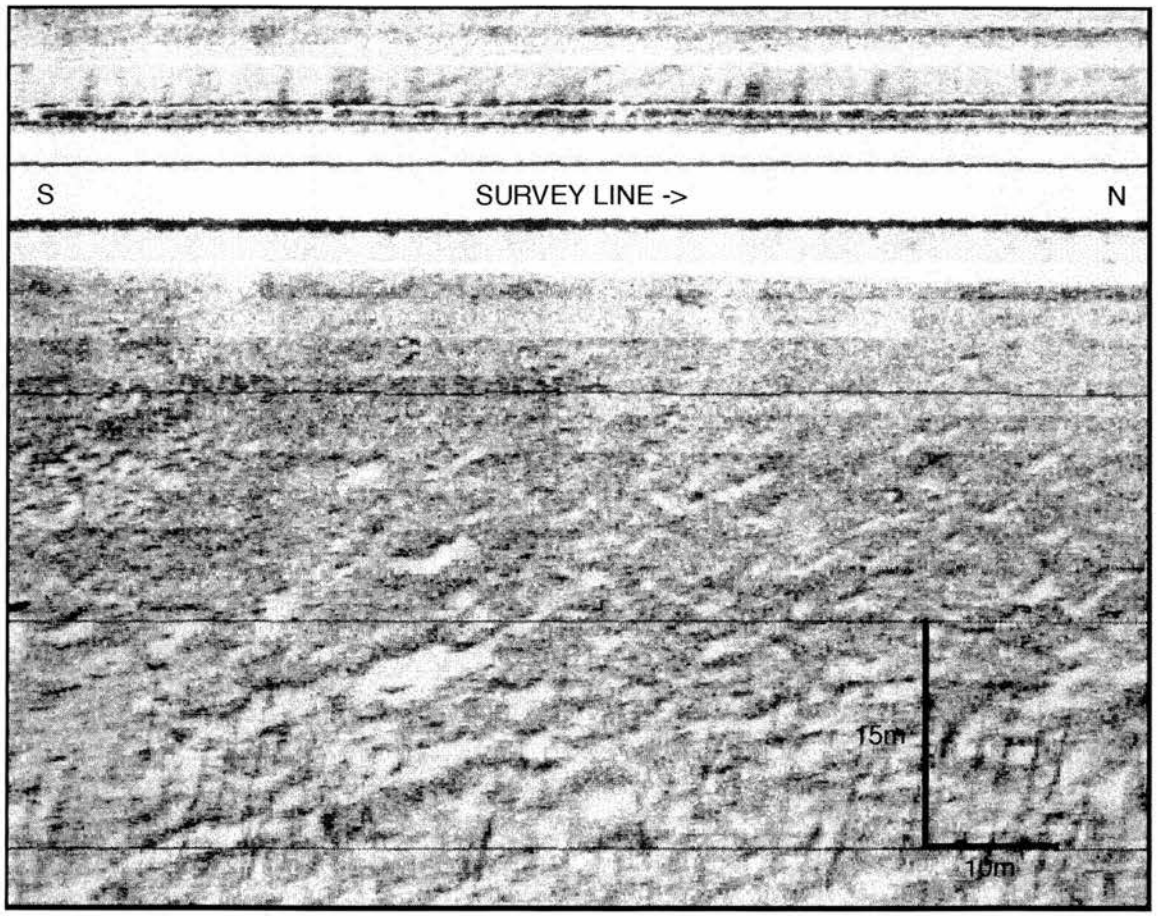

Fig. 8.14: Sonograph of the bed at Station T2-T showing the "patchy, discontinuous" pattern typical of most channel areas.

pebbles and mussels were collected with the van Veen grab indicating, in conjunction with the sinuosity pattern recorded, the existence of strong tidal currents as expected in channel areas.

Current data were recorded on 01.06.78 by R. Peek and S. O'Rourke for a period of 12 hours and 25 minutes from 8:05 until 20:30 with a predicted high tide occurring at 12:28 with a height of 4.6m. Since no measurement was taken of the surface current speed at 20:30, the time series plot (Fig. 8.15a) ends at 20:00. Once more the surface speed is generally stronger than that of the bottom current. Average bottom current speeds were 0.60m/s on the ebb and 0.45m/s on the flood tide, with maximum velocities respectively of 0.98m/s and 0.60m/s, suggesting a strong ebb dominance. The threshold of 0.5m/s was exceeded for 3 hours and 30 minutes on the ebb tide and 4 hours on the flood tide (Fig. 8.15a). However, the flood measurements included two readings below the minimum (0.34 and 0.48m/s) during the exceedance period. The rose diagram (Fig. 8.15b) reveals a range of ebb current directions between 017°-062° (average 045°) and a flood current direction range of 223°-262° (average 238°).

Newport Outer Mooring (NOM)

The current meter Station NOM was positioned at the border of the class of measurable dunes as interpreted from the sonograph (see Chapter 5) which can be seen in Fig. 8.16. The sediment sample collected was classified as silty sand/sandy silt (Table 8.1). The measured dunes at the northern side of the current meter position revealed the "patchy, discontinuous" sinuosity pattern typical for channel areas, commonly related to gravel and pebbles colonised by mussel beds. Dunes indicated a flood dominant asymmetry during both tidal states.

This station was reported to be about 100m off the pier of TERC (McManus, pers. comm.). C. Dobereiner and E. Sarrikostis spent 13 hours collecting data on 21.05.80 between 7:00 and 20:00. This is the only station which revealed bottom current speeds of 0m/s over three measuring intervals (Fig. 8.17a). This is probably related to the neap tidal height of only 4.4m at 8:30 and 4.2m at 21:25. It is therefore not surprising that average bottom current speeds were as low as 0.38m/s on the ebb and 0.28m/s on the flood tide. This would suggest a dominance of the ebb

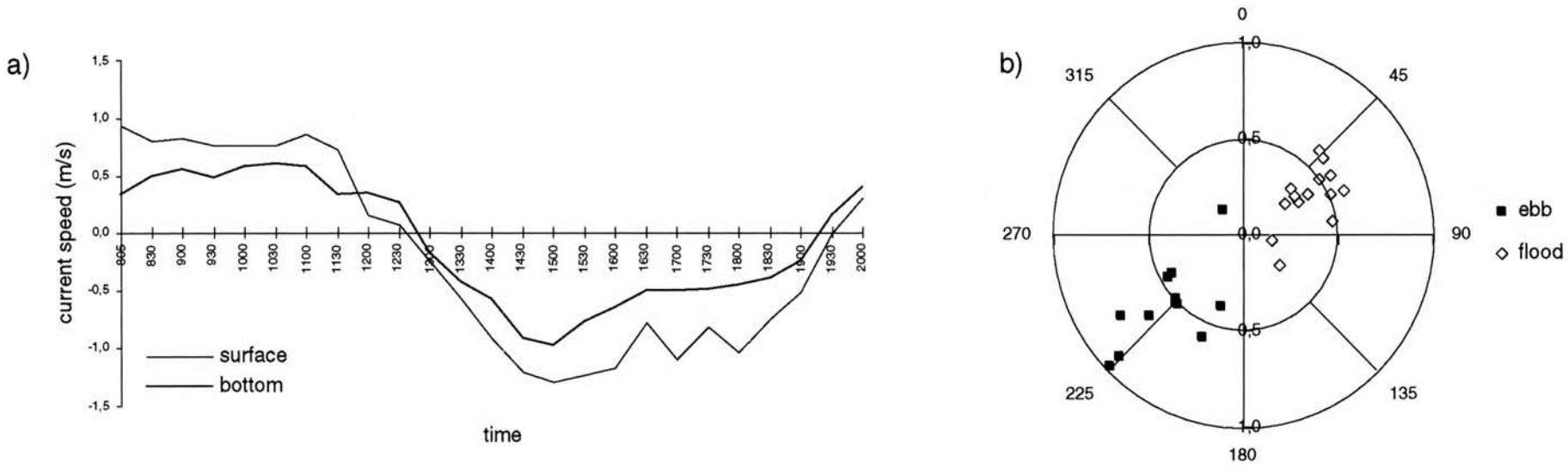

Fig. 8.15: Station T2-T
a) time series plot of surface and bottom current velocities
b) speed and direction of bottom currents

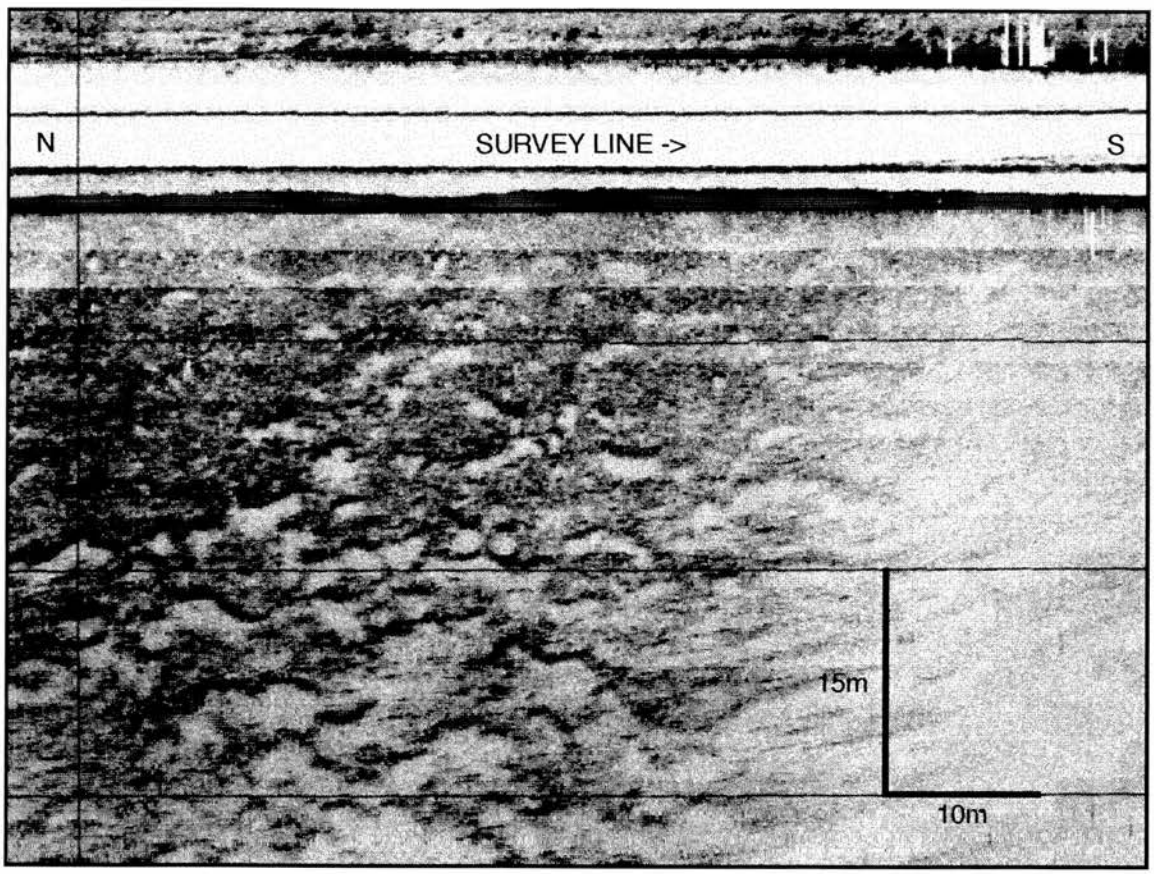

Fig. 8.16: Sonograph of the bed at Station NOM showing the border between the "patchy, discontinuous" pattern in the northern and central section and "no measurable dunes" in the southern section.

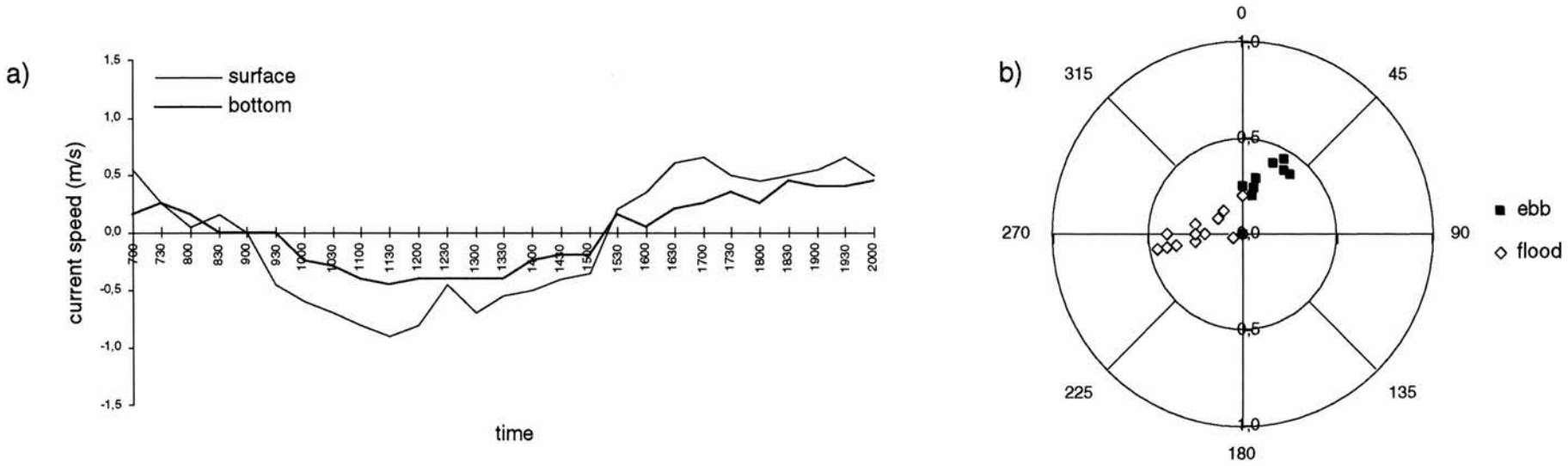

Fig. 8.17: Station NOM
a) time series plot of surface and bottom current velocities
b) speed and direction of bottom currents

flow, but the maximum flow strengths were 0.45m/s on both tides. At this station the threshold of 0.5m/s for dune formation and migration was not exceeded during the recorded tidal cycle (Fig. 8.17a). The rose diagram (Fig. 8.17b) shows that the flow directions were not exactly opposite each other, as at the other stations, but cluster around 036° (015°-040°) on the ebb tide and 269° (240°-300°) on the flood tide.

8.4 Discussion of the current measurements

On the basis of the data obtained a general statement about water circulation in the fieldwork area can be made. At all eight stations stronger surface currents than bottom currents were recorded. Since surface currents are influenced by wind and waves, and do not directly influence the geometry of sedimentary bedforms in deeper waters, they are not included in the further analysis of the data.

The flow strength is closely related to the tidal height so that velocities are relatively slow on neap tides and fast on spring tides. Thus the dates of current metering sessions had to be of similar predicted tidal height to those of the side-scan sonar surveys for comparative purposes, and therefore varied between 4.4m and 5.4m depending on the station. An exact configuration of water circulation should take this into account.

The data acquired at the majority of the stations (B, D, E, QRC, T2-T and NOM) suggest an ebb dominance of bottom current strength according to the maximum current velocity measured (see Fig. 8.18). Average ebb tidal current speeds were between 0.04 and 0.19m/s faster than on the flood tide and maximum speeds up to 0.38m/s faster. The single exception was Station NOM where average ebb current speeds were stronger than flood current speeds but maximum flow strengths were of the same range at both tidal states. The data of the two Stations with dominant flood current flows, A and C, displayed a far smaller difference between both average speeds (A: 0.07m/s, C: 0.10m/s) and for maximum flow strengths (A: 0.07m/s, C: 0.15m/s). However, when examining the length of time in which the current speed exceeds the threshold given for dune occurrence and migration (Dalrymple and Rhodes, 1995), the tidal dominance changes for some of the stations. At Station D the data suggest a symmetric occurrence of current speed for both tides while at Stations QRC and T2-T the threshold was exceeded for a longer time period during

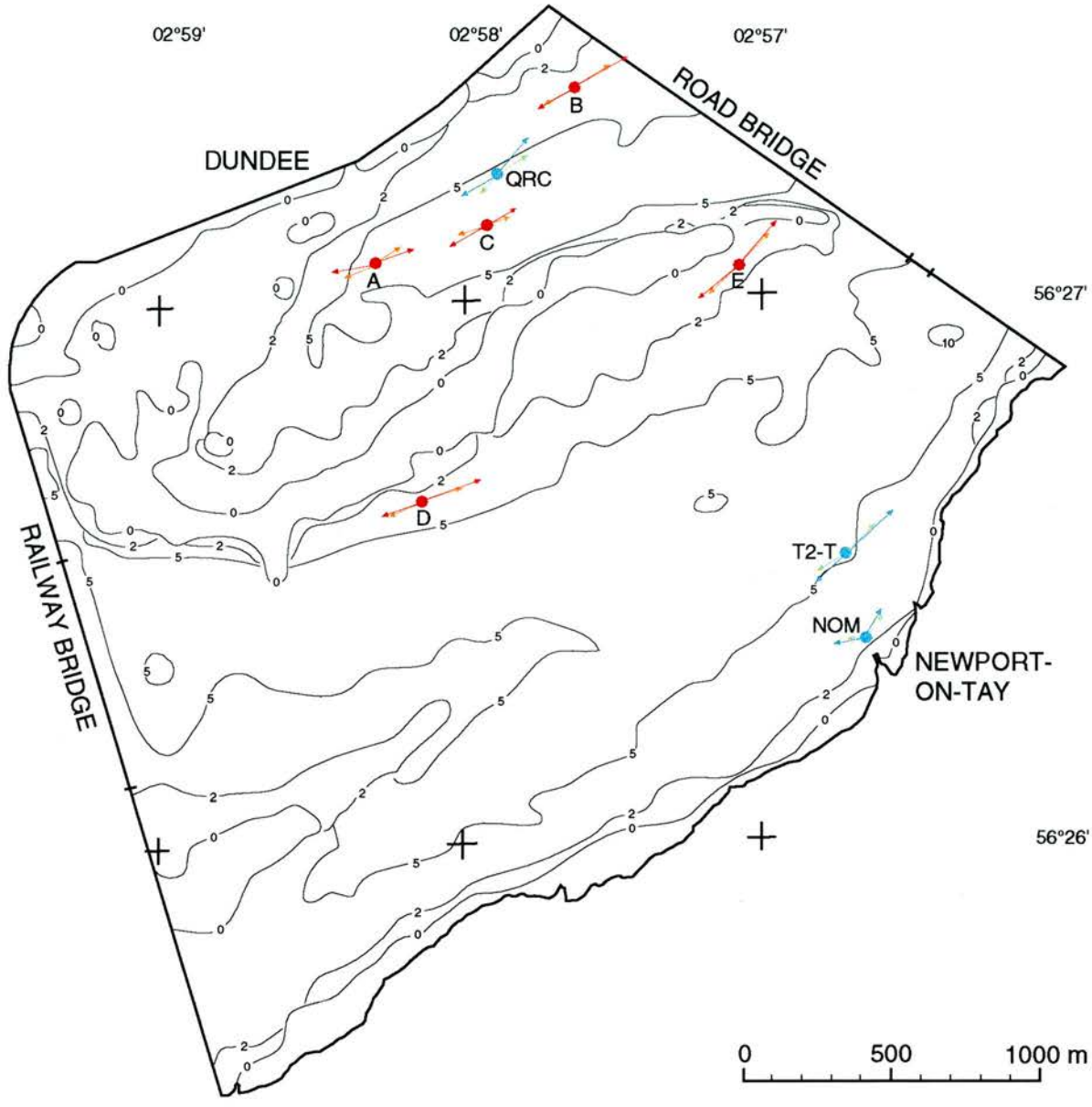

maximum velocity

1.00 m/s

average velocity

1.00 m/s

- A: 29.04.96, 23.07.96
  B: 06.06.96
  C: 24.05.96
  D: 07.05.96
  E: 21.05.96
- QRC: 11.05.78
  T2-T: 01.06.78
  NOM: 21.05.80

Fig. 8.18: Average and maximum current velocities.

flood tidal conditions. At Station NOM the threshold was not exceeded at all which indicates neither the formation nor migration of dunes under the conditions measured.

However, dune asymmetries revealed from sonograph interpretations do not generally support the measurement of maximum and average current velocities at all eight stations. Sonograph interpretation of dune asymmetries and current measurements at Stations C and D coincide revealing flood and ebb dominance respectively. At Station A dune asymmetries were indicative of flood dominant flows during flood tidal conditions and of ebb dominant current flows during ebb tidal conditions although current measurements of one tidal cycle clearly suggested stronger flood currents. At Stations B, E, QRC, and T2-T stronger ebb currents than flood currents were measured which oppose the flood dominant dune asymmetries interpreted from the sonographs during both tidal states. At Station NOM average ebb currents were higher than average flood currents but maximum current speeds measured were the same during both tidal states.

When comparing the length of time at which the threshold for dune occurrence and migration given by Dalrymple and Rhodes (1995) is exceeded with the dune asymmetry as interpreted from sonographs, a correlation was found. At Stations C, QRC and T2-T the threshold of 0.5m/s was exceeded for a longer period of time (between 30 minutes and 1 hour and 40 minutes) during the flood tide, hence coinciding with the flood dominant dune asymmetries recorded by side-scan sonar. Current measurements at Station NOM indicated neither the occurrence nor migration of dunes as can be seen on the southern part of the sonograph shown in Fig. 8.16. At Station D the threshold was exceeded for the same length of time during both tidal conditions and sonographs revealed ebb dominant and mixed dune asymmetries. Although the exceedance of the threshold at Station A indicated a flood dominance, dune asymmetries changed with the tidal state according to the sonographs. At Station B and E flood dominant dune asymmetries were recorded during both tidal conditions even though current measurements clearly revealed an ebb dominance. Nevertheless, a better correlation between dune asymmetries and the exceedance of the given threshold by Dalrymple and Rhodes (1995) was found than between dune asymmetries and maximum and average current velocities, suggesting that the length of time during which

the threshold is exceeded has a stronger effect on the occurrence and asymmetry of dunes than the maximum and average current velocities.

The overall directions of the ebb and flood currents varied from station to station. Average ebb current directions were within the limits of 036°-072° and average flood current directions were between 222°-269°. Apart from station NOM, all current directions were approximately opposite on ebb and flood. Station NOM is probably influenced by its close proximity to the shore (100m off TERC pier).

As already mentioned in Chapter 3 Charlton *et al.* (1975) have investigated the circulation in the Tay Estuary. These authors found that the flood tide is uniformly distributed between the two channels while the ebb tidal flows tend to concentrate in the main Navigation Channel. Float tracking experiments and investigations of salinity variation by McManus and Wakefield (1982) generally support these findings, although they state that the flood tide tends to dominate the northern channel (Queen's Road Channel). When the tide turns, the waters flow southward and then ebb along the southern shore in the main Navigation Channel, resulting in an anticlockwise circulation pattern. However, float tracking experiments measure surface currents only and do not take bottom currents into account. The results of the recent near bottom current measurements do not fully conform to this anticlockwise circulation pattern. Although the data of Stations A and C in the northern channel suggest a flood dominance, the other two stations (B and QRC) appear to be characterised by ebb dominant currents. Both Stations B and QRC are, however, relatively close to the Road Bridge which, according to Charlton *et al.* (1975), causes a significant obstruction to the tidal flow. This may account for the discrepancy. The data of all four stations south of Middle Bank (D, E, T2-T and NOM), along the main Navigation Channel, are indicative of ebb dominant bottom currents and hence support the anticlockwise circulation pattern observed for surface currents.

8.5 Estimation of sediment transport

Numerous methods exist to estimate sediment transport. Heathershaw (1981) has given a summary of commonly used equations and compared the predicted sediment transport rates with those measured in tidal currents. The equations used were Einstein's (1950), Bagnold's (1963)

and Yalin's (1963) bed load equations as well as Ackers and White's (1973) and Engelund and Hansen's (1967) total load equations. Heathershaw (1981) concludes that Bagnold's (1963) bed load equation appears to be the least sensitive while Ackers and White's (1973) total load equation is the most sensitive. Sternberg (1972) modified Bagnold's (1963) equation after further field observations and this equation is applied here since the other equations include variables which could not be measured or estimated in this project and could therefore not be applied. Sternberg's (1972) method has been successfully applied by Harris *et al.* (1979) and Sternberg and Marsden (1979) in Western Port, Australia, by Alizai (1980) in Invergowrie Bay of the Tay Estuary and others.

Initially ebb and flood current velocities from the eight current measurement stations were plotted with their corresponding mean grain diameter of the sediment on a graph after Sundborg (1967) (Fig. 8.19) which is the first step of Sternberg's (1972) method for estimating bed load transport. Sundborg (1967) states that, "the transportation of sediments by flowing water is a process that is intimately connected with the hydrodynamical conditions and the state of movement of the individual grains. This means that also the sorting and segregation of particles according to size, density and shape can be attributed to hydrodynamical forces" (Sundborg, 1967). In the construction of this diagram it was presumed that the velocity refers to the current velocity at 1.0m above the bed and that the sediment consists of uniform materials with a density of 2.65g/cm^3 (quartz and feldspar). The diagram is divided into four fields: A field of transportation of suspended load for small grain diameters, a field of no transportation for larger grain diameters and relatively low velocities followed by an envelope within which cessation of movement occurs as a transition to the field in which bed load transportation takes place in response to the high current velocities (Fig. 8.19).

Sediment samples were collected and analysed (see Chapter 7) and current velocities of eight stations (see Chapter 8) were available to estimate sediment transport. According to Buller and McManus (1975) the sands of the middle reaches of the Tay Estuary are rich in quartz and feldspar permitting the application of Sundborg's diagram. At the eight stations measurements were taken during ebb and flood tidal conditions giving a total of 16 measurements during two tidal states. Of these 16 mean velocities eight plot in the field of bed load transportation, two in the

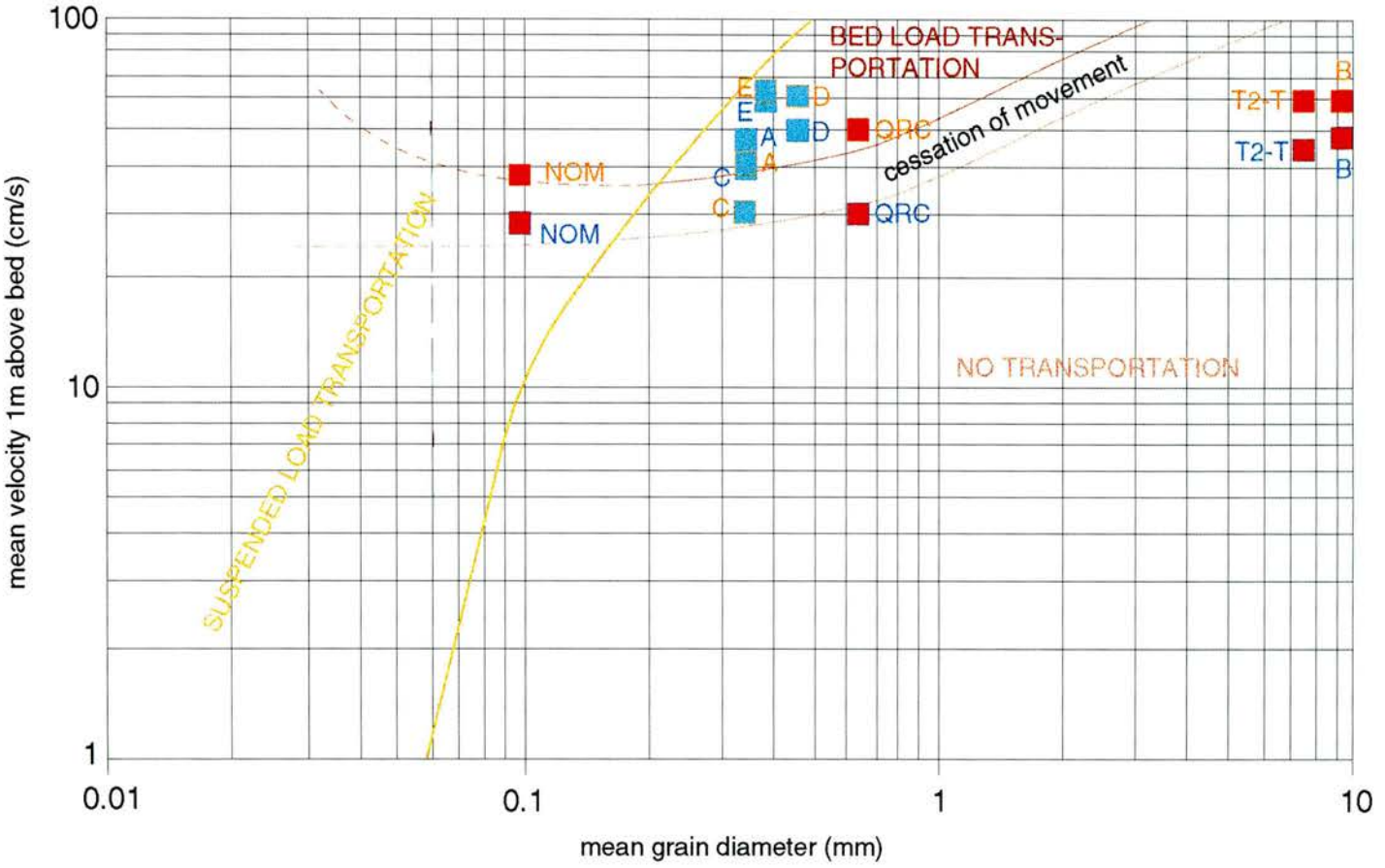

Fig. 8.19: Plot of average current speed (flood and ebb) and corresponding sediment mean grain diameter for all eight stations showing the relationship between grain size, flow velocity and type of sediment movement. Diagram after Sundborg (1967).

field of suspended load transportation, one in the field of cessation of movement and five in the field of no transportation.

The eight measurements plotting in the area of bed load transportation were used to estimate the amount of sediment transported by the tidal currents. The measurements were: Station A - ebb and flood data, Station C - flood data only, Station D - ebb and flood data, Station E - ebb and flood data and Station QRC - ebb data only. The specific steps of the estimation procedure of Sternberg (1972) can be found in Appendix II.

The two data points plotting in the suspended load transportation field of Sundborg's (1967) diagram (Fig. 8.19) relate to Station NOM. The analysis of the collected sediment samples revealed that this part of the estuary is characterised by very fine sands with a mean grain diameter of 0.1mm. Due to this fine mean grain size, the mean current velocities of 0.38m/s during ebb and 0.28m/s during flood tidal conditions are capable of transporting the sediment as suspended load, as seen in Fig. 8.19.

Mean grain size and mean ebb tidal current velocity at Station C plot within the area of cessation of movement on Sundborg's (1967) diagram (Fig. 8.19). Medium sand with a mean grain diameter of 0.37mm was sampled at this station and the average current velocity during ebb tidal conditions was 0.31m/s. According to the diagram of Sundborg (1967) no bed load transport occurs for this type of sediment size with associated flow strength. However, this does not concur with the side-scan sonar observations which revealed flood dominant dune asymmetries during both tidal conditions indicating bed load transport towards the west with the incoming flood tide.

The five measurements which plot in the area of no transportation (Fig. 8.19) differed in grain size as well as current velocities. At Station B no sediment transport could be estimated because the sediment sample contained mainly gravel. Mean current velocities were 0.60m/s on the ebb and 0.48m/s on the flood tide but were not strong enough to cause bed load transportation according to Sundborg (1967). At Station T2-T the same problem was revealed. The sediment sample contained pebbles, mussels and shells and the mean current velocities of 0.60m/s on the ebb and 0.45m/s on the flood tide could not induce bed load transport according to the diagram of Sundborg (1967). At Station QRC the mean

grain diameter of the collected sample was 0.64mm but the mean velocity on the flood tide was as low as 0.31m/s and therefore not high enough to move the coarse sand.

According to Gardiner and Dackombe (1983) the method of Sternberg (1972) has three main limitations:

1) if the method is applied in a tidal environment, the flow should be in an accelerating or relatively steady part of the cycle
2) mean sediment sizes should range from 0.2 to 2.0mm
3) most of the sediment should be transported as bed load and not as suspended load.

The second limitation explains why no estimation could be made for the stations where the samples either contained gravel and pebbles or very fine sediment.

The results of the computation of the eight measurements are presented in Table 8.4. The estimation for ebb and flood tidal data at Station A revealed a net transport of 23g/cm in the flood direction over a full tidal cycle. Flood tidal measurements at Station C revealed a sediment transport rate of 9g/cm during the flood tide. Ebb and flood tidal data measured at Station D displayed a net sediment transport with the ebb tide direction (east) of 8457g/cm over a full tidal cycle. At Station E a higher transport rate during the ebb tide was computed which results in a net sediment transport of 2207g/cm over a full tidal cycle. At Station QRC ebb tidal data revealed that an estimated 1296g/cm of sediment is transported as bed load. The only two stations showing a dominant direction of sediment transport towards the west with the flood tide, are Stations A and C. Both of these were positioned north of Middle Bank. However, Station QRC, also positioned north of Middle Bank, in the Queen's Road Channel, displayed dominant net sediment transport towards the east with the ebb tide. For Station QRC a far higher rate of net sediment transport was computed than the sum of sediment transported as bed load computed for Stations A and C. Estimations of net sediment transport direction at Stations D and E revealed that more sediment is transported towards the east with the ebb tide, especially at Station D which showed the highest rate of net sediment transport of all stations.

Table 8.4: Results of bed load estimation for one tidal cycle according to the method of Sternberg (1972).

Station	tidal state	bed load transport rate (g/cm)	net transport rate (g/cm)
A	ebb	8	
	flood	32	23
C	flood	9	9
D	ebb	8550	8457
	flood	93	
E	ebb	2898	2207
	flood	691	
QRC	ebb	1296	1296

A similar survey was carried out on the tidal flats of Invergowrie Bay, west of the Tay Railway Bridge, where Alizai (1980) measured current velocities and applied Sternberg's method to estimate bed load transport. These data were compared with the results of direct sampling of bed load using a VUV trap. Alizai (1980) measured residual motions with a flood dominance of 233g/cm on the middle and 681g/cm on the outer tidal flats of Invergowrie Bay on a spring tide compared with 141g/cm and 360g/cm on a neap tide, suggesting far lower bed load transport estimates than for the area between the two bridges where at Station D a bed load transport rate of 8457g/cm was estimated for an average tide.

Harris *et al.* (1979) and Sternberg and Marsden (1979) used the same method to estimate bed load transport in a tide-dominated embayment in Victoria, Australia. The maximum net transport rate calculated was 1571g/cm per tidal cycle with an ebb dominance. Gadd *et al.* (1978) estimated bed load transport from near-bottom current measurements on the New York Shelf applying, amongst others, Bagnold's (1963) equation which forms the basis for Sternberg's (1972) modified equation as mentioned earlier. These authors estimated a maximum net bed load transport rate equivalent to 1545g/cm per tidal cycle which is slightly higher than the estimation for Station QRC in this project (1296g/cm). Bed load sampling in a similar environment to the Tay Estuary was carried out by Kostaschuk and Villard (1996) in the Fraser River delta, Canada (tidal range 3-5m; dunes vary in height between 0.3-4.0m and in wavelength

between 4-100m according to Kostaschuk *et al.*, 1989). A Helley-Smith sampler was employed to trap bed load moving in the lower 0.08m of the flow as well as suspended bed material close to the bed but field tests showed that the Helley-Smith oversampled by 150%. Measured mean transport rates for dunes in the Fraser River delta were 0.049kg/m/s which is, assuming a tidal cycle of 12 hours and 30 minutes, equivalent to 22050g/cm over one tidal cycle. However, it is not stated whether this is the net sediment transport. The estimates of sediment transport rates compared with the measured rates by various authors indicate a high deviation of sediment transport rates in tidal environments depending on the method employed.

According to the estimates computed from current measurements in this study, the dominant net sediment transport direction is towards the east with the ebb tide. These results oppose the findings of other researchers (Buller and McManus, 1975). Estimates of the dominant sediment transport direction coincide with the dune asymmetries recorded by side-scan sonar at Stations A, C and D. Bed load transport was higher during the flood tide at Station A where flood dominant dunes were recorded during flood tidal conditions and ebb dominant dunes during ebb tidal conditions. Current measurements taken during flood tidal conditions could be applied only to estimate bed load transport at Station C. This has revealed a flood dominant sediment transport direction which confirms the interpretation of flood dominant dune asymmetries recorded by side-scan sonar during flood and ebb tidal conditions. At Station D sediment was transported as bed load with the ebb tide and sonographs revealed ebb dominant dunes during flood tidal conditions and dunes with mixed asymmetries during ebb tidal conditions. At Stations E and QRC dune asymmetries interpreted from sonographs revealed flood dominant current flows which contradict the estimate of dominant transport direction according to the current measurements of one tidal cycle which indicated an ebb dominance.

However, the estimation is based on average flow strength only and does not include the passing of a threshold for a certain length of time. The results of these estimates do not necessarily mean that the sediments fully leave the estuarine system but may be continuously reworked. Additional data should be collected especially downstream (east) of the study area. It should be noted that the estimate of sediment transported was made for

bed load only and not for suspended load. Including suspended load in the estimate is likely to lead to different results. It is also worth mentioning that the current velocities were measured over one tidal cycle only at various stages of the lunar cycle. Future work should take the various stages of the tide throughout the lunar cycle into account, preferably allowing data collection of flow strength over a higher number of tidal cycles, as well as including all the measurements needed to permit estimation by the more sensitive equation of Ackers and White (1973) for total load.

Chapter 9

KEY FINDINGS, THEIR IMPLICATIONS AND AVENUES FOR FUTURE RESEARCH

9.1 Introduction

Four different types of surveys have been integrated within this project:

a) side-scan sonar surveys giving full coverage of the study area
b) echo-sounding surveys of channel areas and Middle Bank
c) a sediment sampling survey to obtain ground information
d) current measurements.

The results of the four surveys have been described and discussed in Chapters 5, 6, 7 and 8. They were conducted to achieve the following objectives:

1) to carry out the first systematic side-scan sonar survey of the bed of part of the middle Tay Estuary (see Chapter 5)
2) to investigate the bed and establish correlations between the various geometrical parameters of bedforms and water depth (see Section 5.4)
3) to augment the side-scan sonar survey results by echo-sounding surveys in areas where recorded sonographs could not be fully interpreted (see Chapter 6)
4) to investigate the sediment types by means of acoustic remote sensing coupled with direct bottom sampling in order to establish the sediment distribution in the study area (see Chapter 7)
5) to establish a simplified circulation model of the tidal waters of the study area by examining dune asymmetries recorded by side-scan sonar in conjunction with current measurements (see Chapter 8)
6) to estimate bed load transport from current velocities (see Section 8.5)
7) to establish correlations between the geometrical parameters of bedforms, grain size of sediments and current velocities (see Section 9.2).

During the course of the project several ideas and suggestions arose for further research. These are described in Section 9.4 and will, hopefully, be investigated in future projects.

9.2 Relationships between geometrical parameters of bedforms, sediment size and current velocities

All of the bedforms observed by acoustic methods in the study area are dunes of various types (see Chapters 5 and 6). The distribution of dunes and their geometries are controlled by hydrodynamics and sediment characteristics (see Chapter 4). Various researchers (Harms *et al.*, 1975; Dalrymple *et al.*, 1978; Leeder, 1982; Zarillo, 1982; Allen, 1983; Dalrymple and Rhodes, 1995) have found good, positive correlations between mean flow speed and mean grain size and between mean flow speed and flow depth. These authors state that current speed has a major influence on bedform size.

The data collected in this study were analysed to establish correlations between the various geometrical parameters of dunes, sediment size and current velocities. Relationships between the various geometrical parameters of dunes and water depth have already been analysed and discussed in Section 5.4. Correlation coefficients were computed between dune height, dune wavelength, length along dune crest and water depth for:

- total data set
  - during ebb tidal conditions
  - during flood tidal conditions
- subtidal dunes
  - during ebb tidal conditions
  - during flood tidal conditions
- intertidal dunes
  - during ebb tidal conditions
  - during flood tidal conditions

A great variety of relationships was established between these parameters and the results indicate that they do not just depend on one another but are part of a far more complex system. In Chapter 8 dominant current directions, as recorded during one tidal cycle, were compared with the dune asymmetries interpreted from side-scan sonographs. Dune asymmetries as interpreted from sonographs did not generally support the measurements of maximum and average current speed but a correlation was found between dune asymmetry and the length of time at which the threshold for dune occurrence and migration, given by Dalrymple and Rhodes (1995) as 0.5m/s, is exceeded.

The influence of grain size on dune height is complicated. Rubin and McCulloch (1980), Allen (1982) and Flemming (1988) found that dune height decreases as the sediment becomes finer which, according to Allen (1982), is due to the relative proportion of sediment moving as suspended load. The correlation coefficient (r_{cc}) for the total data set is r_{cc}=0.000 (i.e. zero correlation). However, Southard and Boguchwal (1990) have found that a positive correlation between grain size and dune height reverses at grain sizes above 0.5mm, with dune height decreasing as the grain size continues to increase. Mean grain size of the collected sediment samples was correlated with dune height computed from sonographs. When dividing the data set into sub-sets of mean grain sizes of less than 0.5mm and greater than 0.5mm, and correlating these with dune height, the computed correlation coefficients are r_{cc}(<0.5mm)=-0.044 and r_{cc}(>0.5mm)=0.552 indicating no significant correlation (at the 0.01 and 0.05 levels) between fine grain sizes of less than 0.5mm and dune height and a stronger positive relationship between coarser grain sizes over 0.5mm and dune height. When dividing the total data set into subtidal and intertidal dunes, the correlation coefficients between dune height and mean grain size are r_{cc}=0.014 and r_{cc}=0.433 respectively, hence giving no significant correlation (at the 0.01 and 0.05 level). These results do not support the relationships established by the earlier mentioned researchers but suggest that the relationship between mean grain size and dune height is of a more complex nature and requires further investigation.

Another poorly understood relationship exists between sediment grain size and dune wavelength. Flemming (1988) indicates that larger dune wavelengths occur in coarser sediments. This is supported by the observations of Cook and Gorsline (1972) off the southern coast of California and by Dalrymple *et al.* (1978) and Dalrymple (1984) in the Bay of Fundy where "sand waves (large compound dunes according to the classification after Ashley, 1990; see Table 4.2) exist only where the mean grain size is coarser than 0.274mm (1.87phi)"(Dalrymple, 1984). Flume data discussed by Allen (1982) and Southard and Boguchwal (1990) indicate, conversely, that dune wavelength decreases as the sediment becomes coarser. Dalrymple and Rhodes (1995) note that field studies only have reported a positive correlation between dune wavelength and grain size indicating that this relationship is probably affected by other variables such as current speed. However, in this field study the computed correlation coefficient (r_{cc}) was as low as r_{cc}=-0.086 (insignificant at the

0.01 and 0.05 level) for the total data set. Correlation coefficients computed for subtidal and intertidal dunes were also close to 0 being r_{cc}=-0.188 and r_{cc}=-0.099 respectively, indicating no significant correlation (at the 0.01 and 0.05 levels) between dune wavelength and sediment mean grain size.

Since the dune descriptor "length along dune crest" is not referred to in the literature, but has been applied in this study only, no comparison with other observations is possible. Neither the computed correlation coefficient (r_{cc}=-0.031) for the total data set nor the correlation coefficients for subtidal (r_{cc}=-0.164) or intertidal dunes (r_{cc}=-0.184) indicate a significant correlation (at the 0.01 and 0.05 level) between this descriptor and mean grain size.

All computed r_{cc} values between mean grain size and dune height, wavelength and length along dune crest indicate no significant correlation between these variables even when dividing the data set into subtidal and intertidal dunes. It is not possible to fully explain the contradictory findings of this study compared with observations by other researchers since many variables (grain size, current speed, flow depth etc.) influence the occurrence and size of dunes in nature and it is difficult to disentangle the effects of the individual variables.

Bedform phase diagrams (Fig. 4.1) usually relate grain diameter and stream power, flow velocity or shear stress. The problem is that most bedform phase diagrams are based on experimental flume data or on data collected in a natural but uni-directional flow. In this study maximum and average current speeds during ebb and flood tidal conditions were correlated with mean grain diameter giving the following correlation coefficients (r_{cc}):

a) mean grain size/maximum ebb current speed r_{cc}=0.628
b) mean grain size/maximum flood current speed r_{cc}=0.013
c) mean grain size/average ebb current speed r_{cc}=0.487
d) mean grain size/average flood current speed r_{cc}=0.209

The values of the correlation coefficients (r_{cc}) indicate no strong overall relationship between mean grain size and maximum and average current speeds (r_{cc} is insignificant at the 0.01 level). However, a significant correlation (at the 0.05 level) was found between maximum ebb current speed and mean grain size.

The bedform phase diagram established by Harms *et al.* (1975) is based on mean flow velocity and mean grain size (Fig. 9.1), both of which were measured during this study. In Fig 9.1 average ebb and flood current velocities and corresponding mean grain size at the positions of the current measurement stations are plotted according to Harms *et al.* (1975). Stations B and T2-T could not be plotted since the sediment samples contained pebbles and mussels only. Table 9.1 shows a summary of dune sizes, mean grain sizes and average current velocities recorded at all eight stations. As can be seen in Table 9.1 dunes of various sizes were recorded by side-scan sonar at the current measurement stations. Half of the data points plot in the area of dunes as

Table 9.1: Mean ebb and flood tidal current speeds, dune dimensions (nm: not measurable) and mean grain sizes (p+m: pebbles and mussels) at the eight current measuring stations.

Station	dune height (m)	dune wave-length (m)	mean ebb current speed (cm/s)	mean flood current speed (cm/s)	mean grain size (mm)
A	0.45	3.0	40	47	0.37
B	0.35	6.0	60	48	p+m
C	0.59	3.7	31	41	0.37
D	0.40	6.5	61	50	0.48
E	0.45	4.0	63	59	0.39
QRC	nm	10.0	50	31	0.64
T2-T	0.33	3.0	60	45	p+m
NOM	0.23	2.0	38	28	0.10

expected from the interpretation of the sonographs. However, the other half of the measurements plot in the area of "ripples" according to the Harms *et al.* (1975) bedform phase diagram. This may be due to the classification of sedimentary bedforms as described in Chapter 4 but ripples are defined by Harms and Fahnestock (1965) as being under 0.3m in wavelength and under 0.05m in height which does not coincide with the dunes recorded by side-scan sonar at the current stations. Since the bedform phase diagram was established for a uni-directional flow and is mainly based on flume experiments, this result suggests that such a

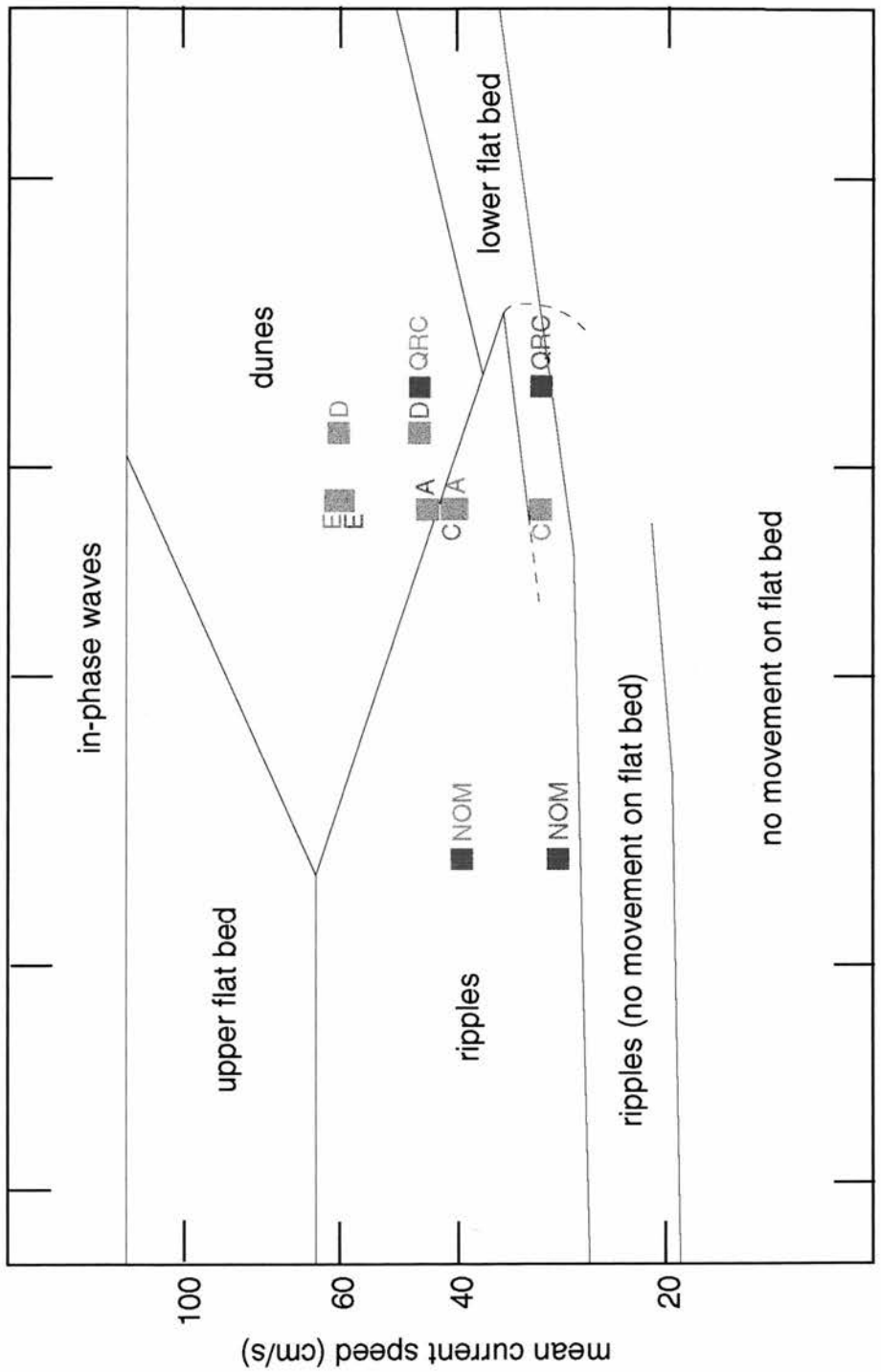

Fig. 9.1: Plot of mean current speed and mean grain size, as recorded at the current stations, on a bedform phase diagram established by Harms *et al.* (1975) (see text).

diagram may give a general indication of the relationship between flow velocity and sediment grain size. The large variety of bedform phase diagrams established by various researchers for uni-directional flow indicates the difficulty of producing a generally applicable diagram. Future work will hopefully include the construction of a bedform phase diagram for the estuarine environment.

Flow strength has a complex influence on bedform size. According to Dalrymple and Rhodes (1995) current speed increases with increasing water depth and dune height increases with increasing current speed if all other variables are constant. This is a generally accepted hypothesis (Rubin and McCulloch, 1980; Allen, 1982). However, water depth varies with the tidal cycle and measurements of water depth depend on the time of the survey. During the current measurement survey, at each of the five positions of this study (A-E), water depth was measured in conjunction with current speed 1m below the water surface and 1m above the bed over one tidal cycle. However, correlation coefficients computed between average water depth and average bottom current speed do not support the generally accepted hypothesis since r_{cc}=-0.94, indicating a significant but negative relationship (at the 0.01 significance level). In order to establish relationships between current speed and dune dimensions, maximum and average current speed measurements from all eight stations were correlated with dune heights measured from sonographs, giving correlation coefficient values (r_{cc}) of between -0.285 and 0.605 (Table 9.2) which are insignificant at both the 0.01 and 0.05 levels. Maximum and average flood and ebb tidal current speeds were also correlated with dune wavelength and length along dune crest (Table 9.2) but no overall strong correlations could be established. All correlation coefficients are insignificant at the 0.01 level but the r_{cc} value of 0.671 for maximum flood current speed and length along dune crest is significant at the 0.05 level.

It is interesting to note that the results of the investigations by Goedheer and Misdorp (1985) also did not support the generally accepted hypothesis, since they found that the "largest bedforms occur in the area with the smallest velocities" in the shallowest parts of their study area, Oosterschelde (Netherlands). However, such a good but negative relationship could not be established in the present study. Sonographs of the middle Tay Estuary revealed subtidal dunes of maximum measured height of 2.2m in water depths of 11.5m with the maximum water depth

being approximately 17.0m during the surveys. Smallest heights detected by side-scan sonar of 0.1m were measured from sonographs in an area where the waters were around 9.0m deep, although minimum measured water depth was 4.0m. Longest wavelengths of 75m were detected in water depths of 10.5m and shortest wavelengths of 0.8m in water depths of 9.0m. Smallest and largest dune heights recorded in intertidal areas during the surveys were 0.20m and 0.90m, respectively. Intertidal dune wavelengths ranged between 1.3m and 15.0m as measured from sonographs. Therefore, dunes of a greater variation in height and wavelength were recorded in subtidal than intertidal areas. In Section 5.4 correlation coefficients (r_{cc}), computed for linear regression analysis of geometrical parameters of dunes and water depth, indicated no significant correlations. The values of maximum and minimum dune height and wavelength in correlation with water depth do not support the generally accepted hypothesis of increasing current speed with increasing water depth or increasing dune height with increasing water depth. Neither do they support the findings of Goedheer and Misdorp (1985) which revealed the highest dunes in the shallowest part of their study area.

Table 9.2: Correlation coefficients (r_{cc}) computed between various geometrical parameters of dunes and maximum and average current speeds.

	dune height	dune wavelength	length along dune crest
maximum ebb current speed	-0.188	0.312	-0.058
maximum flood current speed	0.605	0.127	0.671
average ebb current speed	-0.286	0.328	-0.169
average flood current speed	0.431	-0.129	0.433

However, the finding of no significant correlations (at the 0.01 level) between geometrical parameters of dunes, sediment size and current speed does not prove that these variables are not inter-related. Flume

experiments have shown relationships between dune size, mean grain size and current strength which are partly supported by field observations. In the laboratory it is possible to analyse the relationships between two or three variables only which is impossible in a field study. Building on the conclusion of Dalrymple and Rhodes (1995) it is suggested that an extensive field study should simultaneously determine water depth, current velocity, sediment grain size, sediment availability, water temperature and salinity (which controls the fluid viscosity), flow history and dune size to analyse the complex interplay present in estuaries. The simultaneous measurement of all parameters would permit multi-variate regression analysis if a large number of data sets were to be collected. The results of this field study indicate that no single measured variable can explain the presence and absence nor the distribution of dunes in the middle part of the Tay Estuary.

9.3 Summary and concluding remarks

The sediment distribution and hydrodynamics of the Tay Estuary have been investigated by numerous researchers (Buller *et al.*, 1971; West, 1972; Buller, 1975; Buller and McManus, 1975; Charlton *et al.*, 1975; Al-Ansari and McManus, 1979; Alizai, 1980; McManus, 1982, 1986a and 1986b; Dobereiner and McManus, 1983; McMillan, 1983; Al-Dabbas and McManus, 1987; Gunn and Yenigun, 1987; White, 1992; McClelland, 1994; Carroll, 1995; Maxwell, 1996) especially over the last 30 years. These projects relied mainly on point sampling and only a few short and rather isolated acoustic remote sensing surveys have been carried out. In this project full coverage of the bed between the two bridges crossing the Tay Estuary at Dundee was achieved for the first time by means of side-scan sonar. This acoustic remote sensing technique is most often used in a qualitative sense to locate features of positive and negative relief and to distinguish between major sediment types. Here it has been employed to investigate the bedforms and their geometries, sediment types and facies changes over a relatively large and dynamic area.

Sonographs revealed the general distribution of sedimentary bedforms in the study area. Hitherto unknown, very abrupt facies changes were recorded which could often be related to bathymetrical variations. Sonographs were interpreted especially for the occurrence and distribution

of various types of dunes. Analysis of dune wavelength, height, length along dune crest, sinuosity, superposition, asymmetry and crest orientation was possible from most sonographs. The majority of the dunes recorded were of wavelengths between 0.6 and 5.0m, heights between 0.05 and 0.50m and lengths along dune crests were between 20 and 50m. The dominant sinuosity category was "sinuous out of phase" but a hitherto undescribed pattern referred to as "patchy, discontinuous" was recorded in most channel areas. Dunes were of compound superposition in shallower areas while simple dunes lined the channels. Most dune asymmetries were indicative of flood dominant current flows with generally north-south trending crest orientations.

The results of the side-scan sonar surveys were augmented by echo-sounding data recorded in some channel areas and along Middle Bank where the sonographs did not permit a detailed interpretation. Echograms were analysed for dune wavelength, height, superposition and asymmetry and then compared with the results of the side-scan sonar surveys. Although results were generally similar regarding the distribution of dunes, dune sizes were usually larger when measured from echograms than from sonographs. This is due to the different resolution and beam configuration of the two acoustic surveying systems. However, since the echo-sounder (Lowrance X-16) has the better resolution (which is a function of frequency; Lowrance X-16: f=192kHz; Waverley Sonar 3000: f=100kHz) and therefore permits more precise measurement especially of dune height, this suggests that dune height is underestimated when measured from sonographs recorded with the Waverley Sonar 3000 system. Another explanation is that dune height can be directly measured from echograms but only indirectly from sonographs by measuring the length of the acoustic shadow and calculating the height as described in Section 3.2.2.4. Wavelength, on the other hand, can be measured directly from sonographs and depends on the slant range and the resolution of the system while it has to be computed from echograms by relating the distance travelled between two adjacent GPS fixes to the corresponding fix marks on the echogram. Therefore a more precise measurement of dune wavelength is expected from sonographs.

Although side-scan sonar may be applied by means of acoustic backscatter levels to investigate surficial sediments of the bed, ground

information is essential for calibration since sonographs show relative relationships between tonal intensities and sediment characteristics only. Positions of sediment sampling points were chosen according to the sonographs and collected sediment samples were analysed for grain size distribution. Statistical analysis was carried out to compute median, standard deviation and skewness in order to permit comparison of the results with an earlier survey by Buller and McManus (1975). The dominant sedimentary class found was slightly gravelly sand according to the classification after Folk (1974). Deep areas were lined with coarser fractions such as pebbles, gravelly sand and mussels. Along the shore the sediments consist mainly of silty sand and sandy silt. The distribution of the textural classification of the sediments sampled closely correlates with the bathymetric chart of the study area.

In order to link bedform geometry, as recorded by the two acoustic remote sensing techniques, with sediment transport, it was essential to measure current velocities. Measurements were undertaken at five locations which were complemented by data acquired at three additional positions during earlier surveys. Charlton *et al.* (1975) have investigated the circulation in the Tay Estuary and found that the flood tide is uniformly distributed between the two channels while ebb tidal flows tend to concentrate in the main Navigation Channel south of Middle Bank. The data of the stations south of Middle Bank indicated ebb dominant bottom currents supporting the anticlockwise circulation pattern observed by Charlton *et al.* (1975) for surface currents. Two of the stations (A and C) north of Middle Bank indicated flood dominant current flows while at the other two stations (B and QRC), closer to the Road Bridge, the current flow was stronger during ebb tidal conditions. The measurement of maximum and average current velocities did not fully coincide with the dune asymmetries revealed from sonograph interpretation. At Stations C, D, QRC, T2-T and NOM a relationship between dune asymmetries (or non-existence in the case of Station NOM) and current measurements was found when comparing the former with the length of time at which a threshold (0.5m/s) for dune formation and migration was exceeded (see Section 8.4).

An attempt was made to estimate bed load transport on the basis of current measurements and sediment mean grain size after the method of Sternberg (1972). The results indicate a dominant bed load transport

direction with the ebb tide towards the east. However, this does not conform with the sonograph interpretation of dune asymmetries which indicated an overall flood dominance. As already mentioned in Section 8.5 more data are necessary for an improved estimation of sediment transport.

As discussed in Chapter 5 and Section 9.2, numerous researchers have tried to establish relationships between geometrical parameters of dunes, water depth, sediment size and current velocities, mainly from observations in intertidal environments. Although some researchers have found significant correlations between the above mentioned variables, mainly from flume experiments and occasionally from data collected in field studies, no such correlations could be established from the data collected in this field study. It is therefore suggested that the formerly established relationships should be used for approximate estimations only. Nevertheless, acoustic remote sensing techniques have been successfully employed to systematically investigate the bed, sediment type and facies variations of the middle Tay Estuary.

9.4 Future research suggestions

Throughout this project ideas and suggestions for future research arose. Some of these have been mentioned in Sections 5.5, 6.5 and 8.5 and will be briefly summarised here. Others are related to signatures found on the sonographs which could not be fully explained and require further investigation.

In Section 5.4 the various geometrical parameters of dunes and water depth were correlated. Similarly to Bokuniewicz *et al.* (1977) and Goedheer and Misdorp (1985) but unlike Yalin (1964, 1977, 1987), Allen (1968), Dalrymple *et al.* (1978), Zarillo (1982) and Flemming (1988), no significant correlations were found. The further correlation of the geometrical parameters of dunes not only with water depth but also with flow strength and sediment grain size did not show any significant correlations either but current data were available from eight stations only and a larger data base may alter the results of the statistical correlation analysis. It is therefore suggested that future research should include the use of more current data, as also mentioned in Section 8.5, since a larger

database of current measurements, which should also take the various stages of the tide throughout the lunar cycle into account, would permit a better estimation of bed load transport. As mentioned in Section 8.5 additional data should also be collected downstream (east) of the study area since the present estimation indicated a dominance of bed load transport with the ebb tide towards the east, opposing the interpretation of dune asymmetries which revealed a flood dominance and the findings of other researchers (Buller and McManus, 1975). If the total load of transported sediment is to be estimated, the equation of Ackers and White (1973) should be applied since Heathershaw (1981) suggests that this is more sensitive than the relationship developed by Engelund and Hansen (1967).

As mentioned in Section 6.5, the interpretation of dune asymmetry recorded by side-scan sonar and echo-sounding in the study area suggests a high input of sediment of marine origin which supports the findings of earlier studies by Buller and McManus (1975), Buller *et al.* (1975), McManus (1986) and Al-Dabbas and McManus (1987). However, it must be noted that the majority of the present surveys were carried out on well established flood tides or during high slack water and only a few lines were run during the early stages of the ebb tide. Therefore, it may be assumed that the bedforms might change their size, shape and especially their asymmetry, later during the ebb tide. For better comparison future work should, if possible, include surveys at the end of each tide. However, the areas along the sand banks where changes are expected to occur, would not be accessible as the water depths become too shallow at the end of the ebb tide to permit survey work.

On most days of the side-scan sonar surveys foam lines appeared on the water surface but varied in their extent and location during the tide. Ferrier and Anderson (1995) have investigated the development of such foam lines in the Tay Estuary by means of airborne remote sensing as well as ground sampling from a research vessel. These foam lines are the surface manifestation of convergent fronts which arise at interfaces between water bodies of differing density, due principally to salinity contrasts but also to temperature variations (Ferrier and Anderson, 1996). Convergent fronts can be identified due to distinct changes in water colour and the occurrence of buoyant material at the surface, as well as foam lines.

However, in estuaries it is difficult to recognise the nature, extent and physical relationship of fronts due to the constantly changing current conditions. Ferrier and Anderson (1995) believe that fronts develop due to turbulence caused by the tidal progression over linear bedform features or the development of internal waves at intrusion arms. Convergent fronts have also been investigated in estuaries in England and Wales by Brown *et al.* (1991). These authors point out the important implications of such features for estuarine pollution since the buoyant material will be deposited on the intertidal banks at low water, upstream from its starting point and, furthermore, fronts act as barriers to dispersal of pollutants in the water column.

Since this is particularly relevant for oil spillages, it is important to investigate the presence and effects of convergent fronts. The current distribution in such a convergence zone in an estuary in New Hampshire, U.S.A., has been measured with an acoustic doppler current profiler (ADCP) by Swift *et al.* (1996). The results allowed the production of a model of the flow structure showing the surface convergence and cellular nature of the transverse currents characteristic of axial convergence zones. However, natural channels vary and the results of Swift *et al.* (1996) revealed the importance of the local bed topography on front development and migration. Therefore flow structures and bedforms have to be investigated in each individual estuary before applying a model. On a side-scan sonar record (Fig. 9.2) a convergent front appears as a line of a zone of high acoustic backscatter compared to the surrounding tones.

It is suggested that future work should combine the results of side-scan sonar surveys, to investigate the topographical changes, with current measurements by ADCP to establish a similar model for the Tay Estuary as already produced for the Piscataqua River, New Hampshire, by Swift *et al.* (1996). The temporal and spatial evolution of frontal systems in the Tay Estuary have been extensively studied by airborne remote sensing methods by Ferrier and Anderson (1995 and 1996). It is believed, from the findings of this study, that there are hitherto unrecognised spatial and temporal coincidences between fronts, as observed at the water surface, and the boundaries of active or persistent and inactive or dormant bed load transport pathways. It is important to ascertain the location of sediment sinks, together with the positions and persistence of both the

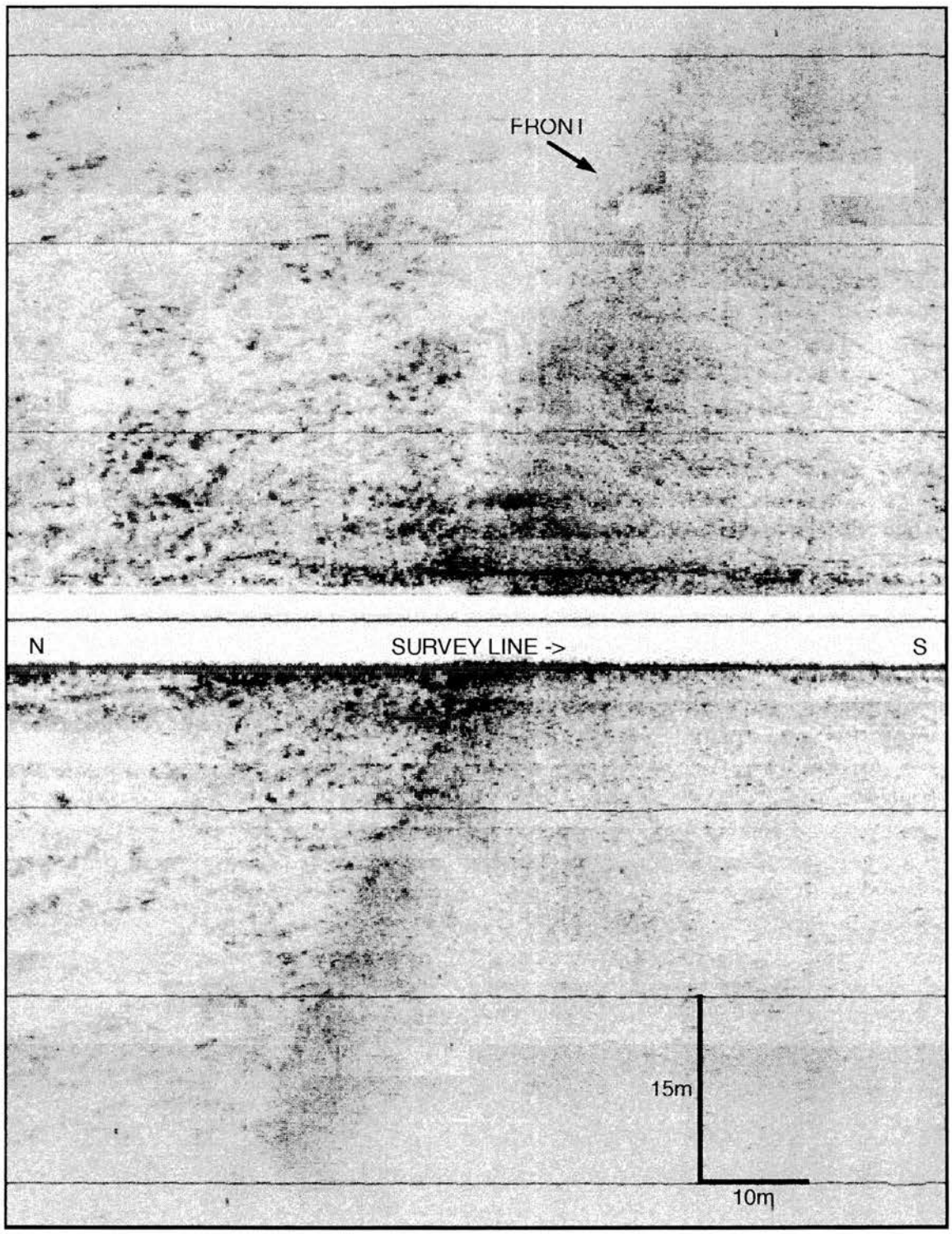

Fig. 9.2: Sonograph recorded when crossing a convergent front in the Tay Estuary. Note high acoustic backscatter from the water column at the convergence zone and no bathymetric correlation with the position of the front.

intra-water column and bottom transport pathways, and under what tidal and hydrological conditions some operate persistently or discontinuously and others cease to function. The long-term dynamics of sediment fluxes in estuaries are a most significant aspect of marine geology and this study has shown that an integrated determination of the whole water/sediment system should be an ultimate goal.

REFERENCES

Ackers, P. and White, W.R. (1973). Sediment transport: new approach and analysis. *Proceedings of the American Society of Civil Engineers*, **HY11**: 2041-2060.

Admiralty (1994). *River Tay:* **1481**.

Agrawal, Y.C., McCave, I.N. and Riley, J.B. (1991). Laser diffraction size analysis. In: Syvitski, J.P.M. (Ed.) *Principles, methods and application of particle size analysis*. Cambridge, Cambridge University Press: 368pp.

Al-Ansari, N.A. and McManus, J. (1979). Fluvial sediments entering the Tay Estuary: Sediment discharge from the River Earn. *Scottish Journal of Geology*, **15**: 203-216.

Al-Dabbas, M.A.M. and McManus, J. (1987). Shell fragments as indicators of bed sediment transport in the Tay Estuary. *Proceedings of the Royal Society of Edinburgh*, **92B**: 335-344.

Al-Jabbari, M.H., McManus, J. and Al-Ansari, N.A. (1980). Sediment and solute discharge into the Tay Estuary from the river system. *Proceedings of the Royal Society of Edinburgh*, **78B**: s15-s32.

Alizai, S.A.K. (1980). *Sediments in the intertidal zone of the upper Tay Estuary.* PhD thesis, University of Dundee.

Allen, J.R.L. (1968). *Current ripples - Their relation to patterns of water and sediment motion.* Amsterdam, North-Holland Publishing Company: 433pp.

Allen, J.R.L. (1970). *Physical Processes of Sedimentation.* New York, Elsevier: 248pp.

Allen, J.R.L. (1976). Conceptual models for dune time-lag: general ideas, difficulties, and early results. *Sedimentary Geology*, **15**: 1-53.

Allen, J.R.L. (1982). *Sedimentray Structures - Their Characteristics and Physical Basis*. New York, Elsevier: 593pp.

Allen, J.R.L. (1983). River bedforms: progress and problems. In: Collinson, J.D. and Lewin, J. (Eds.). *Modern and ancient fluvial systems*. Oxford, Blackwell Scientific Publications: 19-33.

Allen, J.R.L. (1994). Fundamental properties of fluids and their relation to sediment transport processes. In: Pye, K. (Ed.) *Sediment transport and depositional processes*. Oxford, Blackwell Scientific: 25-60.

Allen, J.R.L., Friend, P.F., Lloyd, A. and Wells, H. (1994). Morphodynamics of intertidal dunes: a year-long study at Lifeboat Station Bank, Wells-next-the-sea, Eastern England. *Philosophical Transactions of the Royal Society of London*, **347A**: 291-345.

Anderson, J.M. (1989). Remote sensing in the Tay Estuary using the airborne thematic mapper. In: McManus, J. and Elliott, M. (Eds.). *Developments in estuarine and coastal study techniques*. Fredensborg, Olsen & Olsen: 15-19.

Anonymous (1967). A side-scan sonar plots the sea bed. *New Scientist*, **34**: 648.

Ardö, J. and Pilesjö, P. (1992). On the accuracy of the global positioning system - A test using a hand-held receiver. *International Journal of Remote Sensing*, **13**: 3229-3233.

Armstrong, M., Paterson, I.B. and Browne, M.A.E. (1985). *Geology of the Perth and Dundee district*. London, HMSO: 108pp.

Ashley, G.M. (1990). Classification of large-scale subaqueous bedforms: a new look at an old problem. *Journal of Sedimentary Petrology*, **60**: 160-172.

Bagnold, P.A. (1963). Mechanics of marine sedimentation. In: Hill, M.N. (Ed.) *The Sea*. New York, Wiley-Interscience: 507-582.

Beer, T. (1983). *Environmental Oceanography*. Oxford, Pergamon Press: Belderson, R.H., Johnson, M.A. and Kenyon, N.H. (1982). Bedforms. In: Stride, A.H. (Ed.) *Offshore tidal sands*. London, Chapman & Hall: 27-57.

Belderson, R.H., Kenyon, N.H., Stride, A.H. and Stubbs, A.R. (1972). *Sonographs of the sea floor - A picture atlas*. Amsterdam, Elsevier Publishing Company: 185pp.

Bennett, R.H., Li, H., Richardson, M.D., Fleischer, P., Lambert, D.N., Walter, D.J., Briggs, K.B., Rein, C.R., Sawyer, W.B., Carnaggio, F.S., Young, D.C. and Tooma, S.G. (1992). Geoacoustic and geological characterization of surficial marine sediments by in situ probe and remote sensing techniques. In: Geyer, R.A. (Ed.) *CRC Handbook of geophysical exploration at sea*. Boca Raton, Florida, CRC Press: 295-350.

Berné, S., Castaing, P., Le Drezen, E. and Lericolais, G. (1993). Morphology, internal structure, and reversal of asymmetry of large subtidal dunes in the entrance of the Gironde Estuary (France). *Journal of Sedimentary Petrology*, **63**: 780-793.

Boersma, J.R. and Terwindt, J.H.J. (1981). Neap-spring tide sequences of intertidal shoal deposits in a mesotidal estuary. *Sedimentology*, **28**: 151-170.

Bokuniewicz, H.J., Gordon, R.B. and Kastens, K.A. (1977). Form and migration of sandwaves in a large estuary, Long Island Sound. *Marine Geology*, **24**: 185-199.

Boothroyd, J.C. (1985). Tidal inlets and tidal deltas. In: Davis, R.A. (Ed.) *Coastal Sedimentary Environments*. New York, Springer Verlag: 445-532.

Boothroyd, J.C. and Hubbard, D.K. (1975). Genesis of bedforms in mesotidal estuaries. In: Cronin, L.E. (Ed.) *Estuarine research*. New York, Academic Press: 217-234.

Braystoke Directional Reading Current Flow Meter B.F.M.008 MK3 - Operating and Maintenance Instruction Book and Calibration Chart. Valeport Developments Ltd:

Brown, J., Turrell, W.R. and Simpson, J.H. (1991). Aerial surveys of axial convergent fronts in UK estuaries and the implications for pollution. *Marine Pollution Bulletin*, **22**: 397-400.

Bryant, R.S. (1975). Side scan sonar for hydrography. *International Hydrographic Review*, **11**: 43-56.

Buller, A.T. (1975). Sediments of the Tay Estuary, part II: Formation of ephemral zones of high suspended sediment concentrations. *Proceedings of the Royal Society of Edinburgh*, **75B**: 65-89.

Buller, A.T., Charlton, J.A. and McManus, J. (1972). *Data from physical and chemical measurements in the Tay Estuary for neap and spring tides, June 1972*. Tay Estuary Research Center (TERC), University of Dundee, Report 2.

Buller, A.T., Green, C.D. and McManus, J. (1975). Dynamics and sedimentation: The Tay Estuary in comparison with other estuaries. In: Hails, J. and Carr, A.J. (Eds.). *Near shore sediment dynamics*. London, John Wiley: 201-249.

Buller, A.T. and McManus, J. (1971). Channel stability in the Tay Estuary: Controls by bedrock and unconsolidated post-glacial sediment. *Engineering Geology*, **5**: 227-237.

Buller, A.T. and McManus, J. (1975). Sediments of the Tay Estuary, Part I: Bottom sediments of the upper and upper middle reaches. *Proceedings of the Royal Society of Edinburgh*, **75B**: 41-64.

Buller, A.T. and McManus, J. (1979). Sediment sampling and analysis. In: Dyer, K.R. (Ed.) *Estuarine hydrography and sedimentation*. Cambridge, Cambridge University Press: 87-130.

Buller, A.T., McManus, J. and Williams, D.J.A. (1971). *Investigations in the estuarine environments of the Tay*. Tay Estuary Research Center (TERC), University of Dundee, Report 1.

Carroll, C.J. (1995). *A side scan sonar survey of the bedforms of Middle Bank in the Tay Estuary, Scotland*. MSc thesis, University of Dundee.

Caston, G.F. (1979). Wreck marks: Indicators of net sand transport. *Marine Geology*, **33**: 193-204.

Charlton, J.A., McNicoll, W. and West, J.R. (1975). Tidal and freshwater induced circulation in the Tay Estuary. *Proceedings of the Royal Society of Edinburgh*, **75B**: 11-27.

Chesterman, W.D. (1968). Geophysical exploration of the ocean floor using acoustic methods. *Contemporary Physics*, **9**: 423-446.

Chesterman, W.D., Clynick, P.R. and Stride, A.H. (1958). An acoustic aid to sea-bed surveying. *Acustica*, **8**: 285-290.

Collinson, J.D. and Thompson, D.B. (1989). *Sedimentary structures*. London, Chapman & Hall: 207pp.

Cook, D.O. (1982). Nearshore bedform patterns along Rhode Island from side-scan sonar surveys - discussion. *Journal of Sedimentary Petrology*, **52**: 677-679.

Cook, D.O. and Gorsline, D.S. (1972). Field observations of sand transport by shoaling waves. *Marine Geology*, **13**: 31-55.

Cracknell, A.P.e.a. (1982). Remote sensing in Scotland using data received from satellites: A study of the Tay estuary region using LANDSAT multispectral scanning imagery. *International Journal of Remote Sensing*, **3**: 113-137.

Cunningham, D. (1896). The estuary of the Tay. *Proceedings of the Institution of Civil Engineers*, **120**: 299.

D'Olier, B. (1979). Side-scan sonar and reflection seismic profiling. In: Dyer, K.R. (Ed.) *Estuarine hydrography and sedimentation*. Cambridge, Cambridge University Press: 57-86.

Dalrymple, R.F., Knight, R.J. and Lambiase, J.J. (1978). Bedforms and their hydraulic stability relationships in an tidal environment, Bay of Fundy, Canada. *Nature*, **275**: 100-104.

Dalrymple, R.W. (1984). Morphology and internal structure of sandwaves in the Bay of Fundy. *Sedimentology*, **31**: 365-382.

Dalrymple, R.W., Knight, R.J., Zaitlin, B.A. and Middleton, G.V. (1990). Dynamics and facies model of a microtidal sandbar complex, Cobequid Bay-Salmon River estuary (Bay of Fundy), Canada. *Sedimentology*, **37**: 577-612.

Dalrymple, R.W. and Rhodes, R.N. (1995). Estuarine dunes and bars. In: Perillo, G.M.E. (Ed.) *Geomorphology and Sedimentology of Estuaries*. Amsterdam, Elsevier: 359-422.

Dix, J.K. (1995). *The use of high resolution geophysics for the investigation of submerged Paleo-glaciomarine environments*. PhD thesis, University of St.Andrews.

Dobereiner, C. (1982). *Aggregation and deposition of fine particles in the Tay Estuary*. PhD thesis, University of Dundee.

Dobereiner, C. and McManus, J. (1983). Turbidity maximum migration and harbor siltation in the Tay Estuary. *Canadian Journal of Fisheries and Aquatic Sciences*, **40**: 117-129.

Dobinson, A. and McCann, D.M. (1990). Application of marine seismic surveying methods to engineering geological studies in the nearshore environment. *Quarterly Journal of Engineering Geology*, **23**: 109-123.

Duck, R.W. and Dow, W.M. (1994). Side-scan sonar reveals submerged remains of the first Tay railway bridge. *Geoarchaeology*, **9**: 139-153.

Duck, R.W. and McManus, J. (1985). A sidescan sonar survey of a previously drawn-down reservoir: a control experiment. *International Journal of Remote Sensing*, **6**: 601-609.

Duck, R.W. and McManus, J. (1987). Sidescan sonar applications in limnoarchaeology. *Geoarchaeology*, **2**: 223-230.

Duck, R.W. and McManus, J. (1989). *Bottom and sub-bottom sediments of the lower Tay Estuary*. Tay Estuary Research Centre.

Dyer, K.R. (1972). Sedimentation in estuaries. In: Barnes, R.S.K. and Green, J. (Eds.). *The estuarine environment*. London, Applied Science Publications: 295-310.

Dyer, K.R. (1986). *Coastal and estuarine sediment dynamics*. Chichester, John Wiley & Sons: 342pp.

Einstein, H.A. (1950). The bedload function for sediment transportation in open channel flows. *Soil Conservation Service, US Department of Agriculture, Technical Bulletin*, **1026**: 1-78.

Engelund, F. and Hansen, E. (1967). *A monograph on sediment transport in alluvial streams*. Copenhagen, Technisk Verlag: 62pp.

Ferentinos, G. and McManus, J. (1981). Nearshore processes and shoreline development in St.Andrews Bay, Scotland, UK. *Spec.Publs.int.Ass.Sediment.*, **5**: 161-174.

Ferrier, G. and Anderson, J.M. (1995). *The application of remote sensing data in the study of frontal systems in the Tay Estuary, Scotland*. In: The pplication of remotely sensed data to monitoring coastal processes. University of Dundee, Dundee Centre for coastal zones research.

Ferrier, G. and Anderson, J.M. (1996). The application of remote sensing data in the study of effluent dispersal in the Tay Estuary. *International Journal of Remote Sensing*, **17**: 3541-3566.

Fish, J.P. and Carr, H.A. (1990). *Sound underwater images - a guide to the generation and interpretation of side scan sonar data*. Cataumet, Massachussetts, Lower Cape Publishing: 188pp.

Flemming, B.W. (1976). Side-scan sonar: A practical guide. *International Hydrographic Review*, **53**: 65-91.

Flemming, B.W. (1988). Zur Klassifikation subaquatischer, strömungstransversaler Transportkörper. *Bochumer Geologische und Geotechnische Arbeiten*, **29**: 44-47.

Folk, R.L. (1974). *Petrology of sedimentary rocks*. Austin, Texas, Hemphill Publishing Company: 182pp.

Gadd, P.E., Lavelle, J.W. and Swift, D.J.P. (1978). Estimates of sediment transport on the New York Shelf using near-bottom current meter observations. *Journal of Sedimentary Petrology*, **48**: 239-252.

Gardiner, V. and Dackombe, R. (1983). *Geomorphological field manual*. London, George Allen&Unwin: 254pp.

Goedheer, G.J. and Misdorp, R. (1985). Spatial variability and variations in bedload transport direction in a subtidal channel as indicated by sonographs. *Earth Surface Processes and Landforms*, **10**: 375-386.

Green, C.D. (1975a). Sediments of the Tay Estuary, Part III: Sedimentological and faunal relationships on the southern shore at the entrance to the Tay. *Proceedings of the Royal Society of Edinburgh*, **75B**: 91-112.

Green, C.D. (1975b). A study of hydraulics and bedforms at the mouth of the Tay Estuary, Scotland. In: Cronin, L.E. (Ed.) *Estuarine research*. New York, Academic Press: 323-344.

Gunn, D.J. and Yenigun, O. (1987). A model for tidal motion and level in the Tay Estuary. *Proceedings of the Royal Society of Edinburgh*, **92B**: 257-273.

Harms, J.C. and Fahnestock, R.K. (1965). Stratification, bed forms, and flow phenomena (with an example from the Rio Grande). In: Middleton, G.V. (Ed.) *Primary sedimentary structures and their hydrodynamic interpretation*. Tulsa, Oklahoma, Society of Economic Paleontologists and Mineralogists: 84-115.

Harms, J.C., Southard, J.B., Spearing, D.R. and Walker, R.G. (Eds.) (1975). *Depositional environments as interpreted from primary sedimentary structures and stratification sequences*. Tulsa, Society of Economic Paleontologists and Mineralogists.

Harris, J.E., Hinwood, J.B., Marsden, M.A.H. and Sternberg, R.W. (1979). Water movements, sediment transport and deposition, Western Port, Victoria. *Marine Geology*, **30**: 131-161.

Harris, P.T. and Collins, M.B. (1985). Bedform distributions and sediment transport paths in the Bristol Channel and Severn Estuary, U.K. *Marine Geology*, **62**: 153-166.

Harris, P.T., Pattiaratchi, C.B., Cole, A.R. and Keene, J.B. (1992). Evolution of subtidal sandbanks in Moreton Bay, eastern Australia. *Marine Geology*, **103**: 225-247.

Heathershaw, A.D. (1981). Comparisons of measured and predicted sediment transport rates in tidal currents. *Marine Geology*, **42**: 75-104.

Hine, A.C. (1975). Bedform distribution and migration patterns on tidal deltas in the Chatham Harbor Estuary, Cape Cod, Massachussetts. In: Cronin, L.E. (Ed.) *Estuarine research.* New York, Academic Press: 235-252.

Hobbs, R.R. (1981). *Marine Navigation 2: Celestial and Electronics.* Annapolis, Maryland, United States Naval Institute: 343pp.

Hooper, D.J. (1979). Hydrographic surveying. In: Dyer, K.R. (Ed.) *Estuarine hydrography and sedimentation*. Cambridge, Cambridge University Press: 41-56.

Hunter, R.E., Thor, D.R. and Swisher, M.L. (1982). Depositional and erosional features of the inner shelf, Northeastern Bering Sea. *Geologie en Mijnbouw*, **61**: 49-62.

Ingham, A.E. (Ed.) (1975). *Sea surveying*. London, John Wiley & Sons:
Inman, D.L. (1952). Measures for describing the size distribution of sediments. *Journal of Sedimentary Petrology*, **22**: 125-145.

Inman, D.L. (1963). Ocean waves and associated currents. In: Shepard, P. (Ed.) *Submarine geology*. New York, Harper&Row: 48-81.

Johnson, H.P. and Helferty, M. (1990). The geological interpretation of side-scan sonar. *Reviews of Geophysics*, **28**: 357-380.

Kearey, P. and Brooks, M. (1991). *An introduction to geophysical exploration*. Oxford, Blackwell Scientific Publications: 254pp.

Kelland, N.C. and Hopkins, J.C. (1972). Mosaics from high resolution side scan sonar. *Offshore Services*, **October**: 34-35.

Kjerfve, B. (1979). Measurement and analysis of water current, temperature, salinity and density. In: Dyer, K.R. (Ed.) *Estuarine hydrography and sedimentation*. Cambridge, Cambridge University Press: 186-226.

Klein (1985). *Klein side-scan manual*.

Kostaschuk, R. and Villard, P. (1996). Flow and sediment transport over large subaqueous dunes: Fraser River, Canada. *Sedimentology*, **43**: 849-863.

Kostaschuk, R.A., Church, M.A. and Luternauer, J.L. (1989). Bedforms, bed material, and bedload transport in a salt-wedge estuary: Fraser River, British Columbia. *Canadien Journal of Earth Sciences*, **26**: 1440-1452.

Kostaschuk, R.A., Luternauer, J.L., Barrie, J.V., LeBlond, P.H. and von Deichmann, L.W. (1995). Sediment transport by tidal currents and implications for slope stability: Fraser River delta, British Columbia. *Canadian Journal of Earth Sciences*, **32**: 852-859.

Kumm, W. (1993). *GPS Global Positioning System*. Bielefeld, Delius Klasing: 120pp.

Lafond, E.C., Dietz, R.S. and Knauss, J.A. (1950). A sonic device for underwater sediment survey. *Journal of Sedimentary Petrology*, **20**: 107-110.

Langhorne, D.N. (1973). A sandwave field in the outer Thames Estuary, Great Britain. *Marine Geology*, **14**: 129-143.

Leeder, M.R. (1982). *Sedimentology - Process and Product*. London, Chapman & Hall: 344pp.

Leenhardt, O. (1974). Side scanning sonar - A theoretical study. *International Hydrographic Review*, **51**: 61-80.

Loizeau, J.-L., Arbouille, D., Santiago, S. and Vernet, J.-P. (1994). Evaluation of a wide range laser diffraction grains size analyser for use with sediments. *Sedimentology*, **41**: 353-361.

Lowrance (1985). *Lowrance X-16 Truline Recorder (Manual)*. 25pp.

Magellan (1990). *Magellan NAV 1000 PLUS user guide*. Monrovia, California.

Maxwell, F. (1995). *Comparison between sediment size distribution and remotely sensed acoustic data in the middle reaches of the Tay Estuary*. BSc thesis, University of Dundee.

McCave, I.N. (1979). Suspended sediment. In: Dyer, K.R. (Ed.) *Estuarine hydrography and sedimentation*. Cambridge, Cambridge University Press: 131-185.

McCave, I.N. and Langhorne, D.N. (1982). Sand waves and sediment transport around the end of a tidal sand bank. *Sedimentology*, **29**: 95-110.

McClelland, J. (1994). *Impact of the Tay road bridge on the bedforms of the Tay Estuary: A side scan sonar survey*. MSc thesis, University of Dundee.

McGuinness, W.T., Beckmann, W.C. and Officer, C.B. (1962). The application of various geophysical techniques to specialize engineering projects. *Geophysics*, **27**: 221-236.

McManus, J. (1966). Bottom structures of the Tay and other estuaries. *Scottish Geographical Magazine*, **82**.

McManus, J. (1967). Pre-glacial diversion of the Tay drainage through the Perth Gap. *Scottish Geographical Magazine*, **83**: 138-139.

McManus, J. (1968). The hydrology of the Tay Basin. In: Jones, S.J. (Ed.) *Dundee and district*. Dundee, Dundee Local Executive Committee of the British Association: 107-124.

McManus, J. (1972). Estuarine development and sediment distribution with particular reference to the Tay. *Proceedings of the Royal Society of Edinburgh*, **71B**: 97-113.

McManus, J. (1979). Sediments in estuaries. In: Severn, R.T., Dinely, D. and Hawkes, L.E. (Eds.). *Tidal power and estuary management*. Bristol, Scientechnica: 180-187.

McManus, J. (1982). Salinity - current speed covariation plots from estuaries. In: McManus, J. (Ed.) *Sedimentological, hydrological and biological papers*. Dundee, Tay Estuary Research Center (TERC), University of Dundee: 1-11.

McManus, J. (1984). *Data from tidal cycle measuring stations in the Tay Estuary 1972-82*. Tay Estuary Research Centre, Report 8.

McManus, J. (1984). *Gradients of change in the estuarine environments of the Tay*. In: Remote sensing applications in civil engineering. Dundee, University of Dundee.

McManus, J. (1986a). Land-derived sediment and solute transport to the Forth and Tay Estuaries, Scotland. *Journal of the Geological Society*, **143**: 927-934.

McManus, J. (1986b). *Sediment transport patterns in the Tay Estuary*. In: Wang, S.Y., Shen, H.W. and Ding, L.Z. (Eds.). 3rd International Symposium on River Sedimentation. University of Mississippi, School of Engineering, university of Mississippi: 517-524.

McManus, J. (1988). Grain size determination and interpretation. In: Tucker, M. (Ed.) *Techniques in Sedimentology*. Oxford, Blackwell Science: 63-85.

McManus, J. and Alizai, S.A.K. (1987). Variations in marsh surface levels in the upper Tay Estuary. *Proceedings of the Royal Society of Edinburgh*, **92B**: 345-358.

McManus, J. and Wakefield, P. (1982). Lateral transfer of water across the middle reaches of the Tay Estuary. In: McManus, J. (Ed.) *Sedimentological, hydrological and biological papers*. Dundee, Tay Estuary Research Center (TERC), University of Dundee: 25-37.

McMillan, K. (1983). *Study of sandbank and sediment dynamics in the Tay Estuary and Morecambe Bay usinf LANDSAT multispectral scanner data*. MSc thesis, University of Dundee.

McQullin, R. and Ardus, D.A. (1977). *Exploring the geology of shelf seas*. London, Graham & Trotman: 234pp.

Meade, R.H. (1969). Landward transport of bottom sediments in estuaries of the Atlantic coastal plain. *Journal of Sedimentary Petrology*, **39**: 222-234.

Mill, H.R. (1885). Note on the salinity of the Tay Estuary and of St.Andrews Bay. *Proceedings of the Royal Society of Edinburgh*, **13**: 347-350.

Morang, A. and McMaster, R.L. (1982). Nearshore bedform patterns along Rhode Island from side-scan sonar surveys - reply to Friedrich Werner. *Journal of Sedimentary Petrology*, **52**: 679-680.

Moustier, C.d. and Matsumoto, H. (1993). Seafloor acoustic remote sensing with multibeam echo-sounders and bathymetric sidescan sonar systems. *Marine Geophysical Researches*, **15**: 27-42.

Mudie, J.D., Normack, W.R. and Cray, E.J. (1970). Direct mapping of the seafloor using side-scanning sonar and transponder navigation. *Geological Society of America Bulletin*, **81**: 1547-1554.

Mudroch, A. and MacKnight, S.D. (1991). *Handbook of techniques for aquatic sediments sampling*. Boca Raton, Florida, CRC Press: 210pp.

Open University (1993). *Waves, tides and shallow-water processes*. Oxford, Pergamon Press: 187pp.

Pontin, R.A. and Reid, J.A. (1975). The freshwater input to the Tay Estuary. *Proceedings of the Royal Society of Edinburgh*, **75B**: 1-9.

Pritchard, D.W. (1967). What is an estuary: Physical viewpoint. In: Lauff, G.H. (Ed.) *Estuaries*. Washington, American Association for the Advancement of Science: 3-5.

Proudman, J. and Doodson, A.T. (1924). The principal constituents of the tides of the North Sea. *Philosophical Transactions of the Royal Society*, **A224**: 347-350.

Reid, I. and Frostick, L.E. (1994). Fluvial sediment transport and deposition. In: Pye, K. (Ed.) *Sediment transport and depositional processes*. Oxford, Blackwell Scientific Publications: 89-155.

Rogowski, J.B., Piraszewski, M., Kloze, J., Leszczynski, W. and Mrozinski, J. (1995). *Application of the Global Positioning System in hydrology*. In: General Assembly of the European Geophysical Society. Hamburg.

Rothwell, R.G., Kenyon, N.H. and McGregor, B.A. (1991). Sedimentary features of the South Texas continental slope as revealed by side-scan sonar and high-resolution seismic data. *The American Association of Petroleum Geologists Bulletin*, **75**: 298-312.

Rubin, D.M. and McCulloch, D.S. (1980). Single and superimposed bedforms: a synthesis of San Francisco Bay and flume observations. *Sedimentary Geology*, **26**: 207-231.

Sarrikostis, E. and McManus, J. (1987). Potential longshore transports on the coasts north and south of the Tay Estuary. *Proceedings of the Royal Society of Edinburgh*, **92B**: 297-310.

Scarth, A. (1966). The physical setting of the Tay road bridge. *Scottish Geographical Magazine*, **82**: 104-109.

Simpson, J.B. (1933). The late-glacial readvance moraines of the Highland border west of the River Tay. *Transactions of the Royal Society of Edinburgh*, **57**: 633-645.

Sissons, J.B., Cullingford, R.A. and Smith, D.E. (1965). Some pre-carse valleys in the Forth and Tay basins. *Scottish Geographical Magazine*, **81**: 115-124.

Sly, P.G. (1981). Equipment and techniques for offshore survey and site investigations. *Canadian Geotechnical Journal*, **18**: 230-249.

Southard, J.B. and Boguchwal, L.A. (1990). Bed configurations in steady unidirectional water flows. *Journal of Sedimentary Petrology*, **60**: 658-679.

Stein, R. (1985). Rapid grain-size analyses of clay and silt fraction by Sedigraph 5000D: Comparison with Coulter Counter and Atterberg methods. *Journal of Sedimentary Petrology*, **55**: 590-615.

Stephenson, D. and Gould, D. (1995). *British regional geology. The Grampian Highlands*. London, HMSO.

Sternberg, R.W. (1972). Predicting initial motion and bedload transport of sediment particles in the shallow marine environment. In: Swift, D.J.P., Duane, D.B. and Pilkey, O.H. (Eds.). *Shelf Sediment Transport*. Stroudsburg, Pennsylvania, Dowden, Hutchinson & Ross: 61-82.

Sternberg, R.W. and Marsden, M.A.H. (1979). Dynamics, sediment transport, and morphology in a tide-dominated embayment. *Earth Surface Processes*, **4**: 117-139.

Stride, A.H. (1961). Mapping the sea floor with sound. *New Scientist*, **10**: 304-306.

Sundborg, Å. (1967). Some aspects on fluvial sediments and general fluvial morphology I. General views and graphic methods. *Geografiska Annaler*, **49A**: 333-343.

Swift, D.J.P. and Freeland, G.L. (1978). Current lineations and sand waves on the inner shelf, Middle Atlantic Bight of North America. *Journal of Sedimentary Petrology*, **48**: 1257-1266.

Swift, M.R., Fredriksson, D.W. and Celikkol, B. (1996). Structure of an axial convergence zone from acoustic doppler current profiler measurements. *Estuarine, Coastal and Shelf Science*, **43**: 109-122.

Tucker, M.J. (1966). Sideways looking sonar for marine geology. *Geo-Marine Technology*, **2**: 18-23.

Vries Klein, G.d. (1970). Depositional and dispersal dynamics on intertidal sand bars. *Journal of Sedimentary Petrology*, **40**: 1095-1127.

Vries Klein, G.d. and Whaley, M.L. (1972). Hydraulic parameters controlling bedform migration on an intertidal sand body. *Geological Society of America Bulletin*, **83**: 3465-3470.

Weir, D.J. and McManus, J. (1987). The role of wind in generating turbidity maxima in the Tay Estuary. *Continental Shelf Research*, **7**: 1315-1318.

Wentworth, C.K. (1922). A scale of grade and class terms for clastic sediments. *Journal of Geology*, **30**: 377-392.

Werner, F. (1982). Nearshore bedform patterns along Rhode Island from side-scan sonar surveys - discussion. *Journal of Sedimentary Petrology*, **52**: 674-677.

West, J.R. (1972). Water movements in the Tay Estuary. *Proceedings of the Royal Society of Edinburgh*, **71B**: 115-129.

Wewetzer, S.F.K. and Duck, R.W. (1996). Side-scan sonograph from the middle reaches of the Tay Estuary, Scotland. *International Journal of Remote Sensing*, **17**: 3539-3540.

White, H. (1992). *Topography and morphology of the sediments in the middle reaches of the Tay Estuary*. BSc thesis, University of Dundee.

Williams, D.J.A. and West, J.R. (1973). A one-dimensional representation of mixing in the Tay Estuary. *Tech Pap Wat Pollist Res Dsir*, **13**: 118-125.

Williams, D.J.A. and West, J.R. (1975). Salinity distribution in the Tay Estuary. *Proceedings of the Royal Society of Edinburgh*, **75B**: 29-39.

Williams, S.J. (1982). *Use of high resolution seismic reflection and side-scan sonar equipment for offshore surveys*. U.S. Army Corps of Engineering, Coastal Engineering Technical Aid, 82-5.
Yalin, M.S. (1964). Geometrical properties of sandwaves. *Proceedings of the American Society of Civil Engineers*, **90**: 105-119.

Yalin, M.S. (1977). *Mechanics of sediment transport*. Toronto, Pergamon Press: 298pp.

Yalin, M.S. (1987). On the formation mechanism of dunes and ripples. *Euromech Colloquiem Proceedings*: 261.

Yalin, M.S. (1963). An expression for bedload transportation. *Proceedings of the American Society of Civil Engineers*, **HY3**: 221-250.

Yules, J.A. and Edgerton, H.E. (1964). Bottom sonar search techniques. *Undersea Technology*: 29-32.

Zarillo, G.A. (1982). Stability of bedforms in a tidal environment. *Marine Geology*, **48**: 337-351.

APPENDIX I

The easiest to determine measure is the median diameter (*Md*). It is the grain size diameter corresponding to the 50th percentile on the cumulative curve and thus half of the particles by weight are coarser and half are finer than the median. Since it is not affected by any extremes or asymmetries, Folk (1974) does not recommend its use.

The uniformity or sorting of sediments is equal to the standard deviation of conventional statistics. Inman (1952) defines sorting as:

$$\sigma\phi = (\phi 84 - \phi 16) / 2$$

while Folk (1974) includes 90% of the distribution in his measure known as the inclusive graphic standard deviation:

$$\sigma_I = \frac{\phi 84 - \phi 16}{4} + \frac{\phi 95 - \phi 5}{6.6}$$

The following classification scale for sorting has been derived from measurements for a large number of sediments by Folk (1974).

σ under	0.35ϕ	very well sorted
	0.35-0.50ϕ	well sorted
	0.50-0.71ϕ	moderately well sorted
	0.71-1.00ϕ	moderately sorted
	1.00-2.00ϕ	poorly sorted
	2.00-4.00ϕ	very poorly sorted
over	4.00ϕ	extremely poorly sorted.

Grain size distribution of sediments may be similar in average size and sorting but may differ in symmetry. Skewness measures any tendency of a curve to lean to either side (McManus, 1988). Skewness is expressed by Inman (1952) as:

$$\alpha\phi = \frac{\phi 16 + \phi 84 - 2\phi 50}{\phi 84 - \phi 16}$$

while Folk (1974) expresses inclusive graphic skewness as:

$$Sk_I = \frac{\phi 16 + \phi 84 - 2\phi 50}{2(\phi 84 - \phi 16)} + \frac{\phi 5 + \phi 95 - 2\phi 50}{2(\phi 95 - \phi 5)}$$

The absolute mathematical limits lie within -1 to +1 and Folk (1974) suggests the following limits for skewness:

Sk_I from	+1.0 to +0.3	strongly fine-skewed
	+0.3 to +0.1	fine-skewed
	+0.1 to -0.1	near-symmetrical
	-0.1 to -0.3	coarse-skewed
	-0.3 to -1.0	strongly coarse-skewed.

APPENDIX II

The method of estimating bedload sediment transport in shallow marine environments after Sternberg (1972). The specific steps of this procedure are:

1) Estimate the boundary shear stress τ_0 from the velocity measurements. If the mean velocity at one meter is known then use:

$$\tau_0 = 3 \cdot 10^{-3} \rho \overline{U}_{100}^2$$

with ρ being the fluid density and $\overline{U}_{100}$ the mean velocity 100cm off the bed.

2) Knowing a value of mean sediment diameter (D) estimate from Fig. II.1 the critical shear stress τ_c required to initiate sediment movement.

3) Compute the excess shear stress $(\tau_0-\tau_c)/\tau_c$ and together with the value of D, use Fig. II.2 to estimate the magnitude of the coefficient K.

4) The mass transport as bedload (j) can be estimated from the nomogram presented in Fig. II.3.

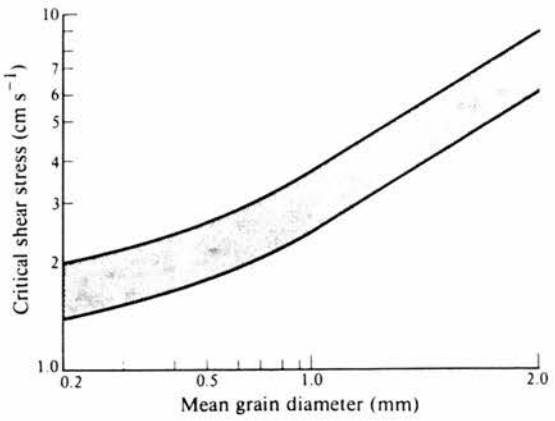

Fig. II.1: Relationship between critical shear stress and mean grain size. The stippled band represents the broad area within which values have been reported (after Inman, 1963).

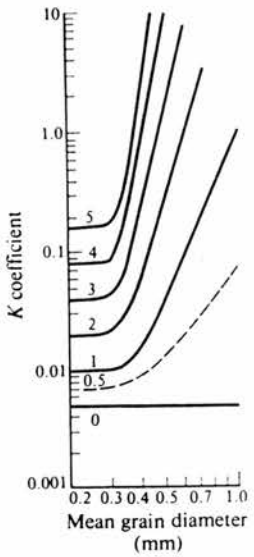

Fig. II.2: Relationship between the K coefficient in the bed load estimation equation and mean grain size for different values of excess shear stress (after Sternberg, 1972). Numbers on curves represent values of excess shear stress (after Gardiner and Dackombe, 1983).

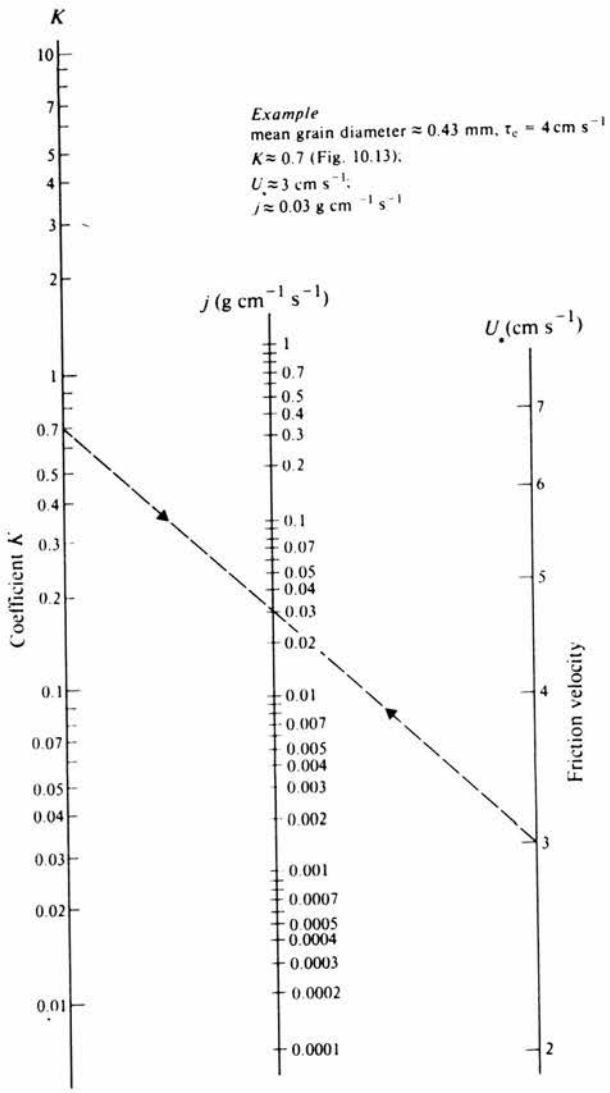

Fig. II.3: Nomogram for evaluation of bed load transport from measurements of the critical velocity and the coefficient K (after Sternberg, 1972).